The photophysics and photochemistry of aromatic 1,3-dicarbonyl compounds used as UVA sunscreens

Coultous, Catherine Jane

The Photophysics and Photochemistry of Aromatic 1,3-dicarbonyl Compounds used as UVA Sunscreens

Catherine Jane Coultous

Department of Chemistry

University of Durham

Submitted in partial fulfilment of the requirements for the degree of

Doctor of Philosophy

November 1999

Abstract

The Photochemistry and Photophysics of Aromatic 1,3-Dicarbonyl Compounds used as UVA Sunscreens

Catherine Jane Coultous

UV radiation can cause harmful effects to human skin, including premature skin ageing and skin cancer. Historically, sunscreens were developed to filter out UVB (290 nm-320 nm), but now the importance of UVA (320 nm-400 nm) sunscreens is realised. The most common UVA sunscreens are based on dibenzoylmethane (1,3-diphenyl propan-1,3-dione, DBM), of which the most common is Parsol 1789 (4'-methoxy 4'-tertiarybutyl DBM). The photochemistry of these materials has, however, been poorly understood. In this work the photophysics and photochemistry of DBM, Parsol 1789, Parsol DAM and ditertiarybutyl DBM have been studied, along with the respective O-methylated and C-methylated compounds of DBM and Parsol 1789.

DBMs exist primarily as an intra-molecularly bonded enol, which absorbs strongly at $\lambda \approx 340$ nm due to a π,π^* transition. The absorption spectra of DBMs also exhibit a smaller peak at $\lambda \approx 250$ nm, due to an n,π^* transition of the diketone content. At low temperature the main absorption band of DBMs shifts to longer wavelengths and vibrational structure can be observed. The enol form of DBMs fluorescence at low temperature, ($v_0' \rightarrow v''_0$ at $\lambda \approx 385$ nm), and phosphorescence can be observed from both the diketone ($\lambda_{em} \approx 495$ nm,) and enol forms ($\lambda_{em} \approx 425$ nm). Thus the triplet energies of the diketones and enols of the DBMs studied have been measured. O-methylated DBMs do not possess an intra-molecular H-bond, and the π,π^* absorption band falls to lower wavelengths than for chelated DBMs. C-methylated DBMs exist as a diketone structure, and display photophysics typical of an aromatic ketone.

It has been suggested that the main process on irradiation of DBM is the formation of a short-lived non-chelated enol, however no direct evidence as to the structure of this species is reported in the literature. Formation of the diketone form of DBM on prolonged irradiation in acetonitrile solution has also been reported, and in this work the quantum yield of this process has been measured; $\Phi \approx 0.01 \pm 0.004$.

In this work, direct (low temperature) IR spectroscopic evidence is presented to prove that the short-lived species produced on irradiation is indeed a non-chelated enol. The infra-red studies also suggest that the non-chelated enol form of DBM form complexes with polar solvents, as has been proposed in the literature. Quantum yields of non-chelated enol formation in cyclohexane at room temperature have been measured to be approximately $\Phi = 0.5 \pm 0.07$. This work indicates that the rate of transient decay is enhanced by the interaction of the transient molecules with chelated enol molecules or other transient molecules. IR studies of low temperature transient formation confirm the interaction of transient molecules by the observation of inter-molecular hydrogen-bonding.

By comparison with the E and Z isomers of O-methylated DBM, it is suggested that at low temperature DBM initially forms a Z-cis non-hydrogen bonded enol, which then converts to an E-trans non-hydrogen bonded enol with further irradiation. The kinetics and the temperature variation of the enol recovery support the theory that there is more than one species formed.

The photochemistry of DBM in emulsions has also been studied in this work. It has been shown that the photochemistry occurring on irradiation is similar to that observed in solutions. This indicates that simple solutions are a good model for actual sunscreen formulations.

Singlet oxygen is a highly reactive species capable of causing serious biological damage, however this work shows that DBM sunscreens generate singlet oxygen by photosensitisation, with quantum yields $\Phi_\Delta \approx 0.005\text{-}0.01$. It has also been shown that the lifetime of the excited state of DBM involved in singlet oxygen production is very short, approximately $\tau < 1$ μs.

Contents

Contents 3

List of Figures 10

List of Tables 17

Abbreviations 19

Chapter 1 - Introduction 22

1.1 Ultra Violet Radiation and Skin 23

1.1.1 Ultra Violet Radiation 23

1.1.2 Penetration of UV radiation into Skin 24

1.1.3 Biological effects of UV radiation 25

1.1.3.1 Vitamin D Synthesis 25

1.1.3.2 Pigmentation 25

1.1.3.3 Keratinisation 26

1.1.3.4 Inflammatory Erythema 26

1.1.3.5 Carcinogenesis 26

1.1.3.6 Photoageing 27

1.1.3.7 Action Spectra 27

1.2 Sunscreens 28

1.2.1 Sun-Protection Products 28

1.2.2 Chemical Sunscreens 29

1.2.3 UVA Sunscreens 30

1.3 Dibenzoylmethanes 31

1.3.1 Keto-Enol Tautomerism of 1,3-Dicarbonyl Compounds 32

1.3.2 Dibenzoylmethanes 34

1.3.3 Parsol 1789 36

1.3.4 C-Methylated Dibenzoylmethanes 37

1.3.5 O-Methylated Dibenzoylmethanes 37

1.4 Aims of this Work 39

1.5 References 40

Chapter 2 - Experimental 42

2.1 Ultra-Violet / Visible Absorption Spectroscopy 43

2.1.1 Room Temperature UV / Visible Absorption Spectroscopy 43
2.1.2 Low Temperature UV / Visible Absorption Spectroscopy 43

2.2 Luminescence Spectroscopy 45

2.2.1 Fluorescence Spectroscopy 46
2.2.2 Phosphorescence Spectroscopy 46
2.2.3 Low Temperature Luminescence Spectroscopy 47

2.3 Infra-Red Spectroscopy 48

2.3.1 Room Temperature Infra-Red Spectroscopy 48
2.3.2 Low Temperature Infra-Red Spectroscopy 48

2.4 Continuous Irradiation 49

2.4.1 Optical Filters 49
2.4.2 Experimental Set-ups 52
2.4.2.1 Photoketonisation Studies *52*
2.4.2.2 Quantitative Photoketonisation Studies *52*
2.4.2.3 Low Temperature Photolysis *53*
2.4.2.4 Photolysis of Solid Samples and Mineral Oil solutions *54*

2.5 Flash Photolysis 54

2.5.1 Excimer Pumped Dye Laser 54
2.5.2 Frequency Tripled Nd^{3+}:YAG laser 55
2.5.3 Data Treatment and Spectra Measurement 57

2.6 Quantum Yield Measurements 59

2.6.1 Quantum Yields of Photoketonisation 59
2.6.2 Quantum Yields of Short-lived Species Formation 62

2.6 Time-resolved Resonance Raman Spectroscopy 64

2.6.1 Raman Scattering 64
2.6.2 Resonance Raman Spectroscopy 65
2.6.3 Time-Resolved Resonance Raman Spectroscopy 65

2.8 Diffuse Reflectance Spectroscopy 68

2.8.1 Introduction 68

2.8.2 Reflection....68
2.8.2.1 Types of Reflection....68
2.8.2.2 Kubelka-Munk Theory....69
2.8.3 Obtaining Diffuse Reflectance Spectra....71
2.8.3.1 Eliminating Specular Reflection....71
2.8.3.2 Sample Preparation....72
2.8.3.3 White Reference Compounds....73
2.8.3.4 Experimental set-up....74
2.8.3.5 Experimental Details for Diffuse Reflectance Absorption spectroscopy used in this work....75
2.8.4 Diffuse Reflection Flash Photolysis....76
2.8.4.1 Theory....76
2.8.4.2 Possible Experimental Set-Ups....76
2.8.5 Experimental Details for Diffuse Reflectance Flash Photolysis used in this work....78

2.9 Singlet Oxygen Detection....79

2.9.1 Quantum Yields of Singlet Oxygen Formation....79
2.9.2 Variable Oxygen Concentration....82
2.9.3 Singlet Oxygen Quenching....83

2.10 Sample Degassing....83

2.11 Temperature Control....83

2.12 Method of separation of the E and Z isomers of O-Methyl DBM....84

2.13 Preparation of Emulsions....84

2.13.1 Sunscreen formulations....84
2.13.2 Preparation of the emulsion....86

2.14 UV/Visible Absorption Spectroscopy of Samples on Transpore Tape....87

2.15 Preparation of Cellulose Samples....87

2.16 Source and Quality of Chemicals used....87

2.17 References....89

Chapter 3 - The Photophysics of Dibenzoylmethanes in Solution....91

3.1 Introduction....92

3.1.1 Basic Photophysics....92
3.1.2 The Photophysics of Carbonyl compounds....93

3.1.2.1 Excited states of Carbonyl Compounds *93*
3.1.2.2 Singlet State Transitions of Carbonyl Compounds - Absorption and Fluorescence *97*
3.1.2.3 Triplet State Transitions of Carbonyl Compounds - Phosphorescence *99*
3.1.3 Photophysics of 1,3-Dicarbonyl Compounds 99
3.1.4 Photophysics of Dibenzoylmethanes 101
3.1.4.1 General *101*
3.1.4.2 Low Temperature Absorption *103*
3.1.4.3 Fluorescence *104*
3.1.4.4 Phosphorescence *104*
3.1.4.5 Other Dibenzoylmethanes *105*

3.2 Results and Discussion **106**

3.2.1 Absorption Spectra 106
3.2.1.1 Absorption Spectra of Dibenzoylmethanes *106*
3.2.1.2 Absorption Spectra of O-Methyl Substituted Dibenzoylmethanes *112*
3.2.1.3 Absorption Spectra of C-Methyl Substituted Dibenzoylmethanes *115*
3.2.1.4 Decomposition of DBM in Alkaline Solution *120*
3.2.2 Low Temperature Absorption Spectra 122
3.2.3 Fluorescence 125
3.2.4 Phosphorescence 127

3.3 Summary **132**

3.4 References **133**

Chapter 4 - The Photochemistry of Dibenzoylmethanes in Solution **135**

4.1 Introduction **136**

4.1.1 Photochemistry of Carbonyl Compounds 136
4.1.1.1 Introduction *136*
4.1.1.2 α-Cleavage Reactions *137*
4.1.1.3 Hydrogen Abstraction Reactions *137*
4.1.1.4 Charge Transfer Complexation *138*
4.1.1.5 Addition to Carbon-Carbon Multiple Bonds *139*
4.1.1.6 Other Reactions *140*
4.1.2 Photochemistry of 1,3-Dicarbonyl Compounds 141
4.1.2.1 Introduction *141*
4.1.2.3 Photoenolisation of 1,3-Diketones *142*
4.1.2.4 Photo-Decomposition of Dibenzoylmethanes *143*
4.1.2.5 Photoketonisation of Dibenzoylmethanes *145*

4.1.2.6 Transient Species Formation in DBM *147*
4.1.2.7 Photo-Isomerisation of O-Methyl DBM *161*
4.1.4 Summary of Photochemistry of Chelated Enol form of DBM 164

4.2 Results and Discussion **165**

4.2.1 Photoketonisation 165
4.2.1.1 Diketone Formation *165*
4.2.1.2 Quantum Yields of Photoketonisation *167*
4.2.2 Flash Photolysis 169
4.2.2.1 Spectra *169*
4.2.2.2 Lifetimes *177*
4.2.2.3 Concentration effects *179*
4.2.2.4 Transient Decay Curve Fitting *183*
4.2.2.5 Temperature Effects *183*
4.2.2.6 Quantum Yields of Transient Formation *189*
4.2.3 Low Temperature Photo-conversion 190
4.2.3.1 Low Temperature Photochemistry *190*
4.2.3.2 Low Temperature Infra-red Spectroscopy *196*
4.2.4 Time Resolved Resonance Raman Spectroscopy 206

4.3 Summary **210**

4.4 References **211**

Chapter 5 - The Photochemistry of Dibenzoylmethanes in Sunscreen Formulations 215

5.1 Introduction **216**

5.1.1 Sunscreen Formulations' 216
5.5.1.1 Types of sunscreen formulations *217*
5.5.1.2 Formulating Emulsions *218*
5.5.1.3 Emulsion Ingredients *218*
5.1.2 Usage Conditions 220
5.1.3 Measuring UV Protection Factors 221
5.1.3.1 Measuring UVB Sun Protection Factors *221*
5.1.3.2 Measuring UVA protection *222*
5.1.3.3 In-vivo Testing Methods for UVA protection *222*
5.1.3.4 In-vitro UVA Testing Methods *223*
5.1.3.5 The Star Rating System for UVA protection *224*
5.1.4 Photochemistry of Sunscreens in Formulations 225
5.1.5.1 Photochemistry of Dibenzoylmethanes in Sunscreen Formulations *225*

5.2 Results and Discussion **226**

5.2.1 Photochemistry of Dibenzoylmethanes in Micellar Systems 226

5.2.2 Photochemistry of Dibenzoylmethane in Emulsion Systems 229

5.2.2.1 The Emulsion System *229*

5.2.2.2 Absorption Spectra of DBM in the Emulsion System *229*

5.2.2.3 Diffuse Reflectance Flash Photolysis of DBM in the Emulsion System *231*

5.2.2.4 Photodegradation of DBM in the Emulsion System *233*

5.2.2.5 Summary *233*

5.2.3 The effect of Amides 233

5.2.4 Photochemistry of Dibenzoylmethanes in Oil-based Systems 235

5.2.5 Photochemistry of Dibenzoylmethane as a Solid 237

5.2.6 Photochemistry of Dibenzoylmethane Adsorbed on Cellulose 240

5.3 Summary **244**

5.4 References **244**

Chapter 6 - Singlet Oxygen Production **246**

6.1 Introduction **247**

6.1.1 Electronic states of molecular Oxygen 247

6.1.2 Singlet oxygen generation by photosensitisation 249

6.1.3 Quantum Yields of Singlet Oxygen Production 250

6.1.4 Photophysical Properties of singlet oxygen 251

6.1.4.1 Non-Radiative Lifetime *251*

6.1.4.2 Kinetics of Formation and Decay *253*

6.1.4.3 Luminescence *255*

6.1.4.4 Singlet Oxygen Quenching *255*

6.1.5 Chemical Properties and Biological effects of singlet oxygen 256

6.1.6 Singlet Oxygen Generation by Sunscreens 257

6.1.7 Singlet Oxygen Generation by Dibenzoylmethane Sunscreens 258

6.2 Results and Discussion **259**

6.2.1 Quantum Yields of Singlet Oxygen Generation 259

6.2.2 Variable Oxygen Concentration 262

6.2.3 Quenching of Singlet Oxygen 265

6.2.4 Sunscreen Formulations and Cellular Environments 266

6.3 Summary **267**

6.4 References **267**

Appendices **270**

1. Publications and Presentations **270**

2. Courses attended **270**

2.1 External Courses 270

2.2 Internal Courses 270

3. Seminars and Lectures attended **271**

Acknowledgements **274**

List of Figures

Chapter 1

Figure 1.1 A portion of the electromagnetic spectrum 23
Figure 1.2 Schematic structure of the skin, indicating penetration of varying UV wavelengths 24
Figure 1.3 Schematic structure of the epidermis of skin 25
Figure 1.4 Structures of common UVB sunscreens 30
Figure 1.5 Structure of 2-hydroxybenzophenone 30
Figure 1.6 UVA sunscreens based on dibenzoylmethanes 31
Figure 1.7 Possible isomers of 1,3-dicarbonyl compounds 32
Figure 1.8 Possible conformations of the diketone form of 1,3-dicarbonyl compounds 33
Figure 1.9 A non-chelated 1,3-dicarbonyl enol 34
Figure 1.10 Structure of crystalline dibenzoylmethane showing chelate ring bond lengths and phenyl ring twist angles 35
Figure 1.11 Two possible chelated enol forms of Parsol 1789 37
Figure 1.12 Structure of C-methyl dibenzoylmethane 37
Figure 1.13 Structures of O-methyl dibenzoylmethane 38
Figure 1.14 Structure of the Z isomer of O-methyl DBM 38

Chapter 2

Figure 2.1 Schematic diagram of the DN1 704 variable temperature liquid nitrogen cryostat 44
Figure 2.2 Optical layout of the LS 50 luminescence spectrometer 45
Figure 2.3 Events occurring during excitation in the phosphorescence mode 47
Figure 2.4 Schematic diagram of the low temperature liquid nitrogen cryostat 49
Figure 2.5 Transmittance spectrum of filter A 50
Figure 2.6 Transmittance spectrum of filter B 50
Figure 2.7 Transmittance spectrum of filter C 51
Figure 2.8 Transmittance spectrum of filter D 51
Figure 2.9 Transmittance spectrum of filter E 51
Figure 2.10 Transmittance spectrum of filter F 51

Figure 2.11 Transmittance spectrum of filter G....51
Figure 2.12 Apparatus for continuous irradiation using tungsen filament lamp....52
Figure 2.13 Apparatus for continuous irradiation using Xe lamp....53
Figure 2.14 Apparatus for nanosecond laser flash photolysis with excitation at 340 nm....55
Figure 2.15 Apparatus for nanosecond laser flash photolysis with excitation at 355 nm....56
Figure 2.16 Transient signals recorded in flash photolysis....57
Figure 2.17 Transient decay....58
Figure 2.18 Difference spectrum at time = t....58
Figure 2.19 Photo-conversions of Aberchrome 540....61
Figure 2.20 Absorption spectra of the two forms of Aberchrome 540....61
Figure 2.21 Possible interactions of infra-red radiation with vibrational energy levels of a molecule....64
Figure 2.22 Apparatus for time-resolved resonance Raman spectroscopy....66
Figure 2.23 Specular reflection....69
Figure 2.24 Diffuse reflection....69
Figure 2.25 Schematic representation of a sample of absorbing and light scattering particles....70
Figure 2.26 Schematic representation of the dependence of the scattering coefficient, S, on the wavelength for various particle sizes....73
Figure 2.27 Conversion of a conventional transmission spectrometer for measuring diffuse reflectance spectra....74
Figure 2.28 Diffuse reflectance spectroscopy using the LS50B luminescence spectrometer....75
Figure 2.29 Set-up for diffuse reflectance flash photolysis (1)....77
Figure 2.30 Set-up for diffuse reflectance flash photolysis (2)....77
Figure 2.31 Set-up for diffuse reflectance flash photolysis (3)....78
Figure 2.32 Apparatus used in this work for diffuse reflectance flash photolysis....79
Figure 2.33 Schematic diagram of the experimental set up for measuring singlet oxygen photosensitisation quantum yields....80

Chapter 3

Figure 3.1 Modified Jablonski diagram summarising the photophysics of organic molecules....92
Figure 3.2 Molecular orbitals of formaldehdye....94
Figure 3.3 Excited electronic states of formaldehyde....95
Figure 3.4 Nature of excited electronic states of formaldehyde....95
Figure 3.5 Molecular orbital diagram of an enone, showing $\pi^* \leftarrow n$ and $\pi^* \leftarrow \pi$ transitions....96
Figure 3.6 Structure of xanthone....97
Figure 3.7 Absorption spectra of benzophenone in ethanol and cyclohexane....98
Figure 3.8 Possible isomers of 1,3-dicarbonyl compounds....100
Figure 3.9 Structures of dibenzoylmethane....102
Figure 3.10 Absorption spectrum of dibenzoylmethane in cyclohexane....102
Figure 3.11 Absorption spectrum of dibenzoylmethane in EPA at room temperature and 77 K....103
Figure 3.12 Trans non-chelated benzoyltrifluoroacetone....105

Figure 3.13 O-methyl substituted DBM 105
Figure 3.14 C-methyl substituted DBM 106
Figure 3.15 Enolate of DBM 106
Figure 3.16 Absorption spectra of dibenzoylmethane in various solvents. 107
Figure 3.17 Suggested complex between acetylacetone and benzene 109
Figure 3.18 Absorption spectra of Parsol 1789 in various solvents at room temperature. 111
Figure 3.19 Absorption spectra of dtDBM and Parsol DAM in cyclohexane at room temperature 112
Figure 3.20 Absorption spectra of E and Z isomers of O-methyl dibenzoylmethane in cyclohexane at room temperature 113
Figure 3.21 Absorption spectra of O-methyl Parsol 1789 in cyclohexane and methanol at room temperature 114
Figure 3.22 Possible isomers of O-methyl Parsol 1789 115
Figure 3.23 Absorption spectra of C-methyl dibenzoylmethane in methanol and cyclohexane 116
Figure 3.24 Absorption spectra of C-methyl Parsol 1789 in methanol and cyclohexane. 117
Figure 3.25 Absorption spectrum of acetophenone in cyclohexane at room temperature 118
Figure 3.26 Structures of 4-tertiary-butyl acetophenone, 4-methoxy acetophenone and C-methyl Parsol 1789 118
Figure 3.27 Changes in absorption spectrum of C-methyl DBM in alkaline and acidic solutions of 9:1 ethanol : water, at room temperature 119
Figure 3.28 Changes occurring in C-methyl DBM on addition of alkali and subsequent neutralisation . 120
Figure 3.29 Changes in the absorption spectrum of DBM in alkaline solution with time 121
Figure 3.30 Absorbance spectrum of DBM in EPA at various temperatures 122
Figure 3.31 Absorbance spectrum of DBM in EPA at 77 K and 298 K 122
Figure 3.32 Absorption spectra of E and Z isomers of O-methyl dibenzoylmethane in EPA at room temperature and 77 K 124
Figure 3.33 Absorption spectra of C-methyl DBM in EPA at room temperature and 77 K 125
Figure 3.34 Fluorescence excitation and emission spectra of DBM in EPA at 77 K 125
Figure 3.35 Fluorescence spectrum of DBM in EPA at 77 K 127
Figure 3.36 Phosphorescence spectrum of DBM in EPA at 77 K 128
Figure 3.37 Phosphorescence spectrum of C-methyl DBM in EPA at 77 K 129
Figure 3.38 Phosphorescence spectrum of DBM in EPA at 77 K 129
Figure 3.39 Chelated enol phosphorescence spectrum of Parsol 1789 in EPA at 77 K 130
Figure 3.40 Diketone phosphorescence spectrum of Parsol 1789 in EPA at 77 K 131

Chapter 4

Figure 4.1 α -cleavage of carbonyl compounds 137
Figure 4.2 Hydrogen abstraction reaction of carbonyl compounds 138
Figure 4.3 Cycloaddition to olefins reaction of carbonyl compounds 139
Figure 4.4 1,3-acyl shift reaction of β,γ unsaturated ketones 140

Figure 4.5 Photochemical reactions of the diketone isomer of 1,3-dicarbonyl compounds 142
Figure 4.6 Photoenolisation of a 1,3 diketone 143
Figure 4.7 Photodegredation of dibenzoylmethanes in solution 144
Figure 4.8 Photoketonisation of dibenzoylmethane in acetonitrile 145
Figure 4.9 Photoketonisation of DBM 146
Figure 4.10 Formation of short-lived species of DBM in cyclohexane 147
Figure 4.11 Proposed photochemical pathway occuring on irradiation of DBM 149
Figure 4.12 Formation of complexes between solvent or additives (A) and the non-chelated intermediate (N) 150
Figure 4.13 Interaction of amines in the conversion from non-chelated enol, *ROH*, to chelated enol ROH 150
Figure 4.14 Re-formation of the intra-molecular hydrogen-bond assisted by an alchohol 151
Figure 4.15 Formation of a complex between DBM and methanol 151
Figure 4.16 Formation of stabilised non-chelated enol in β-keto-esters 152
Figure 4.17 Formation of a complex between excited enol molecules, E* and acetonitrile, A 152
Figure 4.18 Suggested processes occurring on irradiation of DBM 153
Figure 4.19 Structure of the enol form of dimedone 155
Figure 4.20 Formation of possible non-chelated enol rotamers on irradiation of DBM 156
Figure 4.21 Structure of a cyclic β-keto ester 157
Figure 4.22 Stabilisation of the trans non-chelated enol by phenyl group 157
Figure 4.23 Trans-cis isomerisation of enones 158
Figure 4.24 Photoconversion of diaroylacetic acids 159
Figure 4.25 Rotation about the C-C single bond in diaroylacetic acids 159
Figure 4.26 Structure of methylketene dimer 160
Figure 4.27 Photochemical formation of the enolate of DBM 160
Figure 4.28 Structure of E and Z isomers of O-methyl DBM 162
Figure 4.29 Photochemical, radical Z→E isomerisation of O-methyl DBM 162
Figure 4.30 Thermal isomerisation of O-methyl DBM, via protonation 163
Figure 4.31 Photochemical reactions not seen to occur in O-methyl DBM: Rotation about the carbon-carbon or carbon-oxygen single bonds 163
Figure 4.32 Changes in the absorption spectrum of DBM in acetonitrile with irradiation 165
Figure 4.33 Spectra of C-methyl DBM and the diketone form of DBM in acetonitrile 166
Figure 4.34 Recovery of absorbance at 342 nm with time for DBM in acetonitrile following irradiation 166
Figure 4.35 Loss of the enol form of DBM in acetonitrile with time during irradiation at 342 nm 167
Figure 4.36 Formation of the ring closed form of Aberchrome 540 in toluene with time during irradiation at 342 nm 168
Figure 4.37 Typical transient decay curve for DBM in cyclohexane; pumping at 340 nm, probing at 280 nm 170

Figure 4.38 Typical ground state recovery curve for DBM in cyclohexane; pumping and probing at 340 nm 170
Figure 4.39 Difference spectrum after various time intervals for DBM in cyclohexane, pumping at 355 nm 171
Figure 4.40 Approximate transient absorption spectrum for DBM in cyclohexane, pumping at 355 nm. 171
Figure 4.41 Approximate transient absorption spectrum for DBM in ethanol, pumping at 355 nm 173
Figure 4.42 Difference spectrum after various time intervals for Parsol 1789 in cyclohexane, pumping at 340 nm 174
Figure 4.43 Approximate transient absorption spectrum for Parsol 1789 in cyclohexane, pumping at 340 nm 174
Figure 4.44 Difference spectrum after various time intervals for DBM in DMF, pumping at 355 nm 175
Figure 4.45 Transient decayy in DMF, probing at 300 nm 176
Figure 4.46 Transient decay in DMF, probing at 320 nm 176
Figure 4.47 Transient decay in DMF, probing at 345 nm 176
Figure 4.48 Transient decay in DMF, probing at 390 nm 177
Figure 4.49 Graph of concentration vs. First order rate constant for the transient produced from DBM in cyclohexane, pumping at 340 nm 180
Figure 4.50 Graphs of concentration vs. first order rate constant for the transient produced from Parsol 1789 in cyclohexane, pumping at 340 nm 180
Figure 4.51 Two possible routes of recovery of the non-chelated enol transient, N, to the chelated enol, C 181
Figure 4.52 Variation of first order rate constant with laser power for the transients produced from DBM Parsol 1789 in cyclohexane, pumping at 340 nm 182
Figure 4.53 Typical transient decay curves for DBM in 2:1 isopentane:methylcyclohexane 184
Figure 4.54 Variation of the first order rate constant with temperature for the decay of the short-lived photo transient of DBM in 2:1 isopentane : methylcyclohexane 185
Figure 4.55 Variation in initial transient height with temperature for the decay of the short-lived photo transient of DBM in 2:1 isopentane : methylcyclohexane 187
Figure 4.56 Change in absorbance vs. laser power for Parsol 1789 (probing at 358 nm) and Aberchrome 540 (probing at 494 nm), for irradiation at 340 nm 189
Figure 4.57 Changes in DBM absorption spectrum in 2:1 isopentane : methylcyclohexane with irradiation at 340 nm 191
Figure 4.58 Changes in DBM absorption spectrum in EPA at 77 K with irradiation at varying wavelengths 193
Figure 4.59 Absorption spectra of the Z-isomer of O-methyl DBM in EPA at 77 K, and that of the E-isomer formed by iradiation of the Z-isomer 194
Figure 4.60 Possible rotations of DBM following irradiation 194
Figure 4.61 In plane vibrations of the chelate ring of DBM for the C_s and C_{2v} symmetry groups 197
Figure 4.62 Infra-red spectrum of DBM in CCl_4 at 77 K, with solvent spectrum subtracted 198

Figure 4.63 Infra-red spectrum of DBM in CH_2Cl_2 at 77 K, with solvent spectrum subtracted 199
Figure 4.64 Infra-red spectrum of O-methyl DBM in CCl_4 at 77 K, with solvent spectrum subtracted... 200
Figure 4.65 Infra-red spectrum of C-methyl DBM in CCl_4 at 77 K, with solvent spectrum subtracted... 200
Figure 4.66 Infra-red spectrum of the photoproduct on irradiation of DBM in CCl_4 at 77 K, with solvent and DBM spectra subtracted 201
Figure 4.67 Non-chelated enol isomers of malonaldehyde formed on irradiation of the chelated enol form 203
Figure 4.68 Infra-red spectrum of the E and Z-isomers of O-Me DBM in CH_2Cl_2 at 77 K, with solvent spectrum subtracted 204
Figure 4.69 Infra-red spectra of irradiated DBM in CCl_4 at 77 K, with solvent spectra subtracted 205
Figure 4.70 Resonance Raman spectrum of DBM in 1,1,2 trichlorotrifluoroethane; probing at 355 nm . 206
Figure 4.71 Resonance Raman spectrum of O-methyl DBM in 1,1,2 trichlorotrifluoroethane; probing at 295 nm 207
Figure 4.72 Resonance Raman spectrum of C-methyl DBM in 1,1,2 trichlorotrifluoroethane; probing at 295 nm 207
Figure 4.74 Time resolved resonance Raman spectrum of DBM in 1,1,2 trichlorotrifluoroethane; pumping at 355 nm, probing at 295 nm after 1 μs delay. 207
Figure 4.74 Resonance Raman spectrum of 1,1,2 trichlorotrifluoroethane 208

Chapter 5

Figure 5.1 Transient absorption spectrum for DBM in 1% Triton-X-100 reduced in water, pumping at 355 nm 228
Figure 5.2 Absorbance spectrum of 1% DBM in model emulsion system 230
Figure 5.3 Diffuse reflectance absorption spectrum of 0.005% DBM in the model formulation 231
Figure 5.4 Typical transient decay curve for 0.005% DBM in model formulation; pumping at 355 nm, probing at 340 nm 232
Figure 5.5 Diffuse reflectance flash photolysis difference spectrum after various time intervals for 0.005% DBM in the model formulation, pumping at 355 nm 232
Figure 5.6 General structure of amides covered by patent 234
Figure 5.7 Variation of first order rate constant of transient decay for DBM with % N,N-diethyltoluamide in cyclohexane 235
Figure 5.8 Changes in the absorbance spectra of a thin layer of DBM in mineral oil on a quartz plate, with UV irradiation, and on being left to recover for several days in the dark 236
Figure 5.9 Changes in the IR spectrum of a thin layer of DBM in mineral oil between KBr plates with irradiation 237
Figure 5.10 Changes in the absorption spectrum of a thin solid layer of DBM on quartz plate with irradiation and on being left to recover for several days in the dark 238
Figure 5.11 Changes to the IR spectrum of a thin solid layer of DBM with irradiation 239
Figure 5.12 Comparison of IR spectra of DBM, irradiated DBM,O-methyl DBM and C-methyl DBMs 240

Figure 5.13 Structure of cellulose....241
Figure 5.14 Diffuse reflectance absorption spectrum of 0.5 mg/g DBM adsorbed on cellulose....241
Figure 5.15 Difference spectrum after various time intervals for 0.6 mg/g DBM adsorbed on cellulose, pumping at 355 nm....242
Figure 5.16 Transient absorption spectrum for 0.6 mg/g DBM adsorbed on cellulose, pumping at 355 nm....242
Figure 5.17 Typical transient decay curve for 0.6 mg/g DBM adsorbed on cellulose; pumping at 355 nm, probing at 340 nm....243

Chapter 6

Figure 6.1 Schematic molecular orbital diagram for molecular oxygen....247
Figure 6.2 Some electronic excited states of molecular oxygen....248
Figure 6.3 Electronic transitions of molecular oxygen....248
Figure 6.4 Electron transfer between a sensitiser, Sens, and molecular oxygen....250
Figure 6.5 Electronic transitions from the singlet state to different vibrational energy levels of the triplet ground state of oxygen....252
Figure 6.6 Schematic diagram showing the decay kinetics of singlet oxygen, split into the contributions due to formation and decay....254
Figure 6.7 Singlet oxygen decay for photosensitisation by DBM in benzene, as studied by observing 1269 nm luminescence....259
Figure 6.8 Singlet oxygen luminescence signal intensity vs. laser power for photosensitised generation by DBM in benzene....260
Figure 6.9 Singlet oxygen decay traces for varying oxygen concentrations, for photosensitised generation of $^1O_2$ by C_{60}....263
Figure 6.10 Singlet oxygen decay traces for varying oxygen concentrations, for photosensitised generation of $^1O_2$ by DBM....264
Figure 6.11 Variation of (1/initial signal height) vs. (1/oxygen concentration) for the photosensitised generation of singlet oxygen by DBM in benzene....265
Figure 6.12 Concentration of Parsol 1789 vs. observed rate constant for singlet oxygen decay for quenching of singlet oxygen by Parsol 1789 in benzene....266

List of Tables

Chapter 1

Table 1.1 Reported keto : enol ratios for DBM in various solvents 35

Chapter 2

Table 2.1 Description of Optical Filters used in this Work 50
Table 2.2 Standard quantum yields of singlet oxygen generation by photosensitisation 82
Table 2.3 Composition of the FDA standard sunscreen 85
Table 2.4 Purpose of ingredients in the standard sunscreen 85
Table 2.5 Composition of the model sunscreen 86

Chapter 3

Table 3.1 Absorption maxima and extinction coefficients for dibenzoylmethane in various solvents at room temperature. 108
Table 3.2 Absorption maxima and extinction coefficients for Parsol 1789 in various solvents at room temperature. 110
Table 3.3 Absorption maxima for Parsol DAM in various solvents at room temperature. 111
Table 3.4 Absorption maxima for dtDBM in various solvents at room temperature. 111
Table 3.5 Absorption maxima and extinction coefficients for O-methyl dibenzoylmethane in various solvents at room temperature. 113
Table 3.6 Absorption maxima and extinction coefficients for O-methyl Parsol 1789 in various solvents at room temperature. 114
Table 3.7 Absorption maxima and extinction coefficients for C-methyl dibenzoylmethane in various solvents at room temperature. 116
Table 3.8 Absorption maxima and extinction coefficients for C-methyl Parsol 1789 in various solvents at room temperature. 117
Table 3.9 Absorbance data for DBMs and Parsols at 77 K in EPA 123
Table 3.10 Absorption maxima for O-methyl and C-methyl dibenzoylmethane in EPA at 77 K. 124
Table 3.11 Fluorescence data for DBM at 77 K, for excitation at 360 nm and emission at 403 nm 126
Table 3.12 Fluorescence data for Parsols in EPA at 77 K. 126

Table 3.13 Phosphorescence data for dibenzoylmethanes at 77 K 131

Chapter 4

Table 4.1 Reported first-order rate constants for the recovery of the short-lived species of DBM and Parsol 1789 148
Table 4.2 Photoketonization quantum yields for DBM in acetonitrile 168
Table 4.3 Photoketonisation quantum yields for Parsol 1789 in acetonitrile 168
Table 4.4 Transient lifetimes for DBM in various solvents 179
Table 4.5 Variation of the first order rate constant with temperature for the decay of the short-lived photo transient of DBM in 2:1 isopentane : methylcyclohexane 185
Table 4.6 Quantum yields of transient formation for DBM in cyclohexane 190
Table 4.7 Quantum yields of transient formation for Parsol 1789 in cyclohexane 190
Table 4.8 Vibrational band frequencies of DBM 196
Table 4.9 Approximate selected infra-red absorption peak positions for E and Z isomers of O-methyl DBM in CCl_4 and CH_2Cl_2 at 77 K 203
Table 4.10 Approximate selected infra-red absorption peak positions for irradiation of DBM in CCl_4 at 77 K 205
Table 4.11 Position of peaks in resonance Raman spectra for DBM and related compounds 209

Chapter 5

Table 5.1 Ingredients in typical sunscreen emulsions 219
Table 5.2 Absorption maxima for DBM and Parsol 1789 in various solvents at room temperature 227
Table 5.3 Transient lifetimes for DBM in various solvents 227
Table 5.4 Composition of the model sunscreen formulation 229
Table 5.5 Variation of first order rate constant with concentration for the decay of the non-chelated enol species of DBM when adsorbed on cellulose 243

Chapter 6 - Singlet Oxygen Production

Table 6.1 Vibrational stretching frequencies for various hydrogen and deuterium bonds 253
Table 6.2 Singlet oxygen quantum yields and lifetimes for photosensitisation in air saturated methanol solution 260
Table 6.3 Singlet oxygen quantum yields and lifetimes for photosensitisation in air saturated acetonitrile solution 261
Table 6.4 Singlet oxygen quantum yields and lifetimes for photosensitisation in air saturated benzene solution 261
Table 6.5 Singlet oxygen quenching rate constants for DBMs 266

Abbreviations

DBM	Dibenzoylmethane
DMF	N,N-Dimethylformamide
DNA	Deoxyribonucleic acid
dtDBM	4,4'-ditertiarybutyldibenzoylmethane
EC	European Community
EPA	Solvent mixture consisting of 5:5:2 diethyl ether : isopentane : ethanol
FDA	Food and Drug Administration
IR	Infra Red
MED	Minimum Erythemal Dose
NMR	Nuclear Magnetic Resonance
OCR	2-ethylhexyl p-methoy cinnamate
ODPABA	2-ethyl-hexyl p-(dimethylamino) benzate
OMC	2-ethylhexyl salicylate
PABA	p-aminobenzoic acid
Parsol 1789	4-methoxy, 4'-tertiarybutyldibenzoylmethane
Parsol DAM	4,4'-dimethoxy-dibenzoylmethane
PMT	Photomultiplier Tube
RNA	Ribonucleic acid
SPF	Sun Protection Factor
TR^3	Time Resolved Resonance Raman
UK	United Kingdom
US	United States (of America)
UV	Ultra Violet (200 nm < λ < 400 nm)
UVA	Ultra Violet - A (320 nm < λ < 400 nm)
UVB	Ultra Violet - B (290 nm < λ < 320 nm)
UVC	Ultra Violet - C (200 nm < λ < 290 nm)
YAG	Yttrium Aluminium Garnet

Declaration

The work described in this thesis was carried out at the Department of Chemistry, University of Durham, except where otherwise stated, between October 1994 and September 1997. This thesis is the sole work of the author, except where acknowledged by reference, or otherwise stated, and has not been submitted for any other degree.

Statement of Copyright

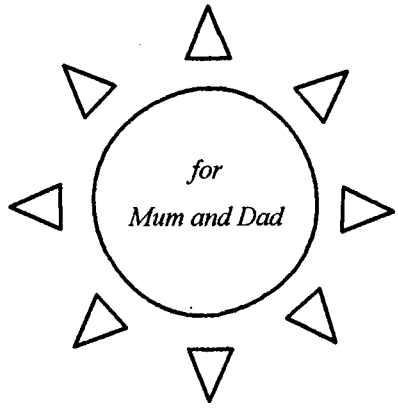
for
Mum and Dad

Chapter 1

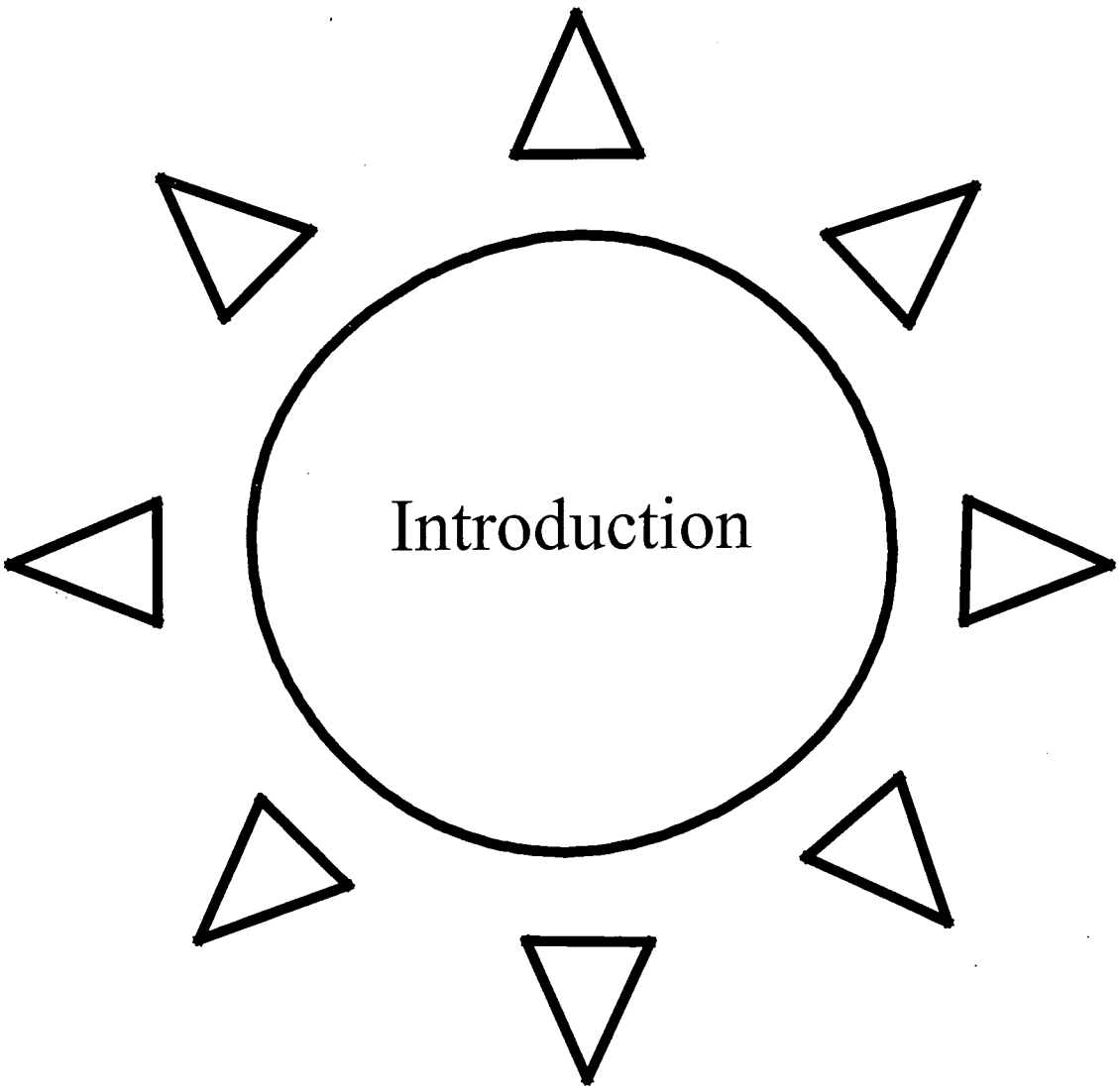

1.1 Ultra Violet Radiation and Skin

1.1.1 Ultra Violet Radiation[1,2]

Electromagnetic radiation is of fundamental importance to life, initiating and regulating a great variety of biological processes, from photosynthesis in plants to vision in animals. The electromagnetic spectrum is divided into different wavelength regions, as indicated in figure 1.1, with the UV region being defined as wavelengths between 200 nm and 400 nm. This can be further subdivided into three divisions, UVA radiation from 320 nm to 400 nm, UVB radiation from 290 nm to 320 nm, and UVC radiation from 200 nm to 290 nm.

A wide range of electromagnetic radiation from the sun reaches the earth's surface. This is mainly in the UV, visible and IR regions, as shown in figure 1.1, although there is also a contribution from longer wavelengths[3]. Atmospheric gases such as oxygen, ozone, carbon dioxide, and water absorb most of the incident radiation reaching the outer atmosphere. The ozone layer is responsible for absorbing most of the UV radiation, and effectively prevents UV radiation below 290 nm (UVC radiation) from reaching the surface.

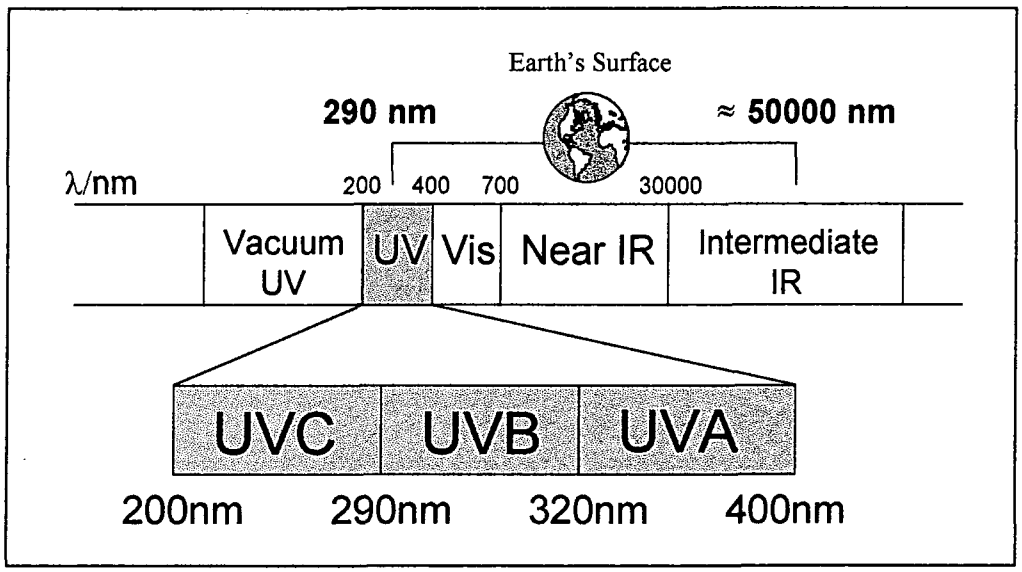

Figure 1.1 A portion of the electromagnetic spectrum
(Indicated boundaries not necessarily to scale)

The sun radiates a continuous spectrum at a constant rate, however there are a great many variables controlling the amount and spectral profile of radiation reaching a given point on the earth's surface. The proportion of solar radiation absorbed by the atmosphere varies with the depth of the atmospheric layer

through which it must pass. This depends on the time of day, with the maximum energy received at noon, and the minimum at midnight. The incident radiation also varies with the time of the year, depending on the earth's axis, with the maximum in the summer and the minimum in the winter. Clearly the position on the earth is also significant, with the maximum radiation falling on the equator, and the minimum at the poles. The scatter of radiation by air-borne particles, such as dust, gives rise to what is known as sky-light, and the amount of UV radiation at the surface due to this effect can exceed that received by direct sunlight. The reflection of radiation from surfaces, such as snow, sand, water and concrete, can also alter the amount of radiation observed at the surface. Consistently measuring the quantity of UV radiation falling at the earth's surface is difficult due to the many factors affecting the intensity of radiation. Reports of the profile and intensity of solar spectra are thus dependent on factors such as geography, weather, season and environment.

1.1.2 Penetration of UV radiation into Skin

The skin is a complex organ, the main function of which is to act as a protective barrier for the internal parts of an organism. The properties of skin, such as the thickness and frequency of hair follicles, vary with the position on the body[5]. The penetration into the skin of the radiation that reaches the earth's surface varies considerably with the wavelength, and also depends on the thickness of the skin involved[4]. The basic structure of the skin and UV penetration depths of a typical sample are shown in figures 1.2 and 1.3.

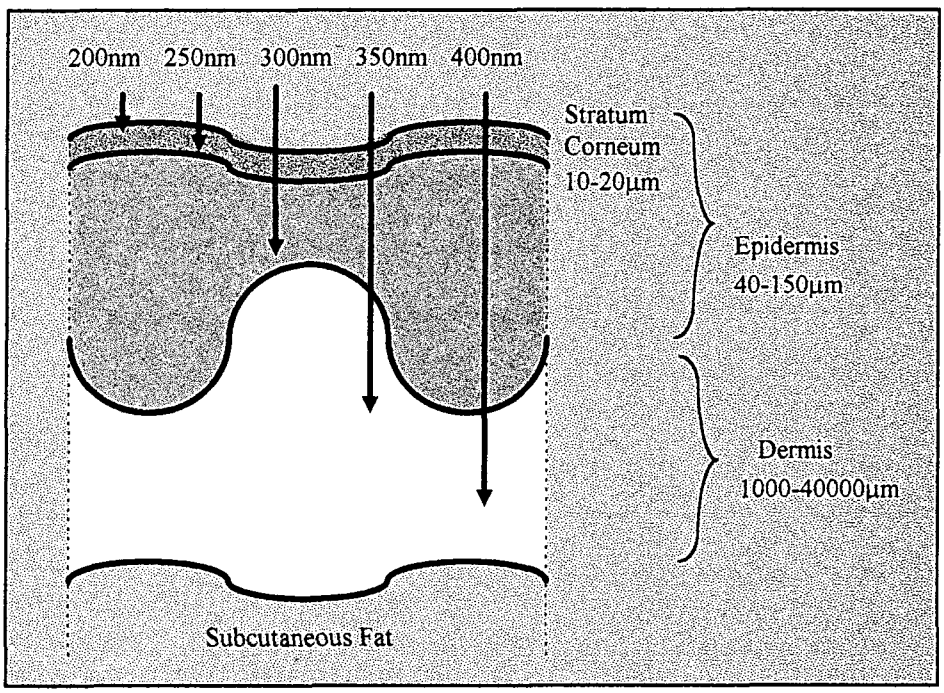

Figure 1.2 Schematic structure of the skin, indicating penetration of varying UV wavelengths[4]

(not to scale)

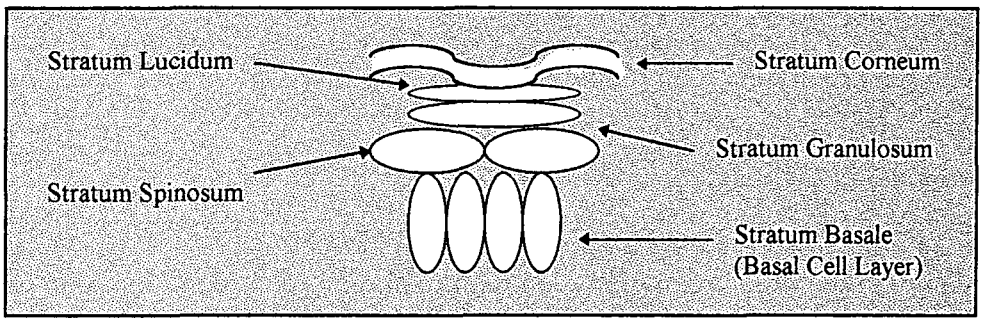

Figure 1.3 Schematic structure of the epidermis of skin[5]

(not to scale)

1.1.3 Biological effects of UV radiation[1,2,6,7]

1.1.3.1 Vitamin D Synthesis[1,2,6,7]

UV Radiation is important in maintaining health because it is directly involved in the synthesis of vitamin D in the skin. Vitamin D is important for healthy bones, and deficiency can lead to problems such as rickets. It is generated in the stratum granulosum layer of the epidermis, see figure 1.3, initiated by the absorption of UV light by the provitamin 7-dehydrocholesterol. Too much vitamin D is toxic, leading to problems such as kidney stones and renal failure. Over-generation of vitamin D is controlled by the natural UV attenuating mechanisms in the skin, pigmentation and keratinization.

1.1.3.2 Pigmentation[1,2,6,7]

The increase in the pigmentation of the skin, otherwise known as tanning, is the most common biological response to UV radiation. There are two distinct types of pigmentation, the immediate and delayed tanning responses. Immediate tanning is caused by photochemical oxidation of melanin granules already present in the epidermis. It reaches a maximum 1 hour after exposure, and fades after 2-3 hours.

Delayed tanning, or melanogenesis is caused by the formation of new melanin pigment in cells found in the basal cell layer of the epidermis, and migration of this pigment towards the skin surface. UV radiation initiates release of a co-ordinated cuprotein by oxidation of the co-ordinating sulphydryl groups. Formation of a dihydroxytyrosine enzyme then initiates melanin production. Delayed tanning begins up to 2 days after the UV exposure, reaching a maximum 2-3 weeks later, and completely fading up to 10-12 months later.

Melanin absorbs UV radiation, limiting the radiation reaching the epidermis and lower layers of the skin, and production of melanin is a natural response to exposure to UV radiation. It can also act as a free-radical scavenger, limiting the possible damage caused by UV, as will be discussed later. Historically, populations living in geographical locations that receive large quantities of UV radiation have deeply pigmented skin from birth, due to a naturally high level of melanin.

1.1.3.3 Keratinisation[1,2,6,7]

The stratum corneum reduces the amount of UV radiation reaching lower layers of the skin because of the highly scattering nature of the keratin in this layer. UV radiation induces the formation of new keratin in the basal cell layer of the epidermis, known as keratinisation. The proteins of keratin also absorb UV, acting as another filter to limit dosage to the skin. The yellow skin tone of mongoloid skin is caused by a high level of natural keratin.

1.1.3.4 Inflammatory Erythema[1,2,6,7]

The most obvious reaction to UV is the induction of inflammatory erythema, commonly known as sun-burn. Erythema is unpleasant and painful, and chronic exposure to UV can lead to swelling and blistering. The mechanism is not well understood, however it is believed to be initiated by absorption of UV radiation by nucleic acids in the basal layer of the epidermis. The primary photochemical reaction results in the formation of unstable radical species, which are then believed to generate stable products such as peroxides or quinone-imines which are known irritants. This also causes effects such as the dilation of small blood vessels, which creates the sensation of heat. Erythema develops 2-3 hours after exposure to UV with the maximum response occurring after 10-24 hours.

1.1.3.5 Carcinogenesis[1,2,6,7]

The processes of Vitamin D production, melanogenesis and erythema are well established and have been studied in depth. There are however, a wide range of more serious effects on the skin of UV exposure, many of which have only recently been identified.

The most serious effect of UV radiation is carcinogenesis, or skin cancer. Studies have shown that cumulative exposure of the skin to UV can result in the formation of benign, premalignant and malignant lesions on the skin. These include seborrheic and actinic keratoses, solar lentigos, keratocanthomas, basal cell and squamous cell carcinomas. Some of these are less serious than others, however some skin

cancers can be fatal. Readers are referred to references 4 and 6 for more detailed discussions of carcinogenesis.

UV radiation can cause covalent linking of adjacent pyrimidine bases on the same strand of DNA, resulting in the formation of pyrimidine dimers. This is believed to be one possible mechanism of cancer formation. UV is also known to inhibit DNA, RNA and protein synthesis, and can thus prevent repair of damaged DNA. UV is believed to have an imunosuppressive effect, and therefore can also encourage the growth of skin cancers once formed.

Skin cancers can develop tens of years after cumulative UV exposure, and studies are therefore difficult due to the time scales involved, and the inability to control or measure exposure. Skin cancer is, however, currently a cause for great concern.

1.1.3.6 Photoageing[1,2,6,7]

Another recent realisation is that UV can cause serious changes to the nature of the skin, resulting in what is referred to as premature skin ageing or photoageing. Photoageing is very different to the normal process of ageing, although the two are often confused. The skin of elderly people in areas that have not been exposed to the sun is often similar in appearance to young skin, indicating that photoageing is the significant factor causing changes to skin over time.

UV causes effects such as thickening of the epidermis, elastosis, caused by the increase of the number and entanglement of elastic fibres in the skin, reduction in the amount of collagen, and microcirculation damage. These effects can give the skin a yellowed, nodular, dry and leathery appearance, with increased wrinkling and sagging. Photoageing is a long-term effect caused by cumulative exposure to UV radiation, and as such is difficult to study. It can also be difficult to separate the normal ageing effects from those caused by the action of UV.

1.1.3.7 Action Spectra[6]

The action spectrum of a biological response describes the range of wavelengths that cause the response and their relative efficiency, and are normally only studied over the wavelength range found at the earth's surface. Action spectra for well-studied responses such as vitamin D synthesis, melanogenisis and erthemya have been widely studied, although reports do not always entirely agree. For responses such as carcinogenesis and photoageing, action spectra are much more difficult to determine, and agreement in the literature is less common.

7-dehydrocholesterol absorbs wavelengths below 320 nm, and thus vitamin D synthesis occurs on UV irradiation below this wavelength, i.e. with UVB irradiation. Tanning and erythema are most effectively induced by UVB radiation, and less effectively by UVA radiation. It is also believed that a tan resulting from UVA irradiation is a less effective filter to UVB radiation than a tan resulting from UVB radiation, due to a different tanning mechanism.

It is believed that the formation of skin cancers results from UVB irradiation, although UVA radiation has not been entirely ruled out as causing, or enhancing the effects. Photoageing is reported to be most effectively caused by UVB radiation, with UVA radiation being less effective. Studies of action spectra for these effects must usually be carried out on animal models because of the ethical and time restraints on using human models, and consequently these action spectra are much less well understood.

Until relatively recently, UVA radiation was not considered to have much effect on the skin due to its lower energy. It was recognised that it can cause pigmentation and erythema, however because it is approximately 1000 times less effective that UVB, its effects were considered negligible next to those of UVB. However, there can be as much as 100-500 times as much UVA radiation in sunlight as UVB radiation, and UVA penetrates deeper into the skin, as indicated in figure 1.2. It is reported that UVA may contribute up to 15% of the erythemal effective radiation at noon, and a greater proportion at other times. It is now recognised that UVA can result in more serious photoageing than UVB radiation, because of the deeper penetration, and it has not been ruled out as a cause of skin cancers. Thus whilst UVB radiation is accepted as the most dangerous UV range, UVA radiation is also considered to be a serious problem.

1.2 Sunscreens

1.2.1 Sun-Protection Products

The long-term harmful effects of UV radiation on the skin have only been realised relatively recently, however because exposure to UV radiation can cause the painful erythema response, there has long been a desire to limit the amount of personal UV radiation received. This has been achieved by the development of sunscreen products, designed to be topically applied to the skin to reduce the amount of UV radiation entering the skin. The first reported commercial availability of a sunscreen product is in the United States in 1928, however is only since the 1970s, with the ease of foreign travel, that commercial sun-protection products have become commonplace in the United Kingdom[4]. The importance of using sun-protection products to protect against skin cancer and photoageing, in addition to erythema, is now

well established, although in western society acquiring a tan is still generally considered to be cosmetically desirable.

Sunscreens were originally used exclusively to protect against sunburn, and because of this, the measurement of the effectiveness of sun-protection products is based on their ability to reduce erythema. The sun protection factor, SPF, label indicates how effective a product is, where the SPF is the ratio of the amount of UV radiation it takes to cause erythema on protected skin to unprotected skin.

Sun-protection products are formulations containing ingredients capable of filtering UV radiation. There are two types of sunscreen ingredients, physical and chemical sunscreens. Physical sunscreens, such as titanium dioxide are effective by reflecting and scattering UV radiation, whereas chemical sunscreens absorb the UV radiation.

1.2.2 Chemical Sunscreens

The majority of sunscreening ingredients are chemical sunscreens, because physical sunscreens can also reflect visible light, which is cosmetically unacceptable. An effective sunscreen chemical must have a strong, broad absorption spectrum in the UV region, and on absorption it must revert quickly to its original form, via safe, non-radiative pathways, without producing harmful intermediates. The compound itself must be non-toxic and non-phototoxic. It must be reasonably photostable over the expected exposure time, and any degradation products must be non-toxic. It should be soluble in an appropriate solvent, and compatible with other ingredients. For cosmetic reasons it should not absorb light in the visible region, and should be odourless.

A great variety of different chemicals have been and are used as sunscreens, and commercial products usually contain more that one absorbing compound. Sun-protection products originally only contained UVB sunscreening chemicals, because of the mistaken belief that the effects of UVA rays were negligible. Consequently there are many UVB sunscreen chemicals available, and relatively fewer UVA sunscreens. However as described above, UVA rays are no-longer considered to be safe. Use of UVB sunscreens has also allowed longer exposure times to the sun, and therefore increased doses of UVA radiation are received, making the inclusion of UVA sunscreens even more necessary. Compounds currently used as UVB sunscreens include methyl benzylidene camphor (3-(4-methylbenzylidene)-bornan-2-one) and octylmethoxycinnamate (2-ethylhexyl-*p*-methoxy cinnamate)[8], as shown in figure 1.4.

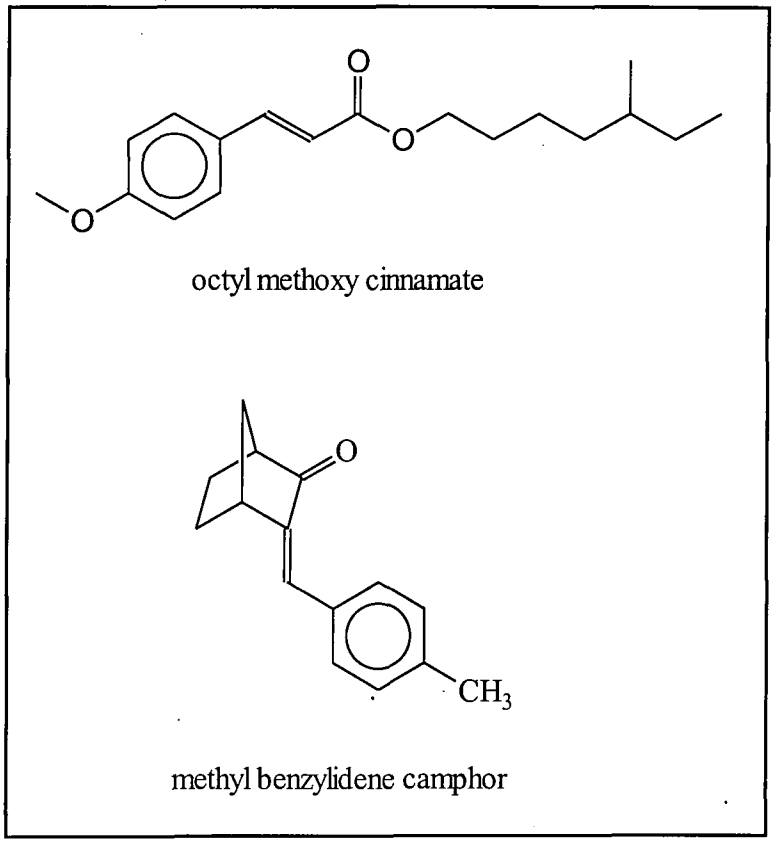

Figure 1.4 Structures of common UVB sunscreens

1.2.3 UVA Sunscreens

The first UVA sunscreens in common usage were based on 2-hydroxybenzophenone[4], figure 1.5, e.g. oxybenzone, 2-hydroxy, 4-methoxybenzophenone. However, these compounds frequently cause allergic reactions, and absorb mainly in the UVB region. Physical sunscreens can also be used to protect against UVA radiation, however, reflection of visible light can also occur, causing an undesirable opaque covering on the skin.

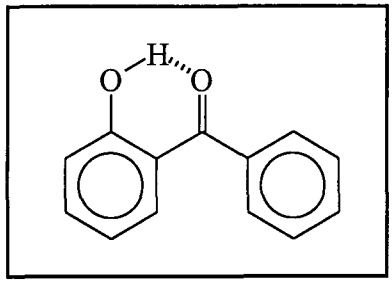

Figure 1.5 Structure of 2-hydroxybenzophenone

The most important family of UVA sunscreens is based on dibenzoylmethane, 1,3-diphenyl propan-1,3-dione, the structure of which is shown in figure 1.6. The sunscreens of this type currently in use are Parsol 1789, 4-methoxy 4'-tert-butyl dibenzoylmethane, Eusolex 8020, 4-tert-butyl dibenzoylmethane and Parsol DAM, 4,4'-dimethoxy dibenzoylmethane. Parsol 1789 is currently the most commonly used UVA sunscreen in Europe[8].

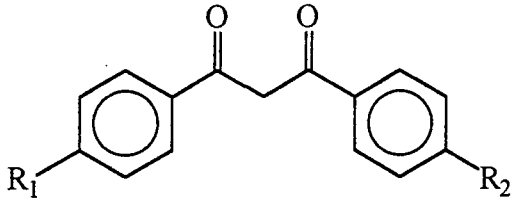

R_1	R_2	Sunscreen
H	H	Dibenzoylmethane
OMe	t-butyl	Parsol 1789
H	t-butyl	Eusolex 8020
OMe	OMe	Parsol DAM

Figure 1.6 UVA sunscreens based on dibenzoylmethanes

The exact photochemical mechanisms occurring on irradiation with UV are poorly understood for these and many other sunscreen chemicals. It is important to understand the photochemistry of such compounds, and particularly to know the nature of excited states and intermediate compounds formed on photolysis. For example, sunscreens are tested on their ability to reduce erythema, and any damage caused by intermediate photoproducts may not be observed. The development of improved sunscreens can also aided by knowledge of the mechanisms involved after the absorption of UV light.

1.3 Dibenzoylmethanes

In order to begin the study of the photochemistry of dibenzoylmethanes, it is first important to understand their structure and properties, as will be discussed in the following sections.

1.3.1 Keto-Enol Tautomerism of 1,3-Dicarbonyl Compounds

Most 1,3-dicarbonyl compounds can in theory exist as one or a mixture of various isomers. Possible isomers include a hydrogen-bonded enol, non-hydrogen bonded enols and diketones, as shown in figure 1.7. If there is no hydrogen present on the α-carbon, the compound cannot enolise and only the diketone can exist. The labelling of different isomers is not always consistent in the literature, and descriptions of various isomers in this work will relate to the structures shown in figure 1.7, where cis and trans refer to the arrangements of the double bonds in the enol structures, and E and Z refer to the arrangement of substituents about the carbon-carbon double bond of the enol.

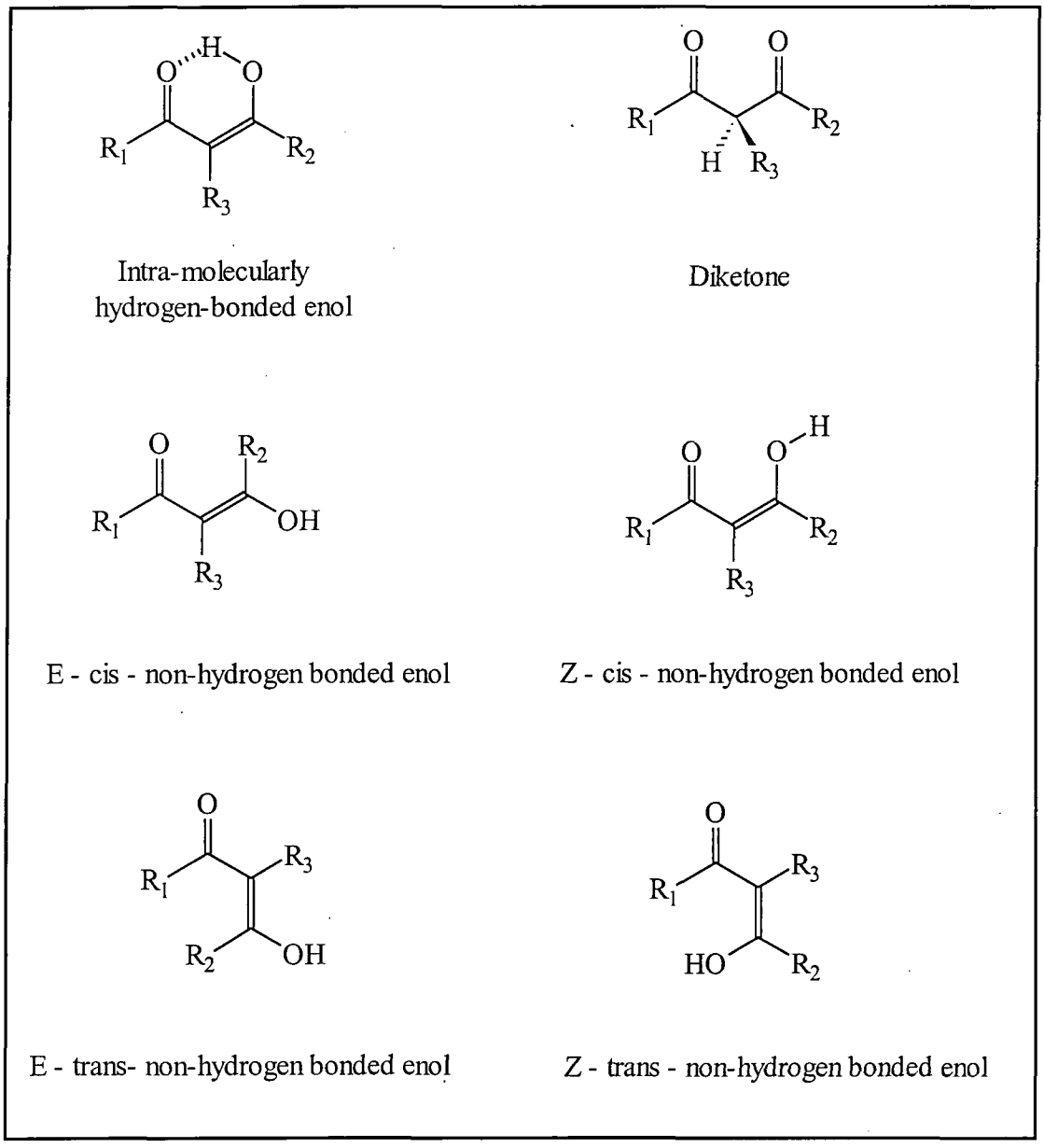

Figure 1.7 Possible isomers of 1,3-dicarbonyl compounds[9]

The diketone isomer can itself exist in different possible conformations as shown in figure 1.8. In the diketone isomer, it is electrostatically most favourable for the carbonyl groups to be arranged in an opposing manner[10], as in structure (b) in figure 1.8. This is because of the repulsive interaction of the oxygen atoms which carry a δ-negative charge. The presence of bulky substituents, e.g. phenyl groups, at R_1 and R_2 can make this arrangement less favourable due to steric hindrance, and conformation (a) in figure 1.8 is then preferred[11]. An intermediate conformation, as shown in (c) in figure 1.8 may also occur[9].

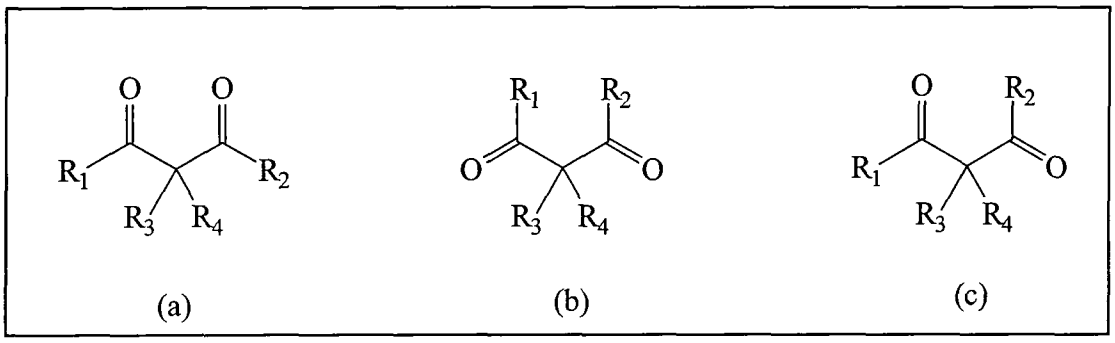

Figure 1.8 Possible conformations of the diketone form of 1,3-dicarbonyl compounds

The nature of the substituents R_1, R_2 and R_3 is the main factor in determining what mixture of the isomers described in figure 1.7 is present in enolisable 1,3 dicarbonyl compounds. The intra-molecular hydrogen bond gives stabilisation to the enol isomer, and consequently this is greatly favoured over the non-chelated forms. Bulky substituents at R_1, and R_2 also favour the chelated structure over the non-chelated structures for similar reasons described above for the diketone form. The non-chelated enols, if present at all, make up less than 3% of the mixture, and the Z-cis non hydrogen bonded enol is not usually considered to be a possible isomer[9,12]. Entropy effects may favour the trans enols at high temperatures[12], however non-chelated enols are generally only observed if the nature of the groups R_1, R_2 and R_3 are such that hydrogen-bonding is not possible, for example in cyclic structures, such as that shown in figure 1.9 [13]. In reference to 1,3-dicarbonyl compounds in this report, the term "enol" will be used to refer to the chelated enol form. The non-chelated form will be referred to specifically as "non-chelated" or "non-hydrogen bonded".

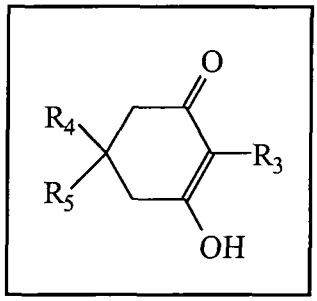

Figure 1.9 A non-chelated 1,3-dicarbonyl enol

Bulky groups at R_1 and R_2 tend to stabilise the enol isomer, as this structure causes the least steric hindrance[10]. Bulky substituents at R_3 also cause steric hindrance, especially if R_1 and R_2 are also bulky, however this favours the diketone structure, which does not need to be planar, and can rotate to relieve strain[10].

Electron-withdrawing substituents at R_3 stabilise the enol form, provided they are not too bulky, where steric effects described above would negate this effect and favour the diketone. Electron withdrawing substituents at R_1 and R_2 also stabilise the enol structure[10].

In solution, the solvent can also have an important effect on the keto-enol equilibrium for 1,3-dicarbonyl compounds. Polar solvents tend to stabilise the keto form more than the enol form[14]. This is because the keto form is more polar than the enol, where the electron density is partially delocalised around the chelate ring. This effect is exaggerated in solvents which can hydrogen bond to the oxygens or the acidic α-hydrogen of the diketone form, stabilising this isomer. Inter-molecular hydrogen-bonding to the enol form would involve breaking of the intra-molecular hydrogen bond, which is unfavourable. Thus as the polarity and hydrogen-bonding ability of solvents are increased, the percentage of diketone content of a solution of a 1,3-dicarbonyl compound increases[14,15,18]. These solvent effects are not great, but can be seen strikingly for aqueous solutions, where the proportions of diketone forms are often higher than would be expected from structural considerations[15].

1.3.2 Dibenzoylmethanes

1,3-Dicarbonyl compounds with at least one phenyl group at R_1 and R_2 (figure 1.7) exist primarily as the chelated enol in the solid and in solution[9]. This is due to the electron withdrawing ability and the bulky nature of the phenyl ring, as discussed above. The actual measured ratios of keto : enol for DBM in the literature vary from source to source, and reported ratios are shown in table 1.1.

Solvent	Percentage enol	Reference
Solid	100	16
Chloroform	100	10
	98	17
Hydrocarbon	98	17
Hexane, Cyclohexane	99	17
Acetonitrile	92	17
Methanol	89.7	10
Water	36.7	18

Table 1.1 Reported keto : enol ratios for DBM in various solvents

The keto : enol ratio is also reported to vary with temperature, such that increasing the temperature causes a slight shift in favour of the keto form in the solid state[19].

The crystal structure of dibenzoylmethane shows that the molecule is not symmetrical about the α-carbon, implying that the chelate ring is not an entirely delocalised system[16]. The structure is shown in figure 1.10.

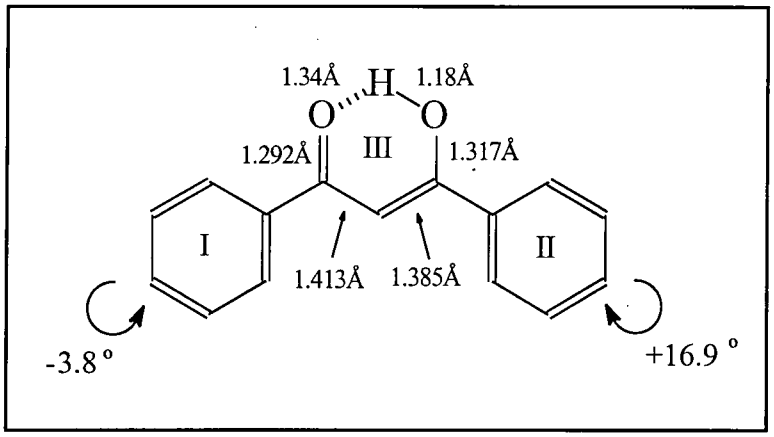

Figure 1.10 Structure of crystalline dibenzoylmethane showing chelate ring bond lengths and phenyl ring twist angles[18]

(I, II and III refer to discussion in the text)

The oxygen-hydrogen bond of the OH group is longer and the hydrogen-bond shorter than in inter-molecularly hydrogen-bonded systems. Similarly, the carbon-carbon double bond is longer, the carbon-

carbon single bond is shorter, the carbon-oxygen double bond is longer and the carbon-oxygen single bond is shorter than in non-chelated systems. This indicates that there is delocalisation in this group.

The chelate ring, III, is planar, although the whole molecule is not because the phenyl rings I and II are twisted out of the plane of the chelate ring. Phenyl ring I, associated with the ketone group, is -3.8° degrees relative to the chelate ring, and phenyl ring II, associated with the hydroxyl group, is +16.9°, in the other direction, relative to the chelate ring[18]. This lack of planarity reduces the extent of conjugation from the phenyl groups with the chelate ring[10].

There is disagreement in the literature as to whether the structure of dibenzoylmethanes in solution is similar to the solid form. Some reports suggest that the chelate ring is not symmetrical, as is the case in the solid[20], while others suggest that in solution the hydrogen is located equidistant between the two oxygen atoms[21].

1.3.3 Parsol 1789

It is difficult to predict whether Parsol 1789 is likely to have a larger or smaller enol content compared to dibenzoylmethane. It has been observed for benzoylacetones, that the substitution of a methyl or methoxy group in the para position of the phenyl ring makes no difference to the percentage of diketone[22], thus it is probable that the ratio of keto to enol for Parsol 1789 is similar to that of dibenzoylmethane due to the very similar structure, and UV spectra observations, as will be reported in chapter 3.

Because of the possible lack of symmetry of the chelate ring, the range of isomers possible for Parsol 1789 is further complicated. The two different phenyl rings mean that there are two different types of chelated enol, depending on which carbonyl group enolises, as shown in figure 1.11.

In solution, and in the pure state, the two tautomers of 1,3 dicarbonyl enols undergo dynamic interchange[23]. For structures with very different groups attached to the carbonyls, one tautomer is likely to be dominant. For example in benzoylacetones, enolisation mainly occurs at the phenyl carbonyl group[22], although it is reported that both forms can be observed by NMR spectroscopy[23]. For compounds like Parsol 1789, where both groups are very similar, it is difficult to predict which form should be preferred. It is likely a relatively balanced equilibrium of the two forms exists, if indeed the chelate ring is not symmetrical in solution.

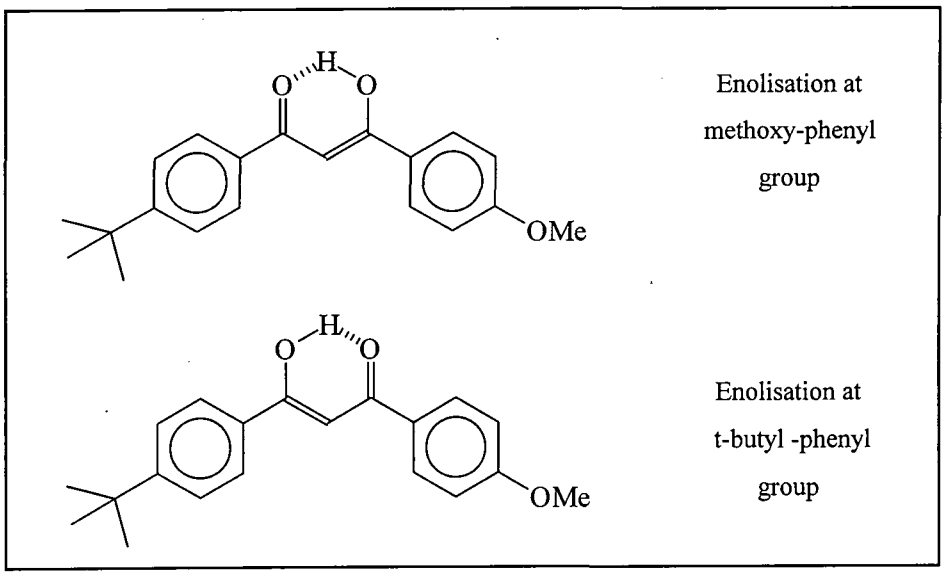

Figure 1.11 Two possible chelated enol forms of Parsol 1789

1.3.4 C-Methylated Dibenzoylmethanes

In C-methylated dibenzoylmethanes (R_3 = Me, figure 1.7) the diketone form is greatly stabilised. This is due to the steric hindrance caused by the methyl group, which can be more effectively relieved in the diketone structure. C-methyl dibenzoymethanes are thus observed to be present entirely as diketones[15], as shown in figure 1.12.

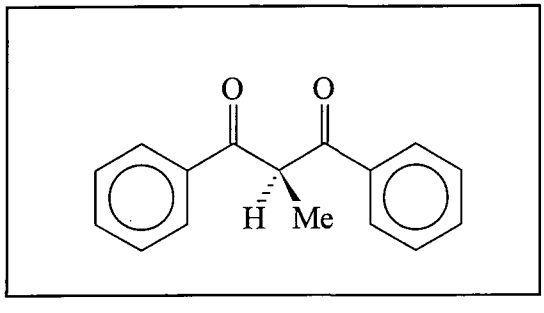

Figure 1.12 Structure of C-methyl dibenzoylmethane

1.3.5 O-Methylated Dibenzoylmethanes

The O-methyl ethers of dibenzoylmethanes, β-methoxy chalcones, have structures similar to a non-chelated enol tautomer of dibenzoylmethane. They exist as an equilibrium mixture of the Z and E isomers[24], as shown in figure 1.13. The E isomer is thermodynamically more stable, with the Z:E ratio in solution reported to be 1:7 [24].

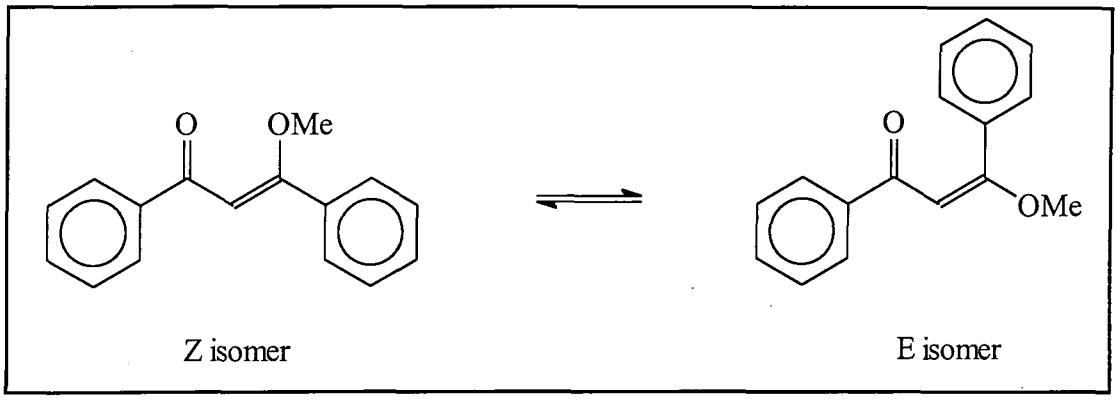

Figure 1.13 Structures of O-methyl dibenzoylmethane

Crystal structures of the two isomers indicate non-planarity. The Z-isomer has similar phenyl group twist angles as found for the chelated DBM enol (see figure 1.10), however the two C-O bonds are no longer in a planar ring, as shown in figure 1.14 [24].

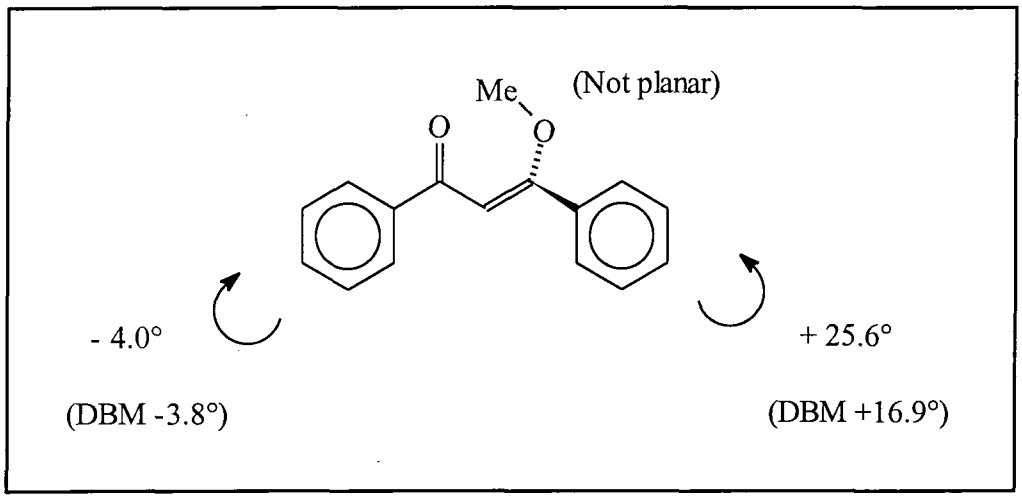

Figure 1.14 Structure of the Z isomer of O-methyl DBM

Synthetic laboratory preparation methods result in production of the Z-isomer, which slowly converts to the thermodynamically more stable E-isomer[24]. In dry non-polar solvents, or as the solid, practically no conversion is noted in the dark. The equilibrium is promoted by H^+, and equilibrium is reached in 2 hours on silica gel, and in 5 hours in methanol solution[24]. The equilibrium is also affected by UV light, as will be discussed in chapter 4.

It is likely that for more general O-methyl dibenzoylmethanes, the preference of Z and E conformations would be affected by similar reasons to those observed for diketones (figure 1.8). The important difference would be that the methyl group makes the Z isomer less stable than the corresponding diketone conformation.

1.4 Aims of this Work

The dibenzoylmethanes are an important family of UVA sunscreens, which are an important component of sun-protection products, providing protection from effects such as erythema and photoaging. However, the photochemistry of such compounds is poorly understood, and this work was undertaken to study the photochemistry of these aromatic 1,3-dicarbonyl compounds.

Chapter 2 contains the experimental details of all the experiments reported in this work, including details of compounds, solvents, equipment and techniques.

Chapter 3 discusses the photophysical properties of dibenzoylmethanes in solution, considering absorption, fluorescence and phosphorescence at room temperature and low temperature.

Chapter 4 contains a discussion of the photochemistry of dibenzoylmethanes in solution and includes a detailed discussion of the literature in this field. Techniques such as UV spectroscopy, flash photolysis and low temperature infra-red spectroscopy have been used to gain important information on the photochemical mechanisms occurring on absorption of UV light.

Chapter 5 describes the photophysics and photochemistry of dibenzoylmethanes in model sunscreen formulations and other environments relevant to usage of sunscreen materials. This work is important, because there is little or no information available in the literature of studies in environments than in solution.

Chapter 6 discusses the singlet oxygen generating properties of dibenzoylmethanes in solution, which also provides further information on photophysical properties.

It is hoped that through this work a greater understanding of the photochemical mechanisms by which aromatic 1,3-dicarbonyl compounds used as UVA sunscreens dissipate the absorbed UV energy can be achieved.

1.5 References

[1] Balsam M S, E Sagarin, "*Cosmetics - Science and Technology*", 2nd Edition, 1972

[2] 6th Congress of the European Society for Photobiology, 3-8th September 1995, Churchill College, University of Cambridge

[3] Revised Nuffield Advanced Science, "*Book of Data*", Longman, 1984, pg. 34

[4] Lowe N J, Shaath N A, "*Sunscreens - Development, Evaluation and Regulatory Aspects*", Marcel Dekker Inc., New York, 1990

[5] Robbins C R, "Skin" in "*Encyclopaedia of Human Biology*", Volume 7, Academic Press, 1991, pg. 41

[6] Fitzpatrick, Eisen, Wolff, Freedberg, Austen, "*Dermatology in General Medicine*", 3rd edition, volume 1, McGraw-Hill, New York, 1987

[7] Shea C R, Parrish J A, "Skin, Effects of Ultraviolet Radiation" in "*Encyclopaedia of Human Biology*", Volume 7, Academic Press, 1991, pg. 65

[8] Sainino E-L, "The ingredients, safety, efficacy and stablity of sunscreens", *National Consumer Administration Publications Series 16 / 1995*, National Consumer Administration, 1995, Helsinki

[9] Markov P, "Light-induced Tautomerism of β-Dicarbonyl Compounds", *Chem. Soc. Reviews*, **13** (1984), 69

[10] Burdett J L, Rogers M T, "Keto-Enol Tautomerism in β-Dicarbonyls Studied by Nuclear Magnetic Resonance Spectroscopy. I. Proton Chemical Shifts and Equilibrium Constants of Pure Compounds", *J. Am. Chem. Soc.*, **86** (1964), 2105

[11] Hammond G S, Borduin W G, Guter G A, "Chelates of β-Diketones. I. Enolization, Ionization and Spectra", *J. Am. Chem. Soc.*, **81** (1959), 4682

[12] Zabicky J, "*The Chemistry of the Carbonyl Group*", Volume 2, Interscience, London, 1970

[13] Grens E, Grinvalde A, Stradins J, "Intra- and intermolecular association and i.r. spectra of dicarbonyl compound enol forms", *Spectrochimica Acta*, **31A** (1975), 555

[14] Rogers M T, Burdett J L, "Keto-Enol tautomerism in β-Dicarbonyls Studied by Nuclear Magnetic Resonance Spectroscopy. II. Solvent effects on Proton Chemical Shifts and on Equilibrium Constants", *Can. J. Chem.*, **43** (1965), 1516

[15] Morton R A, Hassan A, Calloway T C, "Absorption Spectra in Relation to the Constitution of Keto-Enols", *J. Chem. Soc.*, (1934), 883

[16] Williams D E, "Crystal Structure of Dibenzoylmethane", *Acta. Cryst.*, **21** (1966), 340

[17] Moriyasu M, Kato A, Hashimoto Y, "Kinetic Studies of Fast Equilibrium by means of High-performance Liquid Chromatography. Part 11. Keto-Enol Tautomerism of some β-Dicarbonyl Compounds", *J. Chem. Soc. Perkin Trans. II*, (1986), 515

[18] Hay R W, Williams P P, "Proton magnetic resonance of Hydrogen-bonded Chelate Rings", *J. Chem. Soc.*, (1964), 2270

[19] Kuo J, "UV Spectroscopic and Nuclear Magnetic Resonance Studies of the Enol-Keto Tautomerism in β-Diketones", PhD Thesis, Louisiana State University, 1966

[20] Morita H, Nakanishi H, "Electronic Structures and Spectra of the Enol Form of Some β-Diketones", *Bull. Chem. Soc. Jpn.*, **54** (1981), 378

[21] Bratan S, Strohbusch F, "Über den Einfluβ von Substituenten auf die Wasserstoffbrückenbindung von Dibenzoylmethanen", *Chem. Ber.*, **105** (1972), 2284

[22] Lowe J U, Ferguson L N, "The Direction of Enolization of Benzoylacetones", *J. Org. Chem.*, **30** (1965), 3000

[23] Vila A J, Lagier C M, Olivieri A C, "C,O atomic motion associated with solid-state proton transfer in enolic 1,3-diketones", *J.Mol. Struct.*, **274** (1992), 215

[24] Kiuchi F, Chen X, Tsuda Y, "Z-E Isomerisation of β-Methoxychalcones: Preferred Existence of E-Isomers in Naturally Occurring β-Methoxychalcones", *Chem. Pharm. Bull.*, **38(7)** (1990), 1862

Chapter 2

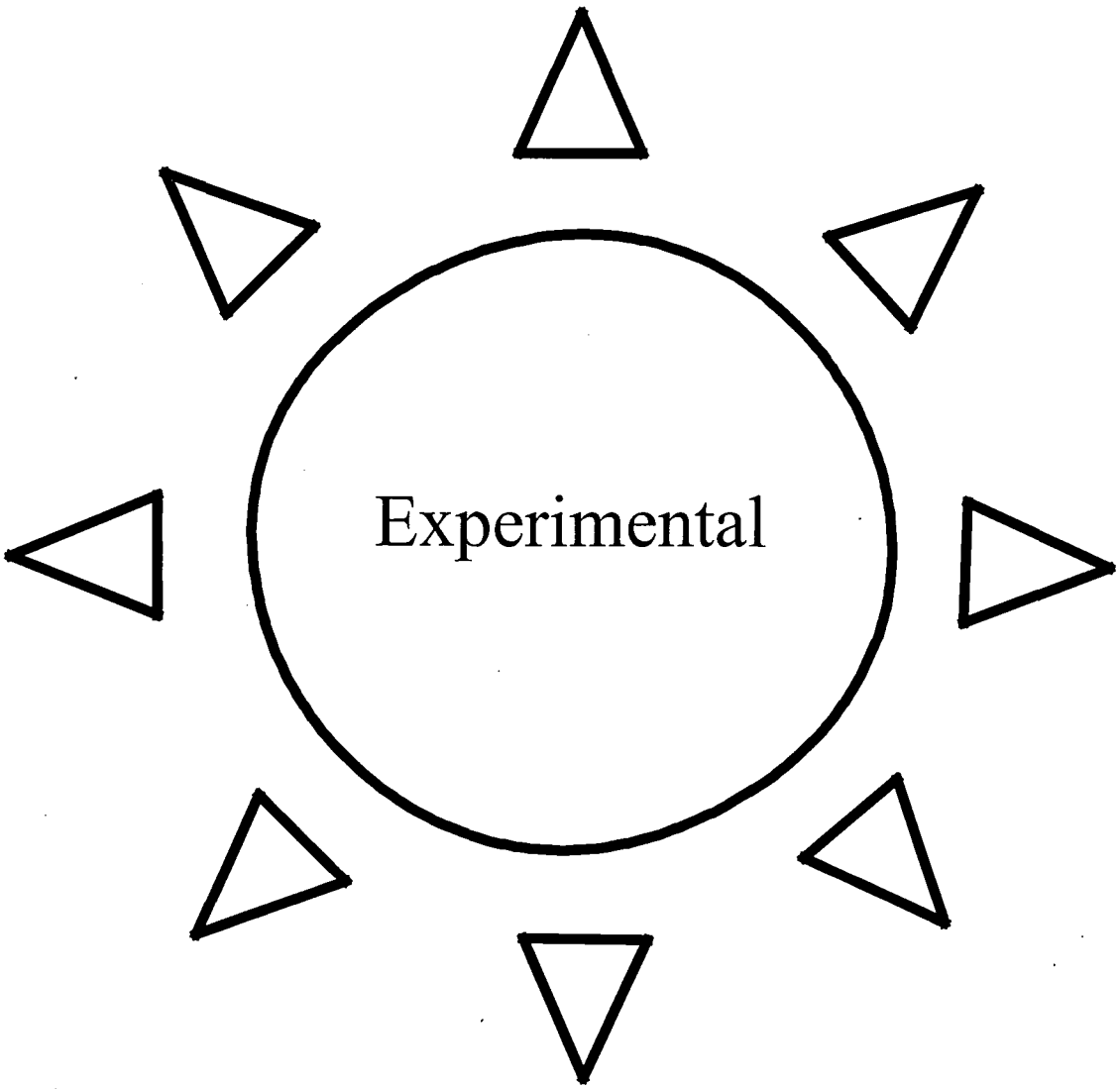

2.1 Ultra-Violet / Visible Absorption Spectroscopy

UV Absorption spectra were obtained using a Unicam UV/Vis Spectrometer UV2-100. A tungsten lamp is used as the source for wavelengths greater than 325 nm, and a deuterium lamp for wavelengths below 325 nm The spectrometer was controlled using Unicam Vision Software Version 3.0 running on a PC.

Spectra intended for calculating absorption maxima and extinction coefficients were measured using a scan speed of 120 nm/minute with data intervals of 0.1 nm. Other modes, such as "Intelliscan" mode (variable scan speed, 120-1200 nm/min) with "Quant" Data interval (0.5 nm), were used for other spectra.

2.1.1 Room Temperature UV / Visible Absorption Spectroscopy

Samples were contained in quartz absorption cuvettes with a path length of 1 cm, unless otherwise stated. All spectra (unless otherwise stated) were run against a reference of pure solvent contained in a matched cell.

Extinction coefficients were calculated using the Beer-Lambert Law (Equation 2.1), where A = absorbance at wavelength in question, ε = extinction coefficient at wavelength in question, c = concentration in mol dm^{-3}, and l = path length in cm.

$$A = \varepsilon c l \qquad \textbf{Equation 2.1}$$

For each system examined, the absorption spectra of several solutions of known concentration, in the range 1×10^{-5} mol dm^{-3} to 1×10^{-4} mol dm^{-3}, were measured. A graph of Absorbance vs. concentration was drawn; the gradient of which gives the extinction coefficient in mol^{-1} dm^3 cm^{-1}.

2.1.2 Low Temperature UV / Visible Absorption Spectroscopy

Low temperature UV/Visible absorption spectra were obtained on the LS50B using a variable temperature liquid nitrogen cryostat from Oxford Instruments (model DN 1704). The layout of the cryostat is shown in figure 2.1

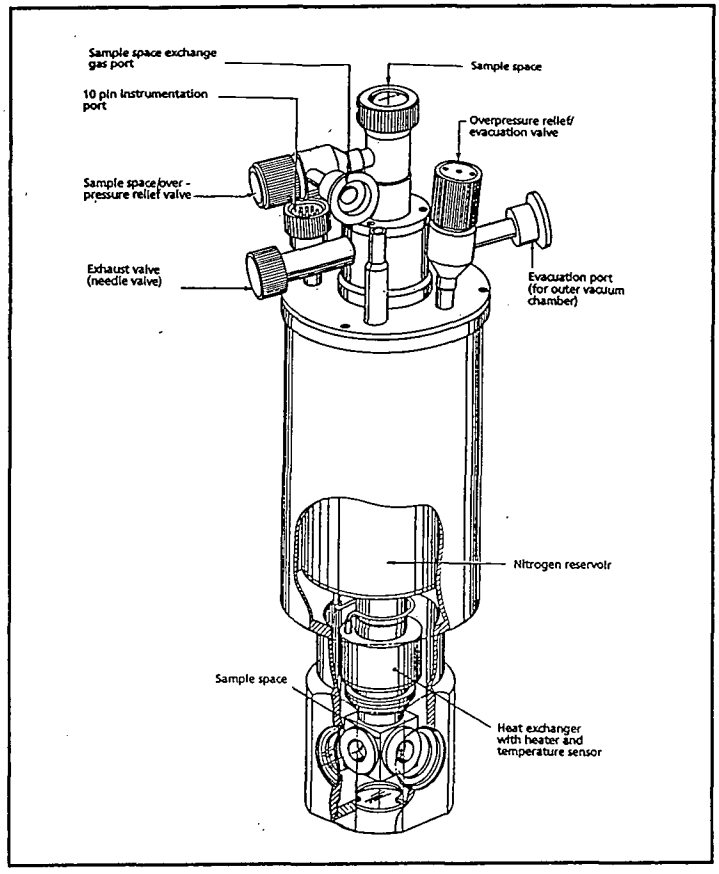

Figure 2.1 Schematic diagram of the DN1 704 variable temperature liquid nitrogen cryostat[1]

The sample is loaded from the top, and positioned at the bottom, in a chamber filled with dry helium. There are four sets of quartz windows for optical access, prevented from misting by an evacuated chamber separating the sample chamber and outer windows. There is a liquid nitrogen (Boiling point = 77 K) reservoir, surrounded by an evacuated chamber, surrounding the upper part of the sample chamber. The sample is cooled by allowing a flow of liquid nitrogen from the reservoir to the heat exchanger. A heating coil and temperature sensor connected to an Oxford Instruments Intelligent Temperature controller ITC4 allows control of the sample temperature.

Spectra in a polar solvent environment were obtained using a solvent mixture of 5:5:2 diethyl ether : isopentane (methyl butane) : alcohol (ethanol), commonly known as EPA. This forms a good quality, clear glass (with no cracks) at 77 K [2]. A mixture of 2:1 methylcyclohexane : isopentane was used as a non-polar solvent which formed a clear glass at 77 K.

2.2 Luminescence Spectroscopy

Fluorescence and phosphorescence spectra were obtained using a Perkin Elmer LS-50B Luminescence Spectrometer, controlled by Perkin Elmer Fluorescence Winlab version 1.02 on a PC. The optical layout of the spectrometer is shown in Figure 2.2

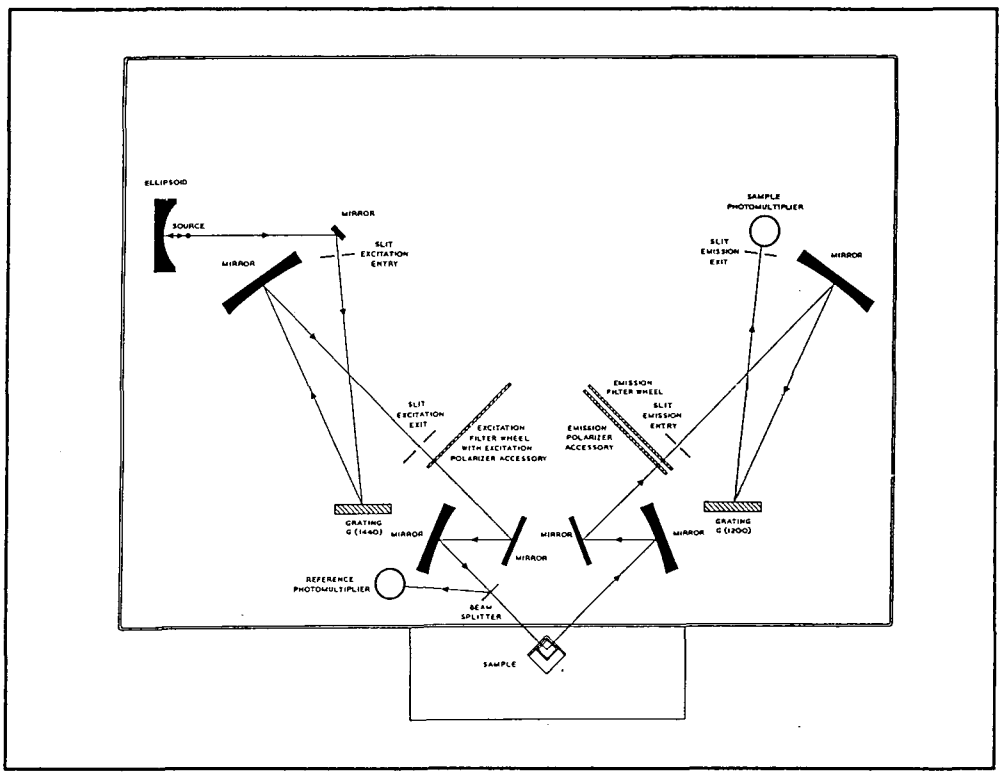

Figure 2.2 Optical layout of the LS 50 luminescence spectrometer[3]

The light source used is a xenon flash tube, which produces an intense, short duration pulse of radiation with a width at half the maximum intensity of less than 10 μs. The light is focused onto the monochromator entrance slit, where it is diffracted on the grating, which is controlled by a stepper motor. A narrow wavelength range emerges. The majority of the excitation beam is focused onto the sample area, and a small proportion is reflected by the beamsplitter onto the reference photomultiplier tube (PMT) and used for spectral correction of the excitation spectra. Light emitted from the sample is focused onto the entrance slit of the emission monochromator, and measured with the sample PMT, model Hanamatsu R928. All emission spectra in this work are reported uncorrected for the PMT response.

Although the range of the excitation monochromator is 200 nm-800 nm, the xenon source has little output below 230 nm, making this a lower usable limit for excitation. The emission monochromator has a range

of 200 nm-900 nm, although the response of the PMT used in this spectrometer limits study of emitted light towards the longer wavelengths.

Luminescence spectra were obtained of solutions contained in 1 cm x 1 cm square quartz fluorescence cuvettes.

2.2.1 Fluorescence Spectroscopy

When operating in the fluorescence mode, the signal is integrated over 80 μs to collect all the light emitted from the sample, for each wavelength studied. The effect of dark current (i.e. the signal detected when no light falls on the detector) is subtracted from the main signals from both reference and sample PMTs. It is measured by gating open both channels a second time before the next flash and measuring the signal as before.

Two types of fluorescence spectra can be obtained. For an emission spectrum, the sample is excited at a chosen wavelength, and emission observed over a range of wavelengths. An excitation spectrum is similar to an absorption spectrum, where a fixed emission wavelength is chosen, and the excitation wavelength varied. This builds a profile of where the samples absorb light that is emitted at a specific wavelength.

2.2.2 Phosphorescence Spectroscopy

Phosphorescence is a much longer-lived process than fluorescence, and phosphorescence lifetimes can cover a very wide range. Hence the gate time, over which the emitted light is integrated, can be chosen to be between 0.01 ms and 500 ms. The delay time between exciting the source and observing the phosphorescence can also be chosen to be between 0-900 ms. (See figure 2.3) The source can also be pulsed between 1 and 10 times to optimise sample excitation. The gate and delay times are measured from the beginning of the last pulse. Again both excitation and emission spectra can be measured.

Phosphorescence lifetimes were measured by fixing both the excitation and emission wavelengths. A set gate time is used, and up to 20 delay times are chosen. After measuring the dark current, the lamp is fired, and the phosphorescence integrated after the first delay time. The procedure is repeated for each delay time, building up a phosphorescence decay profile. Care must be taken to ensure that the gate time is short compared to the phosphorescence lifetime, so that an accurate curve is produced.

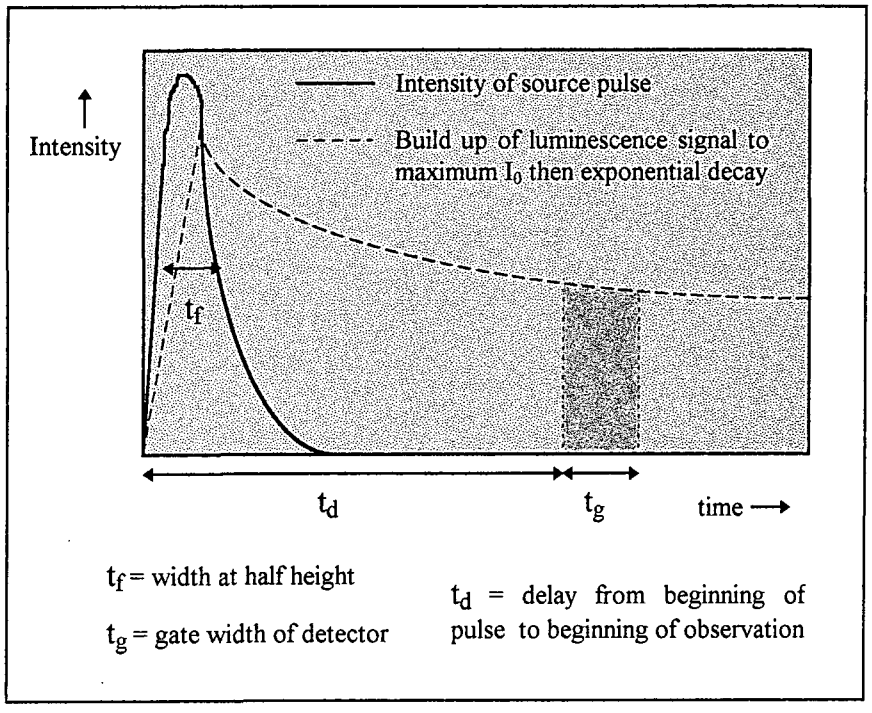

Figure 2.3 Events occurring during excitation in the phosphorescence mode[3]

The phosphorescence decays follow first order kinetics, and have been analysed using a single exponential fit (with offset) on the Data Analysis and Graphics programme, GraFit, (Erithicas Software). (Equation 2.2)

$$I_t = I_0 \exp\left(\frac{-t}{\tau_p}\right) \qquad \textbf{Equation 2.2}$$

Where I_t = Luminescence intensity at time = t, I_0 = Luminescence intensity at time = 0 and τ_p = Phosphorescence lifetime.

2.2.3 Low Temperature Luminescence Spectroscopy

Low temperature fluorescence and phosphorescence spectra were obtained on the LS50B using the variable temperature liquid nitrogen cryostat, described earlier.

The LS50B was adapted to hold the cryostat such that the sample was positioned in a reproducible position at the intersection of the emission and excitation beam paths.

2.3 Infra-Red Spectroscopy

Infra-red spectra were obtained using a Perkin Elmer Paragon 1000 FT-IR Spectrometer, controlled by Perkin Elmer Grams Analyst 1000 version 3.01A level II on a PC.

2.3.1 Room Temperature Infra-Red Spectroscopy

Room temperature spectra were measured using a resolution of 4 cm^{-1}, and taken as the average of 16 scans.

Solution samples were contained in a Graseby Specac, 0.1 mm pathlength CaF_2 heated cell type 20502.

Solid samples as KBr disks were ground together with potassium bromide, and pressed into disks using a hydraulic press. Solid samples were also analysed using a Graseby Specac Golden Gate Attenuated Total Reflection accessory. Liquid samples were run as thin films between potassium bromide plates.

In all cases in this report, spectra are displayed with the solvent spectra subtracted, unless otherwise stated.

2.3.2 Low Temperature Infra-Red Spectroscopy

Infra-red Spectra at 77 K were measured using a home-built low temperature cryostat, as shown in figure 2.4. This consisted of a 0.1 mm CaF_2 solution cell mounted in one end of a hollow copper tube. This tube was surrounded by an evacuated chamber and filled with liquid nitrogen to cool the sample. Outer windows of polished KBr allowed the infra-red beam to pass through and measure spectra.

Due to the basic design of the cryostat, it was necessary to warm the outer wall intermittently using a hot air gun. This was to prevent excessive cooling, and hence misting, of the outer windows.

Spectra were recorded as an average of 300 scans using a resolution of 2 cm^{-1}. Solvent spectra were recorded separately and subtracted.

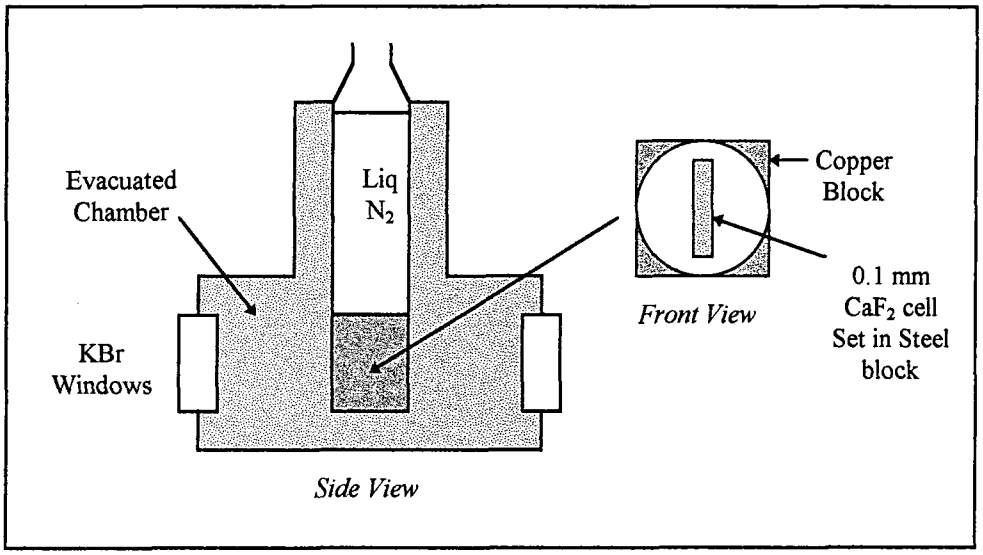

Figure 2.4 Schematic diagram of the low temperature liquid nitrogen cryostat

Despite extensive testing of halogenated compounds and mixtures of these, no solvent forming a glass at 77 K, and having no significant absorption bands was found. Carbon tetrachloride (CCl_4), and also dichloromethane (CH_2Cl_2) were used as solvents, which form white "snows" at 77 K. The pathlength of the cell was such that this did not prevent reasonable spectra being obtained, although interference effects and sloping baselines were evident.

2.4 Continuous Irradiation

A variety of irradiation sources and techniques have been used in this work, to reflect the different reasons for applying continuous irradiation in experiments. The different experimental set-ups and optical filters are described below.

2.4.1 Optical Filters

A variety of filters have been used in this work in order to limit the range of wavelengths of light used in experiments. The filters are of different types and originate from a variety of sources. Descriptions of, and transmission spectra for all of the filters used in this work are given in table 2.1 and figures 2.5 - 2.11. For chemical filters consisting of aqueous solutions, the concentrations varied, and the spectra show merely the general spectral output, and not absolute transmission values.

Filter[a]	Description	Filter Type	Figure no. of Spectra[a]
A	Clear Glass	-	2.5
B	Black Glass	Schott Filter UG 1	2.6
C	Clear Glass	Schott Filter GG 375	2.7
D	Pale Blue Glass	-	2.8
E	Interference Filter for 1270 nm	Infrared Engineering NBD-1270-25-N	2.9
F	aqueous $CuSO_4$ in 5 cm Quartz Cell	-	2.10
G	aqueous $NaNO_2$ in 2 cm Quartz Cell Attenuating Filter	-	2.11

Table 2.1 Description of Optical Filters used in this Work

a) Letters and figure numbers are for reference within this work only and do not correspond to any accepted descriptions

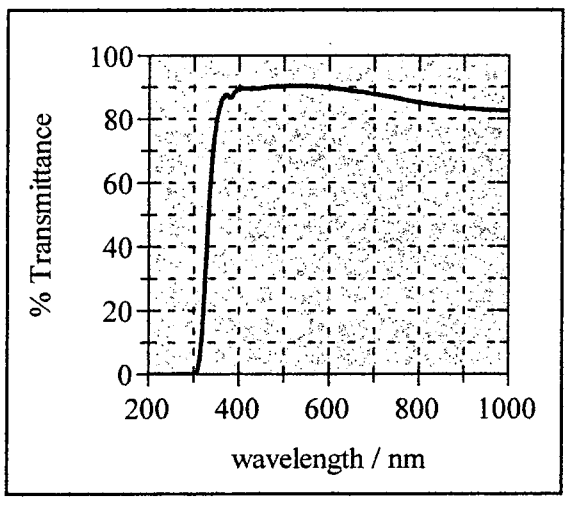

Figure 2.5 Transmittance spectrum of filter A

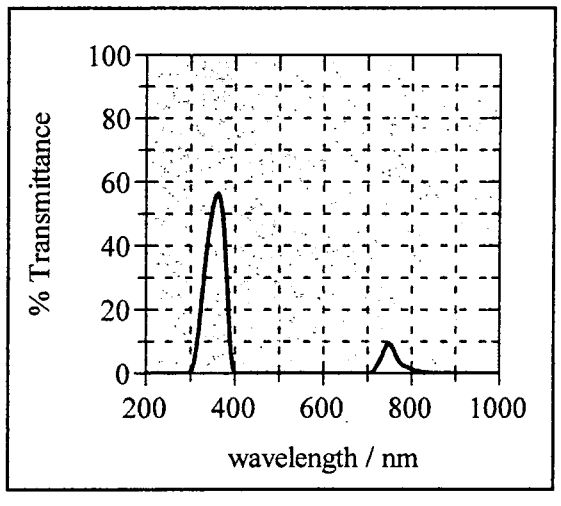

Figure 2.6 Transmittance spectrum of filter B

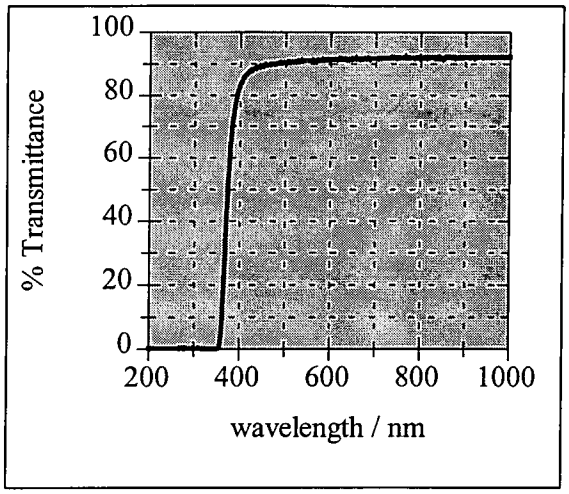

Figure 2.7 Transmittance spectrum of filter C

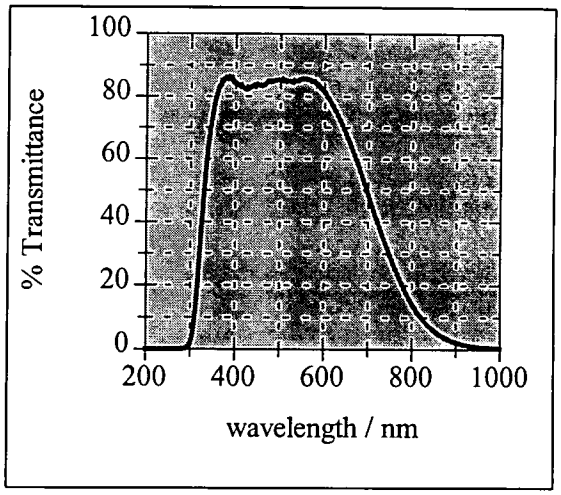

Figure 2.8 Transmittance spectrum of filter D

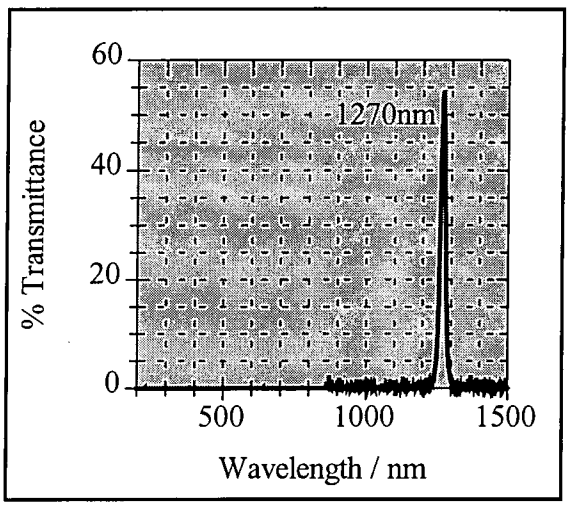

Figure 2.9 Transmittance spectrum of filter E

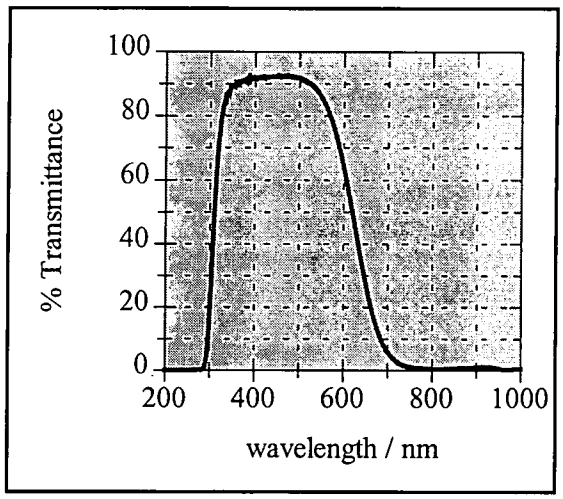

Figure 2.10 Transmittance spectrum of filter F

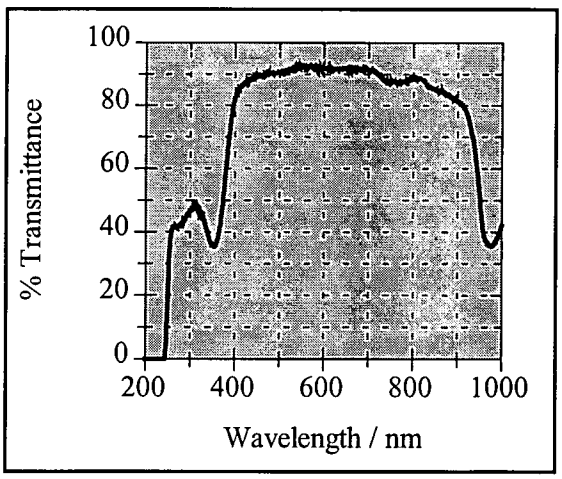

Figure 2.11 Transmittance spectrum of filter G

2.4.2 Experimental Set-ups

2.4.2.1 Photoketonisation Studies

Conversion of DBM from the enol to the keto form was studied using the apparatus described in figure 2.12

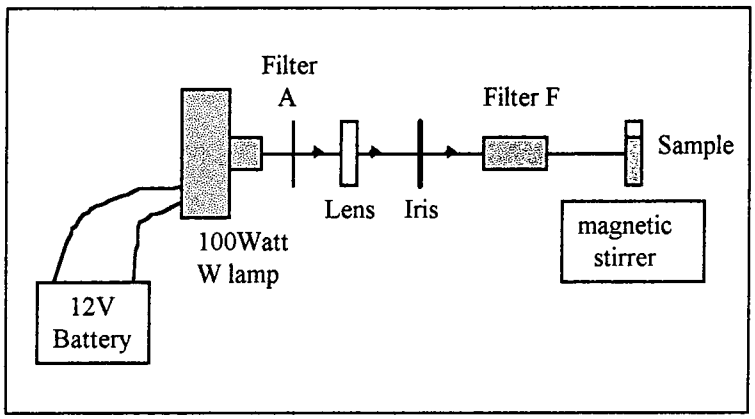

Figure 2.12 Apparatus for continuous irradiation using tungsen filament lamp

An Osram 12 V 100 W tungsten-halogen filament bulb, contained in a home-built housing, was focused and filtered onto the sample, using filters A and F to cut off light below 300 nm, and cut out IR and some visible light. The sample was contained in a quartz absorption cuvette containing a tiny magnetic stirrer bead. This was used with a magnetic stirrer, to ensure mixing, and hence, even irradiation of the sample. The absorption spectrum of each sample was taken at intervals over a period of hours.

The lamp source, however, did not have a constant output with time, due to variation of the battery power, and no quantitative measurements are reported using this apparatus.

2.4.2.2 Quantitative Photoketonisation Studies

Quantitative steady state irradiation of DBM, Parsol 1789 and standards was carried out using the apparatus described in Figure 2.13

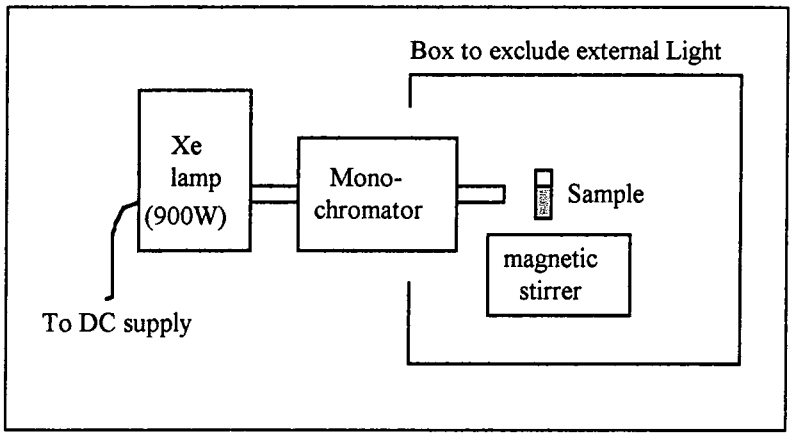

Figure 2.13 Apparatus for continuous irradiation using Xe lamp

A 900 Watt xenon lamp from Applied Photophysics was used as the source. This was converted to a narrow bandwidth source using a f/3.4 monochromator from Applied Photophysics, with both the entrance and exit slits set at 4 mm. Light leaving the monochromator was focused onto the sample, such that the photon flux arriving at the sample was approximately 1.5×10^{16} photons per second at 342 nm, estimated using Aberchrome 540 as an actinometer, as discussed in section 2.6.

The sample consisted of 2.5 cm^3 of the solution under study, contained in a quartz fluorescence cuvette, stirred with a magnetic stirrer as before. The sample was placed in a fixed position for all experiments, ensuring identical conditions. The sample was contained in a light-proof box to ensure no photolysis occurred due to stray light. The absorbance of the sample at the wavelength of interest was measured at intervals over a period of minutes or tens of minutes.

The source had a constant output over a period of hours, allowing quantitative comparison of samples run consecutively. However, due to ageing of the lamp over time, absolute comparison of all samples run was not carried out.

2.4.2.3 Low Temperature Photolysis

Irradiation of frozen solutions of DBM and other molecules, for low temperature absorption and IR specroscopy was carried out using a tungsten-halogen filament lamp, as described earlier, filtered by filter D, to directly irradiate the frozen samples in the cryostats. No stirring was carried out due to the frozen nature of the samples.

Low temperature IR spectroscopy of DBM to distinguish E and Z isomers was carried out using this set-up with the addition of the use of filter C to initially irradiate with wavelengths >375 nm.

Low temperature UV absorption spectroscopy of DBM to distinguish E and Z isomers was carried out after irradiation using a 900 W Xenon lamp and monochromator, as described previously, operating at wavelengths 378 nm, 359 nm and 345 nm using 1 mm slits, and also at 360 nm using 10 mm slits for broad band irradiation.

2.4.2.4 Photolysis of Solid Samples and Mineral Oil solutions

Irradiation of solid samples of DBM and solutions in mineral oil for IR spectroscopy was carried out using a tungsten-halogen filament lamp, as described earlier, filtered by filter D. No stirring was carried out due to the nature of the samples.

2.5 Flash Photolysis

Flash photolysis is a technique which allows the study of short-lived transient species generated by photo-excitation. Two different nanosecond laser flash photolysis set-ups have been used in this work, based on an excimer pumped dye laser, and a frequency tripled Nd^{3+}:YAG laser. Both systems involve the same data acquisition and analysis.

2.5.1 Excimer Pumped Dye Laser

The initial set-up is shown in Figure 2.14. The sample is excited by pulses of laser radiation at 340 nm. This is produced by a Lambda Physik FL2002 dye laser containing para-terphenyl in dioxane (λ_{max}= 343 nm), which is pumped by a Lambda Physik EMG101 (XeCl) Excimer laser at 308 nm. The laser light is collected by a 5 mm liquid light guide, and directed at the sample. This system produces laser pulses at the sample of maximum energies $\approx$ 1 mJ (measured with a calibrated Gentec ED100A power meter), and with a pulse duration of 20 ns. The energy of the pulse was varied using filter G attenuation filters of various transmittances at 340 nm. The relative laser power was measured as a voltage using an ELTEC 420M3 pyro-electric detector, positioned behind the sample holder.

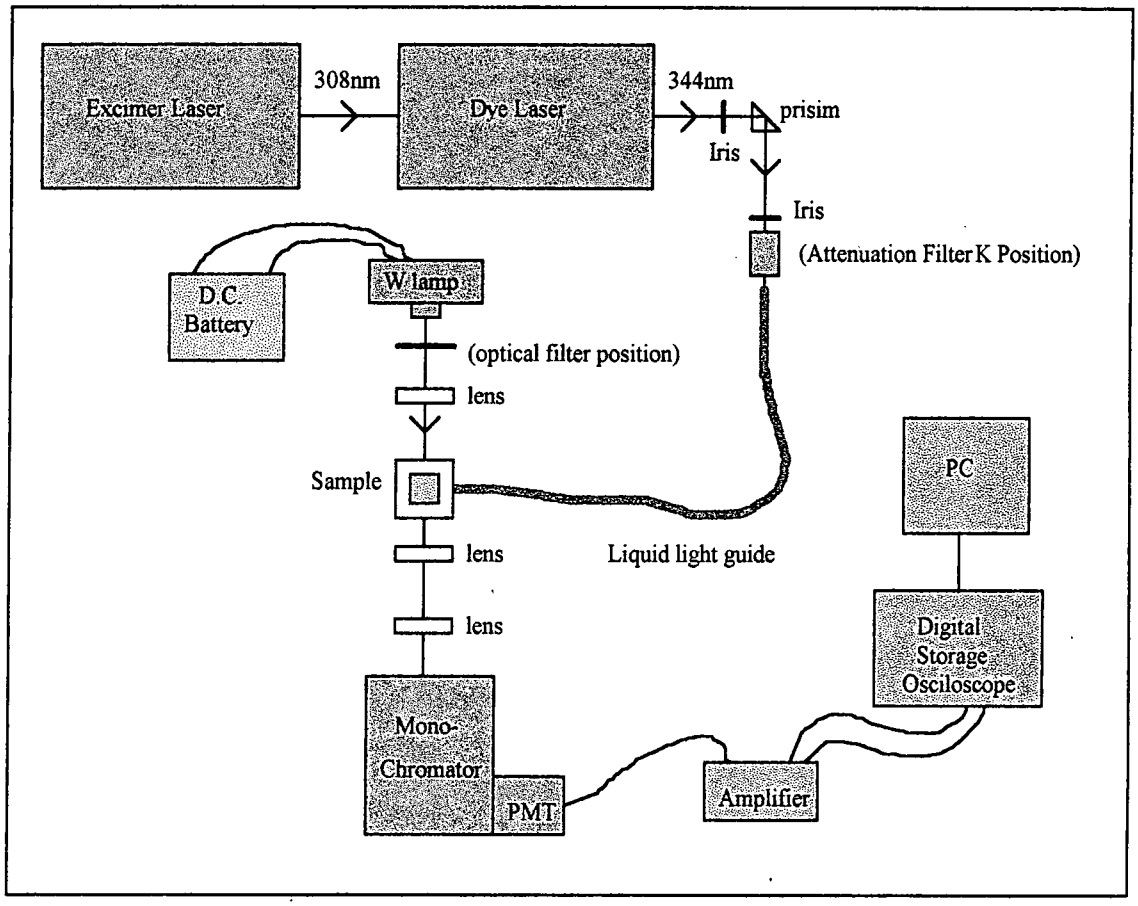

Figure 2.14 Apparatus for nanosecond laser flash photolysis with excitation at 340 nm

The transient produced is observed by absorption spectroscopy, at 90° to the exciting pulse. The source is the 12 V 100 Watt Tungsten filament lamp, powered by a 12 V battery, as described earlier, and focused onto the sample after passing through an optical filter such as filter D. The light is attenuated by the sample, and focused onto a Bentham TM300 Monochromator and the intensity measured using a Hamamatsu R928 photomultiplier tube, PMT. The output from this is sent to a home built DC-10MHz bandwidth amplifier which splits the signal into two components. The first is DC coupled, and represents the (large) I_0 value. The second signal is amplified ×10, and AC coupled, such that only the rapidly changing component of the signal due to the transient decay is seen. Both signals are fed into a 2-channel Tetronix TDS 320 digital storage oscilloscope connected to a PC, and are recorded by a photodiode when triggered with the firing of the laser.

2.5.2 Frequency Tripled Nd^{3+}:YAG laser

The alternative set-up makes use of a Spectra Physics Quanta-Ray GCR-150-10 Nd^{3+}:YAG laser operating in frequency tripled mode at 355 nm as the excitation source, and a 150 W xenon lamp as the analysing source. This is shown in figure 2.15

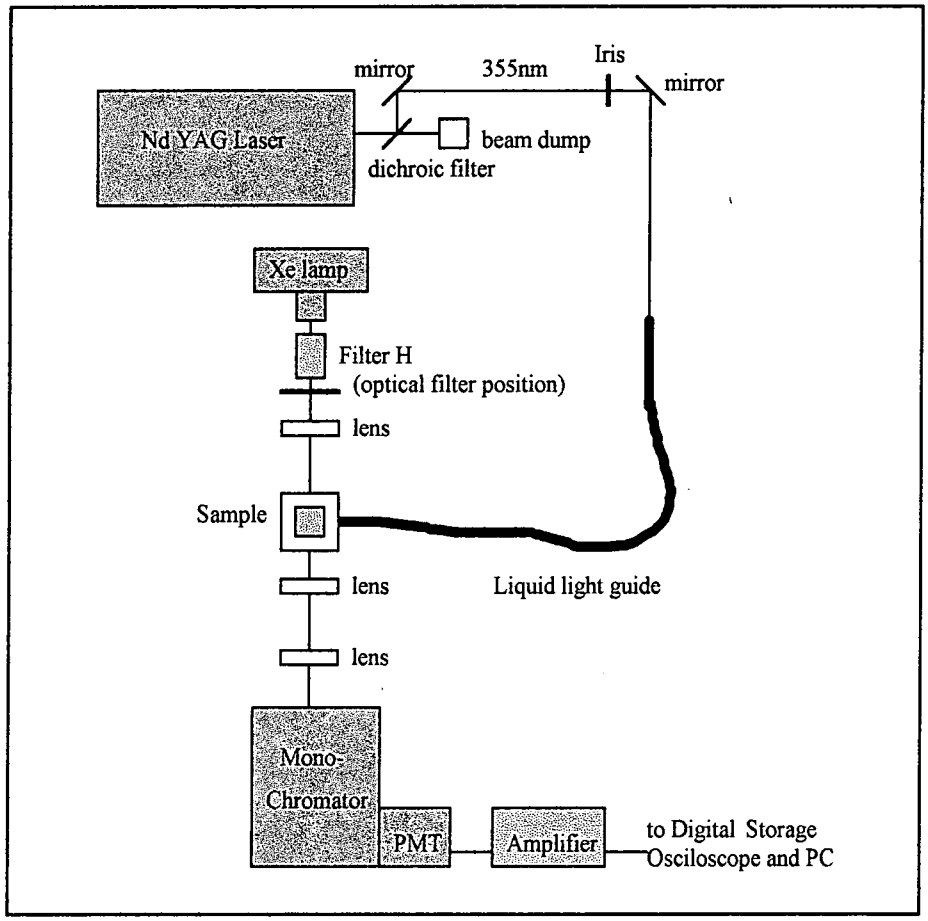

Figure 2.15 Apparatus for nanosecond laser flash photolysis with excitation at 355 nm

The experimental set-up is very similar to that described previously. The sample is excited by pulses of laser radiation at 355 nm, produced by 3rd harmonic generation mixing of 1064 nm and 532 nm light from a Spectra Physics Nd^{3+}:YAG laser. The 355 nm light is separated from the other wavelengths using dichroic mirrors, and part of the laser beam is reflected off a dichroic filter, with the remainder of the 355 nm light produced being dumped. This attenuation is carried out such that laser pulses at the sample are of maximum energies <1 mJ, after passing through a 5 mm liquid light guide to direct the beam to the sample.

The transient produced is observed by absorption spectroscopy, at 90° to the exciting pulse. The monitoring lamp is a Bentham IL6 illuminator, equiped with a 150 W xenon lamp, powered by a Bentham 605 current stabilised power supply, and filtered by filter F. The light is attenuated by the sample, focused onto the monochromator and the signal recorded exactly as described previously.

2.5.3 Data Treatment and Spectra Measurement

The observed signals appear as shown in Figure 2.16 where I_0= Intensity of light before excitation, I_a= change in Intensity of light due to transient, which is considered to be positive as shown in figure 2.16, and I_t = Intensity of light at time = t. In practice, the transient decay is measured as the average of approximately 20 consecutive laser pulses, to increase the signal to noise ratio.

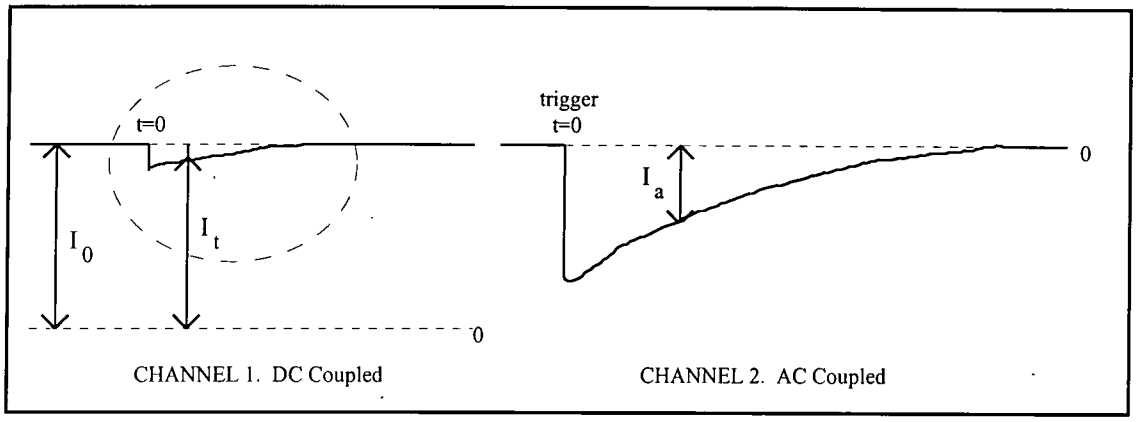

Figure 2.16 Transient signals recorded in flash photolysis

Now to calculate the Absorbance at time = t, equation 2.3 must be used.

$$Abs_t = \log_{10}\left(\frac{I_0}{I_t}\right) = \log_{10}\left(\frac{I_0}{I_0 - \frac{I_a(\text{measured})}{10}}\right) \qquad \textbf{Equation 2.3}$$

Thus the observed signals can be converted to a graph of ΔAbsorbance vs. time, as shown in figure 2.17. Thus the decay of the transient with time is seen, for wavelengths where only the transient absorbs. Where only the ground state absorbs, an inverted trace is seen, corresponding to a bleach and recovery of the ground state.

By observing such decay traces at many wavelengths, a difference absorption spectrum can be constructed. (Figure 2.18), by plotting the transient height at t = 0 or any time interval after excitation. If the ground state does not absorb in the same region as the transient formed, then the spectrum obtained is the transient absorption spectrum. If, however, the transient and ground state have overlapping spectra,

then to obtain the transient spectrum it is necessary to add a scaled ground state absorption spectrum, as shown in equations 2.4 and 2.5, where K is the scaling factor.

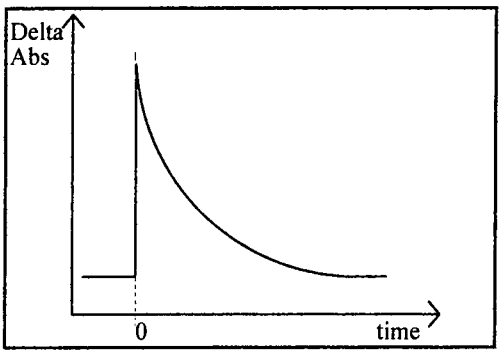

Figure 2.17 Transient decay

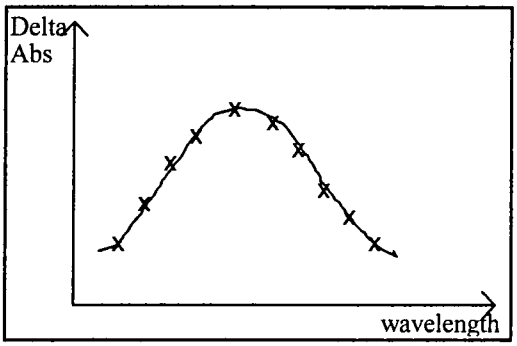

Figure 2.18 Difference spectrum at time = t

$$\Delta Abs = Abs(Transient) + \Delta Abs(Ground\ state) \qquad \textbf{Equation 2.4}$$

$$Abs(Transient) = \Delta Abs + K \times Abs(Ground\ state) \qquad \textbf{Equation 2.5}$$

In many cases the transient decays have been fitted to first order kinetics, equation 2.6, using the data analysis software GraFit (Erithicas Software).

$$Abs_t = -Abs_0 \times \exp(kt) + offset \qquad \textbf{Equation 2.6}$$

The transient lifetime in seconds is related to the first order rate constant by Equation 2.7.

$$\tau = \frac{1}{k} \qquad \textbf{Equation 2.7}$$

2.6 Quantum Yield Measurements

2.6.1 Quantum Yields of Photoketonisation

The quantum yield of photo-conversion of the enol forms of DBM and Parsol 1789 to their diketone forms (Φ_{keto}) is defined in Equation 2.8

$$\Phi_{keto} = \frac{\text{Number of molecules of enol converted to keto per unit time per unit volume of solution}}{\text{Number of photons absorbed per unit time per unit volume of solution}}$$

Equation 2.8

In order to calculate this, the number of photons absorbed must be known. This would be extremely difficult to measure absolutely, so a standard compound, with a known quantum yield of photoconversion from one observable form to another (Φ_{Std}) at the wavelength of interest, can be used, as indicated in equation 2.9.

$$\Phi_{Std} = \frac{\text{Number of molecules of standard converted per unit time per unit volume of solution}}{\text{Number of photons absorbed per unit time per unit volume of solution}}$$

Equation 2.9

Thus, if the standard sample and the test sample are irradiated under exactly the same conditions (i.e. with the same sample positioning, same lamp source, same cuvette, same sample absorbance at wavelength of interest, etc.) then the denominators of Equations 2.8 and 2.9 will be identical. Therefore the quantum yield is given by equation 2.10.

$$\Phi_{keto} = \frac{\text{No. of molecules of enol converted to keto per unit time per unit volume of solution}}{\text{No. of molecules of standard converted per unit time per unit volume of solution}} \times \Phi_{Std}$$

Equation 2.10

For identical conditions, as described, the volumes of the two samples will be the same, and thus this can be cancelled from the equation. By multiplying by Avagadro's number, ΔM_{Keto}= No. of moles of enol converted to keto per unit time, and ΔM_{std} = No. of moles of standard converted per unit time, equation 2.10 can be converted to equation 2.11.

$$\Phi_{keto} = \frac{\Delta M_{Keto}}{\Delta M_{Std}} \times \Phi_{Std} \qquad \textbf{Equation 2.11}$$

It is assumed that all the change in Absorbance of the DBM or Parsol 1789 enol is due to formation of the keto, and a wavelength where only the enol form absorbs was chosen for study. This allows ΔM_{keto} to be followed using the change in absorbance of the Enol form, ΔAbs_{Enol} and ε_{Enol}, because of equation 2.12 (Expanded Beer-Lambert law)

$$\Delta Abs = \frac{\varepsilon \times \Delta M}{V} \times l \qquad \textbf{Equation 2.12}$$

A standard for use in determining the quantum yields of ketonization for DBM and Parsol needs to be a compound with a photochemical change of known quantum yield, occurring on irradiation at about 340 nm-350 nm. It must also have a known extinction coefficient known for a wavelength suitable for observing the change. A suitable standard, used in this work, is Aberchrome 540 [4,5].

Aberchrome 540 ((E)-α-(2,5-dimethyl-3-furylethylidene)(isopropylidiene) succinic anhydride) is a photochromic fulgide, which can be inter-converted between a ring-opened and a ring-closed form by irradiation at appropriate wavelengths, as shown figures 2.19 and 2.20. Both forms are stable in the dark.

The quantum yield of conversion from the ring-opened form (1) to the ring-closed form (2), with irradiation in the region 310-370 nm is Φ=0.20. This value is wavelength and temperature independent in the range specified[4,5]. The extinction coefficient for the absorption peak of the ring-closed form, at 494 nm is 8.2×10^3 dm^3 mol^{-1} cm^{-1} [5]. The ring-opened form does not absorb at 494 nm.

Thus, by assuming that all the ring-opened form is converted to the ring-closed form, ΔM_{Std} can be followed by monitoring the growth of absorbance of the ring closed form at , using ΔAbs_{Std} and ε_{Std}, both measured at 494 nm.

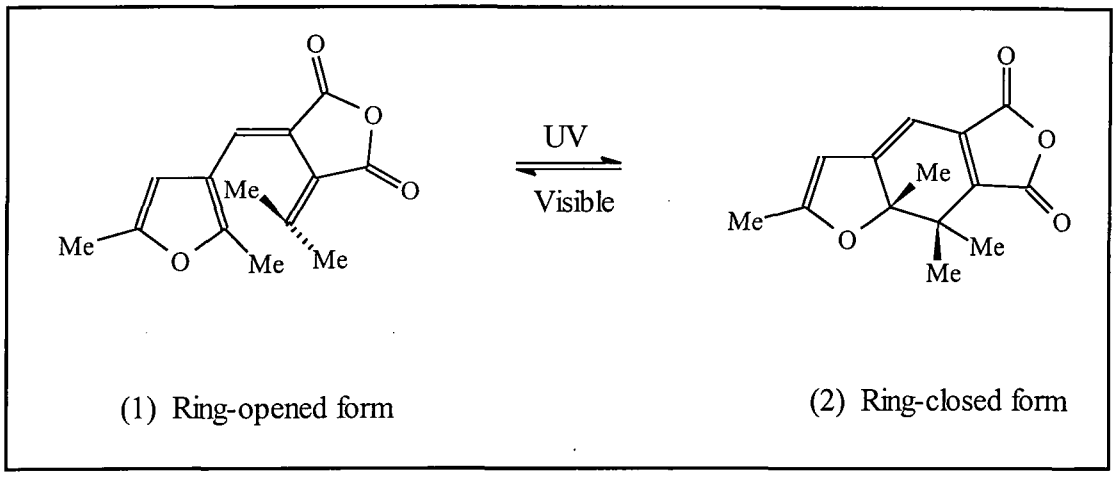

Figure 2.19 Photo-conversions of Aberchrome 540 [5]

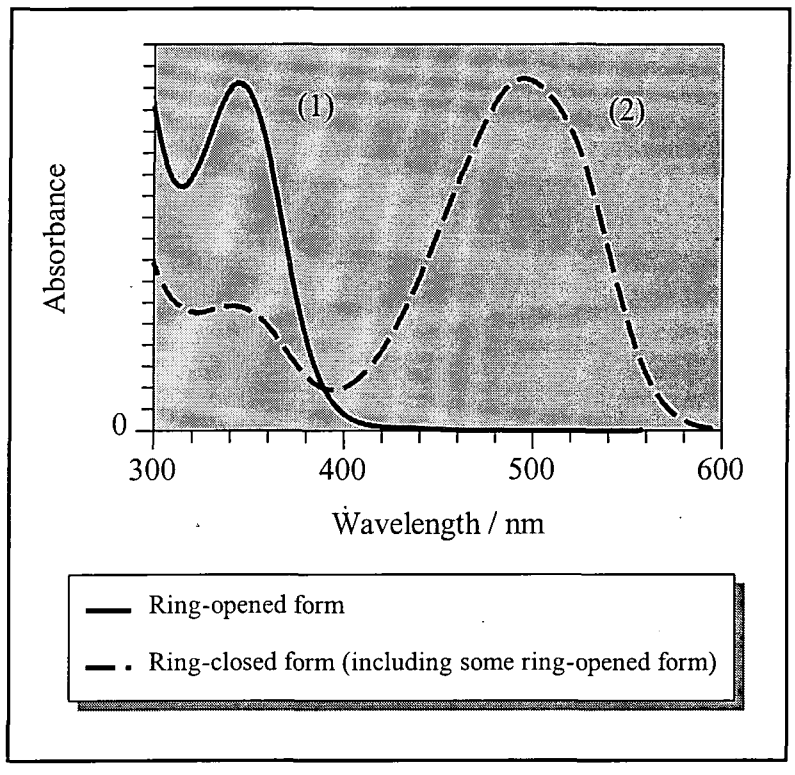

Figure 2.20 Absorption spectra of the two forms of Aberchrome 540 [5]

Now ΔM_{Keto} and ΔM_{Std} are the number of moles converted, of sample and standard per unit time. The rate of change of the these will be different. Thus soon after each experiment has begun, each will be absorbing a different number of photons, making Equation 5. no longer valid. The initial slope of the decay (on a graph of No. of Moles converted vs. time), where the number of photons absorbed is the same in each case, must be used as the ΔM value.

In this work the decays of DBM (to the diketone form) and of Aberchrome 540 (to the ring-closed form) behave as if following first order kinetics, i.e. follow a single exponential decay (Equation 2.13).

$$M_t = -M_0 \times \exp(kt) + \text{offset} \qquad \textbf{Equation 2.13}$$

Where k is the "first order rate constant", and M_0 is the initial number of moles of either sample or standard. By fitting the experimental data to an exponential decay curve, the "first order rate constant" can be easily determined.

Thus, differentiating this equation to give the gradient at time = t, gives Equation 2.14

$$\frac{dM_t}{dt} = -kM_0 \times \exp(kt) \qquad \textbf{Equation 2.14}$$

Hence at time t=0, initial gradient = $-kM_0$.

By replacing the initial gradients for both the sample and standard into Equation 2.10, the quantum yield of photoketonization can be calculated, as shown in equation 2.15.

$$\Phi_{keto} = \frac{k_{Keto} \times M_o^{Keto}}{k_{Std} \times M_o^{Std}} \times \Phi_{Std} \qquad \textbf{Equation 2.15}$$

2.6.2 Quantum Yields of Short-lived Species Formation

The quantum yields of transient formation, were calculated in a manner similar to that for ketonization. The main differences in transient formation over ketonization, is that the change on irradiation is very small, extremely fast, and recovers very quickly. The source used is pulsed, and thus the quantum yield of formation can be amended to equation 2.16.

$$\Phi_{Transient} = \frac{\text{Number of molecules of transient produced per laser pulse per unit volume of solution}}{\text{Number of photons absorbed per laser pulse per unit volume of solution}}$$

Equation 2.16

Thus, ΔM in Equation 2.11 can be interpreted as the number of molecules changed in one laser pulse. This is measured using ΔAbs and ε as described before, but these can be replaced directly in Equation 2.11. as the absorbance of the sample and standard do not change significantly during one pulse If it is assumed that all the change in absorbance of DBM or Parsol is due to the transient formation, then the loss of the absorption of the ground state enol, and its known extinction coefficient can be used instead of the corresponding values for the transient. This gives Equation 2.17 for calculating the quantum yield of transient formation.

$$\Phi_{Transient} = \frac{\Delta Abs_{Enol}}{\Delta Abs_{Std}} \times \frac{\varepsilon_{Std}}{\varepsilon_{Enol}} \times \Phi_{Std} \qquad \textbf{Equation 2.17}$$

Where ΔAbs and ε correspond to the same wavelength, but can be different for the sample and the standard.

In order to increase the accuracy of this experiment, the ΔAbs values are measured at a range of laser powers, and the gradient of a graph of ΔAbs vs. % laser power used in place of ΔAbs in Equation 2.12. The laser power was varied using attenuating filters (G), and the powers measured using a power meter, as previously desribed.

Aberchrome 540, as described in part 2.4.3, was used as the standard. It has been used in such experiments previously[6]. The use of a darkened room, and a filter F to cut out light below 400 nm from the monitoring source, ensured that only light from the laser caused changes in the Aberchrome. The recovery time of Aberchrome under these conditions (due to the monitoring lamp) is much longer than that of the transient species under study. Hence between each averaging laser shot, the sample was stirred in front of the unfiltered monitoring lamp to ensure full conversion back to the ring-opened form.

2.6 Time-resolved Resonance Raman Spectroscopy

2.6.1 Raman Scattering[7]

When a photon interacts with a molecule, it can be transmitted, absorbed or scattered. Rayleigh scattering is due to an elastic "collision" where the photon is scattered with no change in energy, and thus at the same frequency. The photon can be considered to be absorbed by the molecule, raising its energy momentarily to some higher energy level which is not stable ("virtual state"). The molecule therefore immediately loses energy and re-emits the scattered photon, as shown in figure 2.21 a.

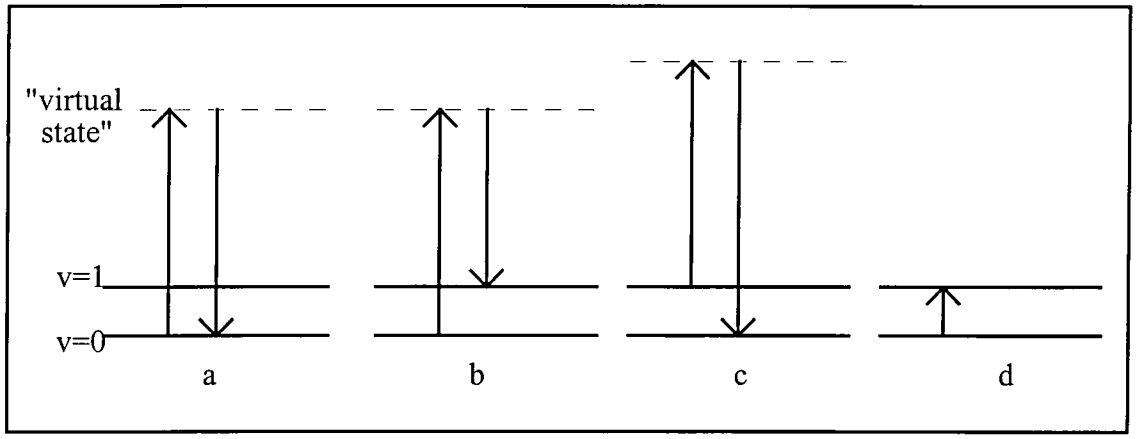

Figure 2.21 Possible interactions of infra-red radiation with vibrational energy levels of a molecule

a) Rayleigh scattering ; b) Stokes Raman scattering c) Anti-Stokes Raman scattering ; d) IR spectroscopy

Two other types of scattering can also be observed; Stokes and Anti-Stokes Raman Scattering. In these cases, the absorbed photon interacts with the molecule and stimulates a vibrational and/or rotational transition. This results in the photon being emitted at a different wavelength, with the difference giving information about the vibrational structure within the molecule, in a similar way to infra-red spectroscopy.

In Stokes Raman scattering, the photon induces a transition from, e.g. the v=0 level to v=1, with the result that the emitted photon is of lower energy, (longer wavelength, smaller wavenumber), as shown in figure 2.21 b.

In anti-Stokes Raman scattering, the photon induces a transition from the v=1 energy level to v=0, and is therefore emitted at a higher energy, (shorter wavelength, longer wavenumber), as shown in figure 2.21 c.

Both Stokes and anti-Stokes Raman scattering are far less intense than Rayleigh scattering, as these processes are much less likely to occur. They can normally only be observed for large sample densities, and using a high powered incident source such as a laser. Anti-Stokes scattering is much less intense than Stokes scattering, because at room temperature, most molecules in a sample exist in the v=0 ground state.

Raman spectra are usually obtained by observing the Stokes Raman scattering, and monitoring the frequency difference between this and the incident light. This gives structural information about the sample, through information about its vibrational and rotational energy levels. Raman spectroscopy and infra-red spectroscopy both give this type of information, but they are complementary techniques. The intensity of bands differ in IR and Raman spectroscopy due to the different mechanisms of the photon-molecule interaction. For a vibrational mode to be IR active there it must involve a change in dipole moment, where as for a mode to be Raman active, it must involve a change in the polarizability of the molecules. Often a strong band in an IR spectrum will be weak in a Raman spectrum of the same sample, and vice versa.

2.6.2 Resonance Raman Spectroscopy[8]

The intensity of Raman scattering is very low. Even when a laser source is used it can be extremely difficult to detect Raman scattering in samples of low concentration. It has been observed that if the incident frequency is at or close to an electronic transition of the molecule, a resonance enhancement of the scattering from the vibrations associated with the chromophore coupled to the electronic excitation is produced. An enhancement of intensity up to 10^6 is possible. Thus by tuning the incident wavelength to an absorption band of a species of interest, resonance Raman spectroscopy can allow the study of samples of low concentration.

2.6.3 Time-Resolved Resonance Raman Spectroscopy[9]

In time-resolved resonance Raman spectroscopy (TR^3 spectroscopy), the resonance Raman spectra of short lived reaction intermediates in solution can be measured, such as those produced on photo-excitation of a sample. This is done in much the same way as the absorption spectra of short lived species are studied using flash photolysis. In TR^3 spectroscopy, one laser is usually used to excite the sample, known as the pump pulse. Another, at a specific interval later, is used to produce resonance

Raman scattering from the transient species in the sample, which is collected and studied. This is referred to as the probe pulse. Usually the concentration of species produced on irradiation is very small, which makes resonance Raman essential in time-resolved studies. Even so, this technique is not nearly as sensitive as flash photolysis, but TR^3 spectroscopy can be a very valuable tool in determining the structure of short lived species.

Time-resolved resonance Raman spectroscopy was carried out at the EPSRC Rutherford Appleton Laboratories, with the help of Sue Tavender, and in collaboration with Prof. G Truscott, Dr. D McGarvey and Miss. L. Mulroy from the University of Keele. The experimental set-up is shown in Figure 2.22.

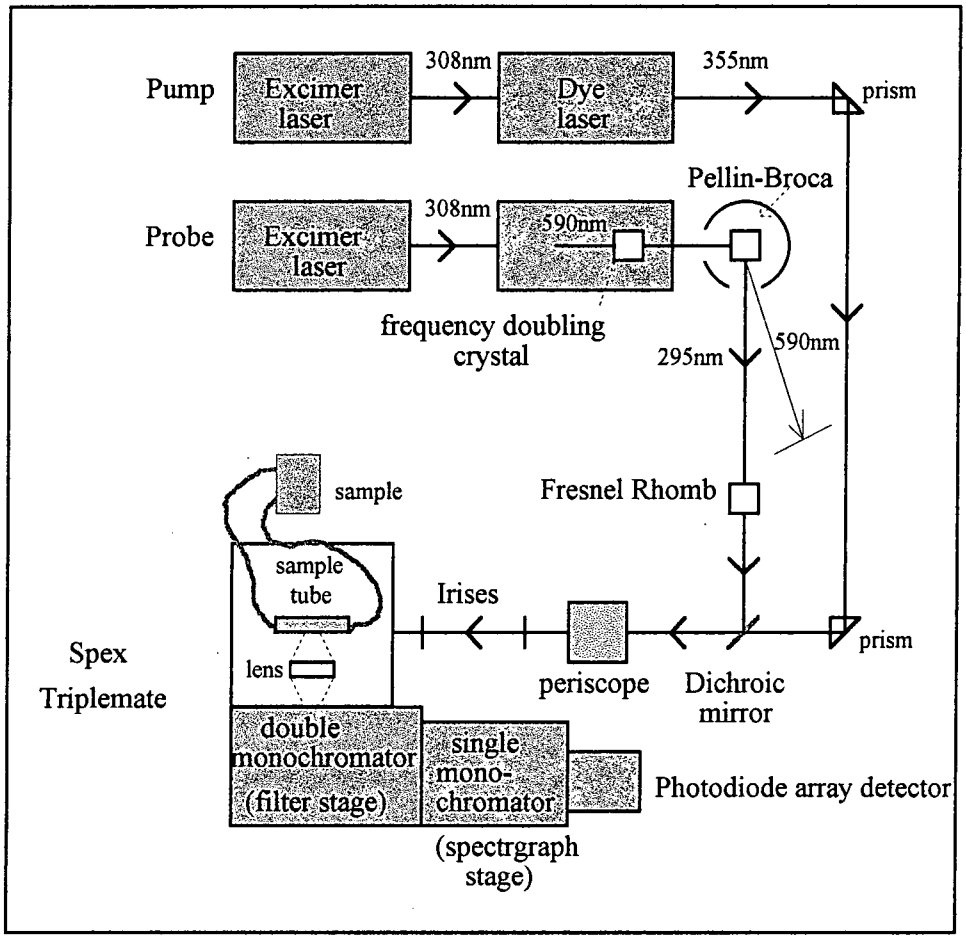

Figure 2.22 Apparatus for time-resolved resonance Raman spectroscopy

The pump laser system consisted of a Lambda Physik FL3002, dye laser containing DMQ in dioxane (λ_{max} =360 nm) pumped by an Lumonics Hyperex 150, XeCl excimer laser at 308 nm. The wavelength of the pump pulse was set to 355 nm. The probe laser system consisted of a similar excimer laser pumped dye laser, containing Rhodamine 6G in methanol (λ_{max} =581 nm). The output from this was set to 590 nm, and then passed through a frequency doubling crystal (BBO). A Pellin-Broca prism was used to

separate the 590 nm and 295 nm radiation, such that the probe pulse was free of red light. It is important that the two laser pulses are of the same polarisation. The frequency doubling crystal rotates the plane of polarisation of the laser light, so a Fresnel Rhomb was used to rotate the plane of polarisation of the probe pulse, such that it was the same as the pump light.

The paths of these two beams were guided so as to follow the same path, and hit the sample in exactly the same place. The two beam paths were combined by use of a dichroic mirror which reflects the probe pulse, but transmits the pump pulse. A periscope was used to raise the beams to the height of the triplemate spectrograph, and irises used to assist in aligning the beams.

A large volume of sample was contained in a pump system, flowing through a quartz tube in the Triplemate. The laser paths were arranged such that they hit the sample from below, in the centre of the tube.

The pump and probe pulses are gated, such that the sample is pumped at 355 nm, then probed at 295 nm, after a time interval of 1 μs. Thus although they follow the same paths, and fall on the sample at the same place, the pump and probe pulses do not actually do so at the same time. Within the 1 μs delay between pump and probe, the solution in the tube is effectively stationary, such that the same portion of solution that is pumped in each case is probed. A large total sample volume is used to prevent degradation of the sample over the course of an experiment, due to the high laser powers.

Scattered Raman light along with Rayleigh scattered probe light is collected and focused into a double monochromator. This acts as a filter, to remove the intense scattered probe light. The transmitted Raman scatter then enters another monochromator, the spectrograph stage, where it is diffracted onto a photodiode array, and the signals recorded and fed to a computer. The whole experiment is carried out in the dark to prevent light form other sources also being detected.

The spectrometer was regularly calibrated by using known Raman peaks for solvents such as acetonitrile (1372 cm^{-1}, 2253 cm^{-1}), cyclohexane (1030 cm^{-1}, 1267 cm^{-1}, 1446 cm^{-1}), ethanol (2928 cm^{-1}) and toluene (1028 cm^{-1}, 1210 cm^{-1}, 1380 cm^{-1}, 1605 cm^{-1}) .

The photodiode array can only record a limited region of the spectrum at any one time. The settings of the filter and spectrograph stages can be adjusted to alter the range observed. In this work done, two ranges were used; 1000 cm^{-1} to 2000 cm^{-1}, where carbonyl peaks are found and 2500 cm^{-1} to 3000 cm^{-1} where OH peaks are located.

Due to the low sensitivity of this experiment, many spectra were recorded over a long period of time, and summed. The repetition rate of the lasers was ≈20 Hz, and the total experiment time was approximately 1½ hours for each different spectrum obtained.

The spectra obtained in the pump and probe experiments are dominated by the solvent with a contribution from the ground state of the samples. Thus in each case, an identical experiment, without the initial pump pulse was carried out, and this was subtracted from the pump-probe experiment. This also eliminates any signals due to background.

Ground state Raman spectra of DBM and Parsol 1789 were obtained using only the laser at 355 nm as the probe pulse. For these a spectrum of the solvent only was subtracted to remove the large peaks due to Raman scattering from the solvent. Ground state spectra of the C-methyl and O-methyl derivatives of DBM and Parsol 1789 were obtained in the same way, but using the only the laser at 295 nm as the probe source.

2.8 Diffuse Reflectance Spectroscopy

2.8.1 Introduction[10]

Diffuse reflectance spectroscopy is a technique for measuring the absorbance spectra of compounds and materials that are opaque, heterogeneous or highly scattering; where the usual transmission spectroscopy is not possible. The spectra are obtained by directing the analysing beam at the sample and then studying the reflected light, using the same techniques as in transmission spectroscopy. It is a very valuable technique in that there are many instances where it is useful to obtain the absorbance spectrum of opaque systems, of compounds that are not readily soluble, and in cases where it is the properties as a solid that are of interest.

Diffuse reflectance flash photolysis takes this one step further, by allowing study of transients produced by excitation with a light source, in the same way as conventional flash photolysis. This technique, however, allows study of samples where due to their opacity, the conventional method using transmission spectroscopy would not be possible.

2.8.2 Reflection[10]

2.8.2.1 Types of Reflection

There are two types of reflection which occur from surfaces. Specular, or regular reflection occurs to a certain extent from all surfaces. It is the reflection most commonly seen on mirrors, or highly polished surfaces, and has been well studied and characterised. Specular reflection occurs at an angle equal to the angle of incidence, relative to the normal, and polarised light falling on a surface will be reflected in this manner such that the polarisation is retained, as shown in figure 2.23.

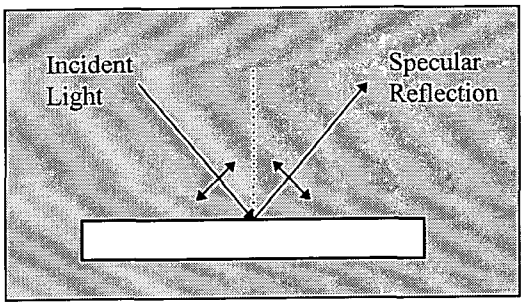

Figure 2.23 Specular reflection

The reflection that occurs from matt surfaces and fine powders will depend on the particulate nature of the medium. It has two components, specular reflection and diffuse reflection. Diffuse reflection arises from light that penetrates below the surface of the sample, suffering multiple scattering at particle boundaries before returning to the surface. Partial absorption occurs within the particles, and hence the diffusely reflected light contains information about the absorption characteristics of the sample. At an absorption band, less diffuse reflection is thus observed, however there is more specular reflection. Diffuse reflection occurs in all directions, as shown in figure 2.24, and polarisation is not retained.

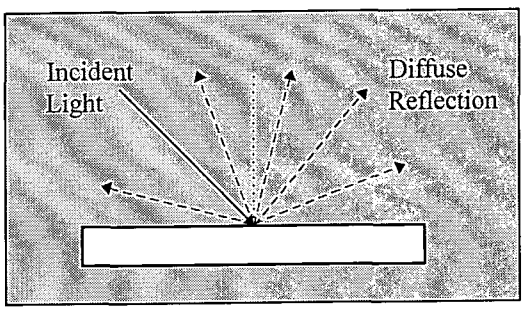

Figure 2.24 Diffuse reflection

There have been many theories to explain diffuse reflection quantitatively. The most commonly used is that known as Kubelka-Munk theory.

2.8.2.2 Kubelka-Munk Theory[10]

Kubelka-Munk theory applies to samples composed of randomly distributed absorbers, and is a good approximation for directed incident beams with weakly absorbing finely divided powders, where the contribution from specular reflection is small.

Kubelka-Munk theory considers two light waves moving in opposite directions, I and J, perpendicular to the irradiated surface at x=0 (see Figure 2.25).

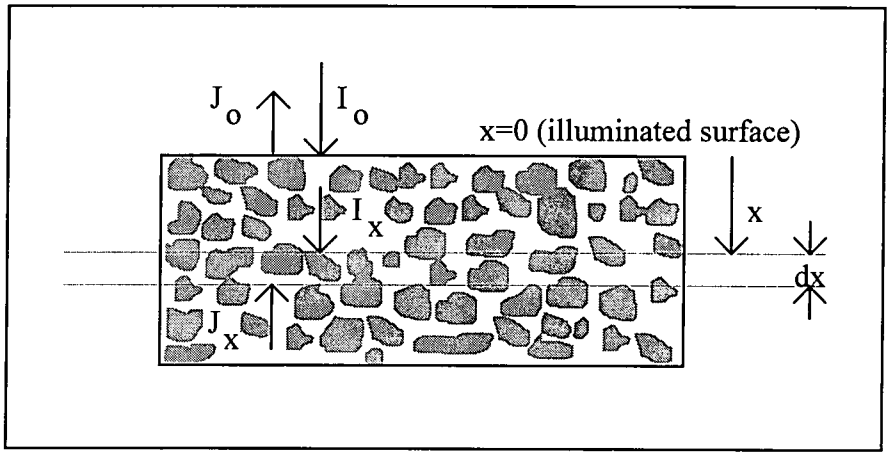

Figure 2.25 Schematic representation of a sample of absorbing and light scattering particles[11].

The changes in intensity of the incident and reflected light beams, on passing dx through the sample, at distance x from the surface, are given by equations 2.18 and 2.19. K is the absorption coefficient, which is related to the extinction coefficient, ε, and concentration, c, by $K = 2\varepsilon c$, and S is the scattering coefficient, both with dimensions of distance^{-1}.

$$dI_X = -I_X(K + S)dx + J_X S dx \qquad \textbf{Equation 2.18}$$

$$dJ_X = J_X(K + S)dx - I_X S dx \qquad \textbf{Equation 2.19}$$

The diffuse reflectance, R, is given by equation 2.20, where I_0 is the incident intensity at the surface, and J_0 is the intensity of the reflected light.

$$R = \frac{J_o}{I_o} \qquad \textbf{Equation 2.20}$$

Equations 2.18 and 2.19 can be solved if K and S are independent of x, i.e. if the sample properties do not change with depth. If the layer is also thick enough such that any further thickness in sample does not affect R, ("optically thick" samples), then the Kubelka-Munk function , F(R) can be derived[10], and is given by equation 2.21.

$$F(R) = \frac{K}{S} = \frac{(1 - R)^2}{2R} \qquad \textbf{Equation 2.21}$$

F(R) vs. wavelength represents the absorption spectrum for diffuse reflectors if S is independent of wavelength. Spectra are displaced by log S, and when S shows some wavelength dependence then the Diffuse reflectance spectrum will not be directly equivalent to the absorption spectrum at all wavelengths.

2.8.3 Obtaining Diffuse Reflectance Spectra

The theory behind the Kubelka-Munk treatment is relatively simple, but it relies on being able to obtain measurements of the pure diffuse reflection from a sample, i.e. without the component of specular reflection. Methods of achieving this are discussed below. There are other practical points which must be considered in order that reliable, reproducible spectra can be obtained, and these are also discussed below.

Kubelka-Munk theory appears to only be valid for samples of weak absorbance[10,12]. In most cases the sample is used highly diluted in a white reference compound, and this can ensure that only small absorbances are present.

2.8.3.1 Eliminating Specular Reflection

There are several methods in which specular reflection can be eliminated. Firstly, if the sample is highly diluted with a non-absorbing white reference compound, and the reflectance spectrum of the diluted sample is measured along with the reflectance spectrum of the pure reference, then the specular reflections of the sample system and the reference are approximately equal. These therefore cancel out, and the ratio gives the pure diffuse reflectance spectrum of the sample. It has been suggested that dilutions with mole fractions in the range 10^{-3} to 10^{-5} are sufficient to ensure the same specular reflectance properties of sample and reference[13]. In some cases such levels of dilution may not be practical, and in these situations other methods can be used.

It has been suggested that if the powder particles are < 10^{-6} m in diameter, and hence of similar dimensions to the wavelength of light, then specular reflectance is almost entirely eliminated[14]. This appears to be a good way to eliminate specular reflectance in cases where high dilution is not practical due to, for example, low absorbances of the sample.

As mentioned previously, specular reflection retains the polarisation properties of the incident light. Diffusely reflected light, however, changes its state of polarisation after multiple scattering at irregular particle boundaries. Hence on shining plane polarised light at the sample (by placing a polariser in the incident beam), the resulting specular reflection is plane polarised, and the diffuse reflectance is not polarised. If a polarising sheet is then placed at right angles to the plane of polarisation of the reflected light, the specular reflection is therefore eliminated. The diffuse reflection is partially transmitted, and thus the reflected light observed is the pure diffuse reflection with no contribution from specular reflection.

2.8.3.2 Sample Preparation

In most cases, a non-absorbing, white standard is used to dilute a solid sample, and to allow calculation of the pure diffuse reflection. Use of a reference also removes any need to collect and measure all the diffusely reflected light. Diluted powdered samples can typically be prepared in two ways. A solution of the compound to be studied can be mixed with the insoluble reference, and the solvent evaporated such that the compound is deposited onto the reference compound. Insoluble compounds can be simply ground together with the reference.

The amount of scattering, and thus the intensity of diffuse reflectance, from a powdered sample is critically dependant on the size of the particles[13]. Smaller particles result in a larger scattering coefficient, and hence less diffuse reflection. It is therefore essential that the sample (diluted in the reference compound) and the reference have identical particulate properties. Samples must have particles of the same size to enable direct comparisons, which can be a difficult task to accomplish in practice. If samples are prepared by grinding together the sample and the reference, this must be done under carefully controlled conditions to ensure identical particle sizes.

Smaller particle sizes can be favourable, in terms of reducing the amount of specular reflection, as described above. However , the scattering coefficient S, begins to show a wavelength dependence as the grain size decreases, as shown in figure 2.26, which can be quite dramatic in the visible and UV regions. Hence coarse grain sizes are required for the Kubelka-Munk function to be valid, particularly at small wavelengths.

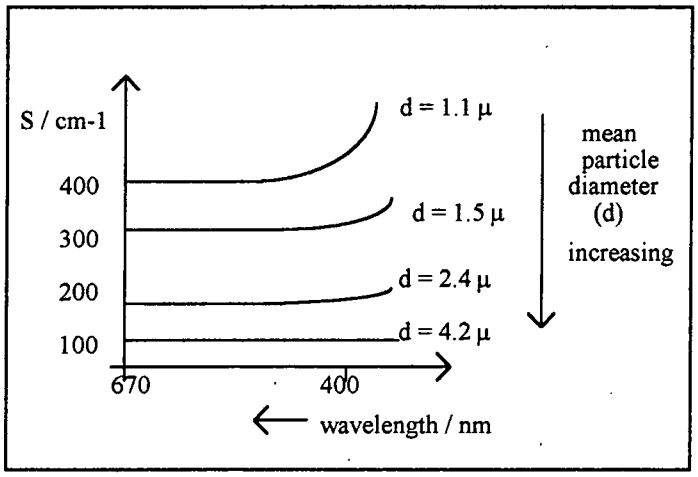

Figure 2.26 Schematic representation of the dependence of the scattering coefficient, S, on the wavelength for various particle sizes[13]

(Example used is ground didymium-glass filter)

Perhaps more important is that the samples have the same packing density, and uniformly flat surfaces. Similar procedures could be used, as when making discs for infra-red spectroscopy, but bearing in mind that samples must be "optically thick", with no transmission of light, in order to ensure validity of the Kubelka -Munk theory.

Zeitlin[15] has used filter paper instead of a powdered sample, and obtained reproducible spectra in the ultraviolet region. His method is to dip pieces of filter paper into solutions of the sample under consideration, and then allow the solvent to evaporate. Untreated filter paper, cut from the same piece, is then used as the reference. Whether this method produces optically thick samples is unclear, especially as Zeitlin also describes using samples prepared in the same way for transmission spectra, however these results seem to be consistent and agree with spectra obtained by transmission measurements.

2.8.3.3 White Reference Compounds[13]

In most cases, a non-absorbing, white reference compound is used to dilute a solid sample, and to allow calculation of the pure diffuse reflection. The most important properties of the standard, are that it must have a reproducible reflectance spectrum itself, and not react or interact with the compound under study, unless these interactions are part of the system to be studied.

The most commonly used standard, for simple solid compounds is magnesium oxide (MgO), however this does not seem to be suitable for use in the UV region, as its diffuse reflectance spectrum in this region seems to vary with time[13]. Frosted glass standards are constant and convenient, but their reflectances decrease sharply below approximately 350 nm, as they absorb UV light. Other possible reference compounds include Li_2CO_3, NaF, LiF, NaCl, $MgSO_4$ etc. The choice of standard will depend

very much on the compounds to be studied, and the spectral region of interest. Silica and microcrystalline cellulose have been commonly used as substrates for diffuse reflectance flash photolysis in recent years, for example see references 16 and 17.

The action of mixing together the sample and the reference can result in adsorption of the sample onto the reference to some extent. Thus in the same way as the spectra of compounds in solution are different to that of the vapour state due to interaction of the solvent molecules, if the dilution is high the spectra obtained by diffuse reflection can be of the adsorbed molecules. Therefore spectra can be different from those obtained by transmission spectroscopy in an inert solvent. The reflectance spectrum of an adsorbed material can be strongly affected by moisture or other solvents, because of a change in particle size, or an interaction with the compound under study.

2.8.3.4 Experimental set-up[11]

A standard transmission spectrometer can be used for measuring diffuse reflectance, with slight modifications; indeed, many attachments are commercially available. The conversion is achieved by reflecting the analysing beam towards the sample, focusing with a lens if necessary, and then reflecting the diffuse beam (with or without specular contribution) back into the original path, towards the detector, as shown in figure 2.27.

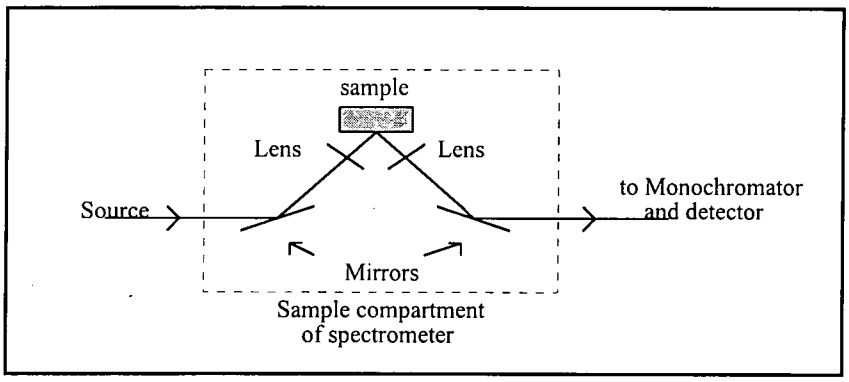

Figure 2.27 Conversion of a conventional transmission spectrometer for measuring diffuse reflectance spectra

Polarisers, as described earlier could be inserted if required, and other modifications could easily be introduced. Clearly, the samples must be placed in identical positions for each experiment. The spectrum of the reference compound is measured separately, and the Kubelka-Munk theory applied. Due to the low light levels that are produced, it is especially important to eliminate stray light.

The angles of incidence and collection have a direct effect on the spectra obtained[18], and thus it is necessary to use exactly the same set up, particularly for measuring the reference spectrum, and in order to be able to make quantitative comparisons between different compounds.

A slightly different set-up collects the reflected light at an angle different to that on the incident radiation, such that much of the specular reflection is eliminated. Use of an integrating sphere is also popular, but this causes problems if the sample luminesces, and is more difficult to set up, with no improvements in spectral quality[13].

2.8.3.5 Experimental Details for Diffuse Reflectance Absorption Spectroscopy used in this work

Diffuse reflectance absorption spectra were obtained using the LS50B Luminescence Spectrometer from Perkin Elmer. Samples were contained in a home-built sample holder with quartz window, and positioned in a home-built accessory. The positioning of the sample was such that the specular reflection was not collected, as shown in figure 2.28.

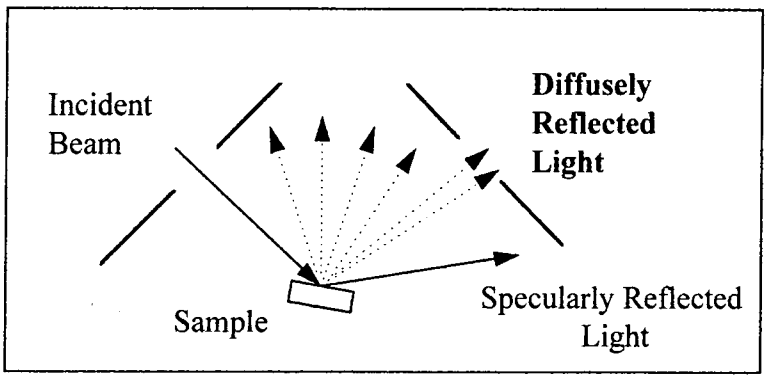

Figure 2.28 Diffuse reflectance spectroscopy using the LS50B luminescence spectrometer

The spectrometer was operated in the synchronous scan mode, such that analysis of collected light was carried out at the same wavelength as the incident light. Slit widths were varied depending on the concentrations of DBM in samples, however were typically used at 2.5mm setting for the excitation slit, and the 0mm setting (minimum width) for the emission slit. Reflectance spectra of each sample, R_S and reference, R_{Ref} were collected separately under identical conditions, and the pure diffuse reflectance, R, due to DBM at each wavelength was calculated as the ratio of these two spectra, as shown in equation 2.22. Kubelka-Munk theory was then applied for each wavelength, as using equation 2.21, to obtain spectra equivalent to the absorption spectra of the samples.

$$R = \frac{R_S}{R_{Ref}}$$ **Equation 2.22**

2.8.4 Diffuse Reflection Flash Photolysis

Diffuse Reflectance Flash photolysis allows opaque samples to be studied in the same manner as transparent samples in normal flash photolysis, but using diffuse reflectance spectroscopy in place of transmission spectroscopy.

2.8.4.1 Theory[10,19]

For an opaque sample, on irradiation with the laser pulse, the initial transient concentration decreases exponentially with increasing penetration depth into the sample. This is true for low laser powers, high ground state concentrations and low extinction coefficients. The Kubelka-Munk function can not be derived as shown earlier to give equation 2.21, because K varies exponentially with x. In this case the total absorbance of the system at wavelength a, after excitation by a laser pulse is given by equation 2.23 (reference 10), where R_B^a is the reflectance of the system before excitation, $R^a(t)$ is the reflectance of the system at time t after excitation and R_T^a is the relative transient reflectance. This equation is very similar to that used in conventional flash photolysis, and hence the same analysis of the results is possible.

$$\frac{\left[R_B^a - R^a(t)\right]}{R^a(t)} = 1 - R_T^a$$ **Equation 2.23**

If higher laser powers are used, a homogenous layer of transient can be produced, and the Kubelka-Munk function described in equation 2.21 can be used, provided the layer produced is "optically thick".

2.8.4.2 Possible Experimental Set-Ups

The basic experimental technique involves a laser and monitoring source directed at the sample, with a lens to collect the diffusely reflected light and direct it into the monochromator and detector e.g. a

photomultiplier tube. The exact geometrical arrangement of these can be one of a set of possible combinations.

Figure 2.29 [10,20] shows the laser path at 45° to the sample, and the analysing lamp at 90° to the sample. The maximum diffusely reflected light is collected, but not the specular reflection. The monochromator angle must be adjusted so that the laser specular reflection does not enter it, as this could be damaging to the detector, and overload the signal. Diffuse reflectance caused by the laser light is eliminated by using a chemical filter, if this is appropriate, or corrected for by measuring the signal observed without the analysing light.

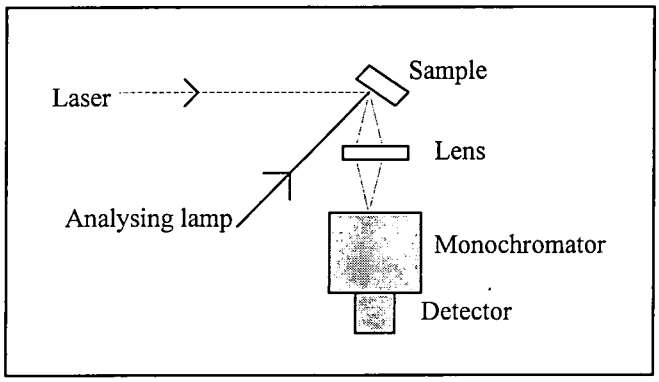

Figure 2.29 Set-up for diffuse reflectance flash photolysis (1)

Another possible set-up is to have the exciting light at 90° to the sample, as shown in Figure 2.30 [21]. This has the advantage of preventing the specular reflection from the laser entering the detector, but care must be taken to prevent specular reflection from the analysing lamp entering the monochromator.

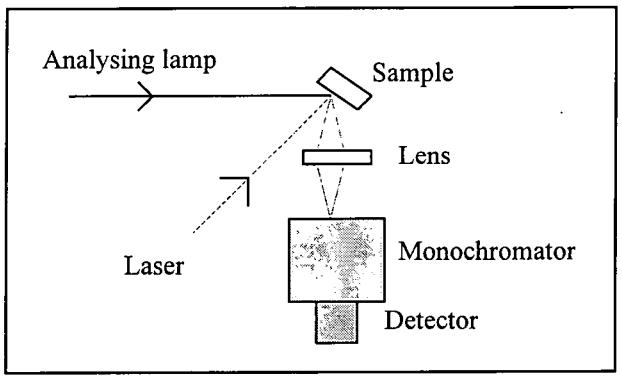

Figure 2.30 Set-up for diffuse reflectance flash photolysis (2)

The third possibility is to have the analysing light at 90° to the sample as shown in figure 2.31 [22], again reducing the chance of laser light and specular reflection from the analysing lamp entering the detector.

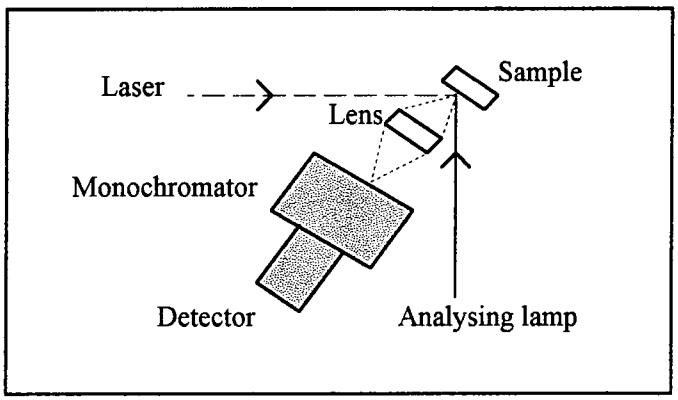

Figure 2.31 Set-up for diffuse reflectance flash photolysis (3)

In each case, transient decays and transient difference spectra are obtained in the same manner as that for transmission flash photolysis, (as described in section 2.5) Diffuse reflectance absorption spectroscopy, as described earlier, can be used to obtain ground state absorption spectra, and thus obtain transient absorption spectra.

Using such experimental set-ups, there have been many literature reports describing nanosecond flash photolysis on opaque or highly scattering materials, with results obtained often comparable to those obtained using transmission flash photolysis[10]. For example the photochemistry of microcrystalline benzophenone has been studied[20], and the photochemistry of ketones, such as acetophenone, adsorbed on surfaces such as zeolites has been investigated using this technique[21,23] .

2.8.5 Experimental Details for Diffuse Reflectance Flash Photolysis used in this work

The experimental set-up used for diffuse reflectance flash photolysis in this work is shown in figure 2.32, and is based on the apparatus shown in figure 2.31.

The sample is contained in a home-built holder with quartz window. The excitation source is a frequency tripled Nd^{3+}:YAG laser, as described in section 2.5.2, with pulse energies <5 mJ, filtered by filter B to remove residual 532 nm light, positioned at > 45° to the sample, to control the path of the specular reflection, and increase the irradiated area. The analysing lamp used was a 150 W xenon lamp, (described earlier), filtered by filter F, positioned at approximately 45° to the sample, and covering a slightly smaller region of the sample than that excited by the laser. Diffusely reflected light was collected at 90° to the sample into a monochromator and PMT, and recorded in the same manner as for transmission flash photolysis, as described earlier.

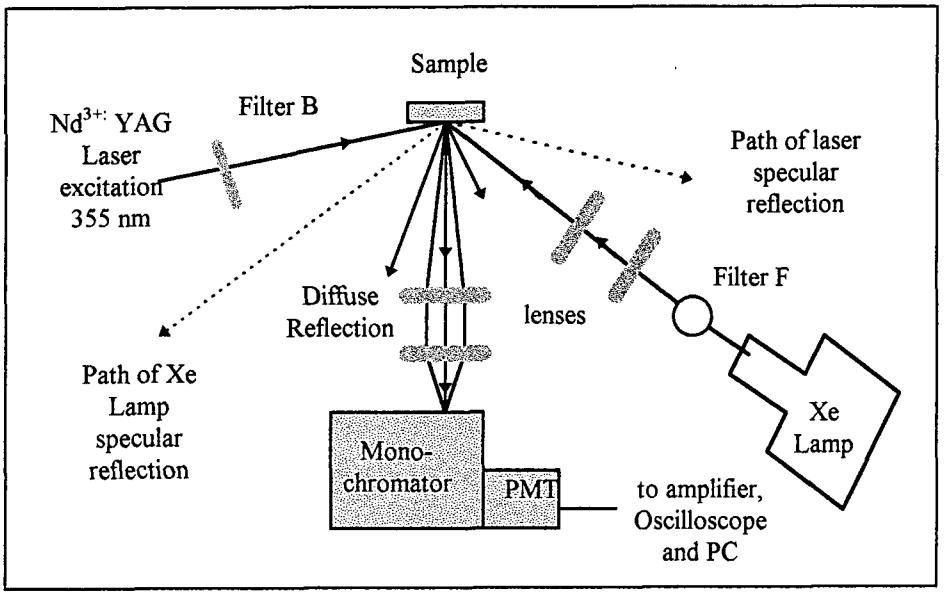

Figure 2.32 Apparatus used in this work for diffuse reflectance flash photolysis

Data analysis was carried out in exactly the same manner as for transmission flash photolysis, using equation 2.3, by assuming the validity of equation 2.23, where the transient concentration in the sample is assumed to vary exponentially with depth.

2.9 Singlet Oxygen Detection

Singlet oxygen measurements were obtained by direct detection of 1269 nm luminescence using time-resolved experiments. Dibenzoylmethane used in these experiments was recrystallised from ethanol to ensure purity.

2.9.1 Quantum Yields of Singlet Oxygen Formation

The experimental set-up is shown in figure 2.33. Much of the equipment has been described previously in section 2.5, and only brief details will be given in this section.

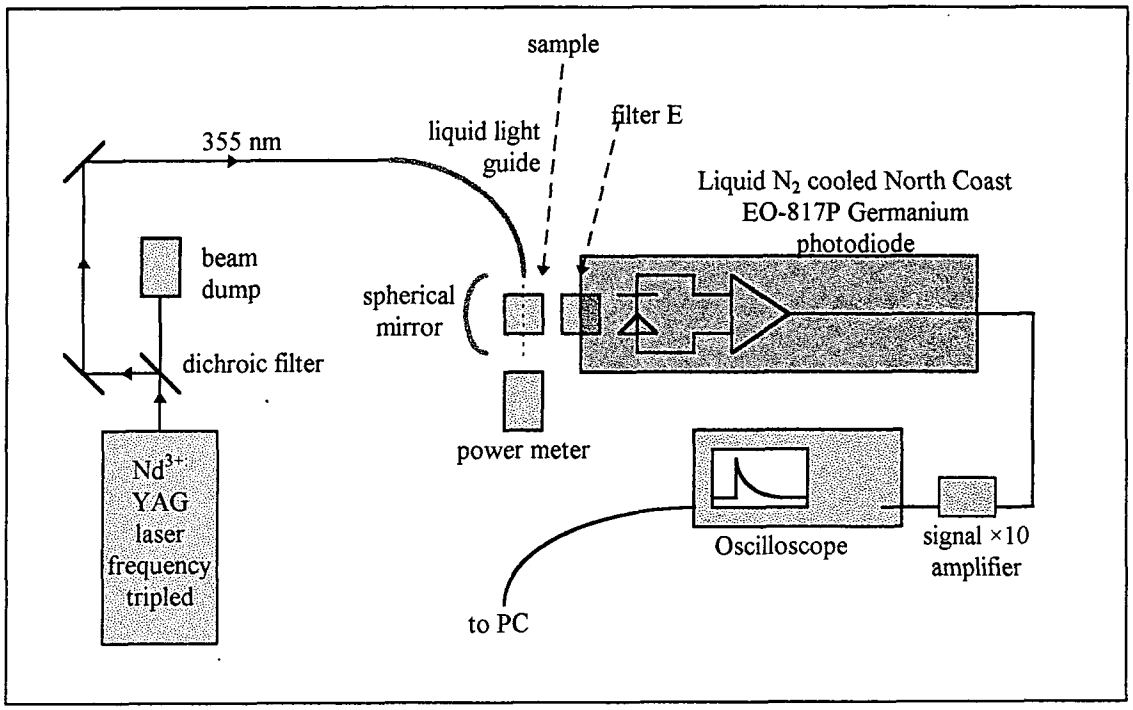

Figure 2.33 Schematic diagram of the experimental set up for measuring singlet oxygen photosensitisation quantum yields

The samples (of absorbance ≈ 0.3 at 355 nm) were contained in quartz fluorescence cuvettes of pathlength 1cm, and excited with laser light from a frequency tripled Nd^{3+}:YAG laser at 355 nm, as described earlier. Pulse energies at the sample were less that 0.3 mJ, and the laser power was varied by changing the energy of the pump lamps for the Nd^{3+}:YAG laser. Relative laser energies were measured with a power meter, as described earlier with the sample removed.

Singlet oxygen luminescence was collected perpendicular to the excitation pulse, and detected using a liquid nitrogen cooled germanium photodiode, (North Coast Scientific Corp. model no. E0-817P). A spherical mirror behind the sample increased the amount of light collected, and filter E, limits detection of scattered laser light, and sample fluorescence if present.

The signal was passed through a x10 amplifier, and the data recorded, using ac coupling, on a digital storage oscilloscope, triggered by a photodiode detecting the laser pulse. Analysis of the decays was performed on a PC to fit a single exponential decay (GraFit).

After obtaining singlet oxygen decay traces, a known singlet oxygen quencher (such as sodium azide) was added if soluble in the solvent, or the sample degassed by the freeze-pump-thaw method, to ensure that the signals obtained were entirely due to singlet oxygen.

Singlet oxygen quantum yields for photosensitisers, (Φ_Δ), are defined as given in equation 2.24.

$$\Phi_\Delta^{Sens} = \frac{\text{Number of molecules of } {}^1O_2 \text{ generated}}{\text{Number of photons absorbed by sensitiser}} \qquad \textbf{Equation 2.24}$$

In order to calculate this, a standard compound, with a known quantum yield of singlet oxygen production, (Φ_Δ^{Std}), is used, defined as shown in equation 2.25.

$$\Phi_\Delta^{Std} = \frac{\text{Number of molecules of } {}^1O_2 \text{ generated}}{\text{Number of photons absorbed by standard}} \qquad \textbf{Equation 2.25}$$

Thus if the standard sample and the test sample are irradiated under exactly the same conditions (i.e. in the same solvent, and with the same sample positioning, same laser power, same cuvette, same sample absorbance at excitation wavelength, etc.) then the denominators of equations 2.23 and 2.24 will be identical. Therefore the quantum yield of singlet oxygen generation by the sensitiser can be calculated as shown in equation 2.26.

$$\Phi_\Delta^{Sens} = \frac{\text{No. of molecules of } {}^1O_2 \text{ generated by sensitiser}}{\text{No. of molecules of } {}^1O_2 \text{ generated by standard}} \times \Phi_\Delta^{Std} \qquad \textbf{Equation 2.26}$$

The amount of luminescence at 1269nm observed is directly proportional to the singlet oxygen concentration, and hence equation 2.26 can be re-written as equation 2.27.

$$\Phi_\Delta^{Sens} = \frac{\text{luminesence signal observed from sensitiser}}{\text{luminesence signal observed from standard}} \times \Phi_\Delta^{Std} \qquad \textbf{Equation 2.27}$$

Singlet oxygen quantum yields, (Φ_Δ), were measured relative to standard sensitisers with known Φ_Δ values. (Because of the solvent dependence of singlet oxygen lifetimes and luminescence quantum yields, it was essential to measure singlet oxygen luminescence from standards and samples in the same solvent.) For each sample, the intensity of the maximum singlet oxygen signal was obtained by fitting an exponential curve to the decay trace, and extrapolating back to t=0. The intensity was measured over a range of laser powers, and the slope of a graph of laser power vs. intensity was calculated using least

squares analysis. The singlet oxygen quantum yield of a sensitiser, Φ_{Δ}^{Sens}, is then given by equation 2.28.

$$\Phi_{\Delta}^{Sens} = \Phi_{\Delta}^{Std} \times \frac{M^{Sens}}{M^{Std}} \qquad \textbf{Equation 2.28}$$

where Φ_{Δ}^{Std} is the quantum yield of singlet oxygen production for the standard and M^{Std} and M^{Sens} are the gradients of the singlet oxygen intensity vs. laser power graphs for standard and sensitiser. If the absorbances of the two solutions were slightly different, this was taken into account in the calculation, by using the modified equation 2.29, where Abs^{Std} and Abs^{Sens} are the absorbances at 355nm of standard and sensitiser respectively. This approximated equation is valid for small absorbances.

$$\Phi_{\Delta}^{Sens} = \Phi_{\Delta}^{Std} \times \frac{M^{Sens}}{M^{Std}} \times \frac{Abs^{Std}}{Abs^{Sens}} \qquad \textbf{Equation 2.29}$$

Standards used, and their quantum yields[24] are given in table 2.2.

Standard	Solvent	Φ_{Δ} values	Φ_{Δ} value used (average)
Acridine	Acetonitrile	0.82 in O_2	0.82
Anthracene	Benzene	0.61 – 1.1	0.88
	Methanol	0.7	0.7
C_{60}	Benzene	0.76 – 1.0	0.97
Rose Bengal	Acetonitrile	0.54, 0.83	0.54
	Methanol	0.8 - 0.91	0.8

Table 2.2 Standard quantum yields of singlet oxygen generation by photosensitisation[24]

2.9.2 Variable Oxygen Concentration

Different concentrations of dissolved oxygen were achieved by varying the pressure of oxygen in the solution. Samples were first degassed, then exposed to a controlled pressure of oxygen, sealed and agitated to allow adequate mixing. The pressure was measured using a MKS Baratron pressure gauge, and correction was made for the partial pressure of solvent vapour using an empirical relationship between pressure and temperature[25].

2.9.3 Singlet Oxygen Quenching

Rate constants for quenching of singlet oxygen were measured using an efficient sensitiser, zinc 2,9,16,23-tetra-tert-butyl 29H 31H-phthalocyanine, to generate singlet oxygen. The experimental set-up was similar to that shown in figure 2.24, but with laser excitation at 680 nm. This radiation was produced by a Nd^{3+}:YAG pumped dye laser (Lambda-Physik FL2002) containing Pyridine 1 (tuning range for 532 nm excitation = 667-736 nm). This system was chosen such that singlet oxygen could be generated by exciting the sensitiser at a wavelength at which dibenzoylmethanes do not absorb.

Singlet oxygen lifetimes were then measured at various concentrations of quencher in the range 0-0.1 mol dm^{-3}, for identical solutions of sensitiser, of absorbance $\approx$ 0.2 at 680 nm, in a 1 cm pathlength cell. The second order rate constant for quenching of singlet oxygen, k_Q was calculated from the slope of a graph of quencher concentration vs. decay rate constant, according to equation 2.30.

$$k_\Delta = k_D + k_Q[Q] \qquad \textbf{Equation 2.30}$$

where k_Δ is the observed rate constant for decay of singlet oxygen, k_D is the rate constant of singlet oxygen decay in the absence of the quencher, k_Q is the quenching rate constant, and [Q] is the concentration of quencher.

2.10 Sample Degassing

No sample degassing was carried out to remove dissolved oxygen unless otherwise specified. In samples where degassing was carried out, this was done using the freeze-pump-thaw method. This involves freezing the solution to 77 K, evacuating the sample, and then allowing the sample to warm to room temperature. This is repeated several times, until no change in pressure is noted on opening the system to vacuum.

2.11 Temperature Control

All work has been carried out at room temperature without regulation, unless otherwise specified. The cryostats previously described were used to study samples at temperatures below room temperature. Flash photolysis at temperatures above room temperature was carried out by using a heated water bath to pump water at the required temperature into a jacket surrounding the sample. This contained holes to allow the laser and monitoring lights to reach the sample.

2.12 Method of separation of the E and Z isomers of O-Methyl DBM

By comparing the UV/Visible absorption spectrum of O-methyl dibenzoylmethane with those reported in the literature for the individual E and Z isomers[26], it is apparent that the O-methyl DBM consists mainly of the thermodynamically less stable Z isomer.

A solution of the O-Me DBM in 1:1 diethylether : isopentane was flowed through a column of silica gel in the dark, and samples collected at regular intervals. By studying the absorption spectra of the consecutive elucidated samples, a slight shift of the λ_{max} towards longer wavelengths followed by a progressive shift towards smaller wavelengths is observed. This indicates that the isomer composition of the consecutive samples changed from mostly the Z-isomer to entirely the Z-isomer to entirely the E-isomer. Complete discrete separation of the two isomers did not occur, because of the rate of Z→E isomerisation on the silica gel, i.e. the isomers were not in fact separated from a mixture of the two, but the E-isomer formed by conversion of the Z-isomer on the silica gel. The solutions of different isomers were kept in the dark, and showed no change in the absorbance spectra over a period of weeks.

2.13 Preparation of Emulsions

2.13.1 Sunscreen formulations

The nature of commercial sunscreen formulations varies considerably depending on the desired cosmetic and protective properties of the product. Sunscreen compounds can be incorporated in a great variety of vehicles, including emulsions, gels, sticks, sprays, and ointments[27]. There is a huge variety of preparations for each category involving different ingredients and combinations, many of which are the subject of commercial patents. This will be further discussed in chapter 5.

With this in mind, a model emulsion system was chosen for this study, based on a United States FDA standard sunscreen formulation for SPF testing[28]. This is an oil in water emulsion containing homosalate (homomenthyl salicylate) as the sunscreen compound, and having the composition as described in table 2.3.

Ingredient	Percentage by weight
Lanolin (wool fat)	5.00
Homosalate (homomenthyl salicylate)	8.00
White petrolatum (mineral oil)	2.50
Stearic Acid (otadecanoic acid)	4.00
Propylparaben (propyl 4-hydroxy benzoate)	0.05
Methylparaben (methyl 4-hydroxy benzoate)	0.10
Edeate disodium (Ethylene diamine tetraacetic acid, disodium salt ; EDTA)	0.05
Proplyene glycol (1,2 propanediol)	5.00
Triethanolamine	1.00
Purified Water	74.30

Table 2.3 Composition of the FDA standard sunscreen[28]

The purpose and properties of each ingredient, as suggested in reference **29**, is given in table 2.4, and further information can be found in chapter 5.

Ingredient	Description
Lanolin	Fatty Substance
Homosalate	Sunscreen
White Petrolatum	Fatty Substance
Stearic acid	Fatty Substance Auxiliary Emulsifying agent
Propylparaben	Preservative
Methylparapen	Preservative
Edeate disodium	Chelate Preservative Antioxidant
Propylene glycol	Solvent Active Substance
Triethanolamine	Emulsifier Neutraliser
Water	Solvent

Table 2.4 Purpose of ingredients in the standard sunscreen[29]

2.13.2 Preparation of the emulsion

The preparation described above was adapted to incorporate DBM in varying concentrations, by substituting it for the homosalate sunscreen. It was decided that the percentage by weight of the other ingredients would remain constant, and varying concentrations of DBM would be achieved by adding appropriate amounts, and varying the water content accordingly. Due to the small nature of the other ingredient quantities, this did not introduce a large variation in the emulsion nature for varying DBM concentrations.

It was also decided to exclude the paraben ingredients, as they absorb strongly in the UV region, interfering with spectral analysis. The main purpose of these ingredients is to act as preservatives, to increase the shelf-life of the product, and the small quantity present is unlikely to greatly alter the nature of the emulsion.

Thus the final procedure for preparing the emulsions used is described below

Ingredients for parts A and B (see table 2.5) were weighed into separate containers, and heated using a stirrer hot-plate to approximately 80°C, with constant stirring using magnetic fleas. Part A was slowly added to part B, with continual stirring of the mixture, and frequent reheating of part A to maintain the temperature. The heat was switched off, and the mixture continually stirred until at room temperature, and the magnetic fleas removed. This resulted in a white creamy emulsion.

	Ingredient	weight / g	% by weight
A	Lanolin (wool fat)	1.00	5.00
	Dibenzoylmethane	x	y
	Mineral oil	0.50	2.50
	Stearic Acid (otadecanoic acid)	0.80	4.00
B	Ethylene diamine tetraacetic acid, disodium salt (EDTA)	0.01	0.05
	Proplyene glycol (1,2 propanediol)	1.00	5.00
	Triethanolamine	0.20	1.00
	Purified Water	16.49-x	82.45-y
TOTAL		20g	100%

Table 2.5 Composition of the model sunscreen

A range of concentrations from 0-5% by weight of dibenzoylmethane were made using this method. The concentrations quoted are guidelines, and emulsion natures varied slightly from sample to sample. The

emulsions used had the consistency of a smooth cream that did not pour. However, overnight, samples tended to become milky and less viscous, indicating that the emulsions were not stable for extended periods of time. Samples were therefore tested as soon as possible after preparation. This problem largely prevented DBM stability studies, due to the changing nature of the emulsion with time.

2.14 UV/Visible Absorption Spectroscopy of Samples on Transpore Tape

Transpore Tape is a polymer-based surgical adhesive tape, manufactured by 3M. It has a regular textured surface with holes, intended to simulate the skin surface.

The absorption spectra of sunscreen formulation samples on Transpore Tape were measured using the following method. Samples were applied evenly onto a piece of Transpore Tape adhered to a quartz slide, and then spread evenly over the surface of the tape. Absorption spectra were measured using the UV/Visible absorption spectrometer, as described in section 2.1, using a reference of Transpore Tape on quartz.

2.15 Preparation of Cellulose Samples

Solutions of known concentration of DBM in methanol were added to 1 g samples of cellulose, and mixed to form a paste. These were then placed under vacuum, and heated gently until all the methanol had evaporated, removing the samples occasionally to stir. Samples were stored under vacuum to prevent the absorption of moisture.

2.16 Source and Quality of Chemicals used

Chemicals used are listed here in alphabetical order, by the names they are most commonly known by, along with the source, quality, and any purification details.

1,1,2-Trichlorotrifluoroethane	B.D.H. SpectrosoL 99.9%
2-Methylbutane	Aldrich 99+%
4-Methoxyacetophenone	Aldrich 99%
4-Tertiary-butyl acetophenone	Aldrich 98%
Aberchrome 540	Aberchromics Ltd.
Acetonitrile	Sigma-Aldrich HPLC grade 99.9+% , dried over molecular sieve

Acetophenone	Aldrich
Acridine	Aldrich
Anthracene	Aldrich
Benzene	Aldrich 99.9%
C-methyl dibenzoylmethane	Prof M J Perkins, Royal Holloway & Bedford College
C-methyl Parsol 1789	Prof M J Perkins, Royal Holloway & Bedford College
C_{60}	Acros 99.9%
Carbon Tetrachloride	M & B
Cellulose	Fluka Cellulose Powder DS-0, dried at 50°C under vacuum
Copper Sulphate	Aldrich
Cyclohexane	B.D.H. GPR 99%
Dibenzoylmethane	Aldrich 98%
Dichloromethane	Aldrich
Diethyl Ether	B.D.H. AnalaR 99.5%
Ethanol	Hayman Ltd. Absolute Alcohol AR Quality 99.9%
Ethylene diamine tetraacetic acid, disodium salt, (EDTA)	Aldrich
Hydrochloric Acid (conc.)	B.D.H. GPR
Lanolin	Aldrich
Methanol	Analar
Methyl cyclohexane	Aldrich 99%
Methylparaben	Aldrich 99%
Mineral Oil	Aldrich
Molecular Sieve	Aldrich 4A beads 1/16-inch 8-12 mesh
N,N-diethyl toluamide	Aldrich 97%
N,N-dimethyl formamide (DMF)	Sigma-Aldrich 99.9%
O-methyl dibenzoylmethane	Gift, Prof M J Perkins, Royal Holloway & Bedford College
O-methyl Parsol 1789	Gift, Prof M J Perkins, Royal Holloway & Bedford College
Parsol 1789 (4-methoxy-, 4'-tertiary-butyl-Dibenzoylmethane)	Gift, Prof M J Perkins, Royal Holloway & Bedford College
Potassium Bromide	Aldrich
Potassium Hydroxide	B.D.H. GPR
Proplyene Glycol (1,2 propanediol)	Aldrich 99%
Propylparaben	Aldrich 99%
Pyridine	Aldrich 99+%
Rose Bengal (3,4,5,6-tetrachloro-2',4',5',7'-tetraiodo flouorescein)	Aldrich, 93%
Silica Gel	Silica Gel 60, Particle size 0.040-0.063mm
Sodium Azide	B.D.H. 99%

Sodium Nitrate	Aldrich
Stearic Acid	Aldrich 95%
Toluene	B.D.H. Analar 99.5%
Triethanolamine	Aldrich
Triton-X 100	Aldrich
Triton-X 100 Reduced	Sigma
Water	purite water (purified using purite water polisher)

2.17 References

[1] Variable Temperature liquid-nitrogen Cryostat DN1 704 Operator's Handbook, Oxford Instruments

[2] Murov S L, Carmichael I, Hug G L, "*Handbook of Photochemistry*", 2nd Edition, Marcel Dekker Inc., 1993

[3] Perkin Elmer LS50 B User's Manual

[4] Heller H G, Langan J R, "Photochromic Heterocyclic Fulgides part 3. The use of (E)-α-(2,5-Dimethyl-3-furylethylidene) (isopropylidene) succinic Anyhdride as a Simple Convenient Chemical Actinometer", *J. Chem. Soc., Perkin trans.*, **2** (1981), 341

[5] Information available on request from Aberchromics Ltd., School of Chemistry and Applied Chemistry, University of Wales College of Cardiff

[6] Wintgens V, Johnston L J, Scaiano J C, "Use of a Photoreversible Fulgide as an Actinometer in One- and Two-laser Experiments", *J. Am. Chem. Soc.*, **110** (1988), 511

[7] Colthup N B, Daly L H, Wiberley S E, "*Introduction to Infra-Red and Raman Spectroscopy*", 3rd Edition, Academic Press, 1990

[8] Bensasson R V, Land E J, Truscott T G, "*Excited States and Free Radicals in Biology and Medicine*", Oxford University Press, 1993

[9] Clark R J H, Hester R E, "*Advances in Spectroscopy*", volume 8, "*Time Resolved Spectroscopy*", , John Wiley & Sons Ltd., 1989, chapter 4

[10] Wilkinson F, Kelly G, Chapter 12 in "*Handbook of Organic Photochemistry*", ed. Scaiano J C, volume I, CRC Press, 1989, Chapter 12

[11] Wendlandt W , Hecht H G, "*Reflectance Spectroscopy*", John Wiley & Sons, 1966

[12] Griffiths T R, Lott K A K, Symons A C R, "Diffuse reflectance Spectrophotometry in the Ultraviolet Using Powdered salts", *Anal. Chem.*, **31** (1959), 1338

[13] Kortüm G, Braun W, Herzog G, "Principles and Techniques of Diffuse Reflectance Spectroscopy", *Angew. Chem. Int. Ed. Eng*, **2** (1963), 333

[14] Kortüm G, Braun W, *Z. physik. Chem. (Frankfurt),* **18** (1959), 242. (Quoted in Reference **15**)

[15] Zeitlin H, Niimoto A, "The Reflectance Spectrum of Acetone-2,4-dinitrohydrazone", *Nature*, **181** (1958), 1616

[16] Wilkinson F, Worrall D R, Williams S L, "Primary Photochemical Processes of Anthracene Adsorbed on Silica Gel", *J. Phys. Chem.*, **99** (1995), 6689

[17] Vieira L F, Oliveira A S, Wilkinson F, Worrall D, "Photophysics of Cyanine Dyes on Surfaces - A new emission from aggregates of 2,2'-cyanines adsorbed onto microcrystalline cellulose", *J. Chem. Soc., Faraday Trans.*, **92** (1996), 1217

[18] Stenium A S, *J. Opt. Soc. Am*, **47** (1957), 995 (Quoted in Reference 11)

[19] Oelkrug D, Honnen W, Wilkinson F, Willsher C J, "Modelling of Transient Production and Decay following Laser Excitation of Opaque materials", *J. Chem. Soc., Faraday Trans. 2,* **83** (1987), 2081

[20] Wilkinson F, Willsher C J, "Detection of Triplet-Triplet Absorption in Microcrystalline Benzophenone by Diffuse-Reflectance Laser Flash Photolysis", *Chem. Phys. Lett.*, **104** (1984), 272

[21] Kessler R W, Wilkinson F, "Diffuse Reflectance Triplet-Triplet Absorption Spectroscopy of Aromatic Hydrocarbons Chemisorbed on γ-Alumina", *J. Chem. Soc., Faraday Trans. 1*, **77** (1981), 309

[22] Wilkinson F, Willsher C J, "Intrazeolite Photochemistry. IV. Studies of Carbonyl Photochemistry on the hydrophobic zeolite-Silicate using time resolved Reflectance techniques", *Can. J. Chem.*, **64** (1986), 539

[23] Turro N J, Gould I R, Zimmt M B, C. Cheng, "Ketone Photochemistry on Solid Silica. A Diffuse Reflectance Laser Flash Photolysis Study", *Chem. Phys. Lett.*, **119** (1985), 484

[24] Wilkinson F, Helman W P, Ross A B, "Quantum Yields for the photosensitised formation of the lowest electronically excited singlet state of Molecular Oxygen in Solution", *J. Phys. Chem. Ref. Data.*, **22**, No 1, 1993

[25] Weist R C, "*Handbook of Chemistry and Physics*", 61st edition, CRC Press, Florida, 1980

[26] Kiuchi F, Chen X, Tsuda Y, "Z-E Isomerisation of β-Methoxychalcones: Preferred Existence of E-Isomers in Naturally Occurring β-Methoxychalcones", *Chem. Pharm. Bull.*, **38** (1990), 1862

[27] Balsam M S, Chapter 7, *"Sunscreen Preparations"* in *"Cosmetics Science and Technology"* 2nd Edition, Volume 1, Edward Sagarin, 1972, pg. 241

[28] "Sunscreen drug products for over-the-counter human use", Federal Register, **58**, No. 90, (1993), Proposed rules, pg. 28299

[29] Saninio E-L, "The Ingredients, safety, efficacy and stability of sunscreens", *National Consumer Administration Publications Series 16 / 1995*, National Consumer Administration, 1995, Helsinki

Chapter 3

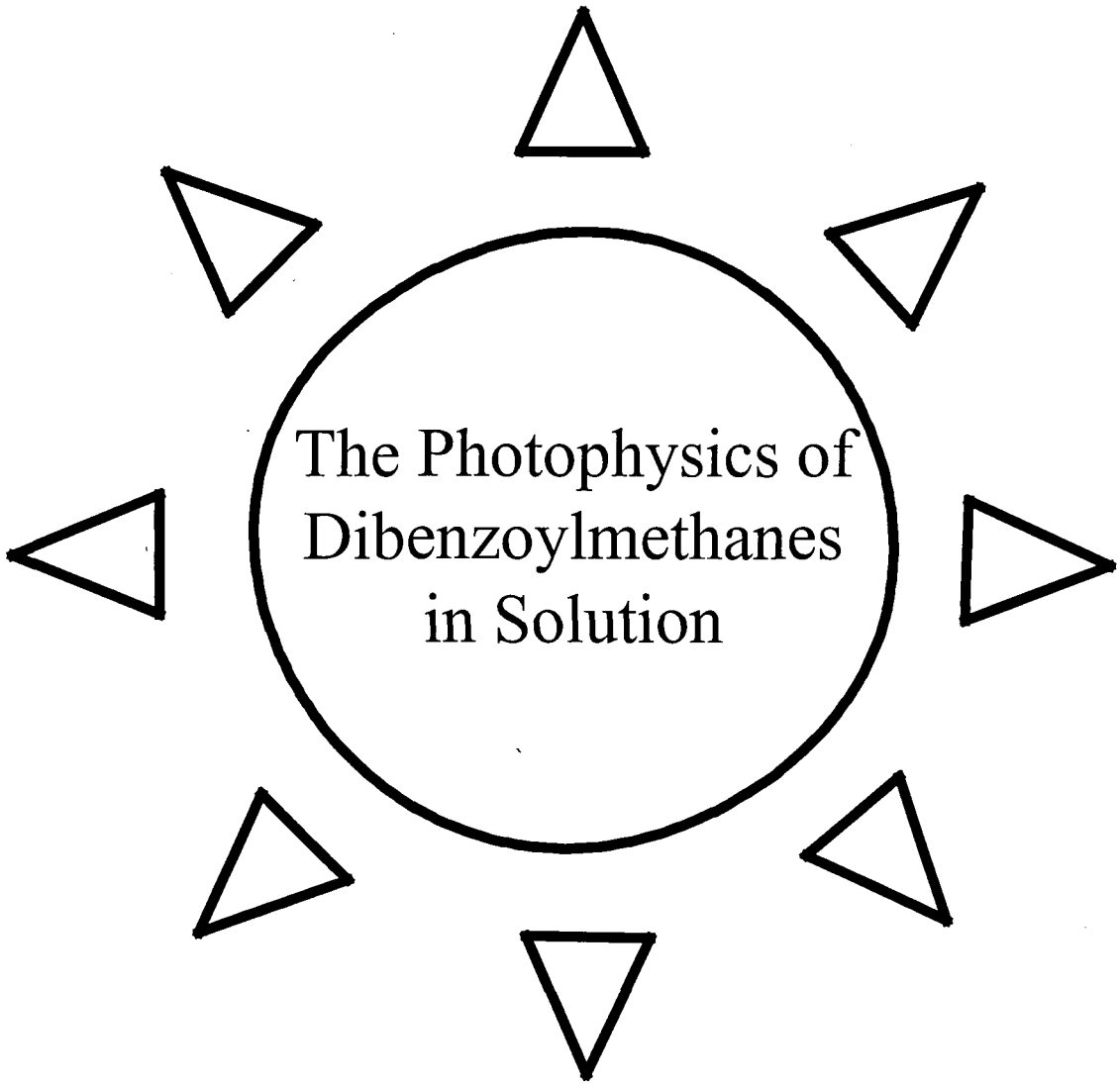

3.1 Introduction

3.1.1 Basic Photophysics

The absorption of light by organic molecules can lead to a great variety of processes, from the conversion of the absorbed energy to heat to the initiation of chemical reactions. An understanding of the excited electronic states and photophysical processes resulting from the absorption of light is of great importance in the understanding of the photochemical properties of a molecule. The photophysics of organic molecules can be summarised in a modified Jablonski diagram, as shown in figure 3.1.

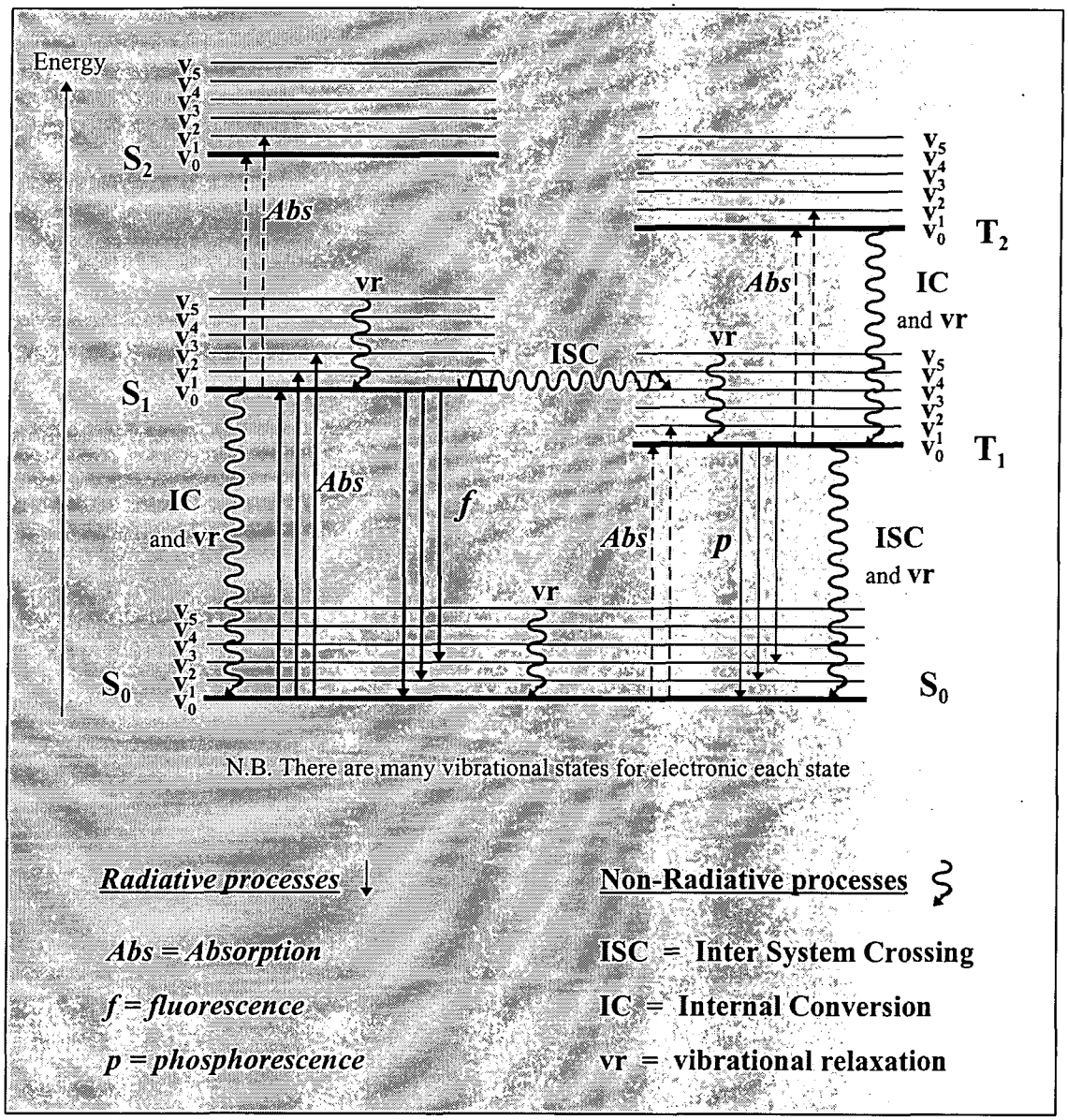

Figure 3.1 Modified Jablonski diagram summarising the photophysics of organic molecules

In most organic molecules, the ground state is a singlet state, i.e. having no unpaired electrons. Absorption of light causes promotion of an electron into a higher energy level. In most cases this occurs with retention of spin, resulting in excitation from the ground state, S_0, to the first singlet state S_1. Absorption takes place from the lowest vibrational state of the ground state, v_0, to a range of higher vibrational energy levels of S_1, however rapid vibrational relaxation occurs such that further processes occur from the v_0 level of S_1. Vibrational relaxation ultimately results in heat transfer to solvent molecules. Further absorption of light to cause a transition to the second singlet state, S_2, is rare, although direct absorption from the ground state to higher singlet states is possible. In these cases the molecule usually reverts to the S_1 state by inter system crossing followed by vibrational relaxation.

The lifetime of the excited singlet state is usually very short, typically $\tau < 10$ns, due to rapid internal conversion to higher vibrational states of the ground state, followed by vibrational relaxation. Relaxation to the ground state can also occur directly by the emission of light, i.e. fluorescence.

A change in the spin state of the excited molecule can occur, resulting in inter-system crossing from S_1 to higher vibrational levels of the first triplet state, T_1, which then vibrationally relax to the v_0 level. Direct absorption from the ground state to the T_1 state can occur, but does so with an extremely small extinction coefficient. The excited triplet state is much longer lived than the excited singlet state, due to the forbidden nature of singlet to triplet and triplet to singlet transitions, however inter-system crossing followed by vibrational relaxation can return the molecule to the ground state. Direct transition from T_1 to the ground state by emission of light, i.e. phosphorescence, can also occur. Triplet to triplet absorption to produce the second triplet state, T_2, is also possible, however the molecule quickly reverts to the T_1 state by inter-system crossing and vibrational relaxation..

The production of an excited state can result in molecular rearrangement or a unimolecular reaction, to produce a different isomer or compound. Alternatively, quenching by other molecules present in solution may lead to a transfer of the absorbed energy, and can result in chemical reactions.

3.1.2 The Photophysics of Carbonyl compounds

3.1.2.1 Excited states of Carbonyl Compounds

The photophysics and photochemistry of carbonyl compounds have been extensively studied over many years, and extensively reviewed in the literature. It is important to understand the nature of the lowest excited states of ketones, as it is from these that the photochemistry of such molecules usually occurs[1].

The molecular orbital diagram of the simplest carbonyl compound, formaldehyde ($H_2C=O$), is shown in figure 3.2, ignoring the orbitals due to C-H bonding.

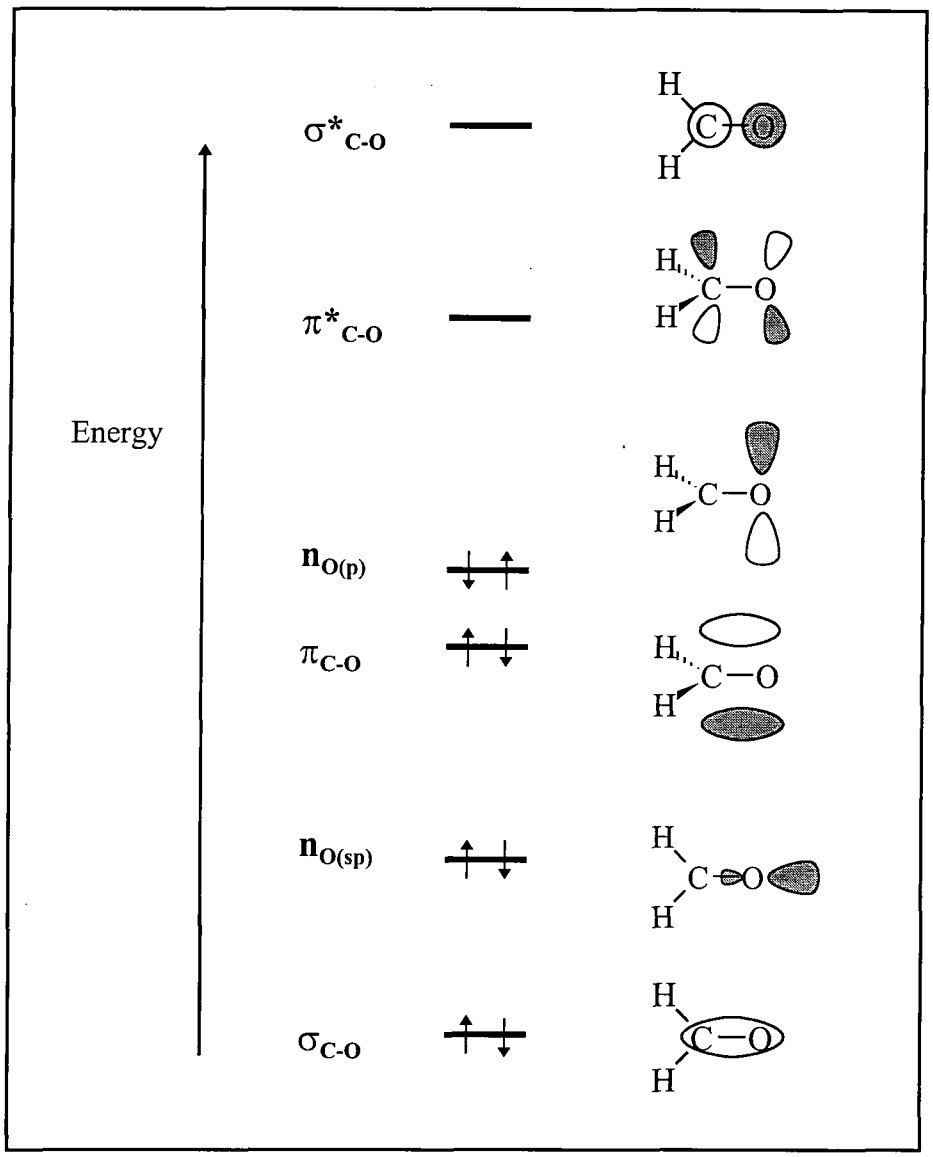

Figure 3.2 Molecular orbitals of formaldehdye[2]

(C-H molecular orbitals excluded, * denotes anti-bonding orbitals)

The most important orbitals in terms of electronic transitions, are the π, $n_{(p)}$ and π^* orbitals, where the non-bonding orbital, $n_{(p)}$, is usually referred to as simply the n orbital. Promotion of an electron to the π^* orbital from either the π or n orbitals can occur, and thus the possible excited singlet and triplet states are as shown in figures 3.3 and 3.4.

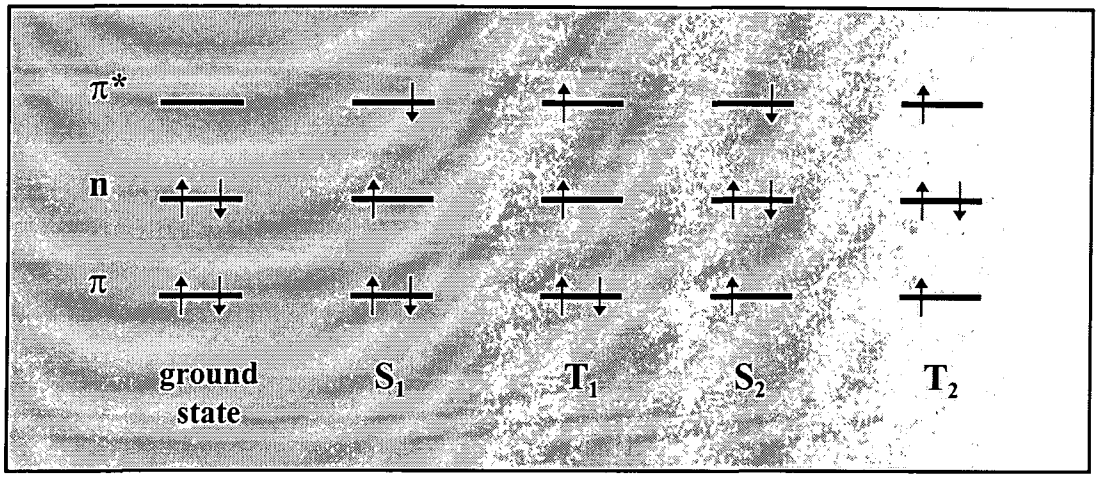

Figure 3.3 Excited electronic states of formaldehyde

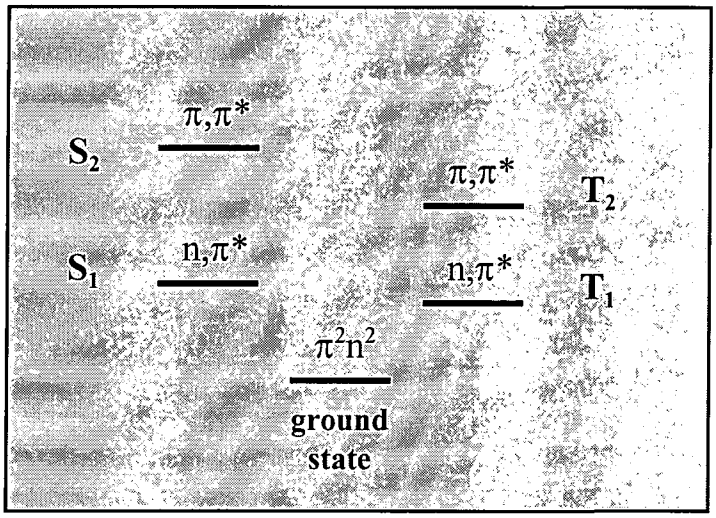

Figure 3.4 Nature of excited electronic states of formaldehyde

This picture becomes more complicated when other substituents on the carbonyl are considered. The energies of the n,π* and π,π* excited states change, depending on the nature of the substituents, such that the first excited state, could be either n,π* or π,π* in nature[3]. Strictly speaking, mixing of the states occurs in all cases, such that even if the lowest excited state is mostly n,π*, it still possesses some π,π* character. Effects such as vibrational motion of a molecule can cause such mixing[1].

In general, the electronic states of aliphatic ketones resemble those of formaldehyde. In aromatic ketones, however, e.g. napthyl ketones, both the n,π* and π,π* states are lowered in energy relative to aliphatic ketones, with the lowering of the π,π* state most notable. This means that the first excited state

of these carbonyls can often be π,π* in character. Phenyl ketones are reported to have n,π* and π,π* triplet states of comparable energy, and therfore a high degree of mixing of the excited states may be expected[3]. Electron donating substituents on the phenyl ring stabilise the π,π* state, where electron density from the benzene ring is transferred to the carbonyl group, and destabilise the n,π* state, in which electron density is transferred to the benzene ring from the carbonyl group. Electron withdrawing substituents can have the opposite effect, except in the case of para substituted groups such as halogens and cyano groups, which can conjugate with the carbonyl group, and thereby stabilise both states. Consequently the nature of the substituents can affect the character of the lowest excited state of aromatic carbobnyl compounds[3].

Enones (R-C=C-C=O) have n,π* and π,π* states that are very close in energy, and depending on the exact structure, the first excited state may be either mainly n,π* or π,π* in character[3]. The molecular orbital diagram of an enone can be created from those of C=C and C=O bonds, as shown in figure 3.5.

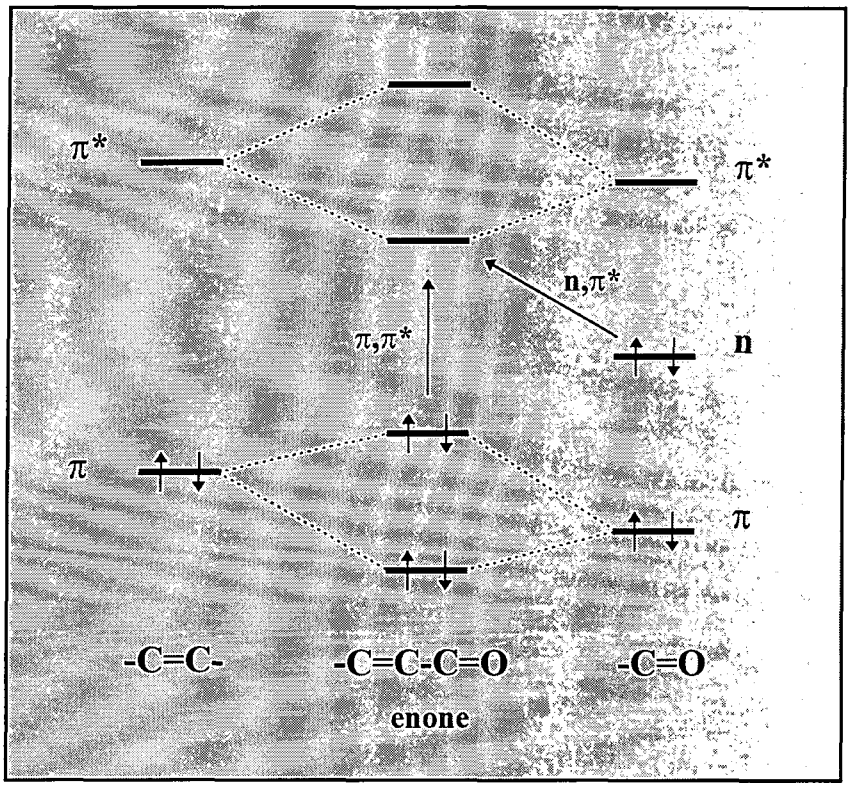

Figure 3.5 Molecular orbital diagram of an enone, showing π*←n and π*←π transitions[3]

The exact nature of the excited states of carbonyls can also be affected by external conditions such as the solvent[1,4]. Excitation from the ground state to the n,π* state involves promoting an electron located in an oxygen non-bonding orbital into an orbital shared by carbon and oxygen (see figure 3.2). Thus electron density on the oxygen is reduced in the n,π* state compared to the ground state, and compared to the π,π*

state. The molecule is therefore less polarised in the n,π* state, than in the ground or π,π* states. Hence in a solvent of high polarity the π,π* state will be more stabilised and have a lower energy, whereas in non-polar solvents the π,π* state is destabilised compared to the ground and n,π* states and has a higher energy. In some cases, the solvent can affect the relative order of the n,π* and π,π* states, and change the nature of the first excited state. This is especially important in compounds where the n,π* and π,π* states lie very close in energy. For example the lowest excited states of the ketone xanthone (figure 3.6) is observed to be of n,π* character in non-polar solvents, and a π,π* character in polar solvents[5].

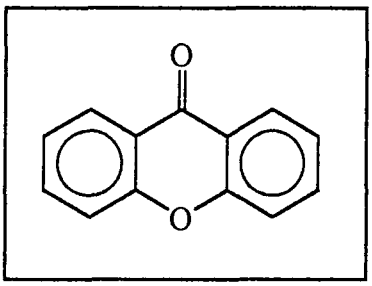

Figure 3.6 Structure of xanthone

3.1.2.2 Singlet State Transitions of Carbonyl Compounds - Absorption and Fluorescence

The absorption spectra of ketones generally fall in the UV range of the spectrum, with the exact position and nature being highly dependant on the substituents. As a general guide, aliphatic ketones have absorptions in the range of $\lambda \approx 280$ nm, and aromatic ketones have bands in the region of $\lambda \approx 340$ nm [2].

Absorption bands exhibit different properties depending on whether the excited singlet state produced is n,π* or π,π* in nature[1,2]. The π*←n transition is forbidden due to symmetry, and hence absorption bands due to such a transition have low extinction coefficients; $\varepsilon < 200$ dm^3 mol^{-1} cm^{-1}. The π*←π transition is symmetry allowed, and thus these bands generally have large extinction coefficients; $\varepsilon > 1000$ dm^3 mol^{-1} cm^{-1} [1,2]. Effects such as vibrational motion, resulting in bending of molecules, can increase the probability of an π*←n transition or lower that for a π*←π transition[1].

Due to the solvent effects mentioned in section 3.1.2.1, a band due to an π*←n transition will show a blue shift, towards shorter wavelengths, with increasing polarity[1]. Bands due to π*←π transitions will show the opposite effect of a red shift, towards longer wavelengths with increasing solvent polarity. It is also reported that the n,π* band of a ketone disappears on protonation[2], where the non-bonding electrons of the oxygen become involved in a new O-H bond.

For some ketones, such as benzophenone, bands due to both $\pi^*\leftarrow n$ and $\pi^*\leftarrow\pi$ transitions can be identified in their absorption spectra, where the above properties, of different extinction coefficients and shifting bands on varying solvent polarity, can be observed, as shown in figure 3.7.

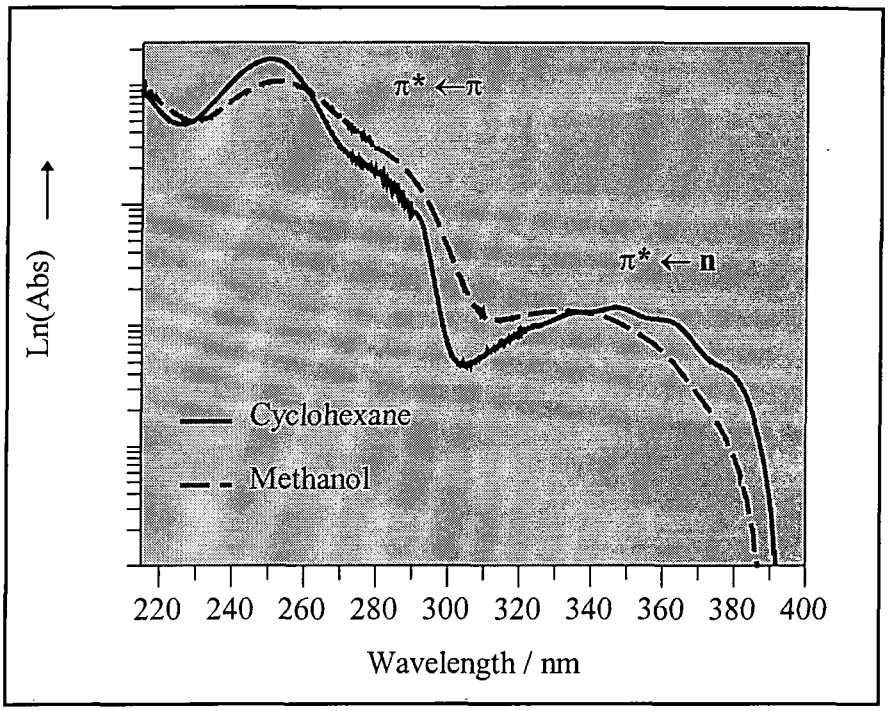

Figure 3.7 Absorption spectra of benzophenone in ethanol and cyclohexane
(data taken from this work; each spectrum obtained from two different solution concentrations)

For most ketones absorption peaks are broadened by vibrations and solvent interactions, such that vibrational structure, with spacings corresponding to C=O stretching frequencies of the excited states, are not seen.

Other absorptions can sometimes also be observed, such as the $\sigma^*\leftarrow n$ transition at wavelengths < 200 nm [2] and $T_1 \leftarrow S_0$ absorptions, which occur with extremely small extinction coefficients, $\varepsilon \approx 10^{-3}$ mol^{-1} dm^3 cm^{-1}.

Ketones can exhibit fluorescence, however they tend to have very low quantum yields of fluorescence due to rapid inter-system crossing to form the triplet state, and a low probability of fluorescence[1]. n,π^* states have lower quantum yields of fluorescence than π,π^* states because of the symmetry forbidden nature of $\pi^*\leftrightarrow n$ transitions[1].

3.1.2.3 Triplet State Transitions of Carbonyl Compounds - Phosphorescence

As mentioned above, inter-system crossing from the singlet to the triplet state is generally very efficient for ketones, and consequently the triplet states of ketones are very important in terms of photochemistry[1,3,5].

The energies of the triplet states lie lower than their singlet state counterparts, with the singlet-triplet splitting typically larger for π,π^* states than for n,π^* states. The nature of the lowest triplet state, as n,π^* or π,π^*, is governed by the same variables described in section 3.1.2.1. for the singlet states, e.g. it is affected by substituents and the solvent. π,π^* triplets tend to be longer lived (τ_p>1s) than n,π^* triplets ($\tau_p<10^{-1}$s)[2].

The triplet energies of aliphatic ketones fall in the range $E_T \approx$ 325-335 kJ mol^{-1}. Phenyl alkyl ketones have lower triplet energies, typically $E_T \approx$ 300 kJ mol^{-1}. For conjugated enones the triplet energy is lower still at $E_T \approx$ 295-300 kJ mol^{-1} [3].

Direct $T_1 \leftarrow S_0$, singlet to triplet absorptions, although highly forbidden, can be observed in the absorption spectrum of concentrated solutions, in a cell of long pathlength, using sensitive equipment[1].

Phosphorescence emission spectra from ketones can often be observed using a rigid matrix at low temperature, and frequently exhibit vibrational structure, where the vibrational spacing matches the stretching vibrations of the carbonyl group[1].

3.1.3 Photophysics of 1,3-Dicarbonyl Compounds

1,3-dicarbonyl compounds can in principle exist as one or a mixture of various isomers, as discussed in chapter 1, shown again in figure 3.8, where the labels cis and trans refer to the arrangement of the double bonds in the enol, and the labels E and Z refer to the arrangement of substituents about the carbon-carbon double bond.

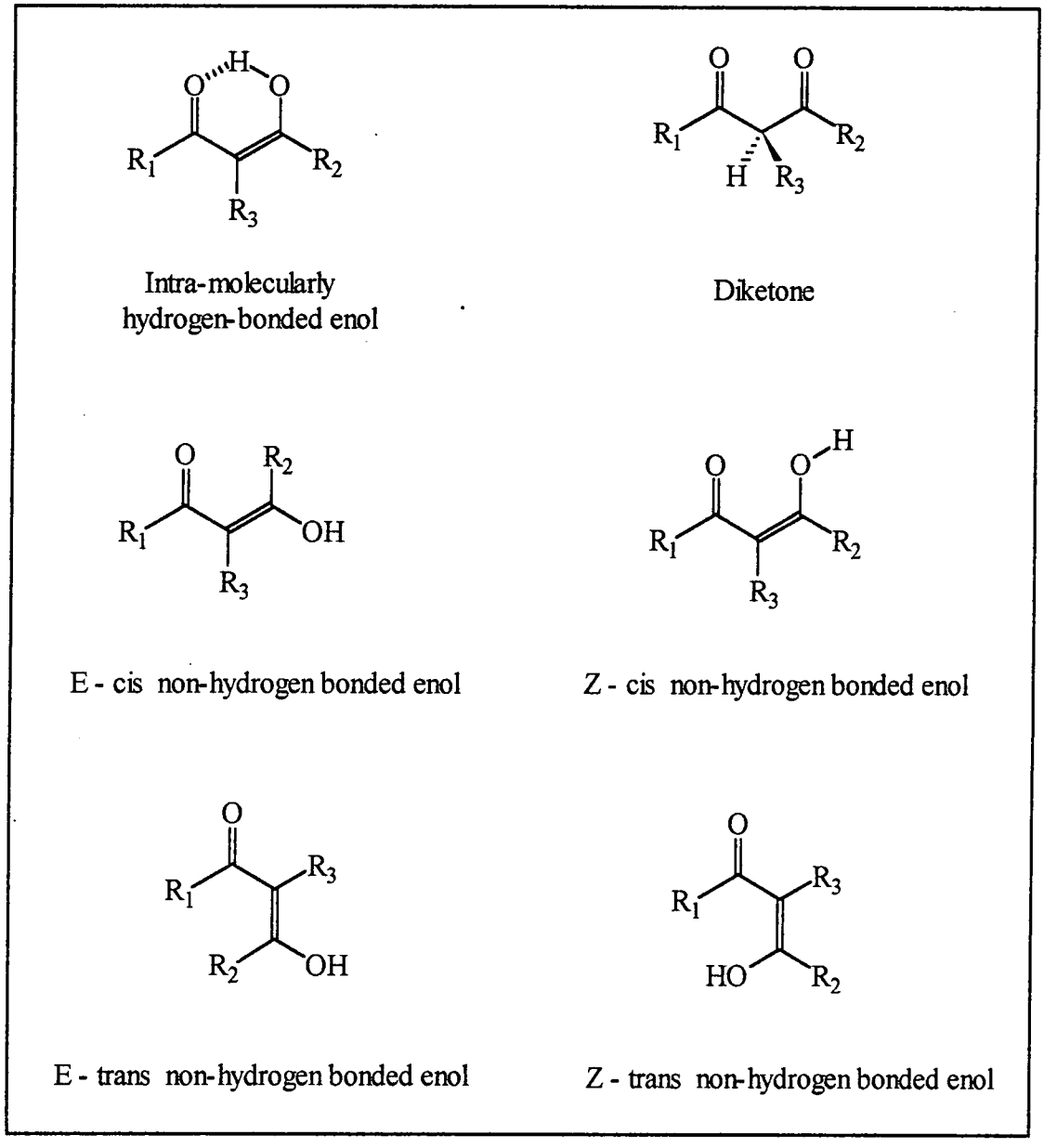

Figure 3.8 Possible isomers of 1,3-dicarbonyl compounds

(R = allyl, aryl or H)

The absorption spectra of 1,3-dicarbonyls exhibit a strong absorption in the 250-300 nm region. Theoretical calculations indicate that this is due to a $\pi^* \leftarrow \pi$ transition in the carbonyl conjugated ethene system of the enol form[6,7]. Calculations also predict two $\pi^* \leftarrow n$ transitions in the visible or near UV range[6], however it is expected that these would be of small intensity. In molecules with aromatic substituents at R_1, R_2 or R_3 (see figure 3.8), the main peak falls at longer wavelengths (lower energy)[6]. Theoretical evidence shows strong π-electron interaction between the enol system and the benzene rings of aromatic 1,3-dicarbonyl compounds. This conjugation gives extra stability to the excited states, accounting for the observed position of the π,π^* absorption bands of these compounds. A detailed

theoretical analysis of the electronic transitions of 1,3-dicarbonyl compounds in the enol form can be found in reference **10**.

Some 1,3-dicarbonyl compounds, e.g. benzoylacetone and ethyl acetoacetate, are reported to have an n,π^* lowest excited singlet state[8,9]. This transition is of low intensity and can masked by the tail of the higher extinction coefficient π,π^* band.

An absorption band in the range 250-260 nm is also visible when aromatic substituents are present[6,7]. This is assigned to be due to the aroyl group of the diketone form[6].

Concentrated solutions ($\approx 10^{-3}$ mol dm^{-3}) of 1,3-dicarbonyl compounds are reported to have a low intensity absorption band in the 290-410 nm region, which is suggested to be an absorption due to dimers formed in solution[11].

1,3-dicarbonyl compounds have generally not been reported to fluoresce when excited at either the enol or the diketone bands[6]. Exceptions can be due to other chromophores present in the molecule[11]. Fluorescence in the region 310-520 nm has been observed, on excitation of the absorption band due to 1,3-dicarbonyl dimers[11].

3.1.4 Photophysics of Dibenzoylmethanes

3.1.4.1 General

NMR and IR studies have shown that dibenzoylmethanes exist primarily in the intra-molecularly hydrogen bonded (chelated) enol form in solution, with the remaining proportion consisting of the diketone form[12] (see figure 3.9).

Dibenzoylmethanes posses a strong absorption band in the region $\lambda_{max} \approx 340$ nm, with an extinction coefficient of $\varepsilon \approx 2 - 2.4 \times 10^4$ mol^{-1} dm^3 cm^{-1} [7,13,14,15]. A smaller peak is also observed in the region of $\lambda_{max} \approx 250$ nm, with an extinction coefficient of $\varepsilon \approx 6 - 10 \times 10^3$ mol^{-1} dm^3 cm^{-1} [7,17]. The absorption spectrum of DBM is shown in figure 3.10.

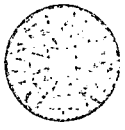

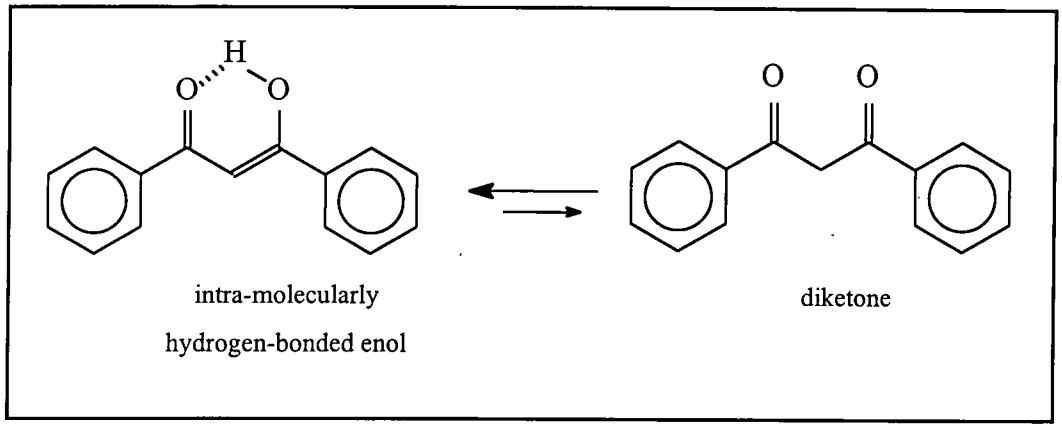

Figure 3.9 Structures of dibenzoylmethane

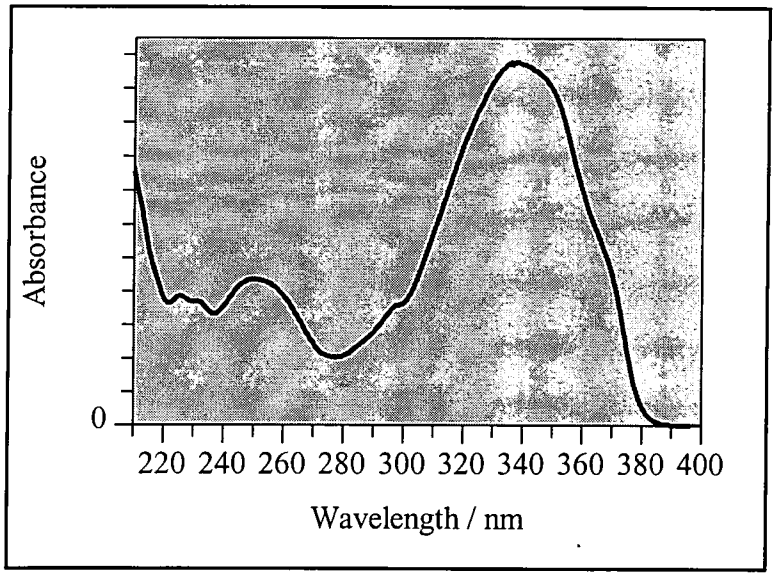

Figure 3.10 Absorption spectrum of dibenzoylmethane in cyclohexane
(data taken from this work - see section 3.2.1.1)

The main band, as previously discussed, can be assigned to a $\pi^*\leftarrow\pi$ transition of the chelated enol form. The peak is more red-shifted than other aromatic 1,3-dicarbonyl compounds due to the strong intra-molecular H-bonding. For example, in the spectra of β-methoxy chalcones[7,16], which share a similar structure, but without the hydrogen bond, this transition is found at shorter wavelengths, $\lambda_{max} \approx 300$ nm. Other studies have suggested the main 340 nm peak to be due in part to charge-transfer interactions[10,17].

It is not clear from the literature, whether the lowest excited state of DBM is π,π^* in character. The π,π^* and n,π^* states of DBM and similar compounds are likely to be close in energy, and as mentioned in the previous section, calculations have predicted $\pi^*\leftarrow n$ transitions in a similar spectral region to the $\pi^*\leftarrow\pi$

transition. Similar compounds such as benzoylacetone and ethyl acetoacetate are reported to have n,π* lowest excited states, as previously discussed, however most literature reports suggest that DBM has a π,π* lowest excited singlet state[10].

The peak at 240 nm is assigned to the π*←π transition of the diketone form[6]. However it cannot be due entirely to this, because the amount of diketone present is very small compared to the size of the peak[7]. Thus it is likely that another transition due to the chelated enol form is included in this band. It has also been suggested that an π*←n transition of the diketone is hidden under the main 340 nm band of the chelated enol structure[8], indicating that the lowest excited state of the diketone is in fact n,π* in nature.

3.1.4.2 Low Temperature Absorption

On freezing a solution of dibenzoylmethane in a rigid matrix, a dramatic change in the absorption spectrum has been reported[8,17], as shown in figure 3.11.

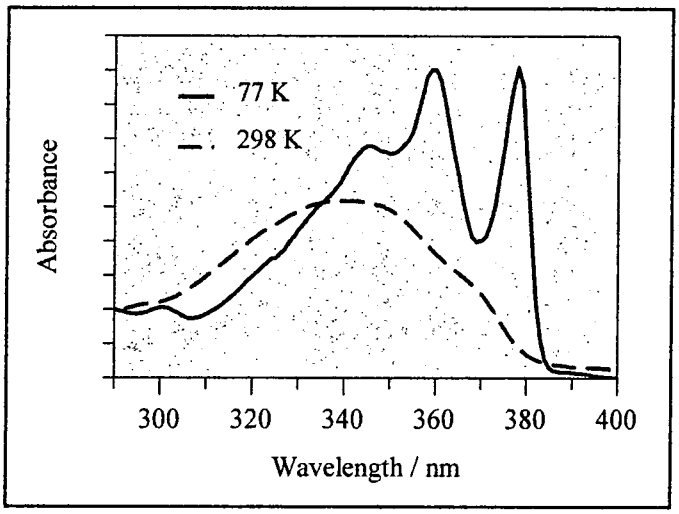

Figure 3.11 Absorption spectrum of dibenzoylmethane in EPA at room temperature and 77 K
(data taken from this work - see section 3.2.2)

The vibrational structure of the absorption band is clearly visible in the spectra at 77 K. A similar effect is seen, but to a lesser extent, with 1,3-diketones such as benzoylacetone, where vibronic coupling between the n,π* and π,π* singlet states has been suggested to reduce the structure observed[8]. It can be noted that the band due to the $v_0' \leftarrow v_0''$ transition is not the most intense. According to the Frank-Condon principle[1], this occurs if an excited state and ground state have significantly different preferred geometries.

3.1.4.3 Fluorescence

It is reported that dibenzoylmethanes fluoresce when excited at the main peak at low temperature[17,18]. Fluorescence is increased if the chelated hydrogen is replaced by a metal ion, such as aluminium[12]. A previous PhD thesis reports that the fluorescence emission spectrum of DBM in EPA has peaks at 386 nm, 400 nm, 420 nm and 445 nm, which correspond to vibrational spacings of 910 cm^{-1}, 1190 cm^{-1} and 1340 cm^{-1} [17], although these observations have not been published in the literature. 1,3-dicarbonyls such as benzoylacetone, with an n,π^* first excited singlet state do not fluoresce as this is a forbidden transition and inter-system crossing to form the triplet state is more likely to occur[8]. Thus the fluorescence of DBM may be evidence that the lowest excited state is π,π^* in nature.

3.1.4.4 Phosphorescence

At low temperature, in a rigid matrix, dibenzoylmethanes have been observed to phosphoresce[8,17]. Excitation of the 250 nm band results in a blue phosphorescence due to the presence of the diketone form[8,17]. This exhibits vibrational structure with a spacing of 1742 cm^{-1} [8], with the $v_0' \rightarrow v_0''$ band at 392 nm in ethanol[8] or 380 nm in EPA[17]. The triplet energy has been calculated to be $E_T = 314$ kJ mol^{-1} [19], and the phosphorescence lifetime is reported to be $\tau_p \approx 50$ ms [17]. This phosphorescence is quite intense, taking into account the amount of diketone present in solution, which is very small. This is consistent with a high rate of inter-system crossing to form the triplet, and a low yield of fluorescence.

Excitation at 350 nm produces a much longer lived green phosphorescence, due to the chelated enol form, which can be easily observed with the eye when the source is removed[8,17]. This also exhibits vibrational structure, with a spacing of 1400 cm^{-1} [8], with the $v_0' \rightarrow v_0''$ band at 490 nm [8,17]. The triplet energy can be calculated to be approximately $E_T = 255$ kJ mol^{-1}. The phosphorescence lifetime is reported by Gacoin[8] to be $\tau_p \approx 16$ ms, however this does not seem to agree with qualitative comments in his report, implying a lifetime of seconds. This phosphorescence has been observed at room temperature for Parsol 1789 in N_2 flushed 2-methylpentane[20]. The vibrational spacing is reported to be 1345 cm^{-1} with the $v_0' \rightarrow v_0''$ band at 486 nm. The triplet energy is reported to be $E_T = 236$ kJ mol^{-1}.

The diketone phosphorescence spectrum can be observed exclusively in very polar solvents and the chelated enol phosphorescence spectrum exclusively in highly non-polar solvents[8].

Triplet-triplet absorption of the chelated enol of DBM, with $\lambda_{max} = 630$ nm, has been observed by flash photolysis of an 3:1 ethanol : methanol solution at 118 K [21,22].

It has been reported that for benzoyltrifluoroacetone a third phosphorescence at 470 nm is observed[8]. This phosphorescence gets more pronounced on dilution, and is assigned as being due to a trans non-chelated enol structure, as shown in figure 3.12. It is suggested that the non-chelated enol is formed from the disassociation of non-luminescent dimers, and is stabilised by the ethanol solvent[8].

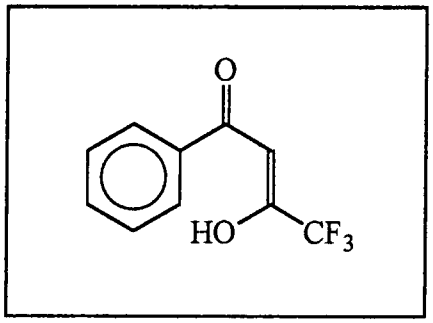

Figure 3.12 Trans non-chelated benzoyltrifluoroacetone

3.1.4.5 Other Dibenzoylmethanes

The O-methyl ethers of dibenzoylmethanes, β-methoxy chlacones, possess a similar structure to the enol form of DBM, but obviously can not form the intra-molecular hydrogen bond. They can exist as one of two isomers, as discussed in chapter 1 and as shown in figure 3.13. The E-isomer is thermodynamically more stable than the Z-isomer[16].

O-methyl dibenzoylmethanes have an absorption peak at approximately $\lambda_{max} \approx 300$ nm, but this varies depending on the extent of E-Z isomerisation[7,16]. The main absorption peak of the Z-isomer is found at longer wavelengths, e.g. 310 nm in 1:1 ether : hexane, than that of the E-isomer which is at 292 nm in the same solvent[16]. The absorbance spectra of O-methyl 1,3 dicarbonyl compounds have been shown to be very similar to the spectra of the corresponding non-methylated, non-hydrogen bonded enol compounds[23].

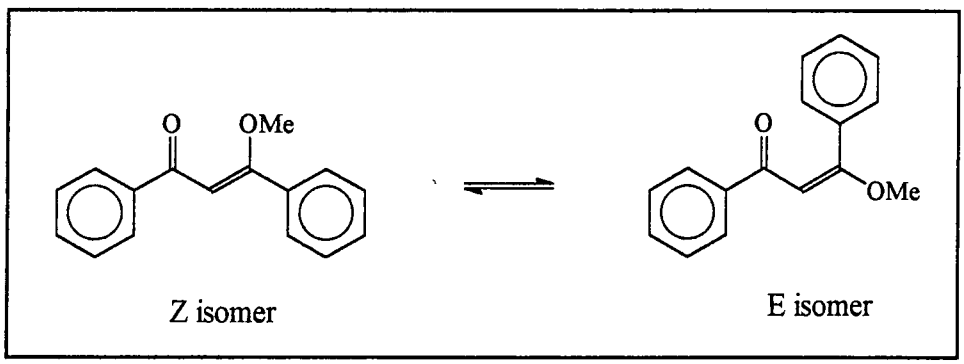

Figure 3.13 O-methyl substituted DBM

C-methyl substituted dibenzoylmethanes are present as the stable diketone form[7], as shown in figure 3.14, and exhibit an absorption spectra similar to those of aromaic ketones such as acetophenone

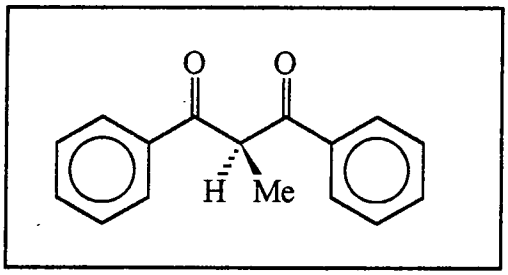

Figure 3.14 C-methyl substituted DBM

In alkaline solution an enolate is formed[10], as shown in figure 3.15. The main absorption peak is red shifted and is assigned to the π,π^* band of the anion with planar chelate ring[10].

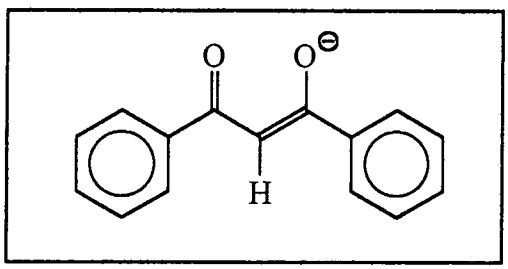

Figure 3.15 Enolate of DBM

3.2 Results and Discussion

3.2.1 Absorption Spectra

3.2.1.1 Absorption Spectra of Dibenzoylmethanes

The absorption spectra of dibenzoylmethane were measured at room temperature in various solvent systems, using the technique described in chapter 2. The spectra all show the same basic shape, as described in section 3.1.4. The absorbance maxima have differing peak wavelengths, depending on the solvent. The molar extinction coefficients, ε, at the wavelengths where the main absorbance peak is

located, λ_{max}, were measured as described in chapter 2, and vary slightly for different solvents. These results are summarised in table 3.1, and selected absorption spectra are shown in figure 3.16.

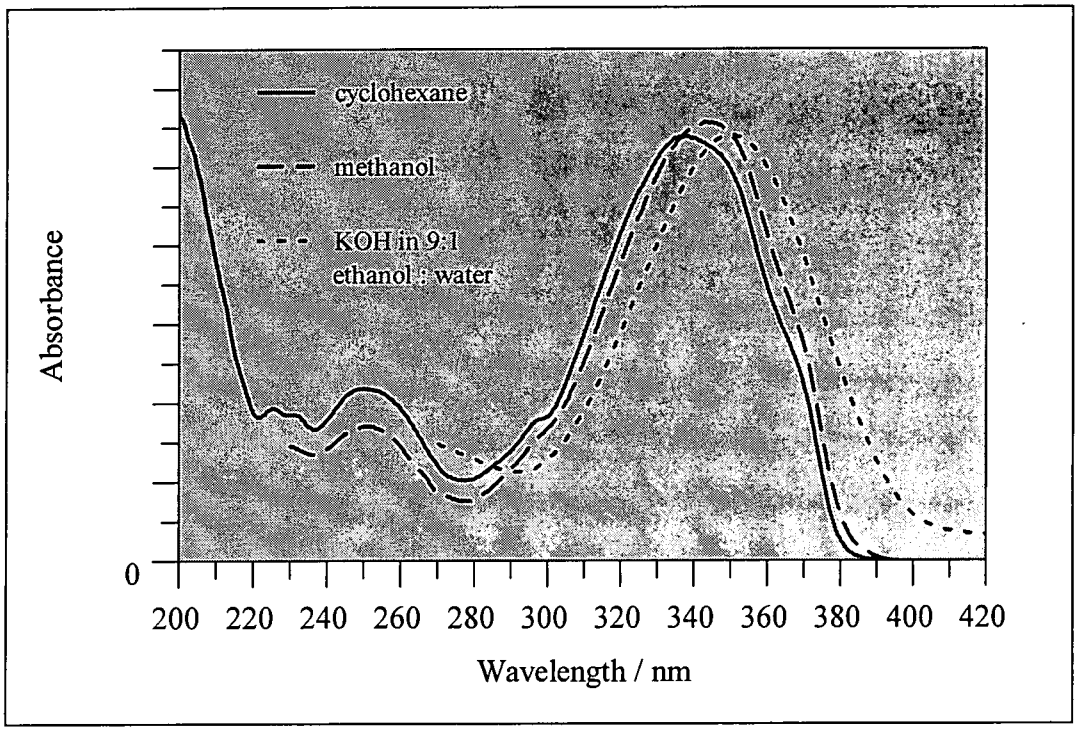

Figure 3.16 Absorption spectra of dibenzoylmethane in various solvents.

It can be observed that both the main peaks display a general shift towards longer wavelengths with increasing solvent polarity, as reported, and expected for $\pi^* \leftarrow \pi$ transitions (see section 3.1.3). In alkaline solution, produced by the addition of KOH, to an ethanol/water mixture, the enolate of dibenzoylmethane is formed, and this new species has a longer observed wavelength maximum than for DBM, with a slightly smoother peak shape, as can be seen in figure 3.16. It is not clear from the absorption spectrum whether the enolate of DBM is formed in N,N-dimethylformamide solution, which is weakly basic.

Solvent	Polarity Scale[a] E_T / kcal mol^{-1}	λ_{max} / nm ± 0.5 nm	$10^4 \varepsilon$ / mol^{-1} dm^3 cm^{-1} ± 5 × 10^2 mol^{-1} dm^3 cm^{-1}	*diketo* λ_{max} / nm ± 0.5 nm
Cyclohexane	31.2	337	2.0	250
Tetrachloromethane	32.5	340	not measured	m
Benzene	34.5	344.5	not measured	m
Dichloromethane	41.1	343	not measured	254.5
N,N-Dimethylformamide	43.8	352	not measured	m
Acetonitrile	46.0	342	2.2	249
Ethanol	51.9	343	2.2	252.5
Methanol	55.5	344	2.2	251
Water	63.1	346	not measured	252.5[b]
1,1,2 -Trichlorotrifluoroethane	-	336	≈ 2	249
1% Pyridine in cyclohexane	-	338	not measured	m
2:1 Isopentane : Methylcyclohexane	-	336	not measured	247
EPA (5:5:2 diethyl ether : isopentane : ethanol)	-	339.5	not measured	m
9:1 ethanol : water	-	344.5	2.1	253.5
9:1 ethanol : water, HCl (acidic solution)	-	344.5	≈ 2.1	253.5
9:1 ethanol : water, KOH (alkaline solution)	-	352	≈ 2.0	m
1% Triton-X 100 in Water	-	348	≈ 1.9	m
1% Triton-X Reduced in Water	-	347	≈ 2.1	m
2% Triton-X Reduced in Water	-	345.5	not measured	m
5% Triton-X Reduced in Water	-	346	not measured	m

Table 3.1 Absorption maxima and extinction coefficients for dibenzoylmethane in various solvents at room temperature.

a) Solvent polarity scale based on "solvatochromic band" shifts of 4-(2,4,6-triphenylpyridinium)-2,6-diphenylphenoxide and its trimethyl derivative[24]. Values increase with increasing polarity
b) diketone peak is larger than chelated enol peak
m) peak masked or distorted by solvent absorption

In benzene solution, the peak is more shifted to the red than would be expected for its polarity. The reason for this is not clear, but could be due to an interaction between the DBM and solvent molecules. Interaction between molecules of 1,3-dicarbonyl compounds, such as acetylacetone, and benzene have been reported in the literature[25]. It is suggested that complexes having the structure shown in figure 3.17 are formed, where the molecule of the chelated enol of acetylacetone is roughly parallel with the benzene molecule, which is placed over a region of large positive charge density on the enol molecule. The structure is also slightly bent, such that the enol proton is in the same plane as the benzene ring. In 1,3-dicarbonyl compounds such as trifluoroacetylacteone and hexafluoroacetylacteone, the complex is suggested to have a structure in which the benzene ring and the chelated enol ring are parallel[25]. Therefore there is evidence that the chelated enols of 1,3-dicarbonyl compounds can indeed interact and form complexes with solvents such as benzene. This results in the absorption for the main $\pi^* \leftarrow \pi$ transition falling at longer wavelength than would be expected from considering only the polarity of the benzene solvent.

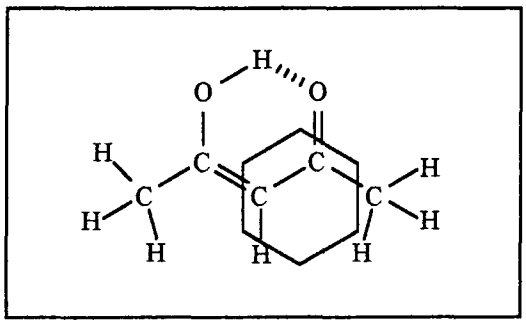

Figure 3.17 Suggested complex between acetylacetone and benzene[25]

(Outline of benzene ring shown, above plane of acetylacetone)

DBM is only slightly soluble in water, and the spectrum obtained in aqueous solution is different to the other solvents, in that the diketone peak is of larger intensity than that of the chelated enol structure. This has been observed in the literature for water containing 2% ethanol[17], and occurs because of the stability afforded to the diketone by extensive hydrogen bonding with the water molecules, meaning a larger percentage of the DBM is present as the diketone structure.

Similar absorption spectra have been obtained for Parsol 1789, Parsol DAM and dtDBM as summarised in tables 3.2 - 3.4 and figures 3.18 - 3.19.

Solvent	Polarity Scale[a] E_T / kcal mol^{-1}	λ_{max} / nm ± 0.5 nm	$10^4 \varepsilon$ / $mol^{-1} dm^3 cm^{-1}$ ± 5×10^2 $mol^{-1} dm^3 cm^{-1}$
Cyclohexane	31.2	355.5	3.0
Tetrachloromethane	32.5	355.5	not measured
Benzene	34.5	358.5	not measured
Dichloromethane	41.1	358.5	not measured
Acetonitrile	46.0	357.5	3.2
Ethanol	51.9	358	3.3
Methanol	55.5	358	3.2
Water	63.1	insoluble	not measured
1,1,2 -Trichlorotrifluoroethane	-	351.0	not measured
2:1 isopentane: Methylcyclohexane	-	350.5	not measured
EPA (5:5:2 diethyl ether : isopentane : ethanol)	-	355	not measured
9:1 ethanol : water	-	360	3.2
9:1 ethanol : water, HCl (acidic solution)	-	360	≈ 3.3
9:1 ethanol : water, KOH (alkaline solution)	-	355.5	≈ 2.6
1% Triton-X 100 in Water	-	361	3.2
1% Triton-X Reduced in Water	-	359.5	3.3

Table 3.2 Absorption maxima and extinction coefficients for Parsol 1789 in various solvents at room temperature.

a) Solvent polarity scale based on "solvatochromic band" shifts of 4-(2,4,6-triphenylpyridinium)-2,6-diphenylphenoxide and its trimethyl derivative[24]. Values increase with increasing polarity

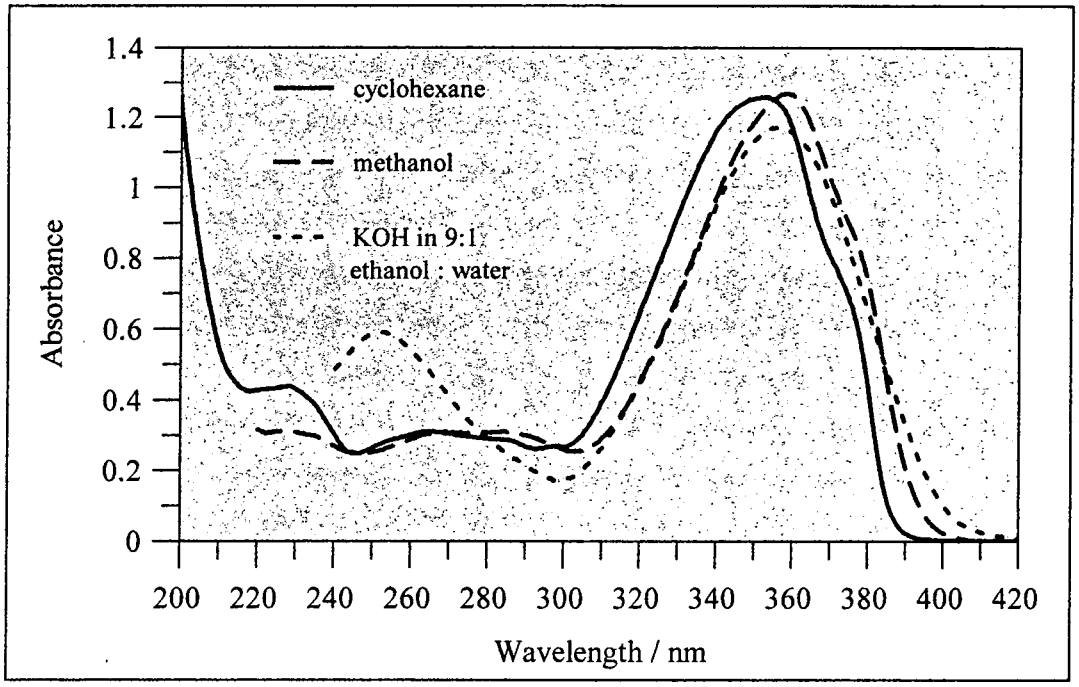

Figure 3.18 Absorption spectra of Parsol 1789 in various solvents at room temperature.

Solvent	λ_{max} / nm ± 0.5 nm
Cyclohexane	357.5
Benzene	362.5
Methanol	361.5
EPA (5:5:2 diethyl ether : isopentane : ethanol)	359.5

Table 3.3 Absorption maxima for Parsol DAM in various solvents at room temperature.

Solvent	λ_{max} / nm ± 0.5 nm	diketo λ_{max} / nm ± 0.5 nm
Cyclohexane	348.5	256
Benzene	352	m
Methanol	352.5	263
EPA (5:5:2 diethyl ether : isopentane : ethanol)	349	257

Table 3.4 Absorption maxima for dtDBM in various solvents at room temperature.

m) peak masked or distorted by solvent absorption

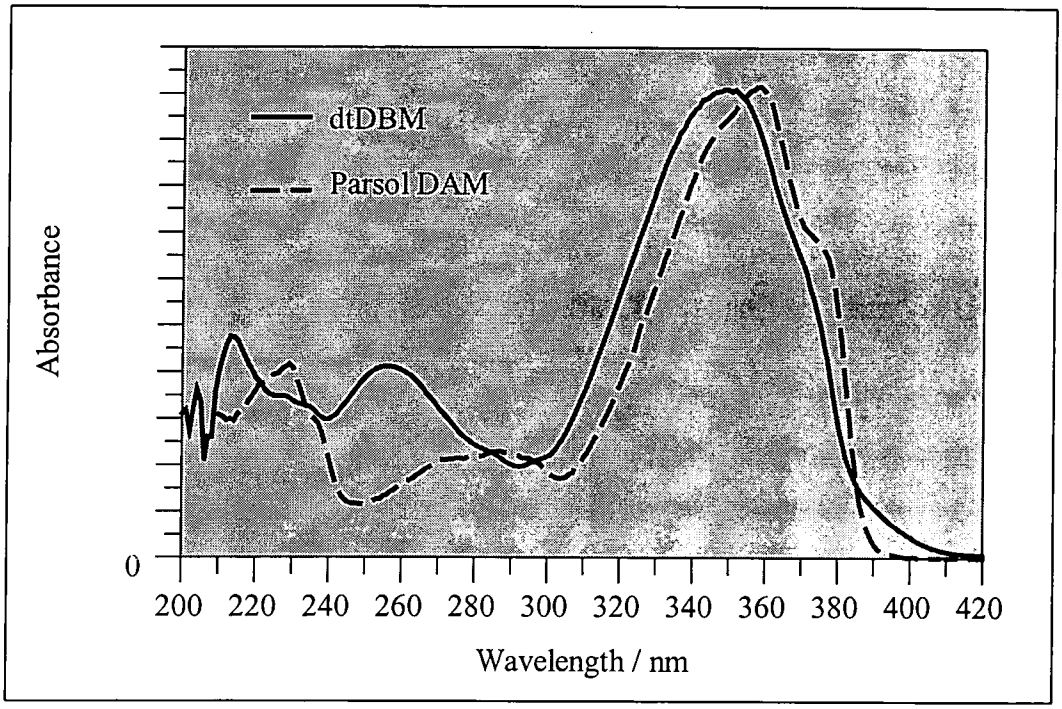

Figure 3.19 Absorption spectra of dtDBM and Parsol DAM in cyclohexane at room temperature.

No absorption at long wavelengths was observed in solutions of concentrations < 5×10^{-4} mol dm^{-3}, and therefore no evidence for dimer formation was observed..

3.2.1.2 Absorption Spectra of O-Methyl Substituted Dibenzoylmethanes

The absorption spectra of the O-methyl substituted dibenzoylmethane and Parsol 1789 have also been studied at room temperature in various solvents, using the technique described in chapter 2.

O-methyl dibenzoylmethanes can exist as one of two possible isomers, with the E-isomer being thermodynamically more stable than the Z-isomer[16]. E↔Z conversion is discussed in chapter 4. The O-methyl dibenzoylmethanes used in this study were primarily present in the Z-isomeric form (see chapter 4), and can be converted to the E-isomers over time (thermodynamically) or with irradiation (photochemically).

The absorption spectra and data for O-methyl Dibenzoylmethane and O-methyl substituted Parsol 1789 are given in tables 3.5 - 3.6 and figures 3.20 - 3.21.

Solvent	Polarity Scale[a] E_T / kcal mol^{-1}	*initial* λ_{max} / nm ± 1 nm	$10^4 \varepsilon$ / mol^{-1} dm^3 cm^{-1} ± 5 × 10^2 mol^{-1} dm^3 cm^{-1}	*E-isomer* λ_{max} / nm ± 1 nm
Cyclohexane	31.2	306.5	1.4	289
Tetrachloromethane	32.5	307	not measured	291
Dichloromethane	41.1	307	not measured	291
Methanol	55.5	306	not measured	296
1,1,2 - Trichlorotrifluoroethane	-	303	not measured	288
1:1 diethyl ether : isopentane	-	306	not measured	290
EPA (5:5:2 diethyl ether : isopentane : ethanol)	-	308	not measured	294
9:1 ethanol : water	-	301	1.2	

Table 3.5 Absorption maxima and extinction coefficients for O-methyl dibenzoylmethane in various solvents at room temperature.

a) Solvent polarity scale based on "solvatochromic band" shifts of 4-(2,4,6-triphenylpyridinium)-2,6-diphenylphenoxide and its trimethyl derivative[24]. Values increase with increasing polarity

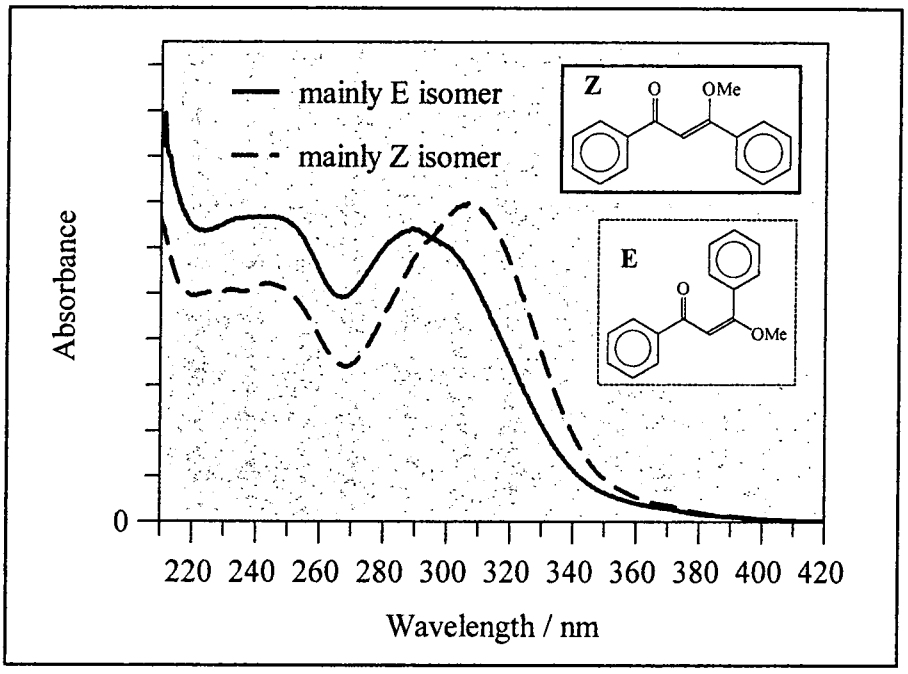

Figure 3.20 Absorption spectra of E and Z isomers of O-methyl dibenzoylmethane in cyclohexane at room temperature

Solvent	*initial* λ_{max} / nm ± 1 nm	$10^4 \varepsilon$ / mol^{-1} dm^3 cm^{-1} ± 5 × 10^2 mol^{-1} dm^3 cm^{-1}
Cyclohexane	300	1.3
Methanol	316	not measured
9:1 ethanol : water	317	1.3

Table 3.6 Absorption maxima and extinction coefficients for O-methyl Parsol 1789 in various solvents at room temperature.

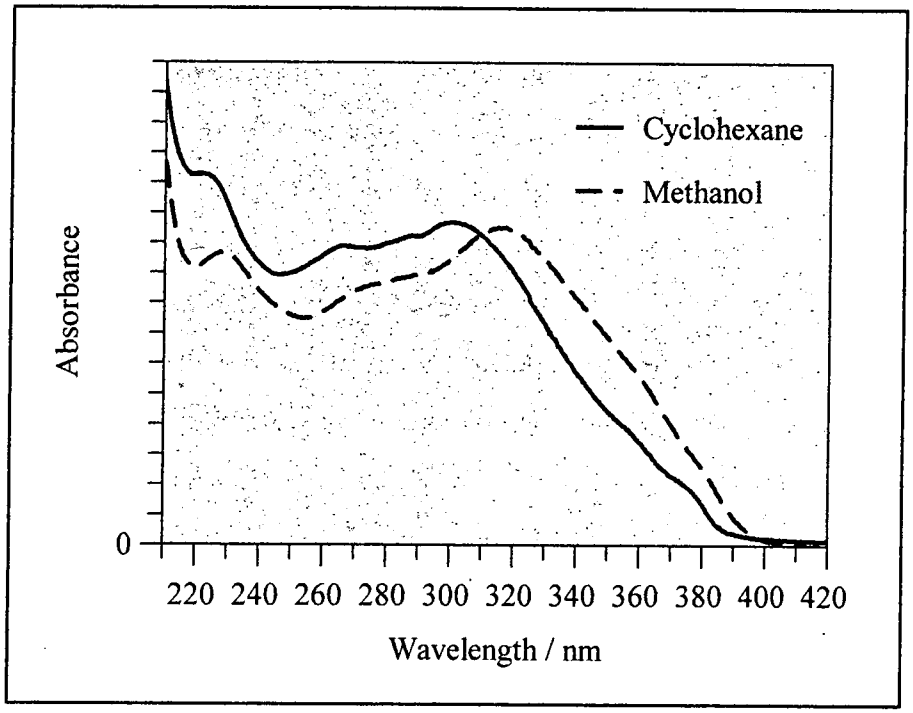

Figure 3.21 Absorption spectra of O-methyl Parsol 1789 in cyclohexane and methanol at room temperature

With no intra-molecular hydrogen bonding possible in O-methyl dibenzoylmethanes, the main peak is found at shorter wavelengths than for DBM, at ≈300 nm. This peak still corresponds to a $\pi^* \leftarrow \pi$ transition, although a red shift to longer wavelengths (lower energy) with increasing solvent polarity is not obvious. It is probably confused with the peak shifts due to varying initial isomer mixtures in different solvents. The shift can be seen more clearly for the spectra of the E - isomers. There is also a $\pi^* \leftarrow \pi$ transition visible at $\lambda \approx 240$ nm for O-methyl DBM.

The spectrum for O-methyl Parsol 1789 is much broader, and appears to be a combination of several peaks. This is most likely to be due to the presence of two different compounds, arising from methylation of the two different acetophenone fragments, with each compound being present as a mixture of E and Z isomers, as shown in figure 3.22

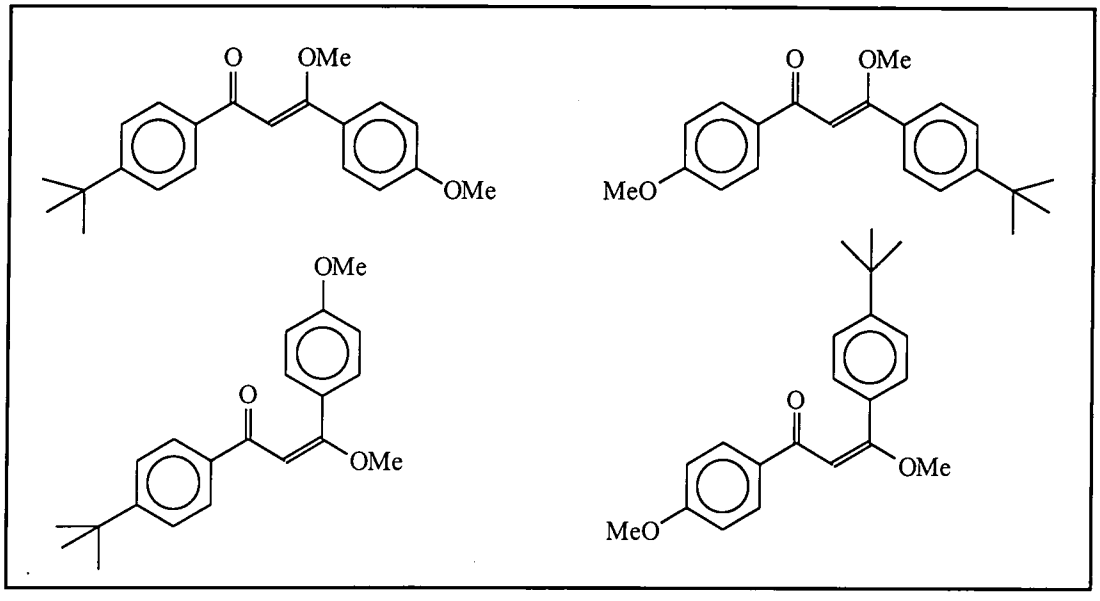

Figure 3.22 Possible isomers of O-methyl Parsol 1789

3.2.1.3 Absorption Spectra of C-Methyl Substituted Dibenzoylmethanes

The absorption spectra of the C-methyl substituted dibenzoylmethane and Parsol 1789 have also been studied at room temperature in various solvents, using the technique described in chapter 2.

The absorption spectra observed for C-methyl dibenzoylmethane and C-methyl Parsol 1789 are summarised in tables 3.7 - 3.8 and figures 3.23 - 3.24.

Solvent	Polarity Scale[a] E_T / kcal mol^{-1}	λ_{max} / nm ± 0.5 nm	$10^4 \varepsilon$ / mol^{-1} dm^3 cm^{-1} ± 5 × 10^2 mol^{-1} dm^3 cm^{-1}
Cyclohexane	31.2	244	2.2
Dichloromethane	41.1	247	not measured
Acetonitrile	46.0	245	not measured
Methanol	55.5	246	not measured
1,1,2 - Trichlorotrifluoroethane	-	244	not measured
EPA (5:5:2 diethyl ether : isopentane : ethanol)	-	243.5	not measured
9:1 ethanol : water	-	247	2.2

Table 3.7 Absorption maxima and extinction coefficients for C-methyl dibenzoylmethane in various solvents at room temperature.

a) Solvent polarity scale based on "solvatochromic band" shifts of 4-(2,4,6-triphenylpyridinium)-2,6-diphenylphenoxide and its trimethyl derivative[24]. Values increase with increasing polarity

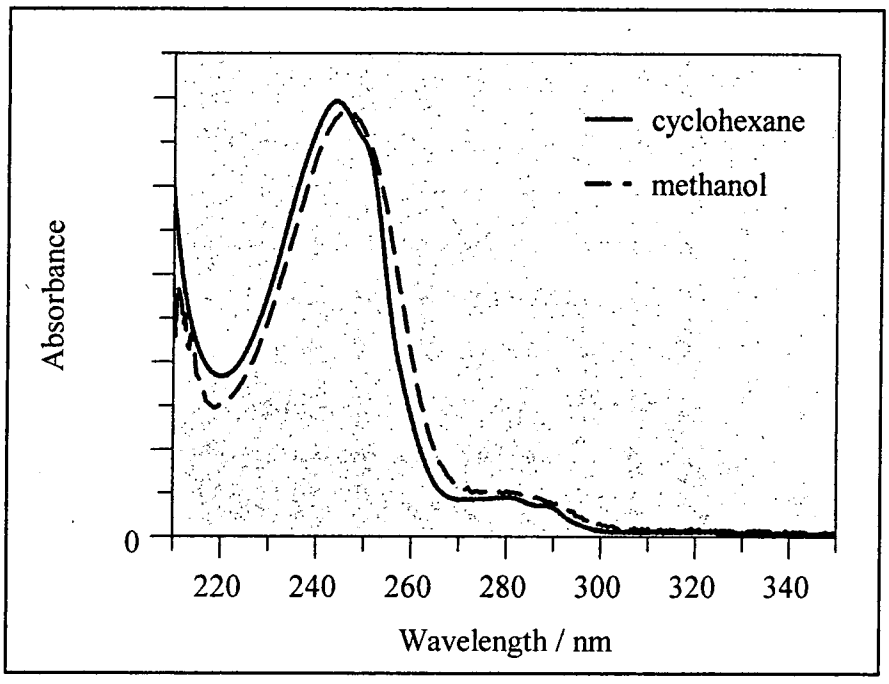

Figure 3.23 Absorption spectra of C-methyl dibenzoylmethane in methanol and cyclohexane.

Solvent	Polarity Scale[a] E_T / kcal mol^{-1}	λ_{max} / nm ± 0.5 nm	10^4 ε / mol^{-1} dm^3 cm^{-1} ± 5 × 10^2 mol^{-1} dm^3 cm^{-1}
Cyclohexane	31.2	262	2.3
Dichloromethane	41.1	264	not measured
Methanol	55.5	263	not measured
1,1,2-Trichlorotrifluoroethane	-	262.5	not measured
9:1 ethanol : water	-	263	2.2

Table 3.8 Absorption maxima and extinction coefficients for C-methyl Parsol 1789 in various solvents at room temperature.

a) Solvent polarity scale based on "solvatochromic band" shifts of 4-(2,4,6-triphenylpyridinium)-2,6-diphenylphenoxide and its trimethyl derivative[24]. Values increase with increasing polarity

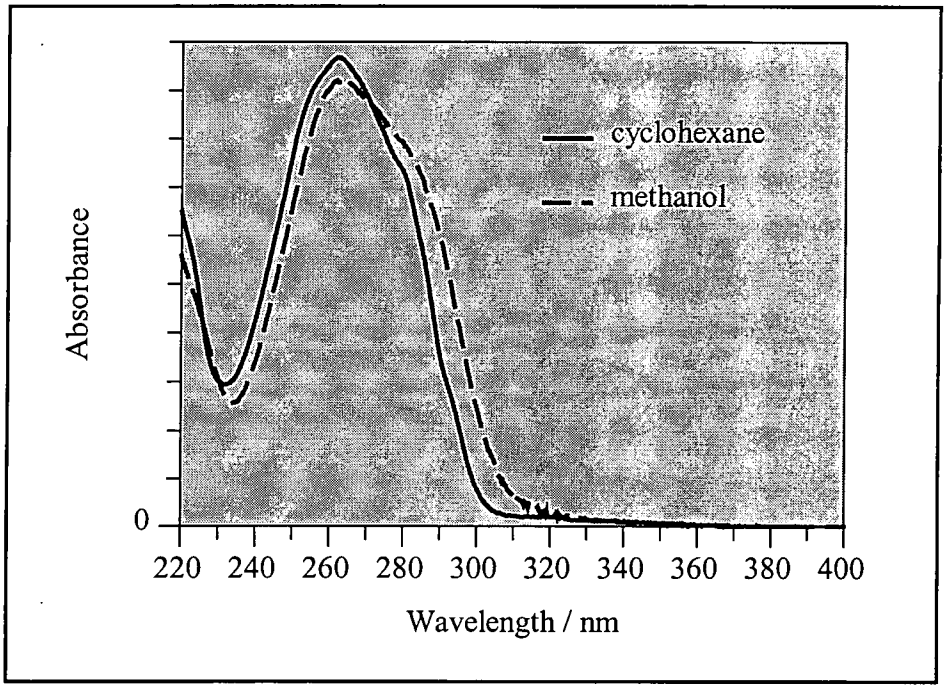

Figure 3.24 Absorption spectra of C-methyl Parsol 1789 in methanol and cyclohexane.

C-methyl dibenzoylmethane shows a spectrum typical of an aromatic ketone, such as acetophenone, the absorption spectra of which is shown in figure 3.25.

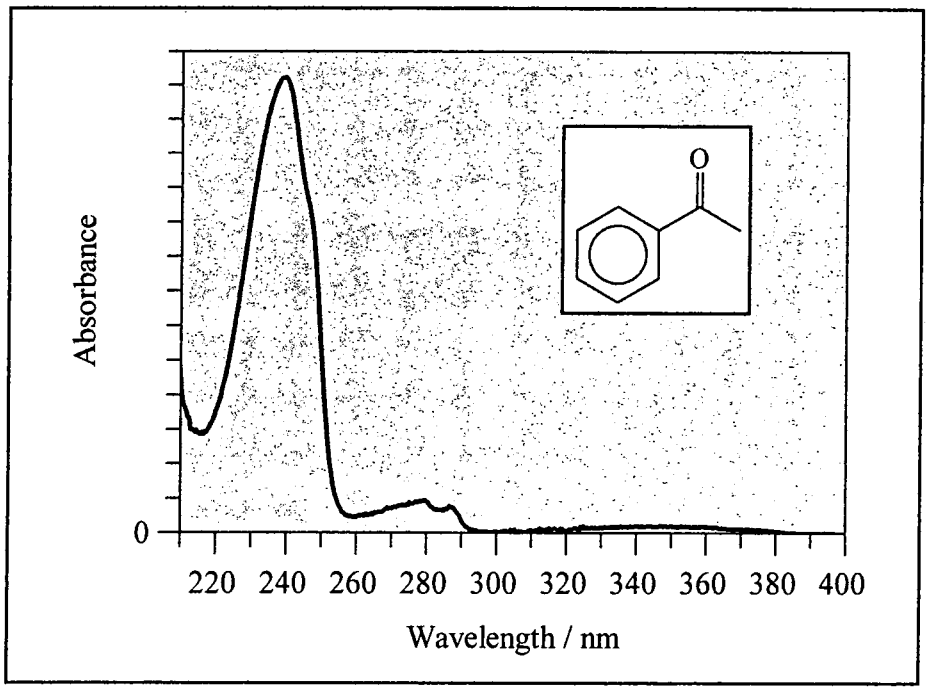

Figure 3.25 Absorption spectrum of acetophenone in cyclohexane at room temperature

The main peak, at $\lambda \approx 245$ nm for C-methyl dibenzoylmethane, is assigned to a $\pi^* \leftarrow \pi$ transition, and can be seen from table 3.5 to display a general shift to longer wavelengths with increasing solvent polarity. The smaller peak at $\lambda \approx 280$ nm, is also a $\pi^* \leftarrow \pi$ transition, and there is a weak $\pi^* \leftarrow$n transition observed at $\lambda \approx 320$ nm.

The spectrum for C-methyl Parsol 1789 appears more structured, and less like that of acetophenone. This effect is due to the contribution of two different spectra from the two different acetophenone fragments, tertiary-butyl acetophenone, and methoxyacetophenone, that make up the molecule, as shown in figure 3.26.

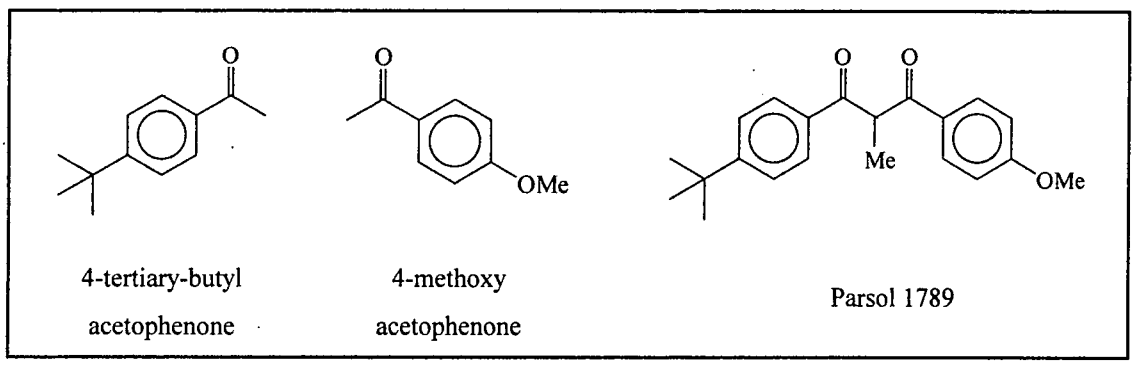

Figure 3.26 Structures of 4-tertiary-butyl acetophenone, 4-methoxy acetophenone and C-methyl Parsol 1789

By adding alkali (KOH) to the C-methyl dibenzoylmethanes solutions, a very large shift in λ_{max} is observed, such that a spectrum is produced that is similar to those seen for the enolates of DBM and Parsol 1789 (see figures 3.16 and 3.18). On neutralising (or acidifying) the solution by adding HCl, the resulting spectrum is similar to that of the dibenzoylmethanes (with no alkali added). Over a period of hours (in the dark) this spectrum slowly reverts to the original spectrum of the C-methyl dibenzoylmethanes. These changes are all shown in figure 3.27.

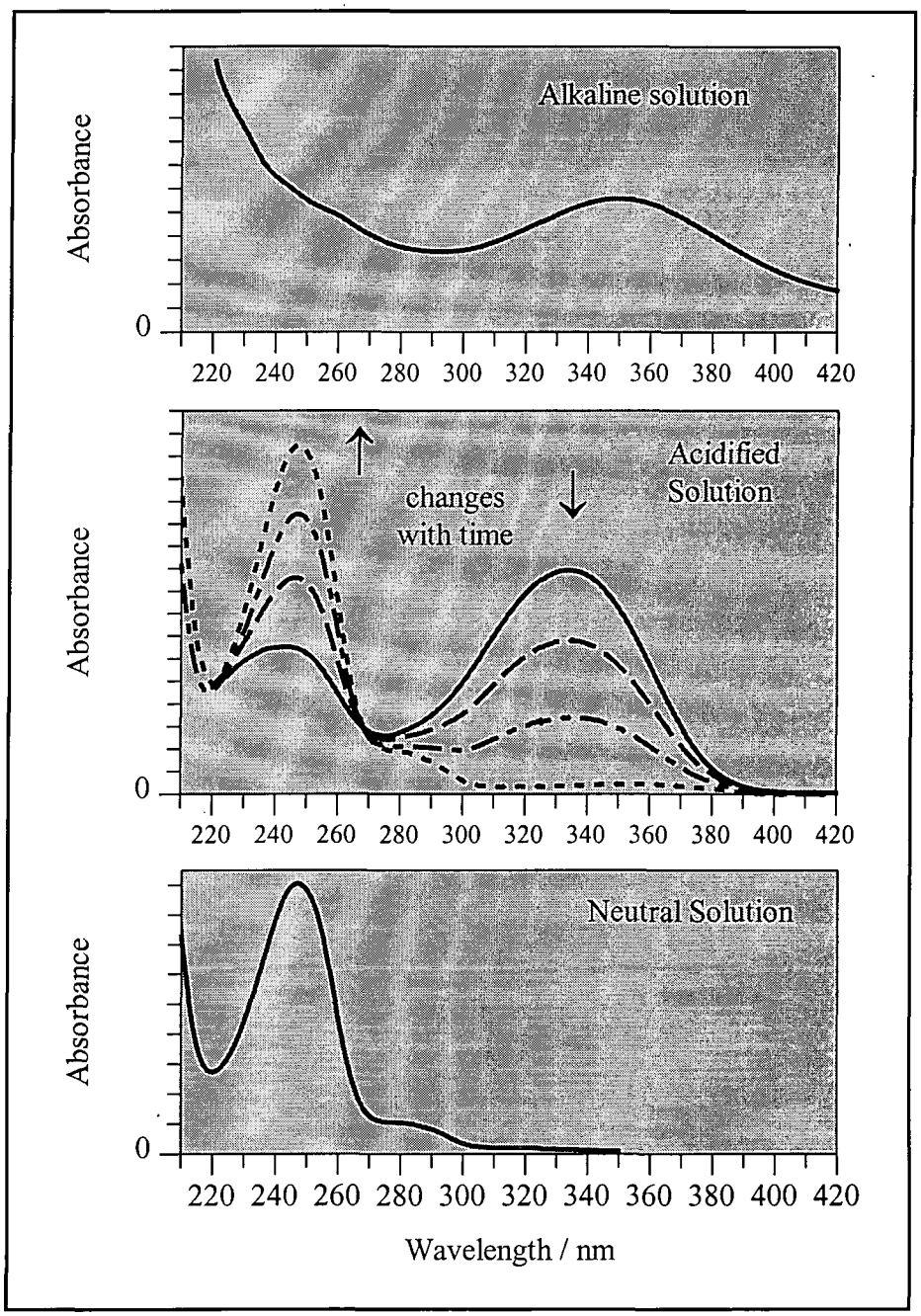

Figure 3.27 Changes in absorption spectrum of C-methyl DBM in alkaline and acidic solutions of 9:1 ethanol : water, at room temperature

These changes are explained by the formation of the thermodynamically unstable enol tautomer of C-methyl DBM. On adding alkali, the enolate of the C-methyl DBM is formed, and has a similar structure to that of the DBM enolates. Addition of acid causes protonation on the oxygen, such that the chelated enol structure is initially formed, and thus the spectrum observed matches that seen for the chelated enol of DBMs. Over time the enol reverts to the thermodynamically favoured diketone structure, and the original spectrum is restored. These changes are shown in figure 3.28.

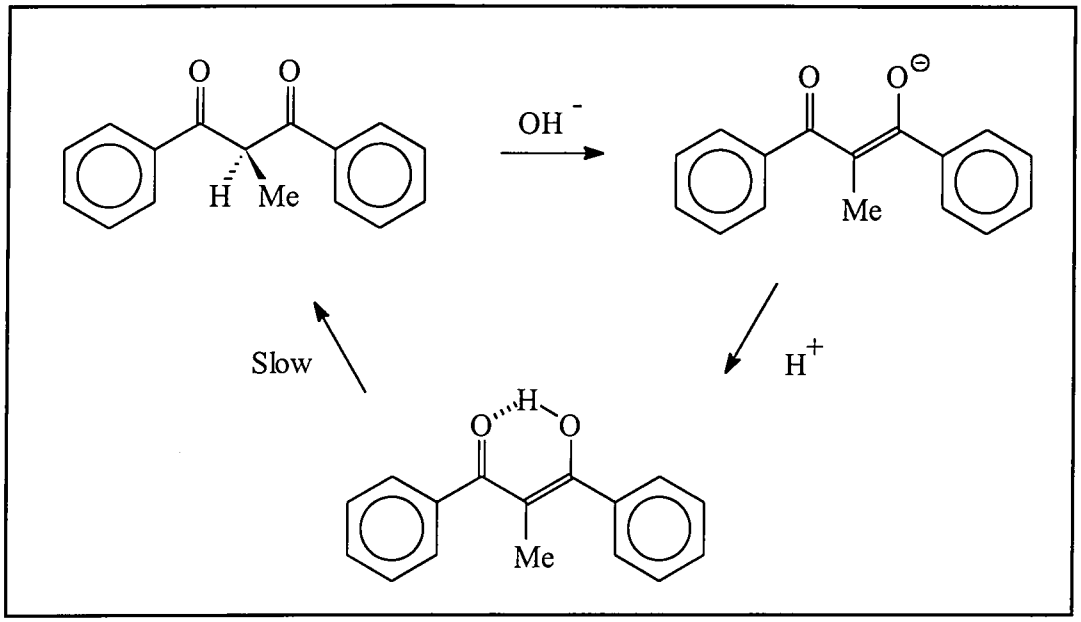

Figure 3.28 Changes occurring in C-methyl DBM on addition of alkali and subsequent neutralisation

The extinction coefficients of the enol forms of C-methyl dibenzoylmethane and C-methyl Parsol 1789 can be calculated from the total C-methyl DBM concentrations and ε for the keto forms. These were measured to be $\varepsilon \approx 2.2 \times 10^4$ mol^{-1} dm^3 cm^{-1} for C-methyl DBM and $\varepsilon \approx 2.6 \times 10^4$ mol^{-1} dm^3 cm^{-1} for C-methyl Parsol 1789, in acidic 9:1 ethanol : water solution. These compare well to the measured extinction coefficients of DBM and Parsol 1789, $\varepsilon \approx 2 \times 10^4$ mol^{-1} dm^3 cm^{-1} and $\varepsilon \approx 3 \times 10^4$ mol^{-1} dm^3 cm^{-1} respectively.

3.2.1.4 Decomposition of DBM in Alkaline Solution

The absorbance spectrum of DBM in alkaline solution, (KOH in 9:1 ethanol : water) as reported in section 3.2.1.1, can be seen to change with time. A reduction in the intensity of the main absorbance

band at $\lambda \approx 350$ nm, accompanied by a slight increase in the intensity of the band at $\lambda \approx 240$ nm, is observed over a period of hours, as shown in figure 3.29

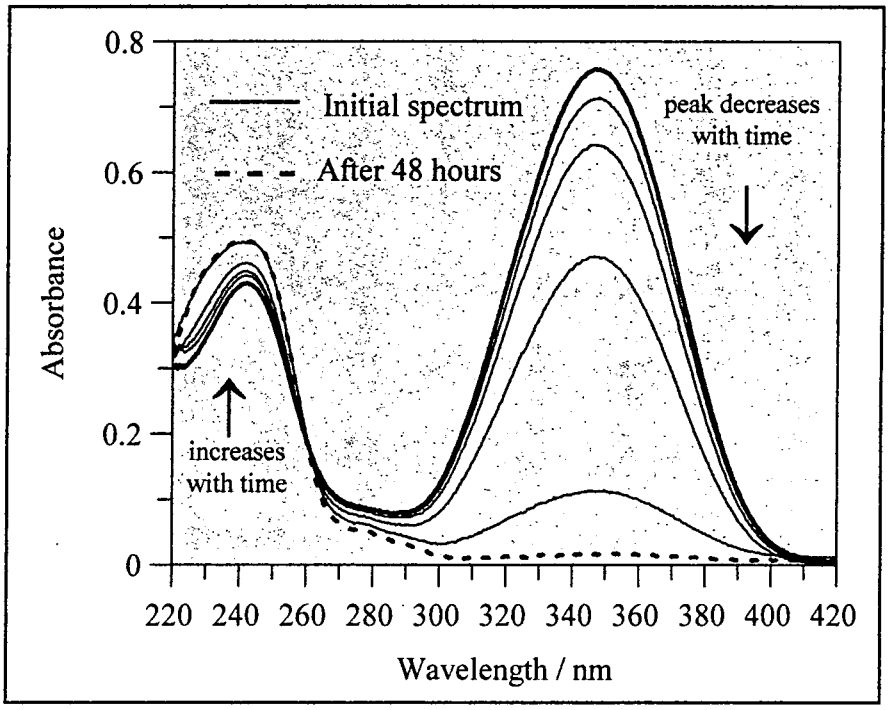

Figure 3.29 Changes in the absorption spectrum of DBM in alkaline solution with time
(solution in 9:1 ethanol : water with added KOH)

These changes have been previously reported in the literature, where the loss of absorbance was observed to decrease exponentially with time, and the first order rate constant of this process was measured to be roughly proportional to the concentration of KOH[10], i.e. it is a pseudo first order process. Morita and Nakanishi suggest that the planar structure of the chelate ring is broken by the action of the KOH, resulting in the loss of the absorption peak due to the π,π^* transition of the chelate ring. If this were the case, it may be expected that restoration of the planar structure would occur on neutralising the solution, however no study of a possible recovery on the neutralisation of the solution was made in their report.

On neutralising the resulting solution after 48 hours, the spectrum of which is shown in figure 3.29, no restoration of the absorbance at $\lambda \approx 350$ nm was observed, either immediately or several days later. It is most likely that the changes occurring are due to decomposition of the DBM, to form ketone products such as acetophenone and ethyl benzoate, and not due to any distortion of the chelate ring. Such a reaction is well precedented in carbonyl chemistry, being the reverse of a Claisen condensation reaction[26].

3.2.2 Low Temperature Absorption Spectra

On cooling solutions of DBM to 77 K, the spectral changes discussed in section 3.1.4.2 can be observed, as shown in figures 3.30 and 3.31.

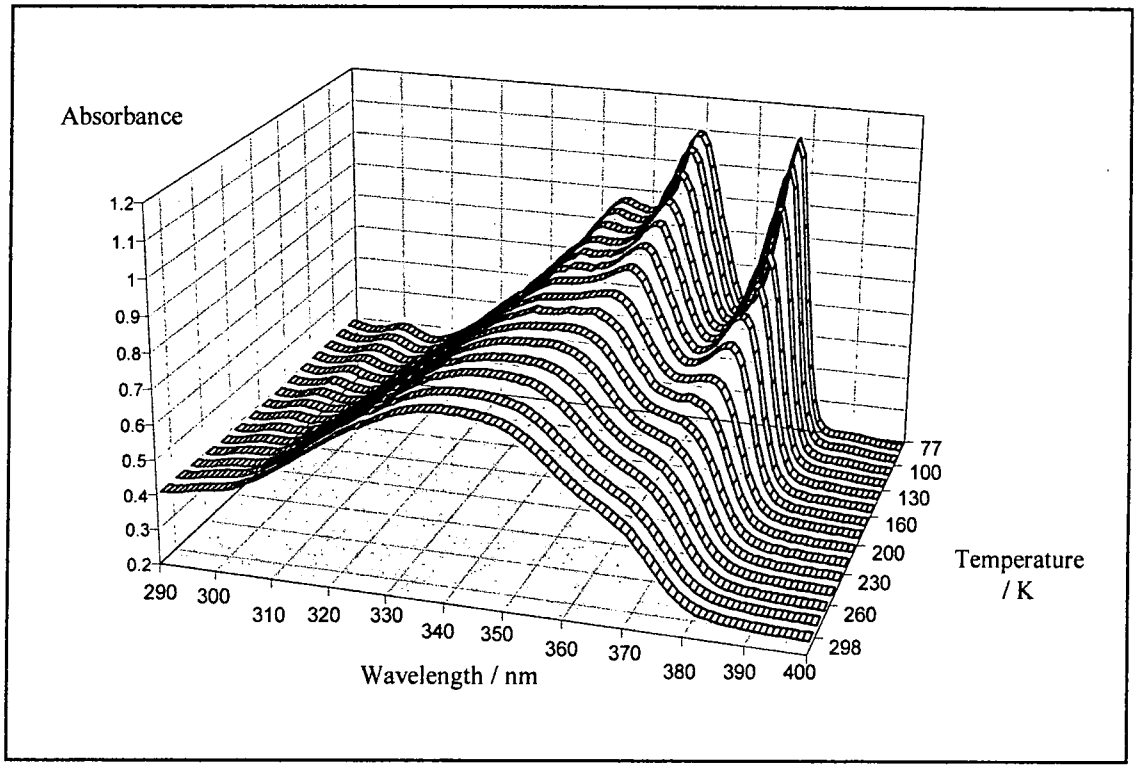

Figure 3.30 Absorbance spectrum of DBM in EPA at various temperatures

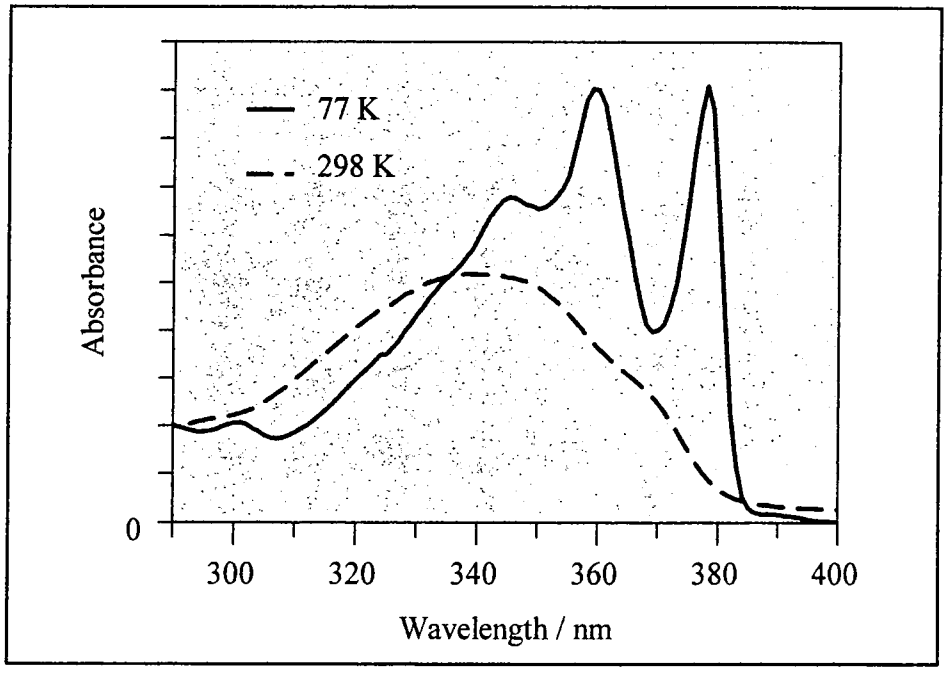

Figure 3.31 Absorbance spectrum of DBM in EPA at 77 K and 298 K

The peaks exhibit a red shift with decreasing temperature. It has been observed that the peak wavelength of electronic absorptions increases, i.e. the energy decreases, with increasing dielectric constant and refractive index of a solvent[27]. Therefore the observed shift is due to an increase in the "solvent concentration" as the temperature decreases, with a corresponding increase in the dielectric constant and refractive index of the solvent. There is also an observed increase in the molar extinction coefficient at the peak wavelength, due to the effective increase in concentration caused by solvent shrinkage. Vibrational structure can be observed, with spacings of 1170 cm^{-1} and 1370 cm^{-1} in EPA, corresponding to vibrations of the excited singlet state of DBM, which are likely to be enolate ring vibrations. The vibrational spectrum of DBM is discussed in chapter 4.

In a 2:1 mixture of isopentane and methylcyclohexane a similar spectrum to that for EPA is observed. The peaks do not appear to be blue shifted, as would be expected in changing from a polar to a non-polar solvent This could be explained by the different solvent systems having different degrees of shrinkage on freezing, causing a different degree of peak shifting in the two cases. For EPA, the ratio of volumes at 77 K and 298 K is V_{77}/V_{293} = 0.778 [29]. No direct data are available for 2:1 isopentane : methylcyclohexane, however the volume ratios for 5:1, 4:1 and 3:1 isopentane : methylcyclohexane mixtures are V_{77}/V_{293} = 0.767, V_{77}/V_{293} = 0.769 and V_{77}/V_{293} = 0.773 respectively [29]. Following this trend, it would be expected that 2:1 isopentane : methylcyclohexane will have a slightly higher volume ratio than that of EPA, although the difference is not significant enough to explain the observed effect.

1,1,2-trichlorotrifluoroethane solution at 77 K does not form a clear glass, and the resultng scattering makes recording spectra difficult. The spectrum of DBM obtained in this solvent at 77 K does not exhibit vibrational structure, but resembles that at 298 K, although slightly red shifted.

Similar spectra are observed for Parsol 1789, Parsol DAM and dtDBM. The positions of absorption peaks are summarised in table 3.9.

	λ_{max} / nm ± 0.5 nm
Dibenzoylmethane	345, 359, 378
Parsol 1789	352[a], 368, 387
Parsol DAM	355, 370, 390
dtDBM	349, 364, 382

Table 3.9 Absorbance data for DBMs and Parsols at 77 K in EPA

a) shoulder

The low temperature absorption spectra of the C-methyl and O-methyl substituted dibenzoylmethanes and Parsol 1789s have the same basic profile as the room temperature spectra, with no vibrational structure visible, although for O-methyl DBM the spectrum at 77 K is less broad. The peaks display a red shift and an increase in intensity, compared to the room temperature spectra, as expected for increasing solvent density. The spectra are summarised in table 3.10 and figures 3.32-3.33.

		λ_{max} / nm ± 0.5 nm
O-Methyl DBM	Z-isomer	318
	E-isomer	306
C-Methyl DBM		244

Table 3.10 Absorption maxima for O-methyl and C-methyl dibenzoylmethane in EPA at 77 K.

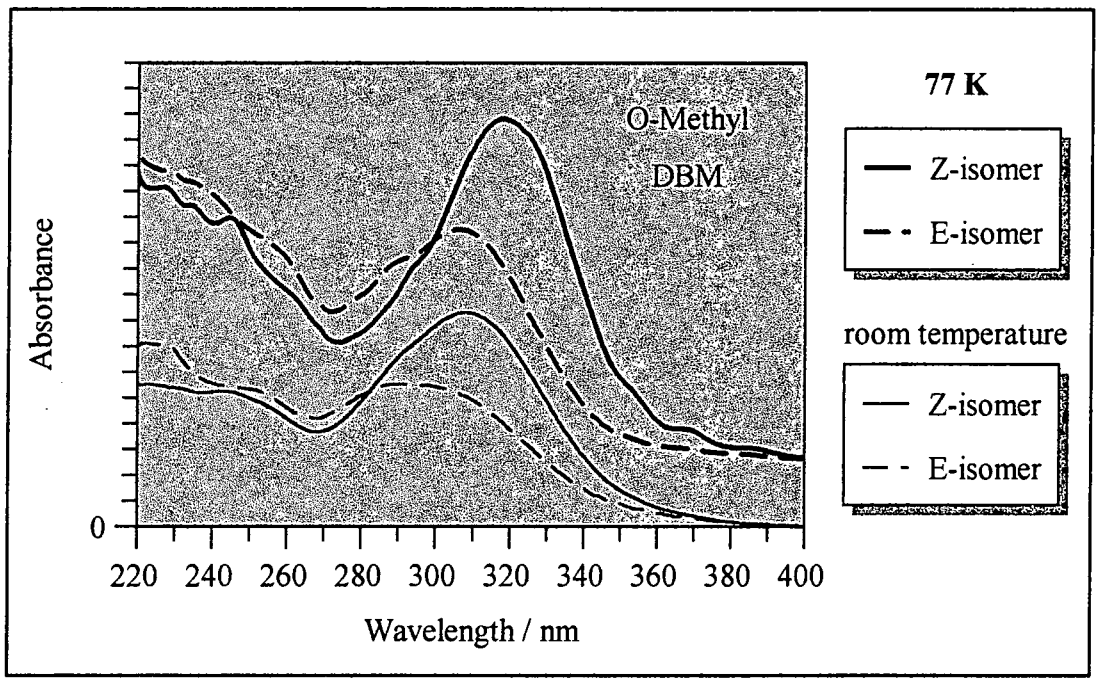

Figure 3.32 Absorption spectra of E and Z isomers of O-methyl dibenzoylmethane in EPA at room temperature and 77 K

(baselines displaced for clarity)

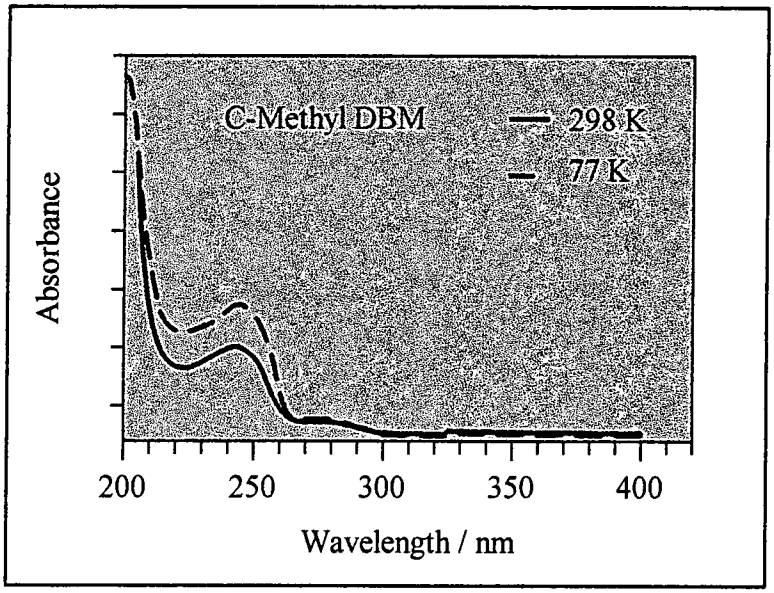

Figure 3.33 Absorption spectra of C-methyl DBM in EPA at room temperature and 77 K

3.2.3 Fluorescence

Dibenzoylmethane samples fluoresce on excitation of the main absorption band at low temperatures. The emission observed reflects the absorption spectrum of the chelated enol. The excitation and emission spectra obtained are shown in figure 3.34, and the results summarised in table 3.11.

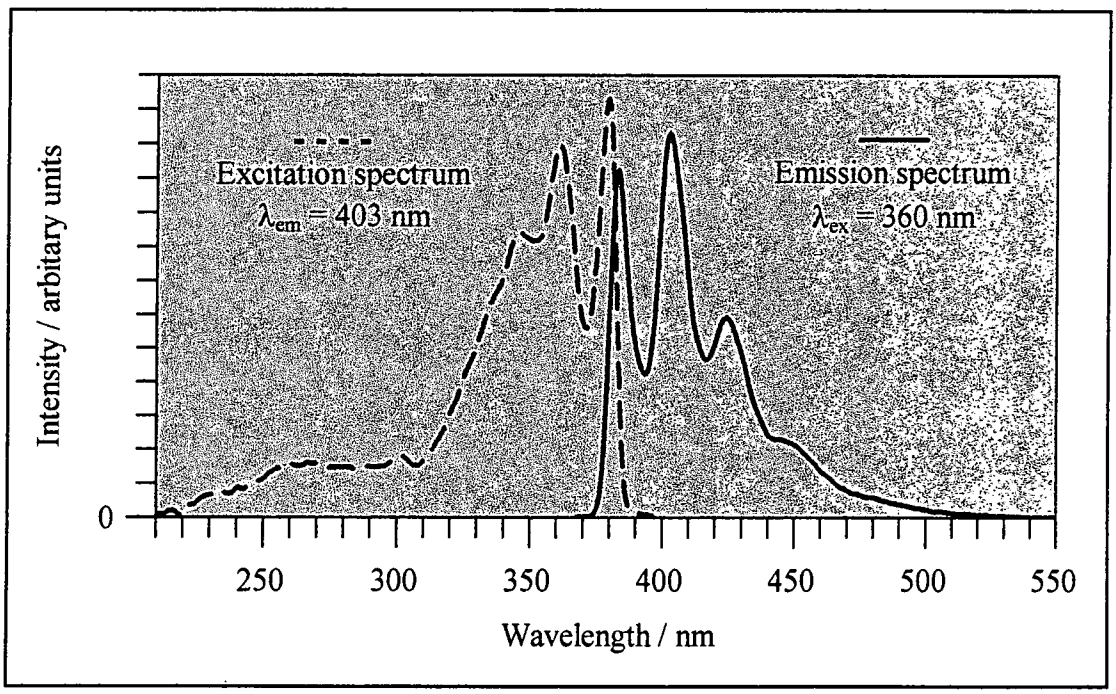

Figure 3.34 Fluorescence excitation and emission spectra of DBM in EPA at 77 K

	Excitation λ_{max} / nm ± 0.5 nm	Emission λ_{max} / nm ± 0.5 nm	Emission vibrational spacing / cm^{-1}
EPA	345.0, 361.0, 379.0	383.5, 402.5, 423.5	1230, 1230
2:1 isopentane : methylcyclohexane	347.5, 363.0, 380.5	387.0, 407.0, 427.0	1270, 1150

Table 3.11 Fluorescence data for DBM at 77 K, for excitation at 360 nm and emission at 403 nm

For DBM in EPA the vibrational spacing is ≈1230 cm^{-1}. This corresponds to a vibration of the chelate ring in DBM[28], which is clearly visible in the infra-red spectrum. (See chapter 4 for more discussion of the infra-red spectrum of DBM.)

Similar fluorescence spectra are observed for Parsol 1789, Parsol DAM and dtDBM, and these results are summarised in table 3.12.

	λ_{em} / nm	Excitation spectrum λ_{max} / nm ± 0.5 nm	λ_{ex} / nm	Emission spectrum λ_{max} / nm ± 0.5 nm	Emission vibrational spacing / cm^{-1}
Parsol 1789	413	353[a], 368.5, 388.0	368	393.5, 413.0, 435.5	1200, 1250
Parsol DAM	414	355.0, 370.5, 390.5	370	394.5, 414.5, 437.0	1225, 1242
dtDBM	407	349.0, 364.5, 383.5	364	387.0, 407.0, 428.5	1270, 1235

Table 3.12 Fluorescence data for Parsols in EPA at 77 K.

a) shoulder

For all the compounds studied, weak fluorescence was also observed for excitation <300 nm. An example is shown in figure 3.35.

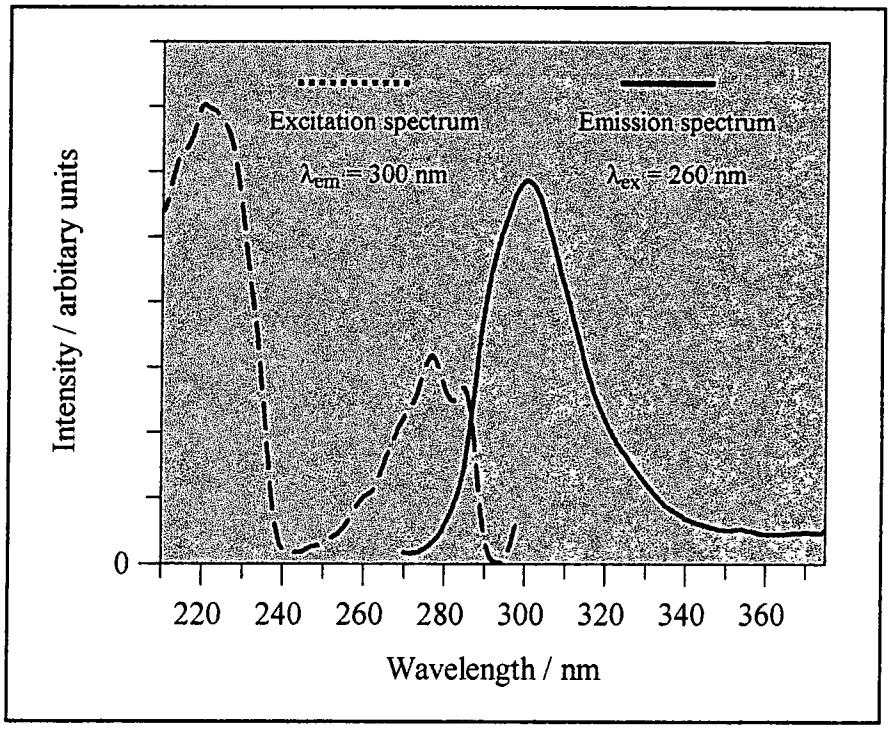

Figure 3.35 Fluorescence spectrum of DBM in EPA at 77 K.

This fluorescence may be due to the diketone component in the samples, however the peak in this excitation spectrum appears to be too far to the red for this to be the case. This may be due to an inner filter effect, where re-absorption of emitted radiation can cause a distortion of the observed spectra. A similar spectrum is observed for C-methyl DBM, suggesting that the diketone structure does weakly fluoresce. Similar fluorescence spectra were also weakly observed at room temperature.

No fluorescence attributable to dimers was observed, and the O-methyl derivatives were not observed to fluoresce at low temperature or room temperature.

3.2.4 Phosphorescence

Two different phosphorescence spectra were observed when different bands of DBMs were irradiated, as has been reported elsewhere (see section 3.1.4.4.)

A blue phosphorescence, due to the diketone component can be observed using 260 nm excitation, as shown in figure 3.36.

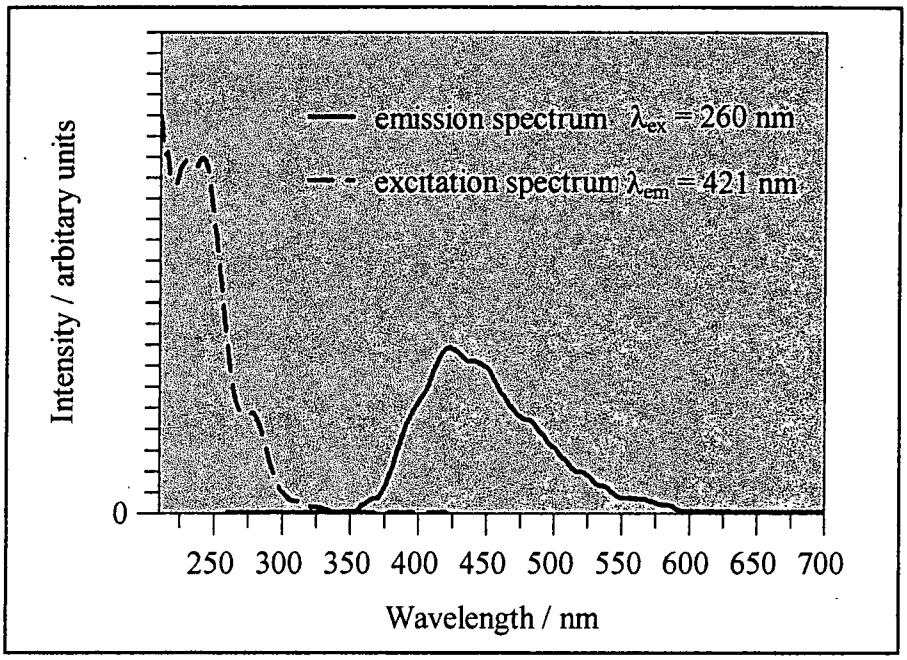

Figure 3.36 Phosphorescence spectrum of DBM in EPA at 77 K

This emission has a blue edge at $\lambda \approx 354$ nm for DBM in EPA, which corresponds to a triplet energy of $E_T \approx 340$ kJ mol^{-1}. This compares to the triplet energies of acetophenone, $E_T = 310$ kJ mol^{-1}, and benzophenone, $E_T = 287$ kJ mol^{-1} [29].

The phosphorescence spectrum is similar to that observed for C-methyl DBM, as shown in figure 3.37, confirming that it is indeed due to the diketone content. The DBM spectrum lacks the vibrational structure seen with C-methyl DBM. This is due to the weak signal, and use of large emission and excitation slits in obtaining the DBM spectrum.

The phosphorescence lifetime of DBM in EPA, λ_{ex}=260 nm, was measured to be approximately $\tau_p \approx 1$ ms, however the signal was very weak. This value compares to that of $\tau_p \approx 50$ ms measured by Kuo[17] under similar conditions. Clearly there is a discrepancy between these two values, the origin of which is not clear. The phosphorescence lifetime of C-methyl DBM was measured to be $\tau_p \approx 6.5$ ms. These values compare to the triplet lifetimes of acetophenone and benzophenone reported in the literature; τ_T=2.1 ms in non-polar solvents and τ_T=5 ms in polar solvents for acetophenone, and τ_T=1 ms in non-polar solvents and τ_T=6 ms in polar solvents for benzophenone[29].

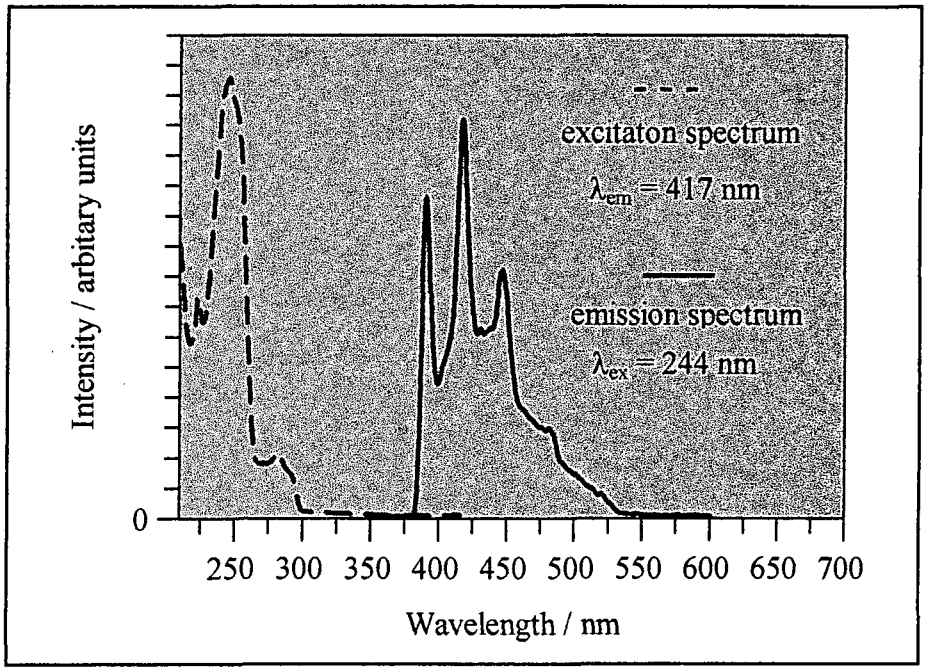

Figure 3.37 Phosphorescence spectrum of C-methyl DBM in EPA at 77 K

A longer lived green phosphorescence is observed for excitation of the chelated enol band of DBM at $\lambda \approx 360$ nm, as shown in figure 3.38.

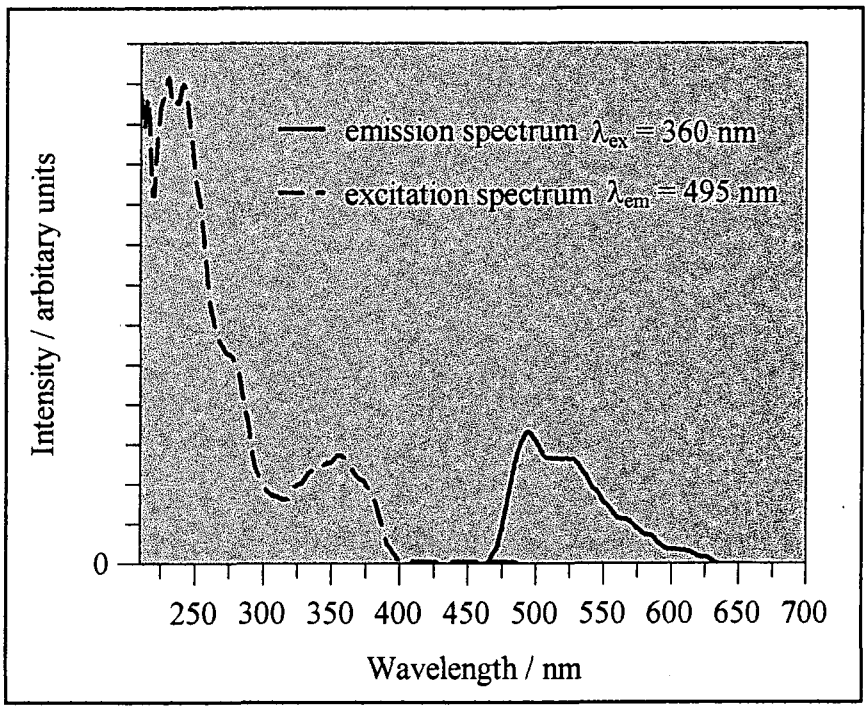

Figure 3.38 Phosphorescence spectrum of DBM in EPA at 77 K

The weakness of the phosphorescence emission limits resolution of vibration bands. The emission has a blue edge at $\lambda \approx 464$ nm for DBM in EPA, which corresponds to a triplet energy of $E_T \approx 260$ kJ mol^{-1}. The excitation spectrum obtained confirms that this phosphorescence is due to the chelated enol form. It was not possible to measure the lifetime due to the low intensity of the signal, although the green phosphorescence was clearly visible with the eye over a period of seconds. A lifetime of $\tau_p > 1$ s is typical of a $\pi^* \leftarrow \pi$ transition (see section 3.1.2.2.) as would be expected for this band.

Similar phosphorescence spectra are obtained for Parsol 1789, Parsol DAM and dtDBM. The spectra obtained for these seem to be of better quality than those seen for DBM. It suggests that the Parsols have a larger quantum yield of phosphorescence. Spectra for the Parsols are given in figures 3.39 - 3.40, and a summary of all the data for dibenzoylmethanes and Parsols are given in table 3.13.

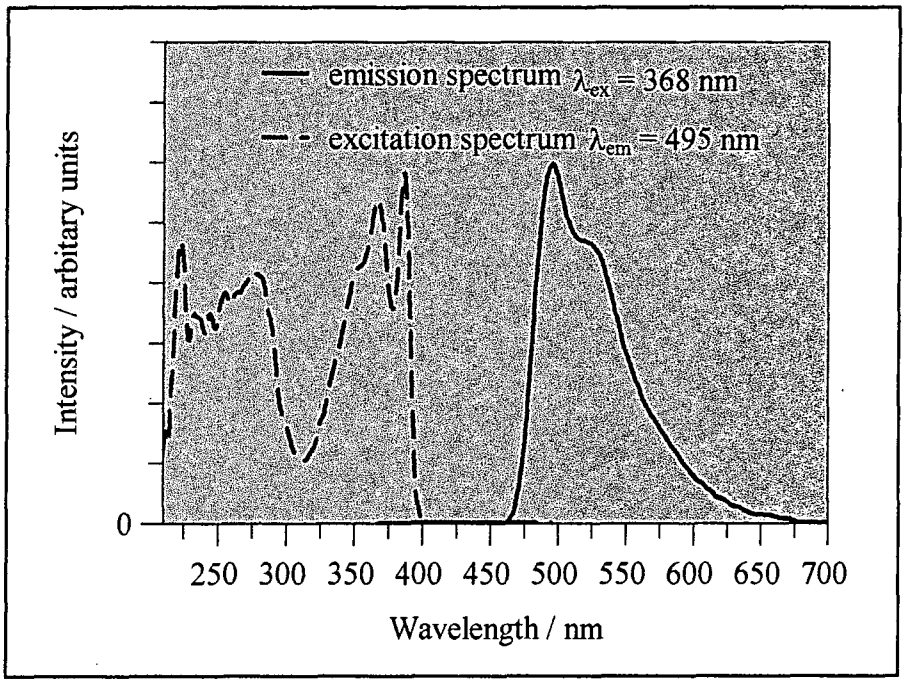

Figure 3.39 Chelated enol phosphorescence spectrum of Parsol 1789 in EPA at 77 K

The triplet energy measured for the chelated enol form of Parsol 1789, $E_T \approx 260$ kJ mol^{-1} at 77 K in EPA, which is the same as the value measured, using the same technique, by Truscott *et al*, $E_T = 260$ kJ mol^{-1}. at room temperature in N_2 flushed 2-methylpentane[20].

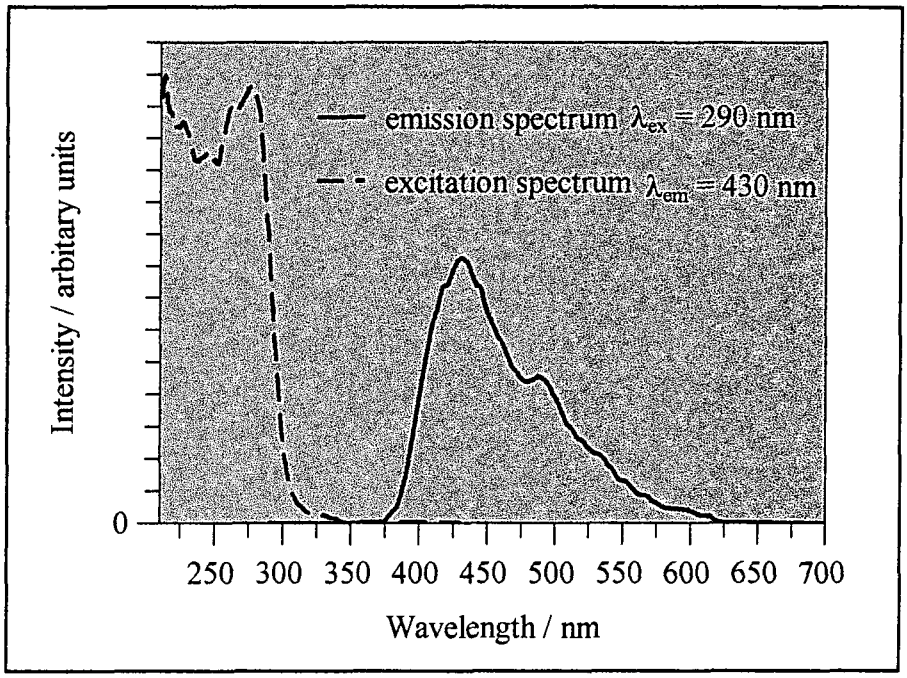

Figure 3.40 Diketone phosphorescence spectrum of Parsol 1789 in EPA at 77 K

	λ_{ex} / nm[a]	Emission spectrum λ_{max} / nm ± 1 nm	Emission blue edge λ / nm ± 2 nm	E_T / kJ mol^{-1} ± 5 kJ mol^{-1}
DBM	360	494	464	260
	260	423	354	340
Parsol 1789	368	495	462	260
	290	430	374	320
Parsol DAM	370	494	459	260
	300	440	382	310
dtDBM	364	495	458	260
	279	421	334	360
C-Methyl DBM	244	390.5, 417.0, 447.0[b]	382	315

Table 3.13 Phosphorescence data for dibenzoylmethanes at 77 K

a) excitation wavelengths not necessarily at centre of absorption peaks

b) data ± 0.5 nm

In a non-polar solvent system of 2:1 isopentane : methylcyclohexane at 77 K, the phosphorescence observed is very much less intense. This is for both the chelated enol phosphorescence and that of the

diketone. As discussed in section 3.1.4.4., in a non-polar environment, it would be expected that the diketone phosphorescence would be reduced, because a smaller quantity is present. The chelated enol phosphorescence should be visible in a non-polar solvent, so it is not clear why it is not.

No phosphorescence was observed at room temperature for any of the compounds, and no phosphorescence was observed for the O-methyl derivatives, at room temperature or low temperature.

3.3 Summary

The photophysics of ketones has been extensively studied over the years, and there are many reviews in the literature. 1,3 dicarbonyl compounds can exist as diketone or enol structures, where the diketone displays the photophysics expected from a ketone compound, however the photophysics of enol can be quite different.

In this work the photophysical properties of dibenzoylmethane, Parsol 1789, Parsol DAM and di-tertiary-butyl dibenzoylmethane have been studied, along with the respective O-methylated and C-methylated compounds of DBM and Parsol 1789. The photophysics of these compounds is important for understanding the photochemistry of dibenzoylmethanes, which is discussed in chapter 4.

Dibenzoylmethanes exist primarily as an intra-molecularly bonded enol structure, which absorbs strongly at $\lambda \approx 340$ nm due to a π,π^* transition. The absorption spectra of DBMs also exhibit a smaller peak at $\lambda \approx 250$ nm, due to an n,π^* transition of the small diketone content. In this work, the absorption peak positions and extinction coefficients of the DBMs in various solvents have been measured. In alkaline solution, the enolate species is formed, with an absorption band at longer wavelength.

At low temperature the main absorption band of DBMs shifts to longer wavelengths, and vibrational structure can be observed. The enol form of DBMs fluorescence at low temperature, with the ($v_0' \rightarrow v''_0$) emission at approximately $\lambda \approx 385$ nm. Phosphorescence can also be observed at low temperature from both the diketone (emission peak at $\lambda \approx 495$ nm,) and enol forms (emission peak at $\lambda \approx 425$ nm). Thus the triplet energies of the diketones and enols of the DBMs studied have been measured.

O-methylated DBMs do not posses an intra-molecular H-bond, and the π,π^* absorption band falls to lower wavelengths than for chelated DBMs, at $\lambda \approx 300$ nm. O-Me DBMs exist as E or Z isomers, where the peak for the more thermodynamically stable E-isomer falls at a slightly shorter wavelength than the Z-isomer. No fluorescence or phosphorescence is observed from O-methyl DBMs at low temperature

C-methylated DBMs exist as a diketone structure, and display photophysics typical of an aromatic ketone such as acetophenone. Phosphorescence can be observed at low temperature.

In summary, many photophysical processes of DBMs have been studied, and as such, this chapter has provided some of the necessary background for understanding the photochemistry of dibenzoylmethanes.

3.4 References

[1] Turro N J, "*Modern Molecular Photochemistry*", University Science Books, California, 1991

[2] Wayne R P, "*Principles and Application of Photochemistry*", Oxford University Press, Oxford, 1988

[3] Wagner P J, "*Topics in Current Chemistry 66 - Triplet States III; Chemistry of Excited Triplet Organic Carbonyl Compounds*", Springer-Verlag, New York, 1975, page 1

[4] Barltrop J A, Coyle J D, "*Principles of Photochemistry*", John Wiley & Sons, Chichester, 1978

[5] Gilbert A, Baggott J, "*Essentials of Molecular Photochemistry*", Blackwell Scientific Publications, Oxford, 1991

[6] Markov P, "Light-induced Tautomerism of β-Dicarbonyl Compounds", *Chem. Soc. Reviews*, **13** (1984), 69

[7] Morton R A, Hassan A, Calloway T C, "Absorption Spectra in Relation to the Constitution of Keto-Enols", *J. Chem. Soc.*, (1934), 883

[8] Gacoin P, "Studies on the Triplet State of Carbonyl Compounds. I. Phosphorescence of β-Diketones", *J. Chem. Phys.*, **57** (1972), 1418

[9] Kittel G, Köhler G, Getoff N, "Sensitised Ketonisation of Ethyl Acetoacetate. A Method for the Determination of Triplet Quantum Yields", *J. Phys. Chem.*, **83** (1979), 2174

[10] Morita H, Nakanishi H, "Electronic Structures and Spectra of the Enol Form of Some β-Diketones", *Bull. Chem. Soc. Jpn.*, **54** (1981), 378

[11] Nikolov P, Fratev F, Petkov I, Markov P, "Dimer Fluorescence of some β-Dicarbonyl compounds", *Chem. Phys Lett.*, **83** (1981), 170

[12] Hay R W, Williams P P, "Proton magnetic resonance of Hydrogen-bonded Chelate Rings", *J. Chem. Soc.*, (1964), 2270

[13] Veierov D, Bercovici T, Fischer E, Mazur Y, Yogev A, "Photoisomerisation of the Enol Form of 1,3-Dicarbonyl Compounds", *J. Am. Chem. Soc.*, **99** (1977), 2723

[14] Veierov D, Bercovici T, Fischer E, Mazur Y, Yogev A, "Photoisomerisation of β-Diketones and β-Keto Esters", *J. Am. Chem. Soc.*, **95** (1973), 8173

[15] Tobita S, Ohba J, Nakagawa K, Shizuka H, "Recovery mechanism of the reaction intermediate produced by photoinduced cleavage of the intramolecular hydrogen bond of dibenzoylmethane", *J. Photophys. Photochem. A: Chem.*, **92** (1995), 61

[16] Kiuchi F, Chen X, Tsuda Y, "Z-E Isomerisation of β-Methoxychalcones: Preferred Existence of E-Isomers in Naturally Occurring β-Methoxychalcones", *Chem. Pharm. Bull.*, **38(7)** (1990), 1862

[17] Kuo J, "UV Spectroscopic and Nuclear Magnetic Resonance Studies of the Enol-Keto Tautomerism in β-Diketones", PhD Thesis, Louisiana State University, 1966

[18] Baczeyñski A, Bissinger J, "Luminescence Properties of β-diketone Chelates. The Vibronic Structure of Emission Spectra of Dibenzoylmethane Chelates", *Bulletin de L'academie Polonaise des Sciences. Série des Sciences math, astr. et phys.*, **16(1)** (1968), 73

[19] Dai G, Qin X, Zhang J, Wu S, "Phototautomerization of β-diketones", *Youji Huaxue (Organic Chemistry)*, **2** (1987), 155, (English translation)

[20] Gonzenbach H, Hill T J, Truscott T G, "The triplet energy levels of UVA and UVB sunscreens", *J. Photochem. Photobiol. B: Biol.*, **16**, (1992), 377

[21] "Triplet-triplet absorption spectra of organic molecules", *J. Phys. Chem. Ref. Data*, **15(1)** (1986)

[22] Astier R, Meyer Y H, "Absorption des β-dicétones sous forte excitation optique", *J. Chim. Phys. Phys-Chim-Biol.*, **65** (1968), 1407

[23] Rhoads S J, Pryde C, "Enolic Concentrations in β-Keto Esters. Correlation of Bromometric and Ultraviolet Absorption Data", *J. Org. Chem.*, **30** (1965), 3212

[24] Taft R W, "An Examination of Linear Solvation Relationships" in "*Progress in Physical Organic Chemistry*", Abboud J L M, Kamlet M J, Taft R W, Volume 13, page 485

[25] Rogers M T, Burdett J L, "Keto-Enol Tautomerism in β-Dicarbonyls studied by Nuclear Magnetic Resonance Spectroscopy", *Can. J. Chem.*, **43** (1965), 1516

[26] McMurry J, "*Organic Chemistry*", 2nd Edition, Brooks/Cole Publishing Company, California, 1988, page 833

[27] Birks J B, "*Photophysics of Aromatic Molecules*", Wiley-Interscience, London, 1970

[28] Tayyari S F, Zeegers-Huyskens T, Wood J L, "Spectroscopic study of hydrogen bonding in the enol form of β-diketones - I. Vibrational assignment and strength of the bond", *Spectrochimica Acta.*, **35 A** (1979), 1265

[29] Murov S L, Carmichael I, Hug G L, "*Handbook of Photochemistry*", Marcel Dekker Inc., New York, 1993

Chapter 4

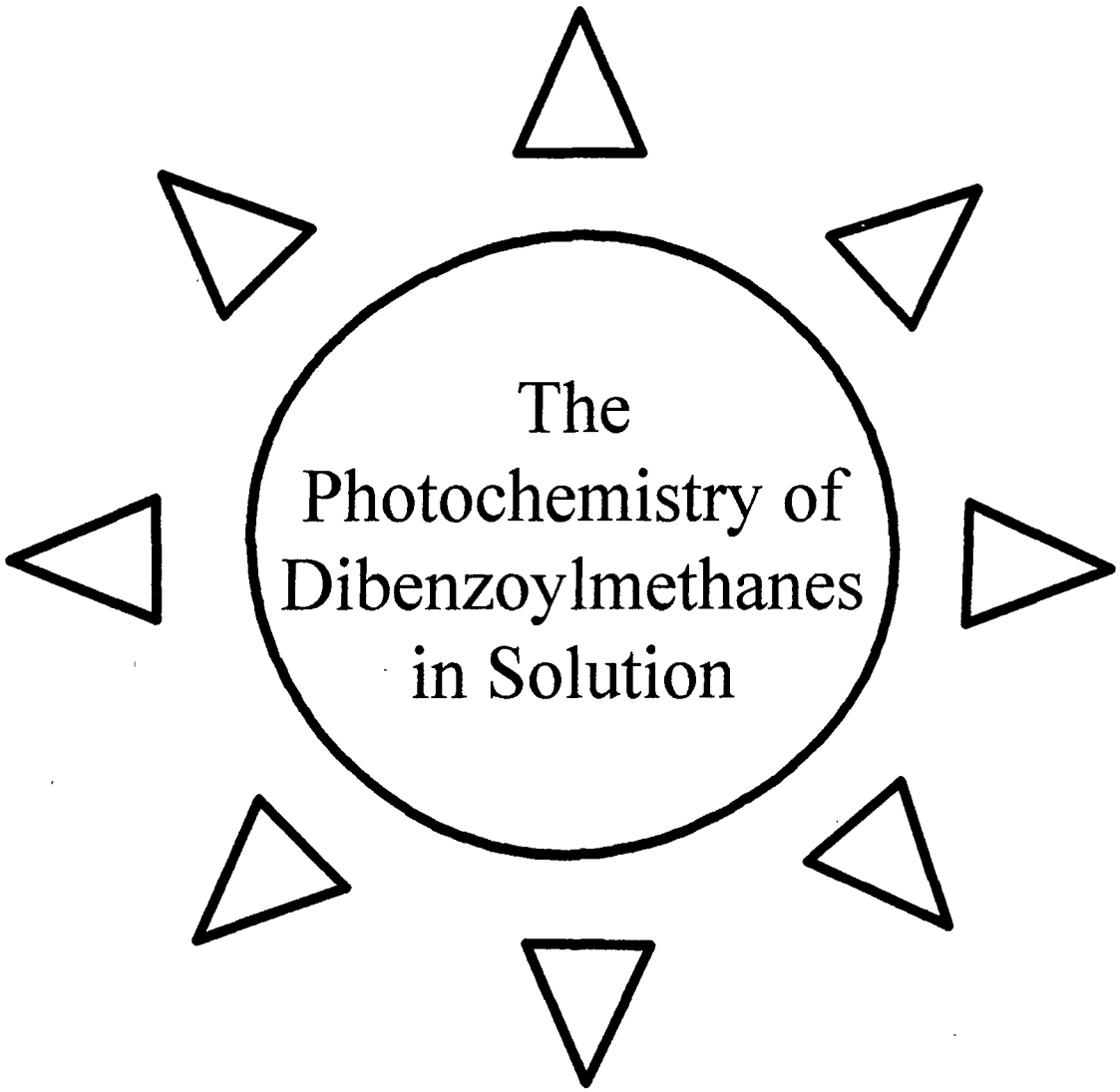

4.1 Introduction

The aim of this work is to improve the understanding of the photochemistry of dibenzoylmethanes in solution, because relatively little is known about the photochemistry of these sunscreens, despite their widespread use. The introduction to this chapter discusses in depth the previous work carried out in this and related fields, however much of the published data and theories are contradictory.

4.1.1 Photochemistry of Carbonyl Compounds[1,2,3]

4.1.1.1 Introduction

Carbonyl compounds undergo a rich variety of chemical and photochemical reactions, and these have been extensively studied over many years. In the ground state, the polarisation of the carbonyl bond is such that the carbon is electron deficient and subject to nucleophilic attack. Promotion of an electron to form an excited state causes a change in the electronic distribution of the carbonyl bond, as described in chapter 3. It is therefore found that the excited state photochemistry of carbonyl compounds is very different to the chemistry observed in the ground state. Furthermore, the chemical behaviour of excited carbonyl compounds can be expected to vary depending on whether the lowest excited state is n,π^* or π,π^* in nature.

In an $\pi^* \leftarrow n$ transition of a carbonyl group, an electron is removed from a non-bonding orbital of the oxygen into a carbonyl π^* orbital, such that the oxygen becomes electron deficient, and the carbon electron rich. The carbon-oxygen double bond is destabilised compared to the ground state, and the chemical behaviour is like that of a diradical. The chemistry of n,π^* excited carbonyls is similar to that of ground state alkoxy radicals, R-O•. In the n,π^* state, the carbon is no longer subject to nucleophilic attack, but can itself act as a nucleophile[1]. Conversely, in a carbonyl $\pi^* \leftarrow \pi$ transition, electron densities at the carbon and oxygen are increased, and the oxygen is observed to be more nucleophilic[3].

The majority of carbonyl photochemistry occurs from the n,π^* excited states[1,2], which is commonly the lowest excited state for carbonyl compounds, as discussed in chapter 3. The main photochemical reactions can be classified into 4 categories; α-cleavage, hydrogen abstraction, charge transfer complexation and attack at carbon-carbon multiple bonds.

4.1.1.2 α-Cleavage Reactions[1,2,3]

The carbon-carbon sigma, or α-bond, of carbonyls in the n,π* excited state is weakened compared to the ground state, by overlap with the vacant n-orbital on the oxygen[1,3]. This has the effect of favouring homolytic cleavage at this α-bond to form two radical species, as shown in figure 4.1. For acyclic ketones a diradical species is formed. This process is known as α-cleavage, and is often referred to as Norrish type I cleavage. The electron in the π* orbital is orthogonal to the reaction co-ordinate and is not considered to be involved in the reaction[3].

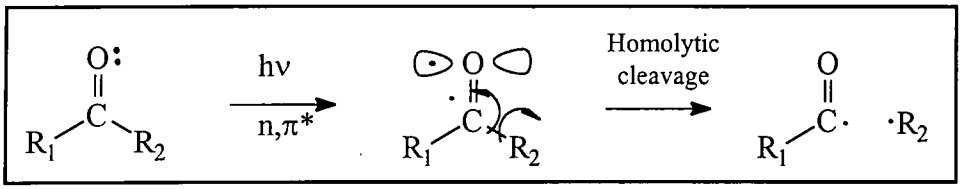

Figure 4.1 α -cleavage of carbonyl compounds[1]

Once α-cleavage has taken place, the radical fragments may undergo several possible fates. They may recombine whilst in the solvent cage, further fragment, or undergo disproportionation and combination, such that a variety of products can be formed, depending on the initial structure of the carbonyl compound[1].

It is possible for α-cleavage to take place from both n,π* singlet and triplet states, however it is usually the triplet state that is responsible, due to the longer lifetime of this species, and the high level of inter-system crossing from the singlet to triplet state[1]. This is especially true for phenyl ketones, where the high level of inter-system crossing from the singlet to triplet state means that reaction takes place exclusively from the triplet state.

4.1.1.3 Hydrogen Abstraction Reactions[1,2,3]

The excited n,π* state of a carbonyl compound is electron deficient and can abstract a hydrogen atom from a nearby C-H bond, in a manner similar to an alkoxy radical[1,2]. This may be from a donor molecule, including the solvent, or the abstraction may occur intramolecularly. The C-H bond cleaves homolytically such that a ketyl radical and an alkyl radical are formed, as shown in figure 4.2.

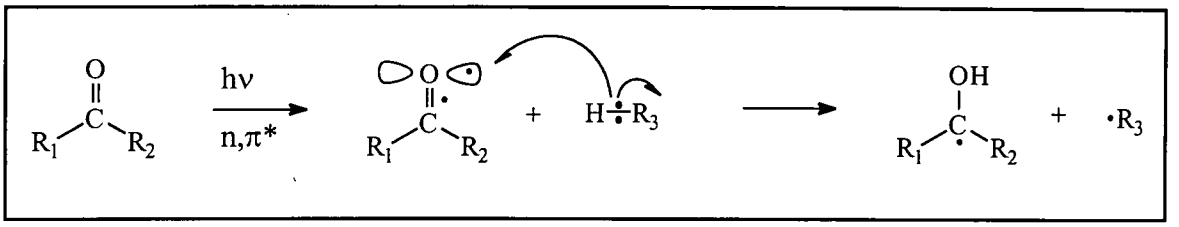

Figure 4.2 Hydrogen abstraction reaction of carbonyl compounds[1]

The radical fragments created may then go on to form a variety of products. The ketyl radical may dimerise to give a pinacol, it may undergo further hydrogen abstraction to produce a secondary alcohol, or it may combine with the donor radical to give a tertiary alcohol[1]. Intra-molecular hydrogen abstraction can result in enolisation[4,5], although other reactions may follow, such that the enol is not isolated.

Intramolecular hydrogen abstraction is favoured in a γ-carbon, and results in a [1,5] hydrogen shift, to generate a biradical. This reaction is known as a Norrish type II process[1].

Reaction is possible from both the singlet and triplet states of carbonyl compounds. However, as for α-cleavage, hydrogen abstraction most commonly occurs from the triplet state than from the much shorter-lived singlet state. In phenyl ketones especially, where a high level of inter-system crossing from the singlet to triplet state, reaction takes place exclusively from the triplet state.

4.1.1.4 Charge Transfer Complexation[3,2]

Excited states are easier to oxidise and reduce than are the corresponding ground states. Carbonyl compounds undergo one electron reductions relatively readily, to produce ketyl radical anions, however, the excited states of carbonyls more commonly form charge transfer complexes with a range of electron donors[3].

The complexes formed are generally considered to be exciplexes, although there is no evidence that they dissociate back to the excited ketone, or phosphoresce, but instead are known to undergo facile chemical rearrangement and radiationless decay[3]. An important reaction of charge transfer complexation is the cycloaddition to olefins, which is discussed in section 4.1.1.5. The transfer of energy from the excited carbonyl to the donor molecule can also occur, such that the donor is left in an excited electronic state[3,2].

The formation of charge transfer complexes acts as an important pathway for the quenching of carbonyl excited states. Many common solvents can act as suitable electron donors, resulting in short observed triplet lifetimes in solution. For example, aromatic compounds such as benzene can act as π-electron donors to quench excited ketones via charge-transfer[3]. In carbonyl compounds such as phenyl ketones, self-quenching can also occur[3].

4.1.1.5 Addition to Carbon-Carbon Multiple Bonds[2,3]

The cycloaddition to a carbon-carbon double bond can occur from the n,π* excited triplet state of a carbonyl compound, resulting in the formation of an oxetane. The reaction proceeds via a diradical intermediate, which can either be formed directly from a carbonyl-olefin charge transfer complex, or exciplex, or via a radical ion pair[2]. The reaction is regiospecific if a radical ion pair is not formed prior to the diradical[2].

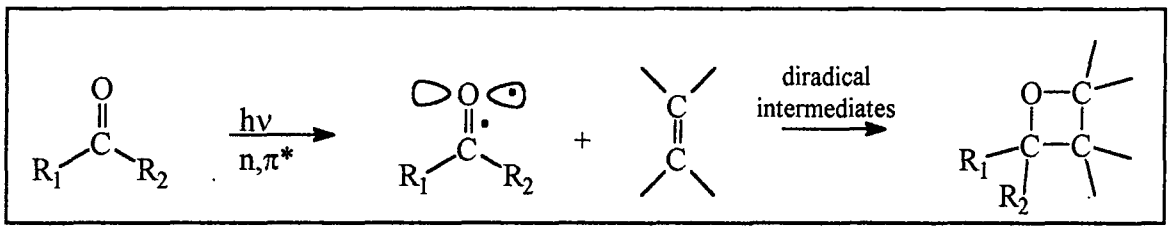

Figure 4.3 Cycloaddition to olefins reaction of carbonyl compounds[2]

Clearly for this type of reaction, a suitable olefin must be present. Intramolecular reaction can occur if there is an accessible carbon-carbon double bond in the carbonyl compound, however this is limited by steric constraints[2]. Such a compound may also dimerise via this reaction.

Addition to carbon-carbon multiple bonds can occur from both the singlet and triplet states of carbonyls, however as mentioned previously, it is usually the longer-lived triplet which reacts[2].

For enones, which possess a carbon-carbon double bond in conjugation with the carbonyl bond, there is the possibility of two different photochemical addition reactions to an olefin. Oxetane formation as described above can occur from the carbonyl functionality, and cyclobutane formation can occur from the carbon-carbon double bond of the molecule[3]. The π,π* and n,π* states of enones are generally close in energy, as discussed in chapter 3, with the nature of the lowest excited state depending on the exact structure of the molecule. It is noted that an enone with an n,π* lowest excited state behaves as for other

carbonyls, and a cycloaddition reaction produces an oxetane. An enone with a π,π* lowest excited state behaves as an olefin and undergoes cycloaddition to form a cyclobutane[3].

4.1.1.6 Other Reactions

The reactions described above are the general types of reactions for excited carbonyl compounds. Other important reactions include the elimination of α-substituents such as halogens, otherwise known as β-cleavage, and photoreduction by amines. β-cleavage is poorly understood, but believed to proceed from ionic or radical cleavage, from singlet or triplet excited states respectively[3]. Photoreduction of carbonyls by amines is similar to hydrogen abstraction, and is believed to proceed via charge transfer intermediates, or by electron transfer followed by proton transfer[3].

For more complex carbonyl compounds, a wider range of reactions, based on those discussed above, become available. For example β,γ unsaturated ketones contain two separate chromophores. Although they are not conjugated, as in enones, the excited states can be mixed to some degree[6]. They are generally considered to have π,π* lowest excited triplet states, but n,π* lowest excited singlet states[6], and consequently the reactions from the singlet state are different to those from the triplet state. Intersystem crossing from the singlet to triplet states is inefficient, and thus the important photochemistry of these compounds is that from the n,π* singlet state. These reactions reflect those previously discussed for n,π* carbonyl compounds.

The most common photochemical reaction of β,γ unsaturated ketones is a 1,3-acyl shift, as shown in figure 4.4, which is initiated by α-cleavage from the n,π* singlet state.

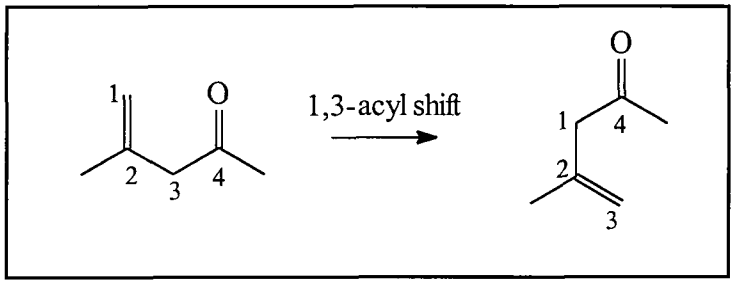

Figure 4.4 1,3-acyl shift reaction of β,γ unsaturated ketones[5]

Other reactions such as decarbonylation and aldehyde formation, are possible alternative fates for the radicals produced from α-cleavage of the n,π* singlet state. Hydrogen abstraction and cycloaddition

reactions, as discussed earlier can also take place. The π,π^* triplet state can undergo a 1,2 shift to form a cyclopropyl ketone.

4.1.2 Photochemistry of 1,3-Dicarbonyl Compounds

4.1.2.1 Introduction

As described in chapter 1, 1,3-dicarbonyl compounds can exist as a mixture of diketone and enol tautomers, which can exist in several different isomeric configurations. The photochemistry of such compounds is directly linked to which tautomers and isomers are present, as these have very different structures and excited states. The diketone forms of 1,3 dicarbonyl compounds have n,π^* lowest excited states, as discussed in chapter 3, and thus are likely to undergo the reactions described above for n,π^* excited carbonyl compounds, e.g. α-cleavage, hydrogen abstaction, charge-transfer complexation and addition to carbon-carbon multipe bonds.

The main reactions of diketones proceed from initial α-cleavage[4]. The radical fragments formed can then undergo further rearrangement and reaction resulting in an overall 1,3-shift or decarbonylation, which involves loss of carbon monoxide. The fragments may also recombine to re-from the initial diketone. These reactions are summarised in figure 4.5.

The 1,3-shift photochemical reaction of 1,3-diketones can be compared to the 1,3-acyl shift reaction of β,γ-unsaturated ketones, figure 4.4, which occurs by the same mechanism. Decarbonylation is also a photochemical reaction of β,γ-unsaturated ketones. 1,3-diketones can also undergo isomerisation on irradiation, via a rotation about a carbon-carbon bond. Different possible diketone conformations were discussed in chapter 1.

1,3-dicarbonyl compounds that do not enolise undergo the above reactions readily, with the major product being a 1,3-shift[4]. The chelated enol isomers of enolisable 1,3-dicarbonyl compounds do not directly undergo these reactions, which may be due to a possible π,π^* lowest excited state, or because of other, pathways, (to be discused later). However, for most dicarbonyl compounds the enol and diketone forms are in equilibrium, and even for those cases where the chelated enol is the major isomer, these reactions can occur via the diketone form.

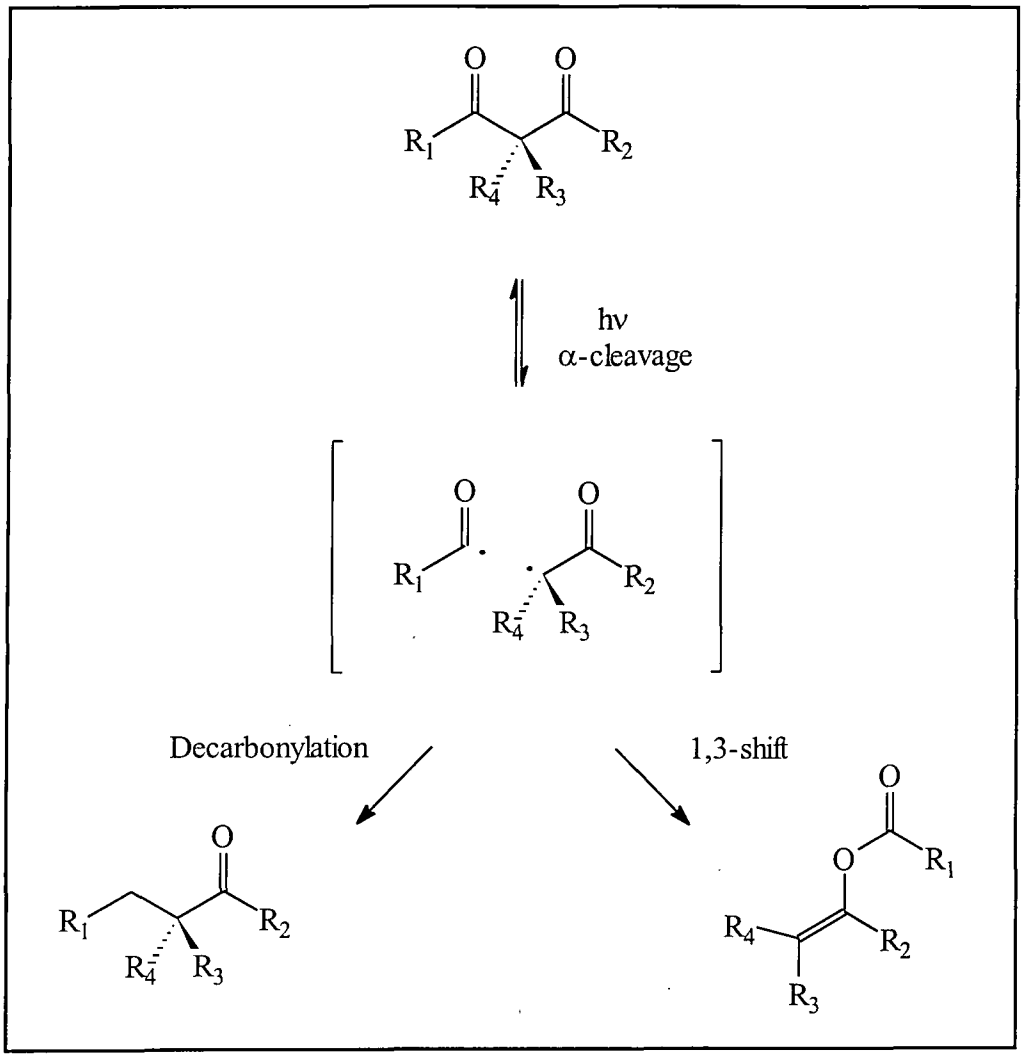

Figure 4.5 Photochemical reactions of the diketone isomer of 1,3-dicarbonyl compounds

4.1.2.3 Photoenolisation of 1,3-Diketones

Another important photochemical reaction of 1,3-dicarbonyl compounds is intra-molecular proton transfer[4]. In many cases this is observed as photoenolisation, which has been widely studied[5]. Photoenolisation occurs via intra-molecular hydrogen abstraction, as discussed in section 4.1.1.3, and is observed to be reversible in the dark.

To enolise diketones that have no α-hydrogen, other parts of the molecule must also be altered, and thus. the reaction that occurs is not photoconversion of the diketone to an enol tautomer. An example of the photoenolisation of 1,3-dicarbonyl compounds is shown in figure 4.6.

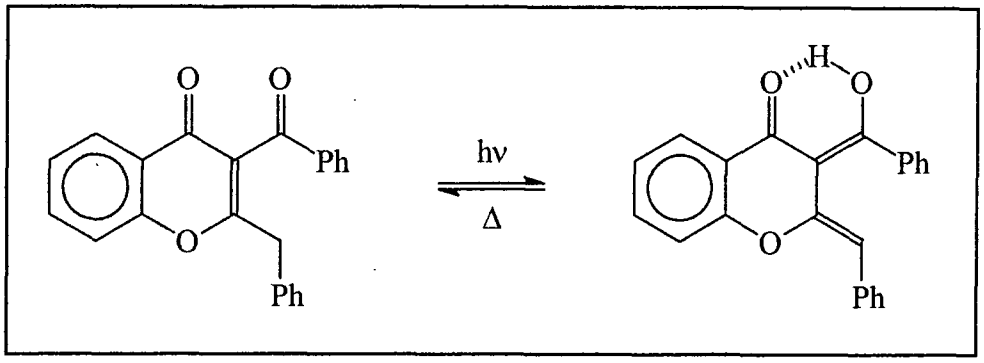

Figure 4.6 Photoenolisation of a 1,3 diketone[5]

4.1.2.4 Photo-Decomposition of Dibenzoylmethanes

Sunscreen formulations containing dibenzoylmethanes, such as Parsol 1789, are known to show a permanent loss in UV absorption with extended irradiation by sunlight or solar simulators[7]. This is caused by irreversible photochemical reactions of the dibenzoylmethanes, resulting in photodecomposition.

The initial reaction is reported to be α-cleavage, to form a pair of radicals, which can then undergo a variety of reactions, including further reaction with each other, ground state molecules, oxygen dissolved in the solvent, and the solvent itself[8,9]. The products of decomposition, which include carbonyl compounds, can then further react and photo-react to result in a wide range of products[8,9]. Some of the products of photodecomposition are shown in figure 4.7.

The α-cleavage reaction is reported to initiate from the n,π* excited state of the diketone[8], as would be expected from the previous discussion of carbonyl photochemistry. Hydrogen abstraction reactions of the dibenzoylmethanes are not observed, even in hydrogen-donating solvents[8].

The degree of decomposition obviously depends on the source and period of irradiation. Decomposition proceeds faster for irradiation in the range $\lambda > 260$ nm, than for the range $\lambda > 345$ nm [8], which can be attributed to greater covarage of the DBM absorption spectrum. Approximately 14% degradation was observed for Parsol 1789 in cyclohexane after 8 hours irradiation with a solar simulator[8]. Under simulated usage conditions of thin layers of 2% Parsol 1789 in a model sunscreen emulsion, 36% degradation has been observed after 1 hour [7]. This is not an entirely accurate model of an actual sunscreen, as incorporation of a UVB filter is usual in a sunscreen. The diketone absorbs mainly in the UVB region, and incorporation of a UVB sunscreen would therefore reduce the rate of degradation of the DBM based UVA sunscreen.

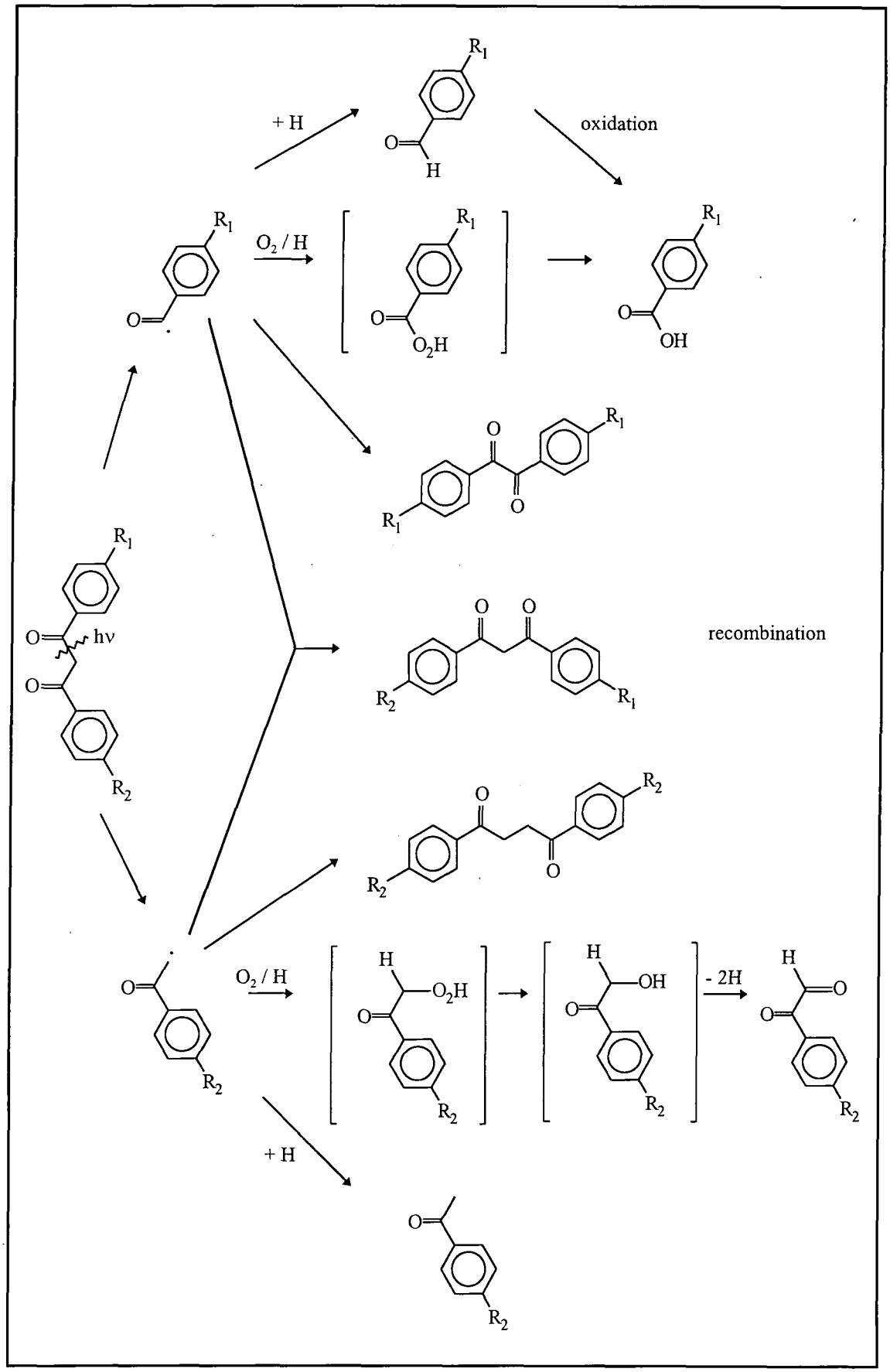

Figure 4.7 Photodegredation of dibenzoylmethanes in solution[8]

Thus although photochemical degradation of dibenzoylmethanes is not an efficient reaction, it could be significant under typical sunscreen usage conditions. This might have serious consequences for two main reasons. Firstly degradation of the sunscreen reduces the UV protective ability, and leaves the user more susceptible to UV damage. Secondly, the other compounds produced by the decomposition could be allergens, photo-allergens, or toxic to the skin.

4.1.2.5 Photoketonisation of Dibenzoylmethanes

It has long been known that prolonged exposure to sunlight or UV radiation causes a change in the observed UV absorption spectra of dibenzoylmethanes and related molecules[4,10,11,12,13,14]. This is characterised by a reduction in the intensity of the main absorption band at $\lambda \approx 340$ nm in dibenzoylmethane, accompanied by an increase in the smaller peak at $\lambda \approx 250$ nm for DBM, on irradiation, as shown in figure 4.8 This change is fully reversible in the dark, with the initial spectrum being fully recovered over a period of hours[4,12,13].

As discussed in chapter 3, the small peak, at approximately $\lambda \approx 250$ nm is assigned to the $\pi^* \leftarrow \pi$ transition of the diketone tautomer, and the main peak, at approximately $\lambda \approx 340$ nm, to the $\pi^* \leftarrow \pi$ transition of the chelated enol tautomer of dibenzoylmethane. Thus the observed spectral change on irradiation is as a result of a shift in the keto-enol equilibrium, to produce more diketone, with the thermodynamic equilibrium being restored in the dark. This is shown in figure 4.9.

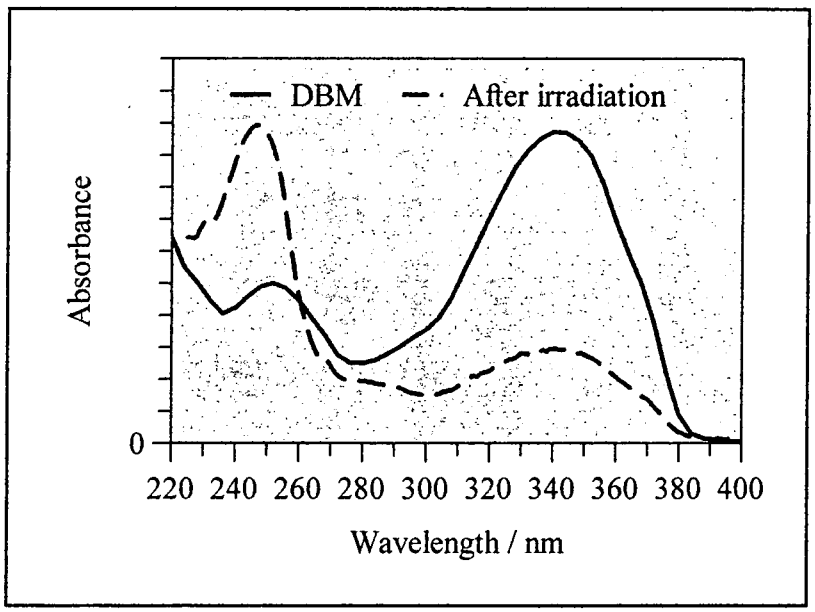

Figure 4.8 Photoketonisation of dibenzoylmethane in acetonitrile
(data taken from this work, see section 4.2.1)

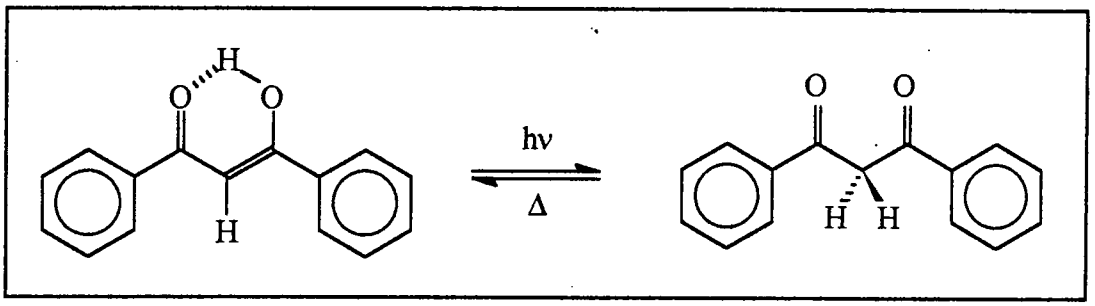

Figure 4.9 Photoketonisation of DBM

This change has been observed for a wide range of 1,3-dicarbonyl compounds in various solvents. The process has been studied by IR and NMR spectroscopy, which support the UV spectral evidence that the reaction occurring is photoketonisation[4,13,14]. Photoketonisation has also been recently observed for Parsol 1789 in acetonitrile solution[15].

The rates of photoketonisation are reported to vary significantly with temperature, solvent and the nature of the irradiation source. However, the actual kinetics do not appear to be universally agreed upon. The formation of the diketone in solution is reported to follow first order kinetics under irradiation at a constant power[16], and second order kinetics in solutions of concentrations above 5×10^{-5} mol dm^{-3} [17]. Other sources report first order kinetics for concentrations below 1×10^{-4} mol dm^{-3} and zero order kinetics for concentrations above this[4,10].

The reported quantum yields of this process also vary. For the photoketonisation of DBM, the quantum yield is reported to be $\Phi = 4.6 \times 10^{-4}$ in hydrocarbon solution[18], $\Phi = 7.3 \times 10^{-5}$ in isooctane and $\Phi = 4.6 \times 10^{-3}$ in acetonitrile[16]. The addition of tertiary amines to the solution is reported to increase the rate of ketonisation, and increase the quantum yield, whilst adding primary amines or ethanol decreases the rate and yield[18]. Other workers report that photoketonisation of DBM can only be observed in acetonitrile solution, and not in hydrocarbon solvents[19]. Photoketonisation is generally reported not to be observed in methanol solution[16,19]. These observations will be discussed further in the next section.

The reverse process of re-enolisation in the dark is reported to follow first order kinetics[12]. The rate constants of re-enolisation at room temperature have been measured to be $k = 6.8 \times 10^{-4}$ s^{-1} in cyclohexane solution and $k = 2.2 \times 10^{-4}$ s^{-1} in benzene[12]. It has also been suggested that re-enolisation can, to some extent, be photochemically enhanced in certain cases. This has been observed for aroylacetic acid esters, or in the presence of tertiary amine catalysts[4,14].

The mechanism of photoketonisation does not appear to have been ascertained. Clearly it involves intramolecular migration of a hydrogen, but the exact route by which this happens, whether this occurs by

hydrogen atom or proton transfer, is not entirely clear[4]. Some workers believe that the tautomerisation can occur directly from excited states of dibenzoylmethanes, whilst many argue that photoketonisation occurs via a short-lived intermediate species formed on irradiation of dibenzoylmethanes.

4.1.2.6 Transient Species Formation in DBM

It has been reported that a short lived species is formed on UV irradiation of the chelated enol form of 1,3-dicarbonyl compounds such as dibenzoylmethane[11,12,13,16,17,18,20,21]. These species have been observed by fast techniques such as flash photolysis, and the absorption spectra measured. A typical example is shown in figure 4.10.

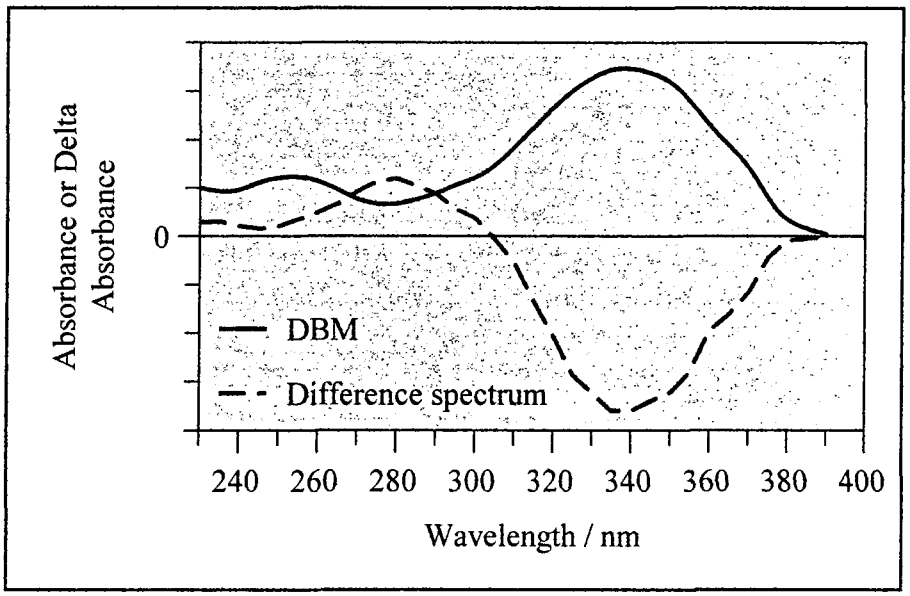

Figure 4.10 Formation of short-lived species of DBM in cyclohexane
(data taken from this work, using flash photolysis, pumping at 340 nm, see section 4.2.2)

For dibenzoylmethane this short-lived species is reported to have two absorption peaks at λ_{max} = 260 nm, ε = 1.3 × 10^4 mol^{-1} dm^3 cm^{-1}, and λ_{max} = 280 nm, ε = 1.4 × 10^4 mol^{-1} dm^3 cm^{-1}, in cyclohexane solution[11,12], or one peak at λ_{max} = 280 nm, in n-hexane solution[19]. The absorption spectrum of this short-lived species can be seen to be located at a shorter wavelength that the chelated enol absorption band, but at a longer wavelength than the diketone absorption band. A similar short-lived species has been reported for irradiation of Parsol 1789 with a peak at λ_{max} = 300 nm, $\varepsilon \approx 2.0 \times 10^4$ mol^{-1} dm^3 cm^{-1} [15].

The short-lived species is reported to revert entirely back to the chelated enol, and it is reported that this process follows first order kinetics. A summary of the reported first-order rate constants for the decay of the short-lived species of DBM and Parsol 1789 is given in table 4.1.

Other workers have reported more complicated kinetic schemes. These involve more than one recovery pathway or short-lived species[17,21], or mixed first and second order kinetics at high laser powers, where recovery can involve the interaction of two transient molecules[19].

	Solvent	τ / ms	k / s^{-1}	Reference
Dibenzoylmethane	Acetonitrile	910	1.1	**19**
		590	1.7	**16**
	Benzene	110	9	**18**
	Cyclohexane	14.3	70	**12 , 18**
	Hydrocarbon	50	20	**11**
	Non-polar hydrocarbon	0.33	3000	**20**
	Isooctane	5×10^{-4}	2×10^{6}	**16**
	Diethyl ether	670	1.5	**19**
	Dimethylsulfoxide	150	6.6	**19**
	Ethanol	1.6	620	**19**
	Methanol	0.37	2700	**19**
Parsol 1789	Acetonitrile	24.40	41.0	**15**
	Benzene	3.50	286	**15**
	Cyclohexane	1.21	826	**15**
	Ethanol	0.24	4167	**15**
	Tetrachloromethane	0.08	12500	**15**

Table 4.1 Reported first-order rate constants for the recovery of the short-lived species of DBM and Parsol 1789

This short-lived species has been extensively studied by various workers, yet the exact structure and the nature of formation and decay remain unknown. Several workers have suggested that the short-lived species is a non-chelated enol, formed by a breaking of the hydrogen-bond on excitation[11,12,13,16,18]. It is also suggested that photoketonisation takes place via a thermal reaction following the photochemical formation of the non-chelated enol[4,13,16,17,18,22]. Thus, on irradiation, the pathway shown in figure 4.11 occurs.

The quantum yield of formation of the short-lived species of DBM is estimated to be $\Phi \approx 1$ in acetonitrile solution, and $\Phi \approx 0.1$ - 0.5 in isooctane solution[16]. This compares to the quantum yields for photoketonisation discussed earlier, of $\Phi \approx 10^{-5}$ - 10^{-3}. If the path shown in figure 4.11 is correct, then clearly $k_1 \gg k_2$, explaining why no diketone product is observed in flash photolysis spectra[12,18].

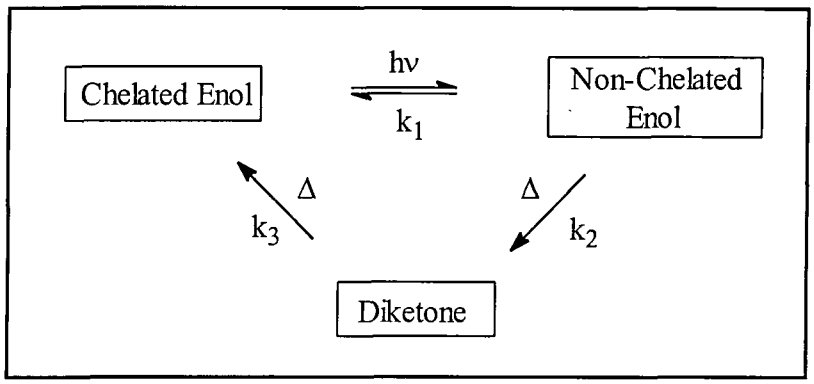

Figure 4.11 Proposed photochemical pathway occuring on irradiation of DBM

Many workers have studied the nature of the short-lived species in order to gain an insight into the mechanism of the photoketonisation of dibenzoylmethane and similar compounds, and as such discussion of the two processes considerably overlap.

The effect of different solvents and additives on the generation and decay of the transient have been studied by various workers[16,18]. It is reported that the extent of the primary photoreaction, (*chelated enol* → *non-chelated enol),* is not affected by the nature of the solvent, or by the addition of amines or ethanol in concentrations $< 10^{-4}$ mol dm^{-3}. The secondary thermal reactions, (*non-chelated enol* → *diketone*, k_2), and (*non-chelated enol* → *chelated enol*, k_1), are strongly affected by the solvent and additives[16,18]. Literature values for k_1 have been listed in table 4.1.

From these results it is assumed that the short-lived non-chelated enol interacts strongly with the solvent or additives by means of the free carbonyl and hydroxyl groups[18]. This results in the formation of complexes between the solvent or additives, A, and the non-chelated intermediate, N, which can then thermally convert to either the diketone, K or the chelated enol, C, as shown in figure 4.12. In the ground state chelated enol, the carbonyl and hydroxy groups are not free, and complexes of this sort are not formed. Hence the additives do not affect the rate of formation of the non-chelated intermediate.

The addition of a tertiary amine, (triethylamine), to a solution of DBM in a hydrocarbon solvent is reported to produce an increase in the quantum yield of photoketonisation. Addition of a primary amine, (ethylamine), or an alcohol, (ethanol), decrease it. It is also noted that in the case of β-keto esters, there

are no rate changes with additives to the solvent[18]. The quantum yields of photoketonisation for β-keto esters are much greater[18], and the rates of non-chelated recovery are faster[12], than for 1,3-diketones.

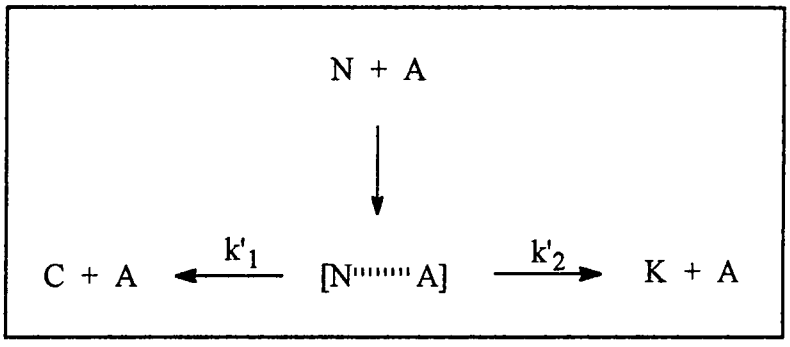

Figure 4.12 Formation of complexes between solvent or additives (A) and the non-chelated intermediate (N)

(K = diketone; C = chelated enol)

The explanations of the effects of the solvent and additives in the literature are somewhat contradictory. It is suggested that primary amines and alcohols enhance the rate of reformation of the hydrogen-bond, k_1, whilst tertiary amines enhance the rate of conversion of the non-chelated form to the diketone, k_2 [18]. Amines and alcohols act as proton-transfer agents, as shown in figure 4.13 making rotation more energetically favourable[17,18]. This increases the rate constant for re-formation of the chelated enol, k_1, and thus reduces the extent of ketonisation. It is also suggested that a primary amine can act as a proton donor, forming a hydrogen-bond with the free carbonyl group of the non-chelated intermediate. This promotes proton transfer from one oxygen to the other, rather than from the oxygen to the α-carbon, which needs to occur for ketonisation. This does not occur in tertiary amines because of steric constraints[18].

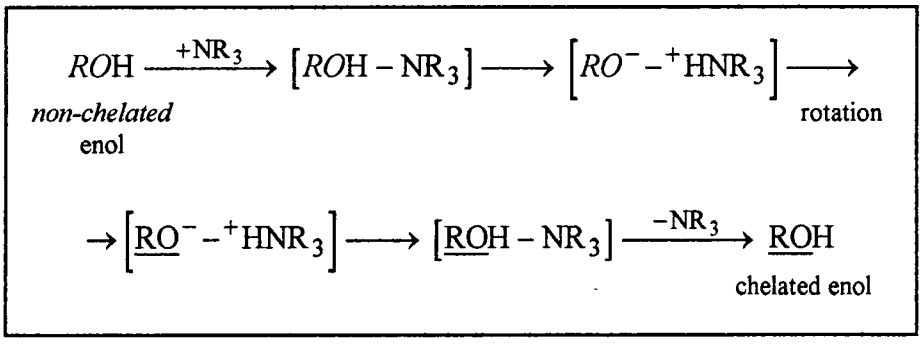

Figure 4.13 Interaction of amines in the conversion from non-chelated enol, *ROH*, to chelated enol ROH (reference 17)

In a theory similar to that outlined above, it has been suggested that alcohols may participate in a mutual hydrogen exchange with the non-chelated intermediate, via inter-molecular hydrogen-bonding, as shown in figure 4.14. In this way the intra-molecular hydrogen-bond is re-formed more efficiently, and the initial structure restored at a greater rate in alcohols[19].

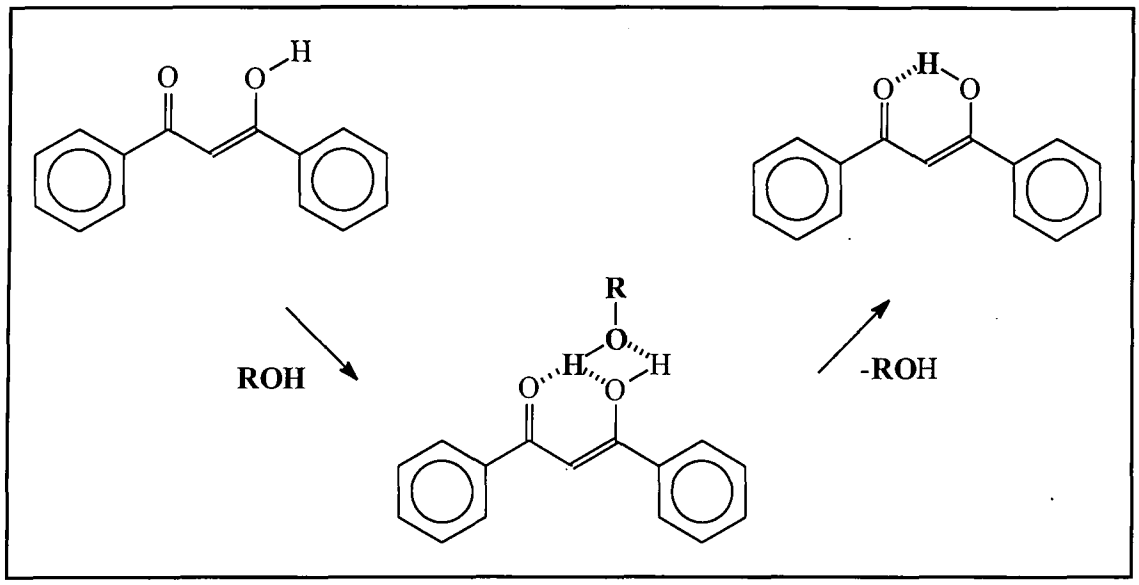

Figure 4.14 Re-formation of the intra-molecular hydrogen-bond assisted by an alchohol[19]

Other workers have suggested that a complex is formed in methanol, as shown in figure 4.15, where a partial proton transfer to the methanol occurs. In this case ketonisation, k_2, is reduced because of an increased energy barrier, such that re-formation of the chelated enol, is favoured[16].

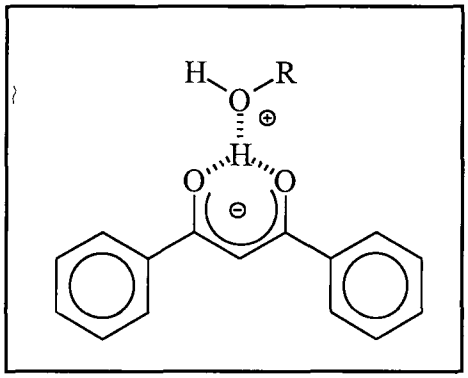

Figure 4.15 Formation of a complex between DBM and methanol[16]

The role of tertiary amines may be similar to the effect reported for β-keto-esters, where the oxygen of the ether group stabilises the non-chelated enol, as shown in figure 4.16. This reduces the rate of re-chelation k_1, and as a result increases the yield of diketone product[11,18].

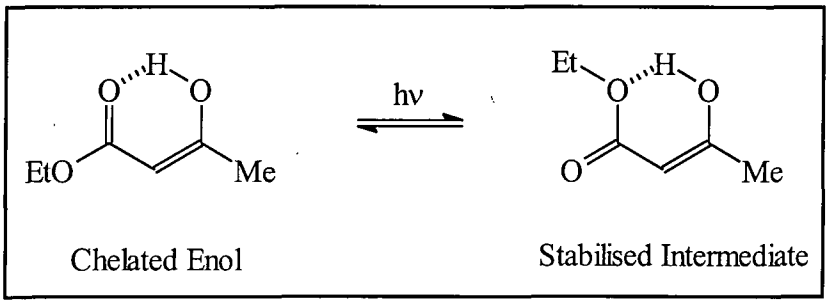

Figure 4.16 Formation of stabilised non-chelated enol in β-keto-esters[18]

As discussed in the previous section, photoketonisation is most readily observed in acetonitrile solution, a polar aprotic solvent[16,19]. This is explained as being due to the inability of the solvent to act as a proton donor, coupled with the formation of a complex between the excited enol and acetonitrile molecules, as shown in figure 4.17. The nature of the complex may involve partial hydrogen transfer from the excited enol to the acetonitrile molecule. The result is that the short-lived intermediate is then greatly stabilised, such that k_1 is reduced, and ketonisation increased[16].

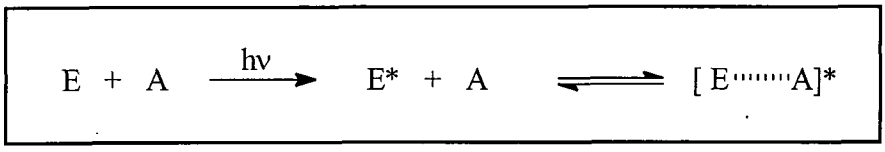

Figure 4.17 Formation of a complex between excited enol molecules, E* and acetonitrile, A[16]

It has been pointed out that there is a large loss in entropy on recovery of the chelated enol[19]. Because of this the enthalpy change on re-chelation is very important. In acetonitrile solution, which has a high dielectric constant, and is thus very polar, the chelated enol is destabilised, and hence there is only a small enthalpy change on formation. This could explain the slow rates of re-chelation in acetonitrile solution, and why the diketone product is favoured[19]. The formation of complexes with protic solvents reduces the entropy loss on re-chelation, and makes this route more favourable. In protic solvents chelated enol recovery is thus faster than in aprotic solvents.

Various workers have suggested possible complex formations and hydrogen transfers, which they use to explain the effects of different solvents and additives, but rather unsatisfactorily. The reason why a tertiary amine should enhance photoketonisation, whilst a primary amine inhibits it has not been explained satisfactorily. There are also great differences in the reported lifetimes of the short-lived intermediate, as was seen in table 4.1. It is generally reported that polar protic solvents speed up the rates of non-chelated intermediate decay, k_1, whilst 1,3-diketones in acetonitrile, a polar non-protic solvent, have low values for k_1, and high ketonisation quantum yields. It has also been suggested in the literature that the addition of water to various solvents may have an effect on the rate constants[18].

It is also reported that in concentrated solutions, $> 5 \times 10^{-4}$ mol dm^{-3}, dimers of the short-lived species may be formed. This is the source of the observed higher order kinetics of recovery of the chelated enol[20]. These dimers are either formed by the interaction of two molecules of the short-lived species, or by the formation of a dimer of the chelated enol which is then excited. The dimers are reported to have faster decay rates than non-chelated monomers[20], meaning that the measured relaxation rates of the transient species will depend on the concentration of the solution, because this affects dimer formation[23].

Other reports suggest a more complicated scheme of products, with two or more different excited states produced, on excitation of DBM[16,17]. A detailed scheme has been proposed by Yankov and co-workers[17], and is summarised in figure 4.18.

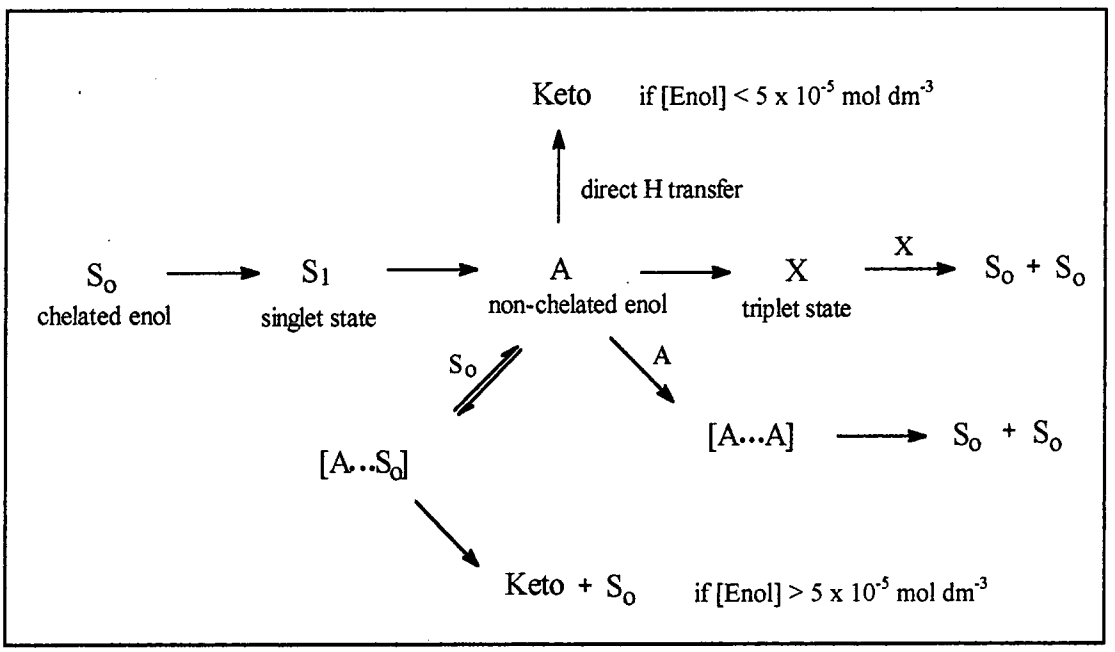

Figure 4.18 Suggested processes occurring on irradiation of DBM[17]

(see text for discussion)

It is suggested in the literature that on irradiation, the excited singlet state, S_1, is formed which rapidly isomerises to form the non-chelated enol rotamer, A. This can directly ketonize through direct hydrogen transfer. It can also convert to a triplet state, X, or combine with either a ground state enol, or another excited isomer to form dimers $[A\cdots S_0]$ or $[A\cdots A]$. $[A\cdots S_0]$ can convert to one diketone molecule, Keto, and a ground state chelated enol, S_0, or revert back to the non-chelated enol, A, and a ground state chelated enol, S_0. $[A\cdots A]$ thermally reverts to two ground state enols, S_0, as does the triplet state, X interacting with another triplet molecule. Formation of dimers $[A\cdots S_0]$, is reported to become a significant deactivation pathway at concentrations approximately > 5 x 10^{-5} mol dm^{-3}, whereas below this concentration direct hydrogen transfer is most important.

The lack of fluorescence from the singlet state, S_1, is explained by the fast conversion to the non-chelated rotamer, A [17]. The reported fluorescence at low temperature, as discussed in chapter 3, might therefore be observed because this thermal pathway is hindered by the rigid matrix. There is a very high observed rate of formation of $[A\cdots A]$, and this is explained as being due to the existence of weakly bonded dimers present in the ground state[17,24].

The effect of oxygen on the lifetime of the short lived species, and on ketonisation is not entirely clear, in that it is only ever briefly discussed in the literature. It has been reported that oxygen in solution has no effect on the quantum yields of ketonisation[19,22], and no effect on the extent of formation or rate of decay of the short-lived intermediate[12]. It has also been reported that the lifetime of the short-lived species is reduced by 20% in aerated solutions[24] , although this is suggested to be due to the change in pH due to dissolved CO_2, as will be discussed later. Oxygen flushed solutions have also been reported to increase the quantum yield of ketonisation, but reduce the yield of the short-lived species, suggesting that oxygen enhances the change from short-lived species to diketone, whilst inhibiting the change from chelated enol to short-lived species[12]. Oxygen quenching of excited states and singlet oxygen formation are discussed in chapter 6.

The discussion concerning the exact structure of the short-lived species is extensive. Most workers tend to agree that it is a non-chelated enol formed by rotation about one of the chelate ring bonds[4,11,12,13,16,18,21]. Theoretical calculations support this theory[22,25], but little direct evidence has been presented. The absorption spectra of the short-lived species, obtained by flash photolysis, have been compared to the spectra of the O-methyl ethers of 1,3-dicarbonyls, the β-methoxy chalcones, which are discussed in chapter 3, and have been shown to be very similar[12]. 1,3-dicarbonyl compounds which are structurally fixed in a trans configuration and hence unable to intra-molecularly hydrogen-bond, e.g. dimedone, figure 4.19, have also been studied. The UV / visible absorption spectra of these have been shown to change very little with O-alkyl substitution, to form the corresponding β-alkoxy chalcones[26]. These results provide support for the theory that the short-lived species is a non-chelated enol.

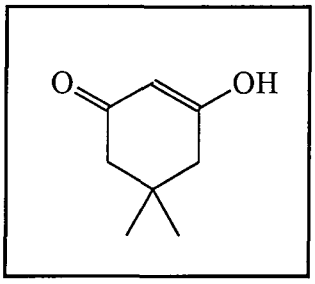

Figure 4.19 Structure of the enol form of dimedone

As discussed in chapter 3, ethyl acetoacetate is reported to have an n,π* lowest excited triplet state[4,22]. In this compound the first excited states have an electron deficient oxygen, and consequently an intra-molecular hydrogen-bond is unfavourable. Rotation to form a non-chelated species, where the carbonyl and hydroxyl hydrogen are separated, is therefore a likely relaxation process of the lowest excited states[4]. This supports the theory that the transient observed on irradiation of 1,3-dicarbonyl compounds is a non-chelated rotamer.

It is generally reported that the lowest excited singlet and triplet states of DBM have π,π* character, as discussed in chapter 3. This would mean that the above explanation is not valid for DBM, because in a π,π* excited state electron density is increased at the carbonyl, making a hydrogen-bond more favourable in the excited state. However in 1,3-dicarbonyl compounds such as DBM the n,π* and π,π* states are generally considered to be close in energy, as discussed in chapter 3, and it is possible that the lowest excited states of DBM have n,π* character. Because other evidence suggests that a non-chelated enol is formed on irradiation of DBM, it is probable that rotation to form this species does take place from an n,π* excited state, where the intra-molecular hydrogen-bond is unfavourable.

The discussion of the structure of the transient becomes complicated when trying to determine exactly which non-chelated enol isomer is formed. The possible routes to formation of the non-chelated enol on irradiation are rotation about, a) the carbon-oxygen single bond, b) the carbon-carbon double bond, or c) the carbon-carbon single bond, as shown in figure 4.20 for DBM [4,11,12,13,16,18,21]. The labelling of these different rotamers in the literature is sometimes confusing, and hence the labelling system discussed in chapter 1 will be used in this work. The product formed by rotation about the C-C single bond, route c, will be referred to as the Z-trans non-chelated enol, and that formed by rotation about the C=C double bond, route b, as the E-cis non-chelated enol, where the cis and trans refer to the arrangement of the double bonds, and Z and E refer to the arrangement of substituents about the carbon-carbon double bond. The product formed by rotation about the C-O single bond, route a, will be referred to as the Z-cis non-chelated enol.

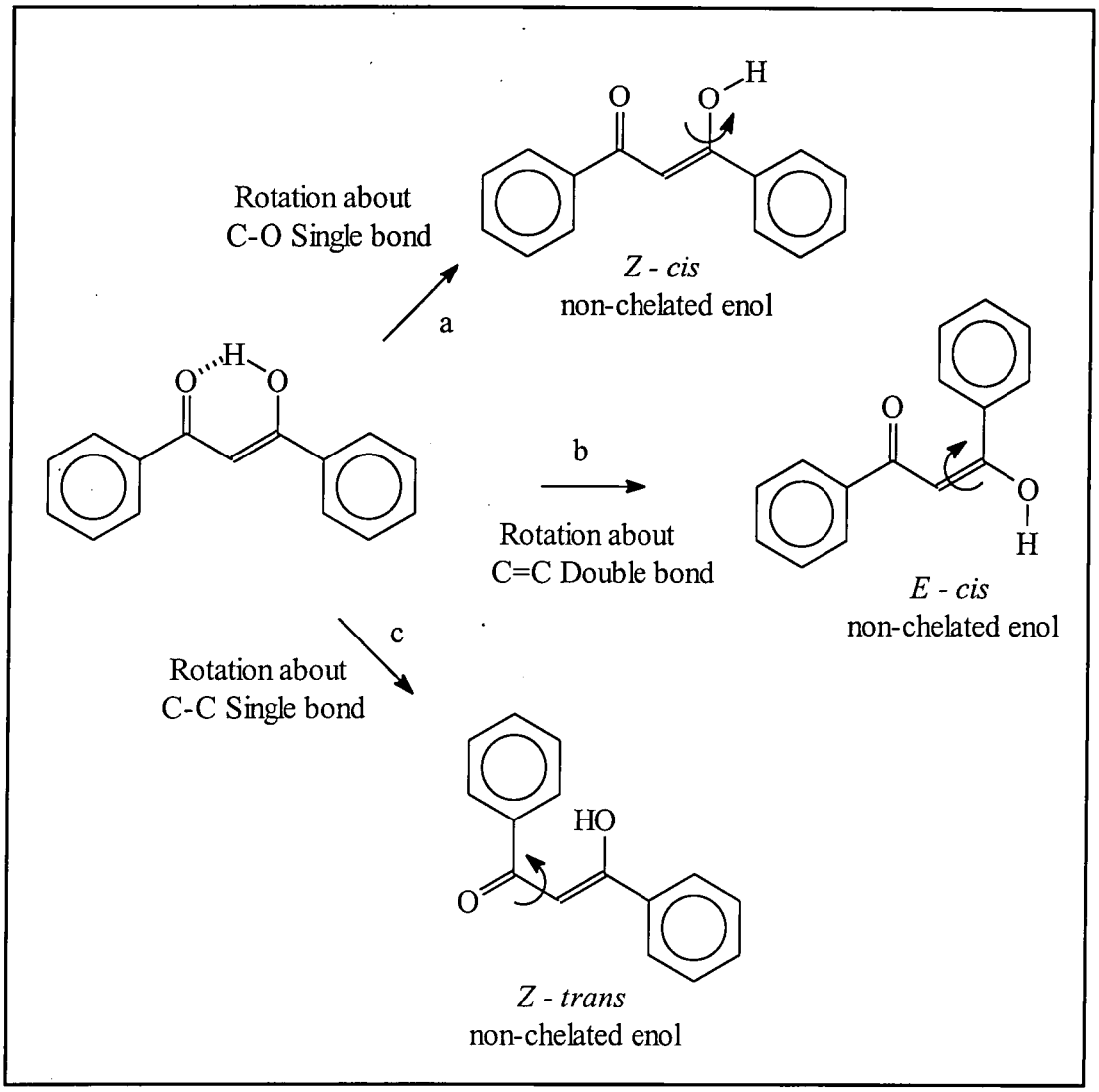

Figure 4.20 Formation of possible non-chelated enol rotamers on irradiation of DBM

Rotation about the single C-O bond is not usually considered to occur[4], although the resulting structure has been used to explain the interactions with solvents discussed earlier[19], and some workers have suggested it as a possible route[21]. Energy barriers to C-O rotation are reported to be higher than for C-C rotations, and in malonaldehyde this species is reported to have a higher energy that other non-chelated species formed by other rotations[27]. The main discussion in the literature covers whether the short-lived species is formed via rotation about the C-C single bond, route b, or C=C double bond, route c.

Rotation about the C-C single bond, route b, has been suggested to occur on irradiation[13]. Support for this theory comes from considering cyclic β-keto esters of the structure shown in figure 4.21.

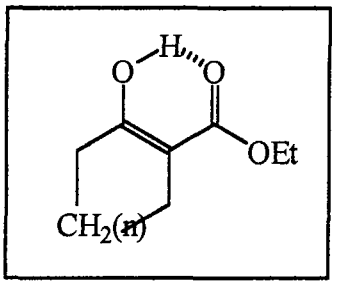

Figure 4.21 Structure of a cyclic β-keto ester

(Enolised structure shown)

These compounds undergo photoketonisation and formation of the short-lived intermediate, as for the other 1,3-dicarbonyl compounds[10]. These compounds enolise preferentially as shown in figure 4.21. It is therefore concluded that rotation to form the non-chelated enol must occur via rotation about the C-C single bond, as the steric structure prevents rotation about the double bond[10]. This evidence is not entirely convincing, however, because it has also been suggested that enolisation could occur the other way round to some extent in this molecule, and hence allow rotation about the double bond to produce the intermediate.

It is also suggested that in DBM such a product would be stabilised by a hydrogen-bond type interaction between the free OH group and the π-system of the phenyl group[13], as shown in figure 4.22. Similar interactions between hydrogens and π-electrons of unsaturated groups have been reported in the literature[28,29].

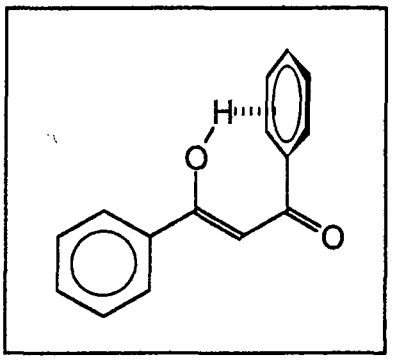

Figure 4.22 Stabilisation of the trans non-chelated enol by phenyl group[13]

The main argument in favour of single bond rotation appears to be the higher energy barrier for rotation about the double bond[11]. However, it is generally accepted that in the excited state, the order of the

double bond is reduced[4,16], so this argument becomes less valid. It is suggested that in the singlet state of DBM the bond orders of the single and double bonds are nearly equal[21].

Rotation about the double bond appears more likely to produce a species suitable as an intermediate to ketonisation. Hydrogen migration or proton transfer to the α-carbon is likely to be most efficient from the E-cis non-chelated enol due to the physical proximity of the hydrogen and the α-carbon in this structure [16], as can be seen from figure 4.20. If the diketone product initially formed was the trans diketone isomer, as discussed in chapter 1, then this is a sensible option for the structure of the intermediate.

Strong support for the rotation about the carbon-carbon double bond, route b in figure 4.20, is provided on considering deactivation of the excited states of enones. On irradiation of an enone, it is reported that trans → cis isomerisation, i.e. rotation about the single bond as shown in figure 4.23, is unlikely due to the high activation energy[30].

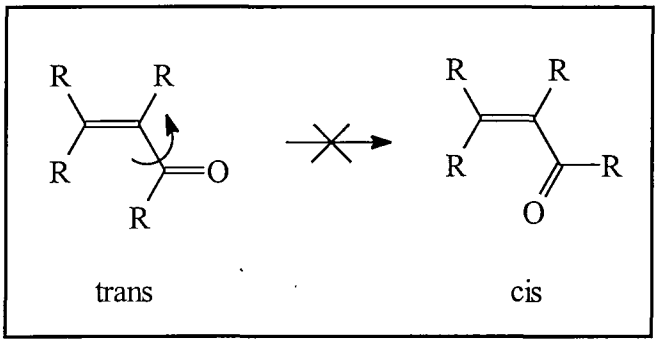

Figure 4.23 Trans-cis isomerisation of enones

Twisting of the double bond, however, allows inter-system crossing due to an equalising of the S and T energies, and is thus an efficient relaxation pathway of the lowest triplet state[30]. 1,3-diketones share a similar structure to enones, and it can be inferred that the rotation about the carbon-carbon double bond, route b, is an efficient relaxation pathway in these compounds[22]. Indeed, calculations suggest that the S_1 and T_1 energies of DBM become equal on a 90° rotation of this bond[21,31]. Hence an E- trans non-chelated enol is the likely photoproduct.

Further evidence is presented by considering the photochemical inter-conversion of diaryol acetic acids[4], as shown in figure 4.24. On irradiation, rotation about the carbon-carbon double bond occurs to form another intra-molecularly hydrogen-bonded species[32].

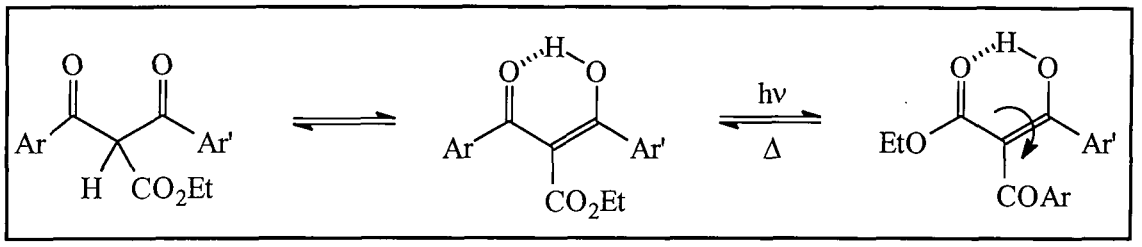

Figure 4.24 Photoconversion of diaroylacetic acids[32]

This evidence however is again not entirely reliable, because another species, shown in figure 4.25, is also a photo-product. In this case, rotation occurs about the carbon-carbon single bond, after the initial double bond rotation. It is also possible that enolisation can occur at the aryl group, such that the initial rotation is actually about the single bond.

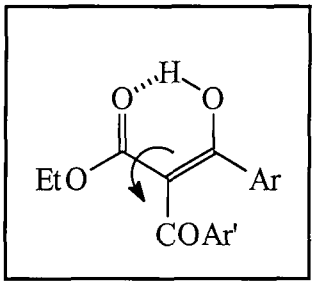

Figure 4.25 Rotation about the C-C single bond in diaroylacetic acids

Photochemical formation of another short-lived species has also been reported to occur for DBM in basic solutions[19]. Ethanol solutions with added potassium hydroxide or triethanolamine were used, such that the solution was basic, but the enolate anion was not formed significantly in the ground state. On excitation a new absorption band appears, with a maximum at 355nm, and the recovery of the main peak at 340nm shows double exponential kinetics. The new peak is assigned to the enolate anion of DBM, which is formed from the non-chelated short-lived intermediate produced on irradiation of DBM.

Enols that are fixed in the non-chelated configuration such as dimedone, figure 4.19, and methylketene dimer, figure 4.26, are known to be acidic. The pKa values of these two compounds are pK_a = 5.2 and pK_a= 2.8 respectively[33], c.f. ethanoic acid, pKa= 4.75 [34]. Therefore it can be expected that the non-chelated intermediate of DBM is quite acidic, whereas the chelated enols are less acidic because of the strong chelate bond, c.f. 2,4-diketopentane, pK_a=8.09, and 1-ethoxy-2,4-diketopentane, pK_a=8.13 [12]. Thus even in a slightly basic solution it is quite feasible that the non-chelated species can easily lose a

proton to form the enolate. This also supports some of the other additive theories, which suggest partial proton transfer takes place between the non-chelated species and the amine or alcohol.

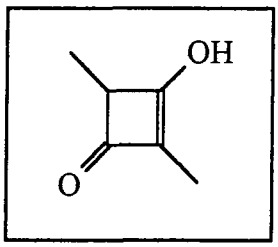

Figure 4.26 Structure of methylketene dimer

The enolate has also been reported to be observed in degassed ethanol or in pyridine solution[24]. It is suggested that aerated solutions of ethanol are too acidic for enolate formation, because of dissolved CO_2. In flash photolysis experiments, the enolate species can be seen to grow in with first order kinetics as the non-chelated species decays, and then decays following first order kinetics to re-form the chelated enol, as shown in figure 4.27. Overall, recovery of the chelated enol is reported to be enhanced relative to similar solutions in aerated ethanol[24], or pure ethanol[19].

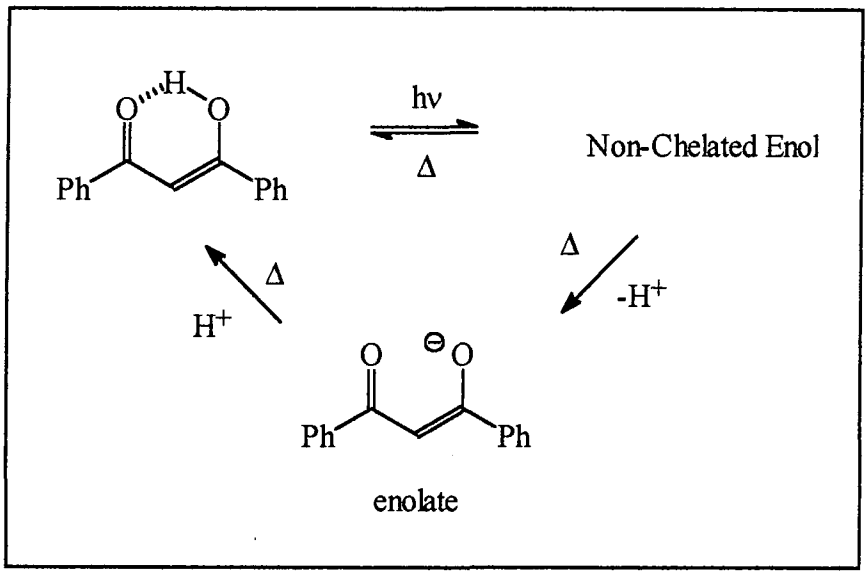

Figure 4.27 Photochemical formation of the enolate of DBM

There are also arguments as to from which excited state the formation of the non-chelated isomer occurs. It has been suggested that photoketonisation takes place from the singlet excited state of 1,3-dicarbonyl

compounds including DBM, but further irradiation then produces the triplet state of the diketone[35]. Other workers report that the ketonisation of ethyl acetoacetate can be sensitised by known triplet sensitisers, and therefore photoketonisation probably occurs from the triplet state of this 1,3-diketone[22], although it is reported that there is evidence that the reaction also occurs via the singlet state[4]. The formation of the non-chelated enol from is reported to by Yankov and co-workers to occur from the singlet state, as discussed earlier[17]. In an earlier report they claim that formation of the Z-trans rotamer occurs from the triplet state, whilst rotation about the carbon-oxygen single bond occurs from the singlet state[21]. The lack of influence of molecular oxygen is suggested to indicate that DBM isomerises rapidly from the singlet state, however other workers have shown an effect of oxygen, as has been mentioned, which could implicate a triplet state. It is also generally accepted that carbonyl compounds of this type undergo rapid intersystem crossing, as discussed in chapter 3, suggesting that isomerisation takes place from the triplet state. The deactivation of enones by twisting of the double bond has also been shown to occur from the triplet state[30], and the same process for 1,3-dicarbonyl compounds is also considered to occur from the triplet state[31]. The luminescence studies in chapter 3 show that at low temperature both phosphorescence and fluorescence can be detected from the chelated enol species, showing the presence of both singlet and triplet states.

If the reaction takes place from the triplet state, it could still be possible that the lowest excited singlet state is π,π^* as discussed in chapter 3. On inter-system crossing, the lowest excited triplet state may in fact be n,π^*, which, from earlier discussions, favours the formation of a non-chelated enol.

4.1.2.7 Photo-Isomerisation of O-Methyl DBM

As was discussed in chapter 1, O-methyl dibenzoylmethanes, can exist as either the Z-isomer, or the more thermodynamically favourable E-isomer, as shown in figure 4.28. The structures were determined by X-ray crystallography of solid samples of the isomers, and it is assumed that the structures found in solution are the same[36].

It has been observed that the action of light induces and accelerates the conversion from the Z to the E isomer, i.e. the conversion can occur photochemically as well as thermally[36]. In hexane solution an equilibrium mixture of 1:6 Z-isomer : E-isomer was achieved within 20 minutes of irradiation with visible light, compared to a non-observable change from pure Z-isomer, in the dark. In methanol solution, visible light caused equilibrium to be achieved in 40 minutes, compared to several hours in the dark[36].

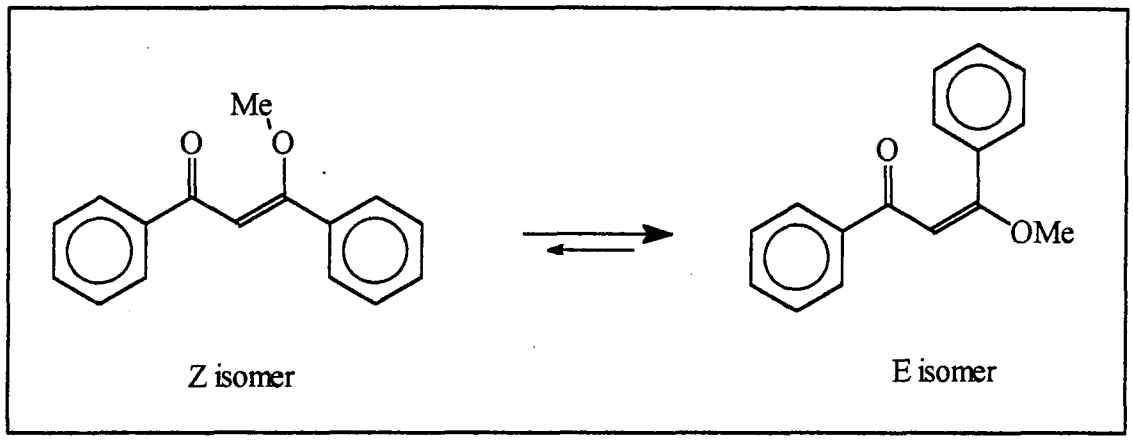

Figure 4.28 Structure of E and Z isomers of O-methyl DBM

It has been proposed that whilst Z→E isomerisation in the dark occurs via protonation, photochemical Z→E isomerisation can occur via a radical route[36], as shown in figures 4.29 and 4.30. However, as was discussed earlier, the chemistry of the excited states of carbonyls can be similar to that of radicals, and thus actual radical formation may not occur, although a radical mechanism for DBM rotation has been suggested[21].

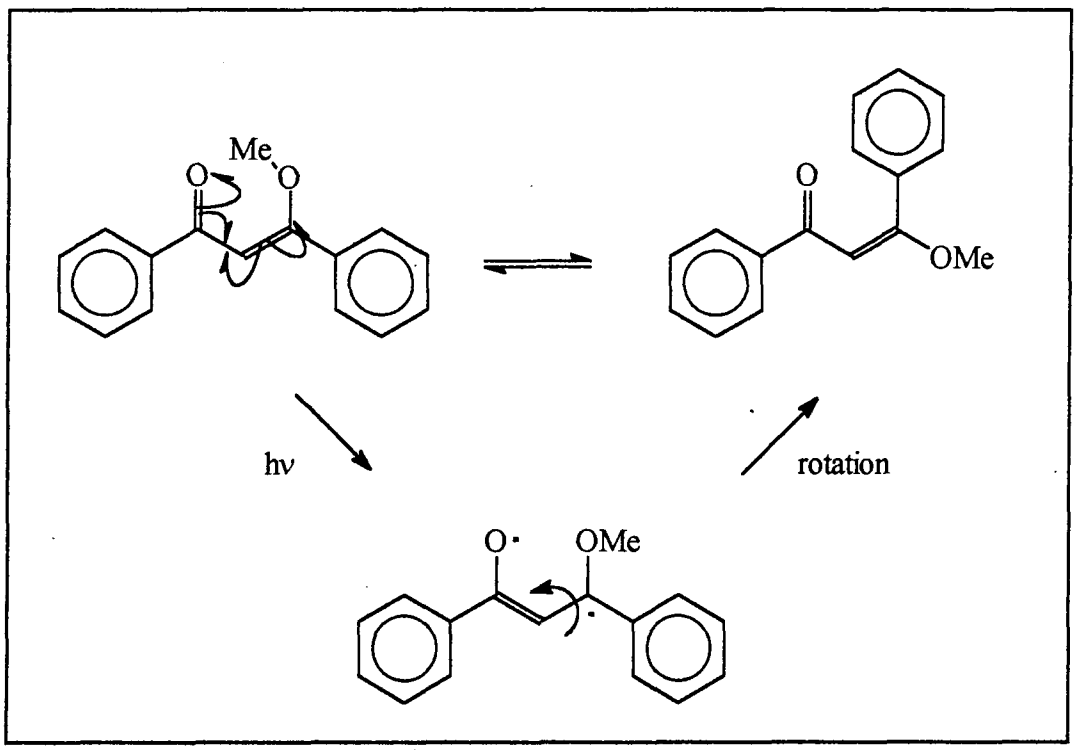

Figure 4.29 Photochemical, radical Z→E isomerisation of O-methyl DBM[36]

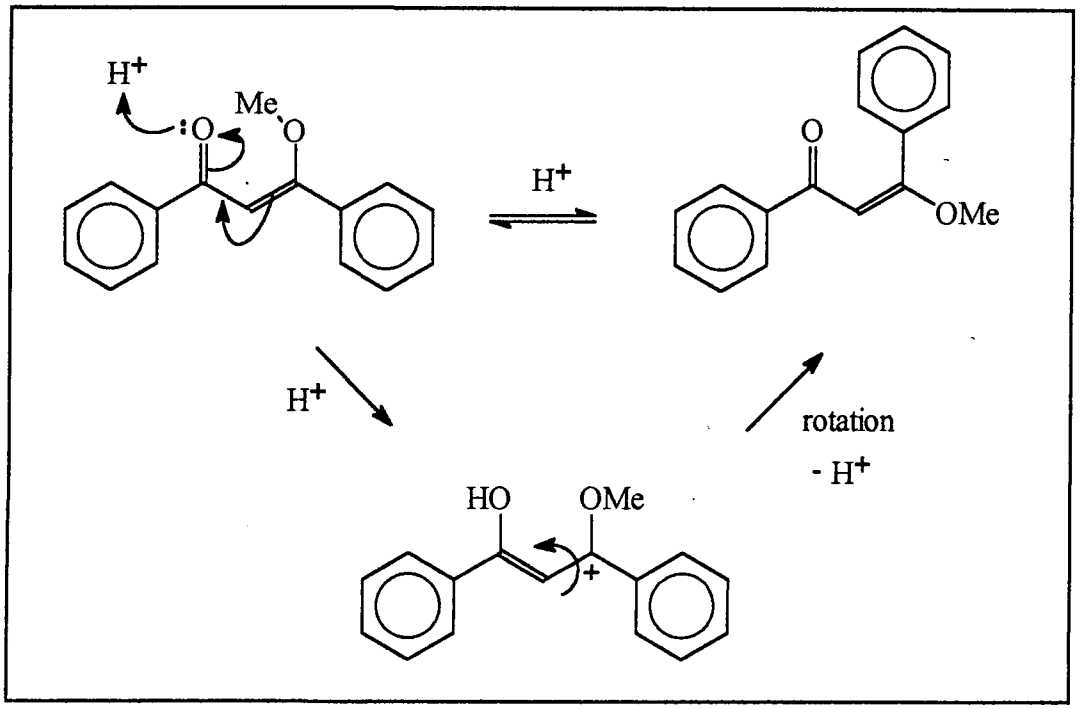

Figure 4.30 Thermal isomerisation of O-methyl DBM, via protonation[36]

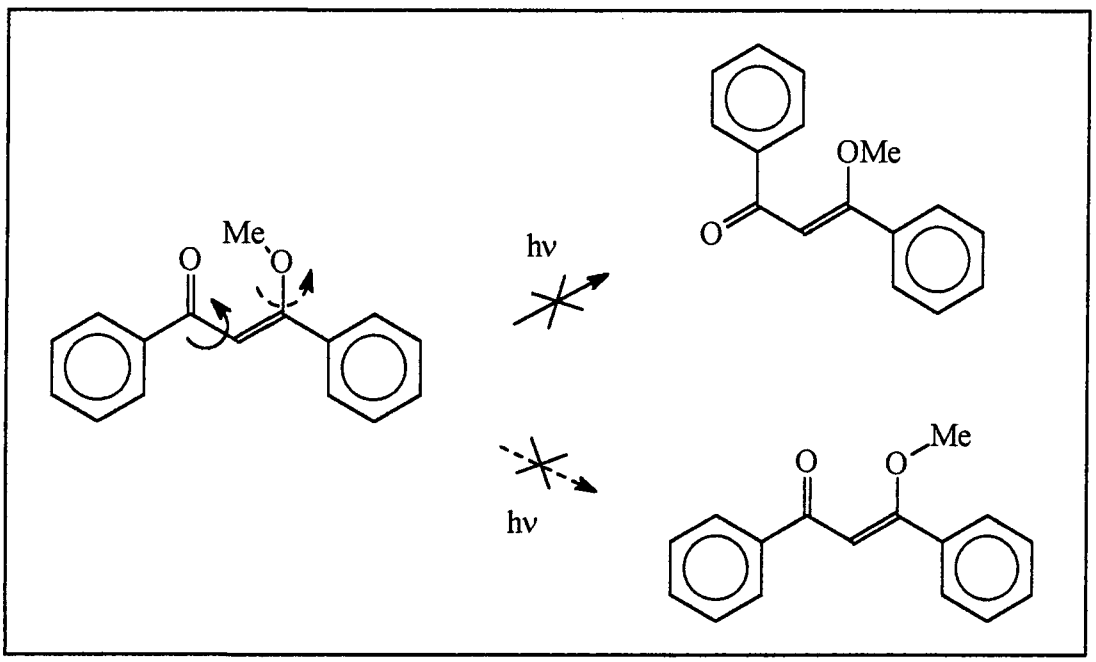

Figure 4.31 Photochemical reactions not seen to occur in O-methyl DBM: Rotation about the carbon-carbon or carbon-oxygen single bonds

The importance of this observation in understanding the photochemistry of DBM is significant. Firstly the preference for the E isomer indicates that in dibenzoylmethane it is mainly the intra-molecular hydrogen-

bonding that means the cis structure is favoured. If no H-bond stabilisation occurs in the molecule, then sterically a non-chelated rotamer is probably preferred.

Secondly, isomerisation occurs via a rotation about the carbon-carbon double bond in the O-methyl DBM to produce exclusively the E-isomer. No structures corresponding to rotations about the carbon-carbon single bond or the carbon-oxygen single bond, figure 4.31, are observed. This has important parallels in the structure of the short-lived non-chelated photoproduct of DBM.

4.1.4 Summary of Photochemistry of Chelated Enol form of DBM

By comparison with other similar compounds that exhibit similar properties to DBM, it appears that DBM has n,π^* lowest excited singlet and triplet states, although probably of comparable energy to π,π^* states, which are usually reported as the lowest states. In the n,π^* excited states there is no intra-molecular hydrogen-bonding, and fast relaxation by rotation takes place to produce a non-chelated rotamer. Rapid intersystem crossing takes place from the initially excited singlet state, such that isomerisation most probably takes place from the triplet state

By comparison of Z $\leftrightarrow$ E isomerisation of O-methyl DBM, and by considering other evidence described, this isomerisation most probably occurs via a rotation about the carbon-carbon double bond of the chelate ring to produce a Z-trans non-chelated enol. However, the other possible rotamers caused by rotation about the carbon-carbon or carbon-oxygen single bonds may also occur, and no reports have considered the possibility of more than one rotation occuring, to form of a mixture of isomers.

The non-chelated enol then reverts thermally to the ground state chelated enol, or can undergo fast hydrogen (or proton) transfer to form the diketone species. The diketone reverts thermally slowly back to the chelated enol.

In basic solutions the enolate anion may also be formed thermally from the non-chelated intermediate, which then reverts to the chelated enol.

Despite all the studies of the photochemistry of dibenzoylmethane over many years, there has been no direct evidence presented as to the structure of the short-lived intermediate, and no direct evidence that ketonisation occurs via this species. Because dibenzoylmethanes are commonly used as sunscreens, it is important to fully understand the processes occuring on irradiation, the nature of the photochemcial species produced, and the rates at which they recover back to DBM. It has been the aim of the work in this chapter to try and provide further insight into the photochemistry of dibenzoylmethanes in solution.

4.2 Results and Discussion

4.2.1 Photoketonisation

4.2.1.1 Diketone Formation

The effect of significant exposure to UV light of solutions of dibenzoylmethane in various solvents was investigated using the tungsten filament lamp apparatus as described in chapter 2.

When DBM solutions in ethanol, cyclohexane and trichlorotrifluoroethane, of concentrations ≈ 2.5×10^{-5} mol dm^{-3}, were irradiated, a small change in the intensity of the main absorption peak was observed after a few hours. In these solutions, the changes did not appear to be reversible after standing for a week in the dark, and hence are attributed to result from degradation of the sample. Thus in ethanol and cyclohexane solutions, photoketonization is not observed under these conditions, although the literature suggests it does occur in aliphatic hydrocarbon solvents[11,12,13,16], for example hexane, heptane, cyclohexane and isooctane.

In acetonitrile, photoketonization, and recovery of the chelated enol, was readily observed. Figure 4.32 shows the changes observed over a period of two hours of irradiation, with the intensity of the main peak at 342 nm decreasing as the intensity of the diketone peak increases.

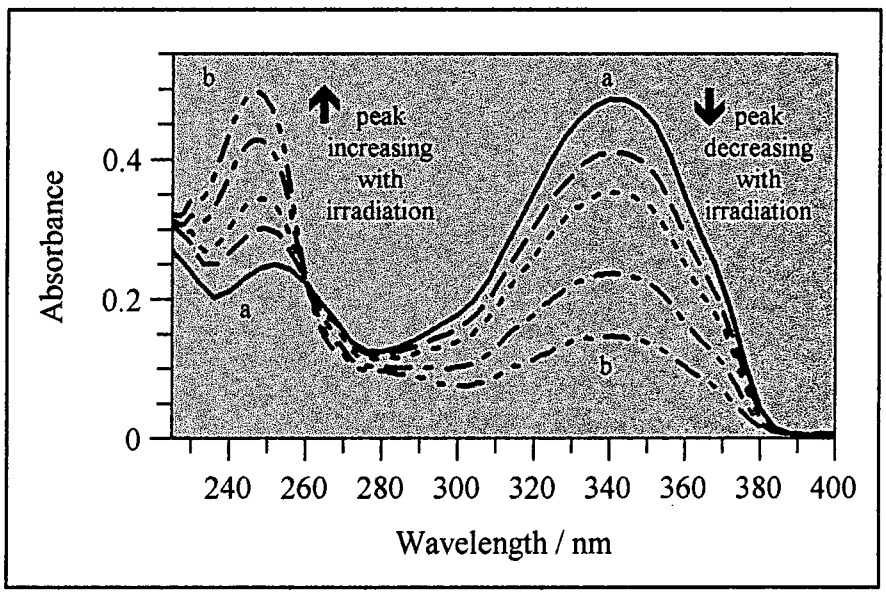

Figure 4.32 Changes in the absorption spectrum of DBM in acetonitrile with irradiation
(irradiation λ > 300 nm; a) initial spectrum; b) spectrum after 2 hours irradiation)

By subtracting a scaled absorption spectrum of unirradiated DBM from the spectrum obtained after two hours of UV irradiation, the spectrum of the diketone form is obtained (figure 4.33). This corresponds well with the spectrum of C-methyl DBM, indicating that it is indeed the diketone product that is formed on irradiation. The recovery of the enol after irradiation was also followed, and found to follow a first order rate law. An example is given in figure 4.34.

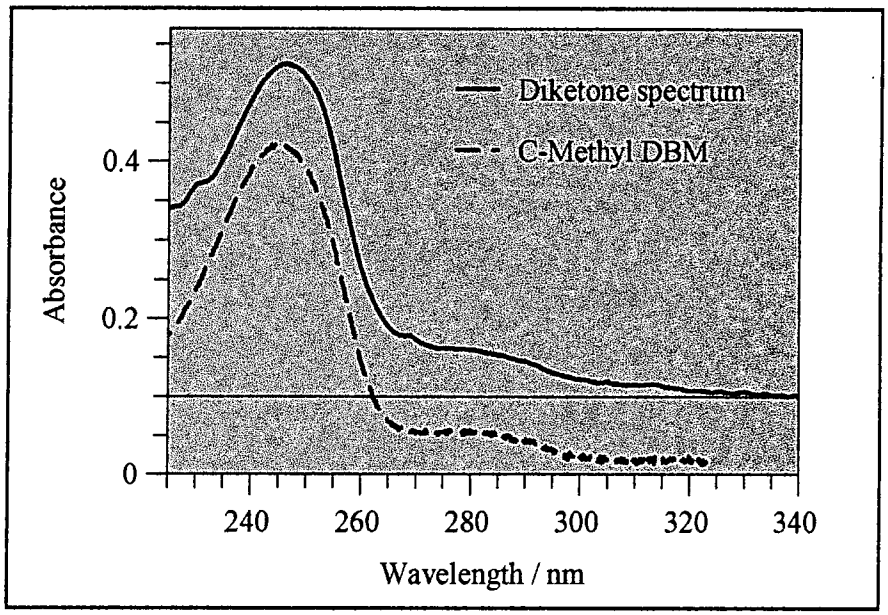

Figure 4.33 Spectra of C-methyl DBM and the diketone form of DBM in acetonitrile
(spectrum of diketone of DBM obtained by subtracting a DBM spectrum from the that of the irradiated product; baselines displaced for clarity)

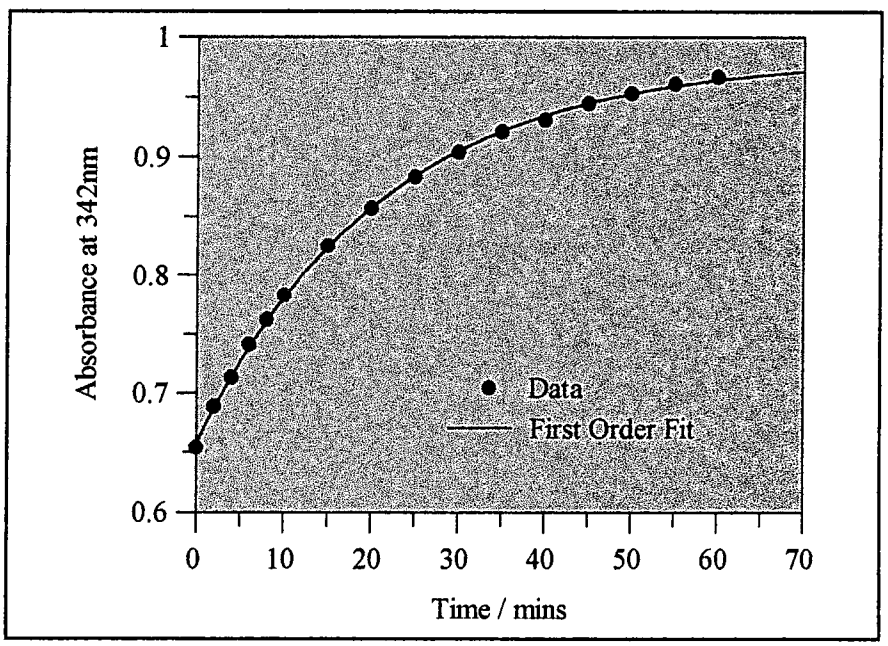

Figure 4.34 Recovery of absorbance at 342 nm with time for DBM in acetonitrile following irradiation

The first order rate constants of this recovery over a concentration range 5 x 10^{-6} mol dm^{-3} to 1 x 10^{-4} mol dm^{-3} were calculated, with an average value of $k \approx 1 \times 10^{-3}$ $s^{-1} \pm 5 \times 10^{-4}$ s^{-1}. This compares to a literature value of $k = 6.8 \times 10^{-4}$ s^{-1} in cyclohexane[12]. A large error was associated with this result, which could be due to many factors, including the presence of water in the acetonitrile solutions. Water was found to affect the rates of transient decay in flash photolysis, and thus it is possible that water could affect the recovery rates after ketonisation. If differing amounts of water were present in each sample, this could account for some of the observed differences in rate constants.

4.2.1.2 Quantum Yields of Photoketonisation

The quantum yields of ketonization of DBM and Parsol 1789 in acetonitrile (dried over molecular sieves) were measured as described in chapter 2, using the Xe-lamp, over a range of concentrations. Typical curves for the loss of DBM enol, and the growth of the ring-opened form of Aberchrome are shown in figures 4.35 and 4.36 respectively. The quantum yields obtained are given in tables 4.2 and 4.3.

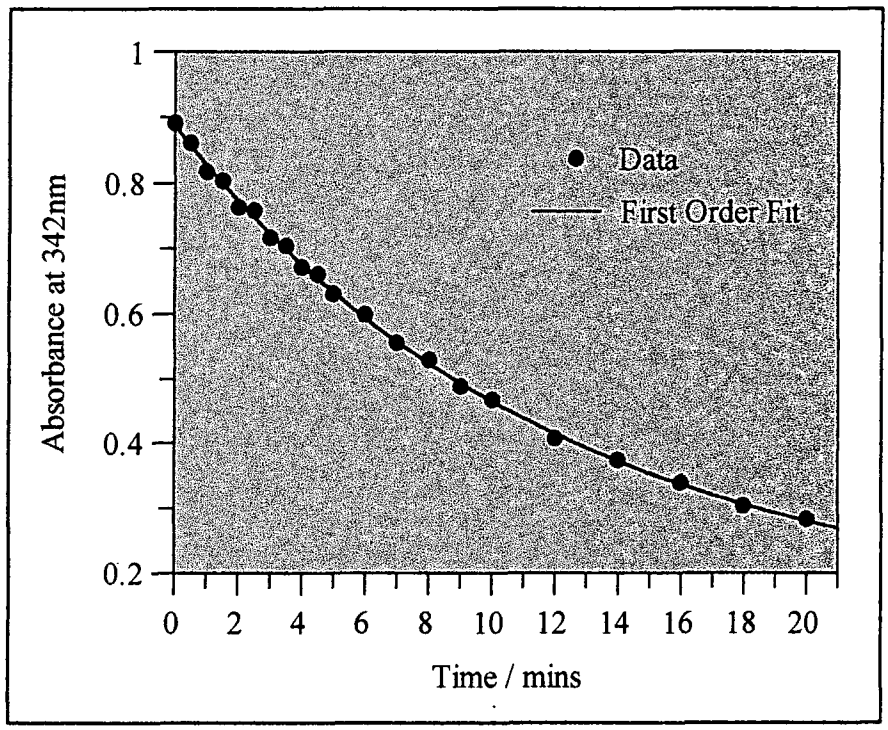

Figure 4.35 Loss of the enol form of DBM in acetonitrile with time during irradiation at 342 nm

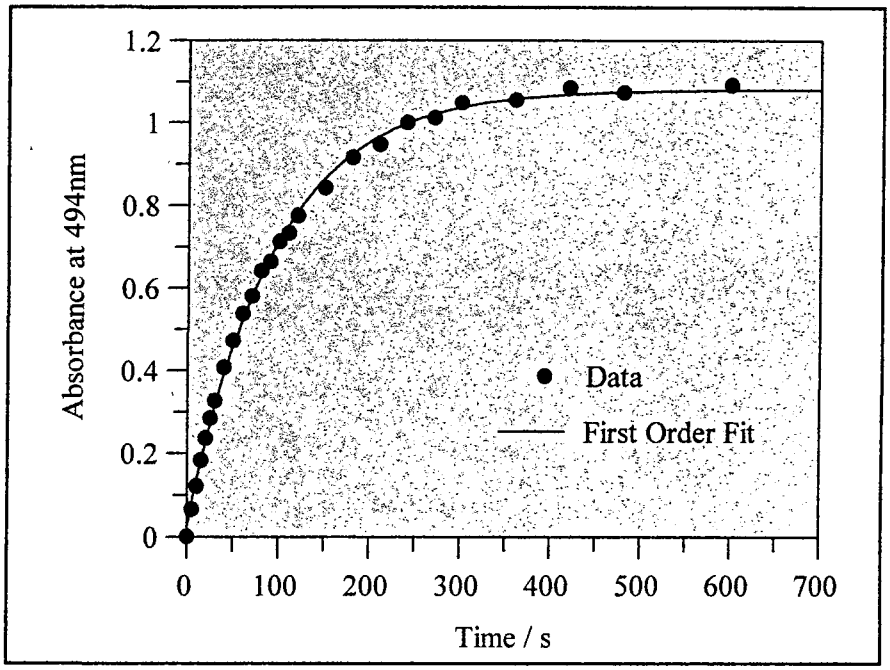

Figure 4.36 Formation of the ring closed form of Aberchrome 540 in toluene with time during irradiation at 342 nm

10^5 x Concentration / moldm^{-3}	$\Phi_{Ketonisation}$
1.1	0.017
1.3	0.0071
2.0	0.0087
3.1	0.011
4.0	0.0080
6.3	0.0086
average	**0.01 ± 0.004**

Table 4.2 Photoketonization quantum yields for DBM in acetonitrile

10^5 x Concentration / moldm^{-3}	$\Phi_{Ketonisation}$
0.87	0.0038
1.5	0.013
2.1	0.013
3.0	0.0048
3.5	0.0078
average	**0.008 ± 0.004**

Table 4.3 Photoketonisation quantum yields for Parsol 1789 in acetonitrile

The values in tables 4.2 and 4.3 compare to the literature value of $\Phi_{Ketonisation}$ = 0.0046 for DBM in acetonitrile[16]. These quantum yields follow no general trends with concentration. As can be seen, there is a considerable error in these results, but they do show that this process is a very inefficient one, with only ≈ 1% of excited molecules undergoing conversion to the diketone.

The large errors involved may be due to a number of factors. DBM and Parsol 1789 recover to the enol form thermally, and thus during the experiment, some recovery may have occurred. The recovery process is slow ($k = 1 \times 10^{-3}$ s^{-1} in the absence of UV), but this will have significance given the time scale of these experiments, (e.g. DBM decay rates measured as $k \approx 1 - 5 \times 10^{-2}$ s^{-1}), which would result in a lower than expected value for the quantum yields.

Photodegradation is also possible within the time scale of the experiments, which would also give an inaccurate value for $\Phi_{Ketonisation}$, because the formation of the diketone was measured by monitoring the loss of the DBM or Parsol 1789.

4.2.2 Flash Photolysis

The short-lived species produced initially on irradiation of dibenzoylmethane and Parsol 1789 at $\lambda \approx 340$nm has been investigated using the technique of flash photolysis, as described in chapter 2.

4.2.2.1 Spectra

Typical change in absorbance versus time curves for transient decay, and ground state recovery are shown in figures 4.37 and 4.38. The curves follow first order kinetics, and can be seen to share the same lifetimes, i.e. the kinetics of the recovery of the chelated enol are the same as the kinetics of the decay of the transient.

By studying such traces at varying wavelengths, difference and transient absorption spectra have been obtained, as described. The transient absorption spectra of dibenzoylmethane in various solvents have been studied. The spectrum in cyclohexane solution is given in figures 4.39 and 4.40. Similar spectra were obtained in 1,1,2-trichlorotrifloroethane and acetonitrile solutions.

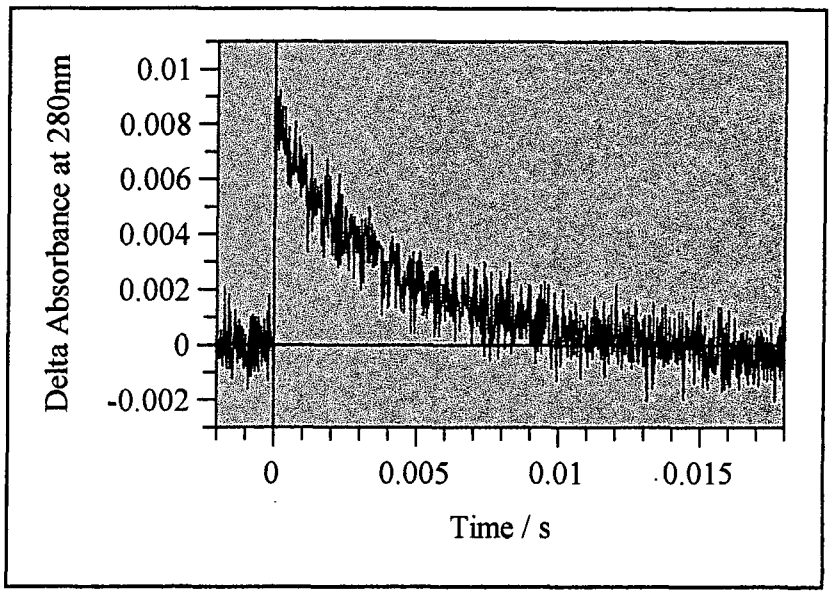

Figure 4.37 Typical transient decay curve for DBM in cyclohexane; pumping at 340 nm, probing at 280 nm

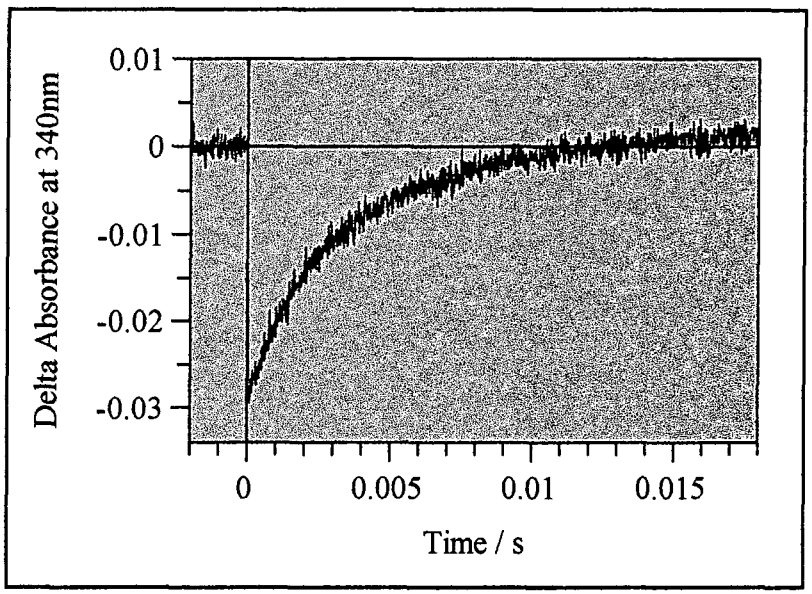

Figure 4.38 Typical ground state recovery curve for DBM in cyclohexane; pumping and probing at 340 nm

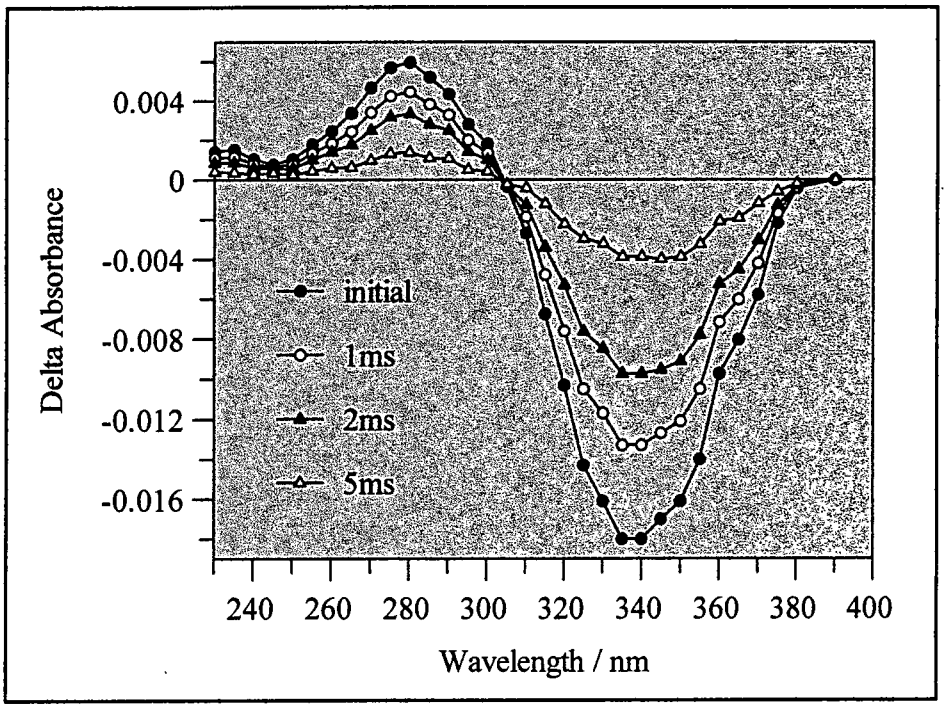

Figure 4.39 Difference spectrum after various time intervals for DBM in cyclohexane, pumping at 355 nm

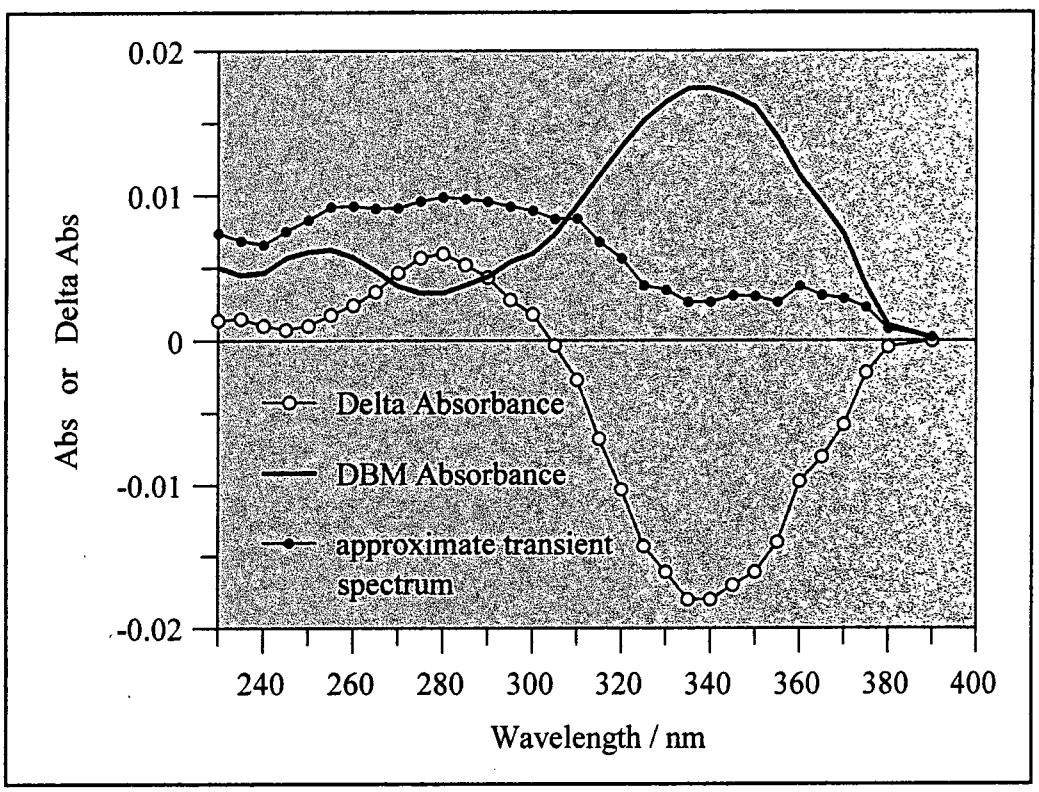

Figure 4.40 Approximate Transient absorption spectrum for DBM in cyclohexane, pumping at 355 nm

(initial delta absorbance values plotted)

The transient absorption spectrum indicates the formation of a short-lived species with an absorption peak at about 270 nm - 280 nm, which is consistent with those reported in the literature[12,17]. Although two absorption bands at 260 nm and 280 nm were reported, the results obtained in this work appear only to show a single, broad peak spanning this region. The spectrum could be interpreted as two peaks at approximately $\lambda \approx 260$ nm and $\lambda \approx 280$ nm, however the quality of the spectra makes it difficult to say if this is merely an artefact.

It appears from the calculated transient absorption spectrum, that there is a small degree of negative correlation of the graph, in the region of the main DBM absorption peak. This is not due to an under-addition of the DBM ground state spectrum, because this spectrum "dip" can not be eliminated with the addition of a larger proportion of ground-state spectrum. It is most likely that this feature is caused by an experimental artefact, linked to the different techniques used to measure the ground state spectrum and the transient difference spectrum. The ground state spectrum is measured using a fixed band width, however this is not possible with the flash photolysis experimental set-up. In experiments to measure the transient difference spectrum, the monochromator slit widths were manually adjusted to optimise sensitivity at different wavelengths. Thus the band width varied over the wavelength range of the transient difference spectrum. Larger slit widths, and therefore band widths, were used for smaller transient difference signals, to increase signal intensity. Because this effect does not occur in the ground state spectrum, this could explain the apparent rise in the calculated transient absorption spectrum towards the longer wavelengths, causing the apparent "dip" in the spectrum.

The maximum extinction coefficient of the short-lived species in cyclohexane had been estimated to be $\varepsilon = 1.4 \times 10^4$ mol dm^{-3} cm^{-1} at $\lambda = 270$ nm. This compares to a value of $\varepsilon = 2 \times 10^4$ mol dm^{-3} cm^{-1} at $\lambda = 340$ nm for DBM, as reported in chapter 3.

It is important to point out a flaw in the method of calculating the transient absorption spectrum. The method used, as described in chapter 2, involves adding a scaled ground state absorption spectrum to the difference spectrum measured in the flash photolysis experiments. Dibenzoylmethanes exist as a mixture of the chelated enol and the diketone, as discussed, however in these experiments we are only exciting the chelated enol, and are assuming that only this species is involved in the short-lived species formation. Thus we should only add a scaled ground state absorbance spectrum corresponding to the chelated enol only, and not the diketone, however, this is not practical because the DBM diketone spectrum and proportion is not known for all solvents. Thus the diketone spectrum is also added, and this results in an apparent "extra" absorbance contribution to the transient spectrum, in the 250 nm region. The transient spectra reported in this work, and in the literature, are therefore distorted by the diketone spectrum. If this effect did not occur, the transient peak obtained would be much less broad, with a peak in the region of $\lambda_{max} \approx 290$ nm.

The spectra obtained in ethanol, micellar solutions of 1-5% Triton X-100 (reduced) in water, and EPA appear to have a slightly different shape, as shown in figure 4.41.

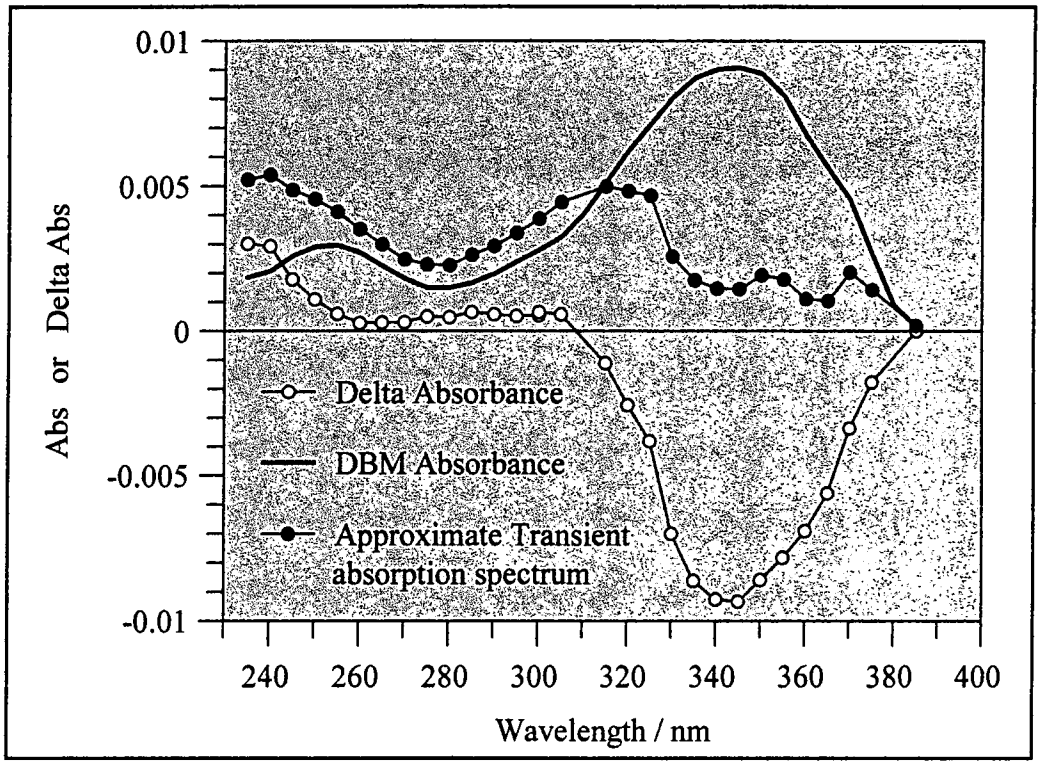

Figure 4.41 Approximate transient absorption spectrum for DBM in ethanol, pumping at 355 nm (initial delta absorbance values plotted)

The absorption peak is now seen to fall at approximately 310 nm. It appears that in protic solvents the absorption spectrum of the short-lived species is shifted towards longer wavelength (lower energy), compared to the spectrum in hydrocarbon or non-protic solvents. This is consistent with the literature discussions of solvents such as ethanol forming complexes with the transient species. The same apparent atefact of negative correlation can also be seen to occur, as was discussed previously.

Parsol 1789 behaves in the same way as DBM, with similar spectra obtained. The transient spectra for Parsol 1789 in cyclohexane are given in figures 4.42 and 4.43.

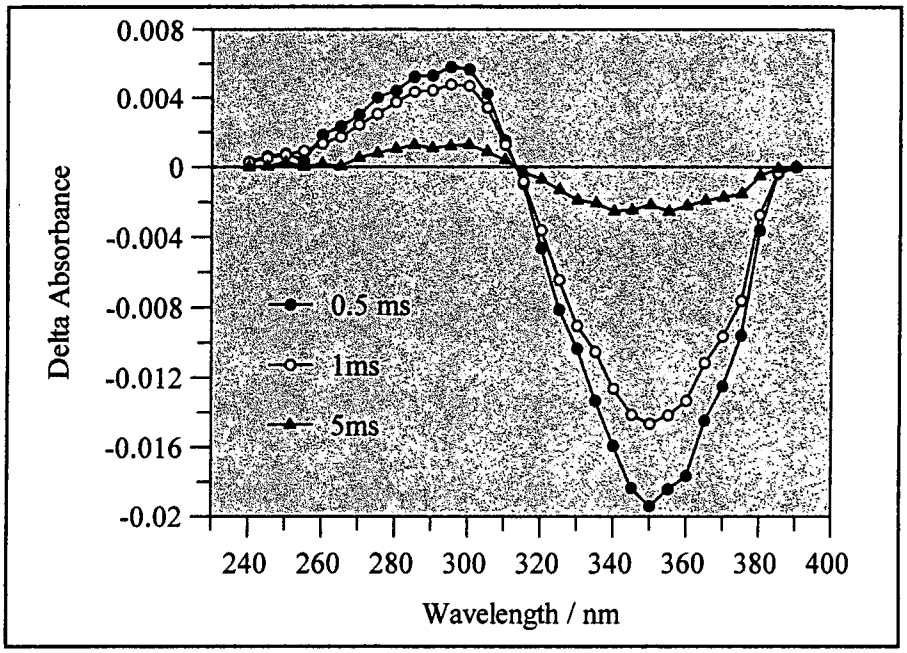

Figure 4.42 Difference spectrum after various time intervals for Parsol 1789 in cyclohexane, pumping at 340 nm

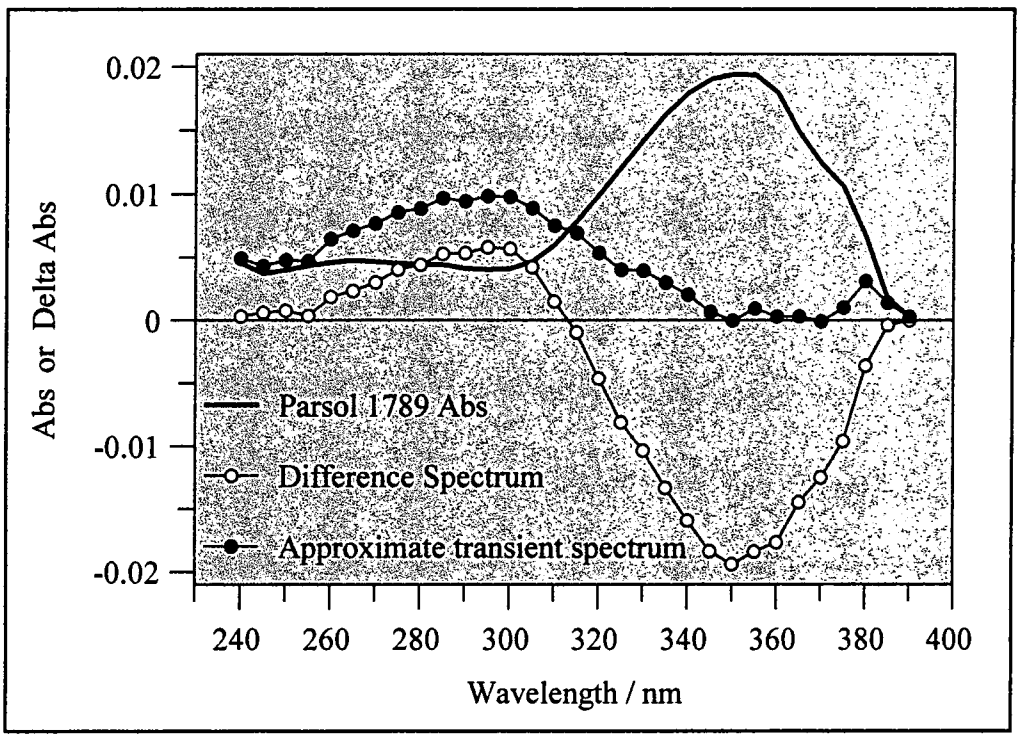

Figure 4.43 Approximate transient absorption spectrum for Parsol 1789 in cyclohexane, pumping at 340 nm

(initial delta absorbance values plotted)

No evidence of the enolate transient at 380 nm [18] was observed in ethanol or 1% pyridine in cyclohexane solutions, although study was not undertaken in degassed solution. In N,N-dimethylformamide, (DMF), solution, enolate formation was observed, although a high rate of sample degradation limited the quality of spectra obtained. The appearance of a new species at 390 nm was, however, clearly observed, as is shown in figure 4.44.

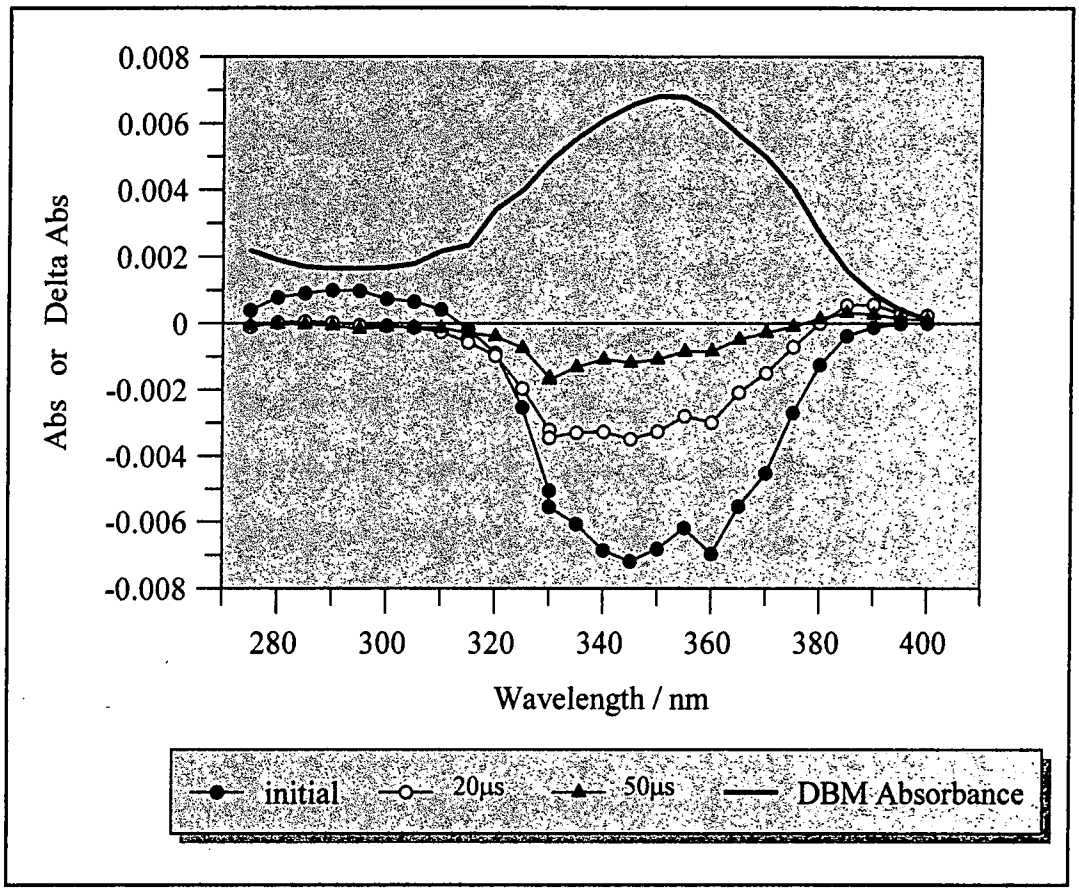

Figure 4.44 Difference spectrum after various time intervals for DBM in DMF, pumping at 355 nm

Transient decays were fitted to double exponential curves. At wavelengths in the region of 390 nm, a growth, followed by decay, of a short-lived species is observed. Wavelengths around 320 nm also produced a similar curve over a similar time scale, but with negative delta absorbance values. At wavelengths in the region of 300 nm a sharp decay followed by slight recovery was observed. Wavelengths in the region of 345 nm fitted well to a single exponential decay. These decay curves are shown in figures 4.45 to 4.48.

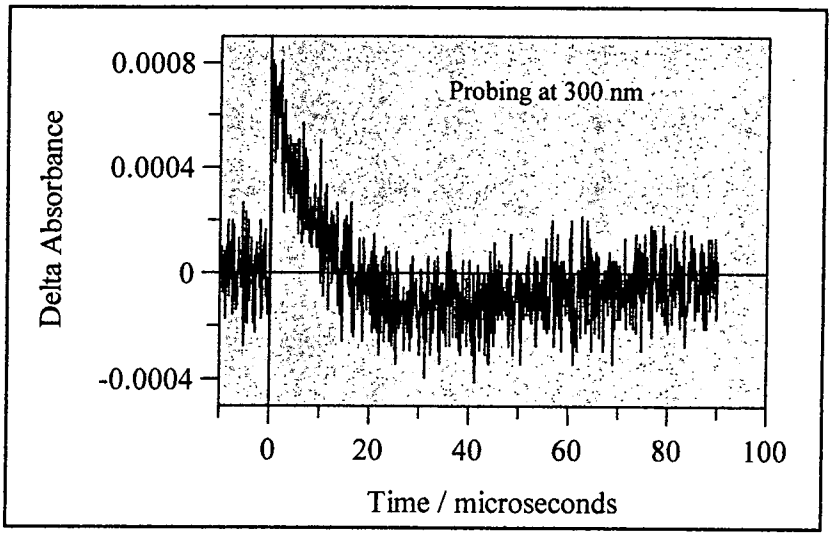

Figure 4.45 Transient decay in DMF, probing at 300 nm

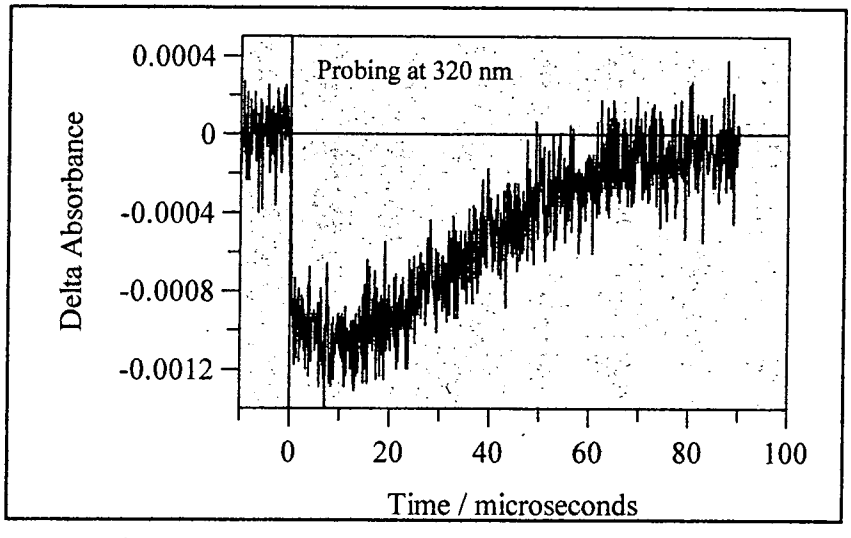

Figure 4.46 Transient decay in DMF, probing at 320 nm

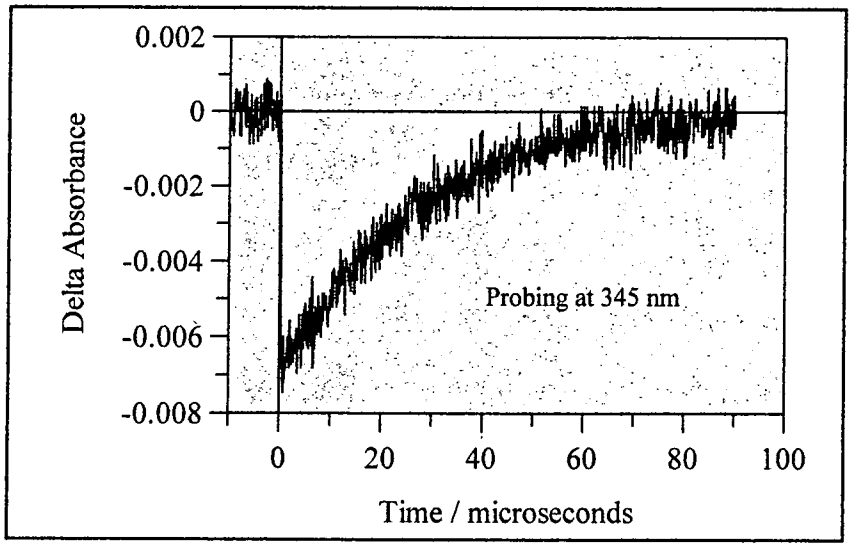

Figure 4.47 Transient decay in DMF, probing at 345 nm

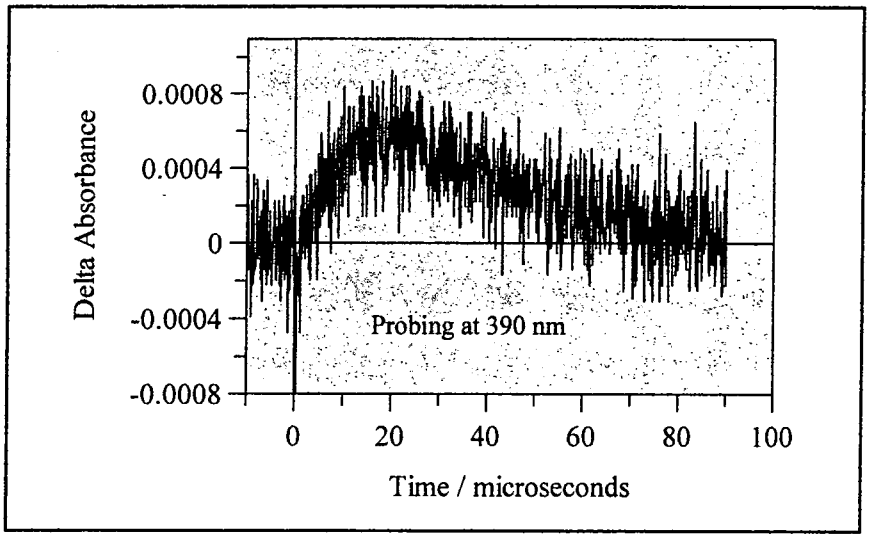

Figure 4.48 Transient decay in DMF, probing at 390 nm

These results show that flash photolysis of DBM in DMF solution produces the enolate of DBM, as has been observed in the literature for basic solutions, as discussed in section 4.1.2.5 Initially the non-chelated intermediate is formed, which then decays to the enolate, which can be seen to grow in with matching kinetics. The non-chelated enol also decays directly back to the chelated DBM. The enolate reverts to the original chelated dibenzoylmethane, at a slower rate than its formation. The overall lifetime in DMF solution was much shorter than in the other solvents studied, which will be discussed in the next section. The effect of the addition of amides to sunscreen formulations containing DBM based sunscreens has been the subject of a patent, and is discussed in chapter 5.

Enolate formation was not observed in any other solvents, although this does not exclude the formation of small amounts, or the formation of an enolate that reverts to the chelated enol at a faster rate than its formation.

4.2.2.2 Lifetimes

The first order rate constants of the decay, and thus lifetimes, τ, of the transient species of dibenzoylmethane were observed to be different in each solvent system. In each case, excluding DMF solution as discussed, they were found to be independent of the probe wavelength, and the rate constants for decay of the transient were the same as those for recovery of the enol.

The measurement of transient decay rates proved to have many problems. The rates of transient decay were consistent for experiments carried out over a period of a few days, however there were large

differences noted in the lifetimes measured at different points in time, e.g. experiments carried out months apart, for identical experimental conditions. The source of the discrepancies could not be identified or eliminated despite rigorous investigation. The effects of DBM concentration and temperature on the decay rates were investigated, as will be discussed later, however for experiments carried out in the same solvent at the same concentration and at the same temperature, consistent lifetimes could not be obtained.

Extended exposure to the laser light and monitoring lamp can produce a loss in absorbance of DBM due to decomposition, which would affect the concentration and composition of the DBM solutions. However, no significant changes in lifetime were seen if a sample was irradiated for many laser shots, or left in the monitoring lamp of the flash photolysis set-up, before measuring the transient lifetime. In any case samples were changed frequently from a stock solution.

The possible effect of the solution age was also investigated. Transient lifetimes for freshly made DBM solutions, and those kept for several days in the dark were measured, and no differences were noted.

It was observed that the addition of water in acetonitrile or ethanol solutions had a marked effect on lifetime. The possiblity that varying traces of water in the solvents could be responsible for the lifetime discrepancies was therefore invesitigated. Solutions of DBM in cyclohexane dried over molecular sieves were prepared, and the solutions spiked with varying amounts of water. No significant changes in the measured rate constants of transient decay were observed. Thus it appears water is not sufficiently soluble in cyclohexane for water traces to be the cause of inconsistent results. With other, hydrophilic, solvents such as acetonitrile, water traces have proven to be a problem, which is not entirely overcome by careful solvent drying. However other factors must also be involved, affecting the rates of decay, to account for the difference in other solvents.

The effects on transient lifetime of varying the laser power were also investigated. It was found that decreasing the laser power resulted in a decrease in the first order rate constant for decay, which corresponds to an increase in the lifetime, as will be discussed later. According to those results, however, the small variations in laser power occurring each time the flash-photolysis equipment was set-up would not have a significant effect on the lifetimes.

The most likely reason for the lifetime differences observed is the presence of traces of water or pH differences in the solvents. As has been discussed, the literature reports that very different lifetimes are observed for the addition of various additives at concentrations $< 10^{-4}$ mol dm^{-3} [16,18]. It is possible that solutions made up from a bottle of fresh solvent will exhibit different lifetimes to those made up with an bottle of solvent previously exposed to the air, due to absorption of water. Solution pH may also have an effect; it was noted in the literature that degassed and aerated solutions of ethanol exhibited different decay kinetics due to the formation of the enolate species[24]. Thus it is possible that subtle pH changes due to differing amounts of dissolved CO_2 from the air may contribute to the changes in lifetime.

Clearly the situation is complicated and a number of factors are likely to be involved. The problems discussed make it difficult to compare the transient decay rates for different solvents, and could explain the differences in lifetimes reported in the literature.

The values of the first order rate constants, and lifetimes obtained in this work, for solutions of absorbance, Abs = 0.3 at 355 nm, measured in various solvents, are given in table 4.4.

These values vary considerably from reported literature values, probably for the reasons discussed. They indicate that the transient has a longer lifetime in acetonitrile than in cyclohexane, which in turn is much longer than in ethanol. They also show that the addition of water to the ethanol vastly increases the rate of decay of the transient, and aqueous micellar solutions have extremely short lifetimes. The addition of pyridine to cyclohexane greatly reduces the lifetime of the short-lived species.

Solvent	k / s^{-1}	τ / ms
Acetonitrile	200	5
Cyclohexane	300	3.4
Ethanol	3900	0.25
1% Triton X-100 (reduced) in water	60000	0.017
2% Triton X-100 (reduced) in water	52000	0.019
5% Triton X-100 (reduced) in water	52000	0.019
1% Pyridine in Cyclohexane	60	17
EPA	450	2.2
9:1 Ethanol : Water	15000	0.07

Table 4.4 Transient lifetimes for DBM in various solvents

4.2.2.3 Concentration effects

The observed first order rate constants of the transient decay are dependent on the initial concentration of dibenzoylmethane or Parsol 1789. Although variations in the absolute calculated rate constants occur, for the reasons explained above, the dependence of the transient decay on the concentration of DBM or Parsol 1789 can be studied by carrying out experiments at differing concentrations, but under the same conditions, for example, using solvents from the same source, and on the same day.

This has been done for DBM and Parsol 1789 in cyclohexane, at room temperature. As explained earlier, the recovery of the chelated enol follows the same kinetics as for the decay of the transient, as seen in

figures 4.37 and 4.38. Therefore the rate constants for transient decay can be measured by studying the recovery of the chelated enol. The recovery of the ground state was observed at 5 probe wavelengths about the main absorption peak, and the average value of the rate constants and lifetimes taken. The results are shown below in figures 4.49 and 4.50, where the data have been fitted to straight lines.

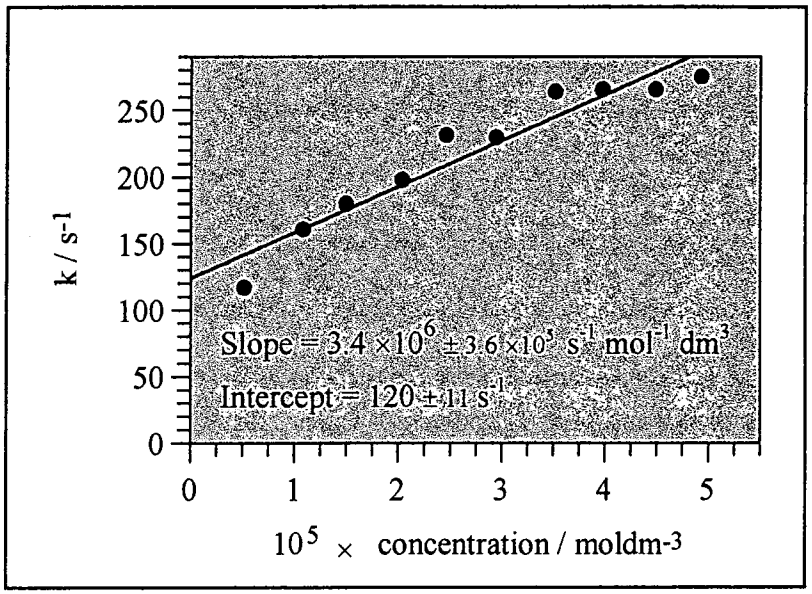

Figure 4.49 Graph of concentration vs. First order rate constant for the transient produced from DBM in cyclohexane, pumping at 340 nm

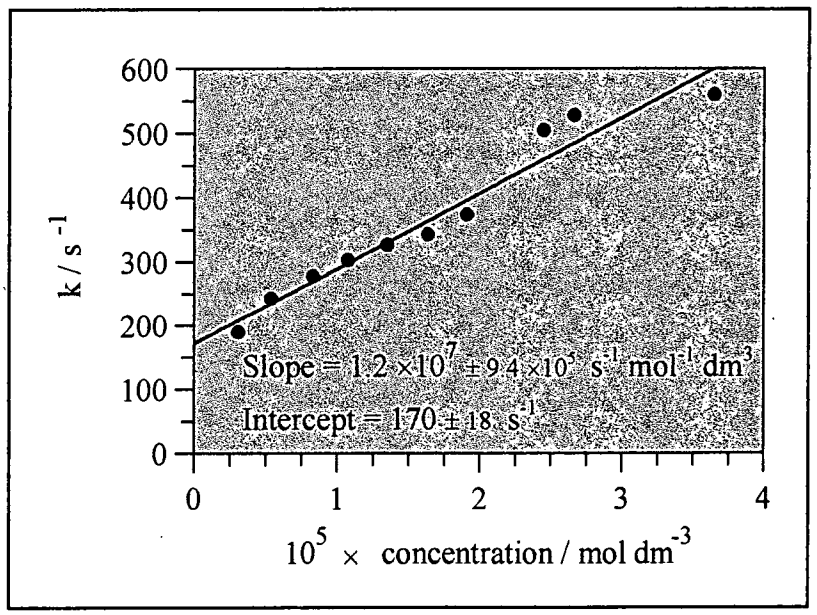

Figure 4.50 Graphs of concentration vs. first order rate constant for the transient produced from Parsol 1789 in cyclohexane, pumping at 340 nm

From these results it is clear that the concentration of dibenzoylmethane in solution does affect the observed first order rate constant of transient decay. This suggests that interaction with ground state DBM molecules is a decay pathway for the transient species, resulting in an enhanced rate of chelated enol recovery, and the observed kinetics are pseudo first order. However, the fact that the relationship is not one of direct proportionality suggests that this pathway occurs in addition to direct recovery of the transient, as indicated in figure 4.51.

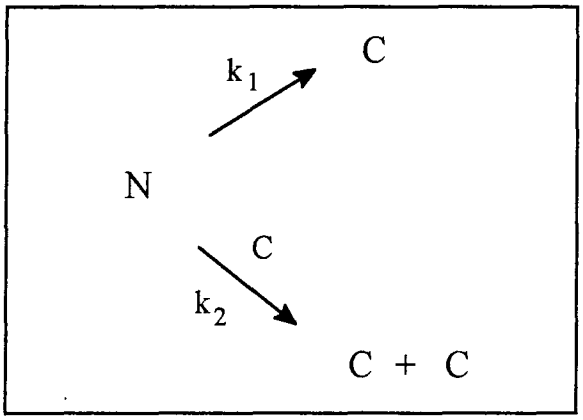

Figure 4.51 Two possible routes of recovery of the non-chelated enol transient, N, to the chelated enol, C

If the scheme shown in figure 4.51 occurred, the the rate of loss of the non-chelated enol would be described by equations 4.1 and 4.2, where [N] represents the concentration of non-chelated enol and [C] is the concentration of the chelated enol. Assuming that [C] » [N], the observed first order rate constant is then given by equation 4.3.

$$\frac{d[N]}{dt} = -k_1[N] - k_2[C][N] \qquad \textbf{Equation 4.1}$$

$$\frac{d[N]}{dt} = -\left(k_1 + k_2[C]\right)[N] \qquad \textbf{Equation 4.2}$$

$$k_{obs} = k_1 + k_2[C] \qquad \textbf{Equation 4.3}$$

In the above kinetic scheme, the variation of observed first order rate constant, k_{obs}, with the concentration of chelated enol, [C], would result in a straight line graph with a gradient of k_2 and an intercept of k_1. The results from the above experiment seem to fit this relationship, suggesting that the scheme of transient decay shown in figure 4.51 does occur - the non-chelated enol of DBM can either recover directly to form the chelated enol, or can recover by interaction with a chelated enol ground state molecule.

The above kinetics are however a simplification for the situation of DBM transient decay, and assume that only a small fraction of DBM is converted to enol, which may not be appropriate, as will be shown later. Varying the ground state DBM concentration or the illumination conditions also necessarily varies the amount of transient produced, the effects of which are discussed below. Thus the actual kinetics are likely to be much more complex that those presented above.

The effect of varying the laser power on the rates of transient decay in cyclohexane was also investigated, using attenuating filters to alter the laser power. A linear relationship was observed, as shown in figure 4.52.

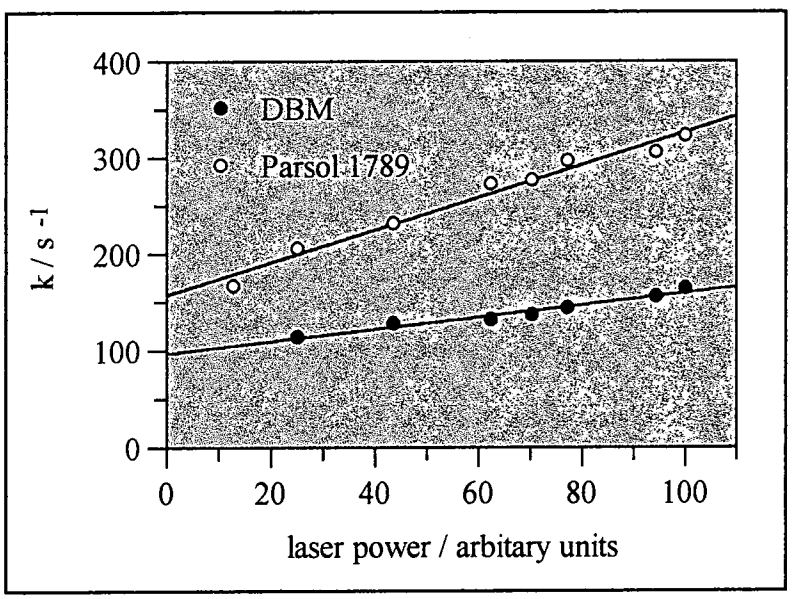

Figure 4.52 Variation of first order rate constant with laser power for the transients produced from DBM Parsol 1789 in cyclohexane, pumping at 340 nm

(Linear fits: DBM slope = 97 ± 4 s^{-1}; Parsol 1789 slope = 157 ± 7 s^{-1})

The short-lived species thus appears to decay more quickly with increasing laser power, i.e. with increasing transient concentration. This complements the concentration study, and suggests that the transient species interact with one another, and the rate of decay is enhanced. This effect has been reported in the literature,

where it is observed that on increasing the laser power, the rate of transient decay is increased as a second order reaction component becomes more significant[19].

In the literature, it was suggested that the short-lived non-chelated enol form can interact with ground state molecules, and other transient molecules, to form dimers[17,20], as discussed earlier. Recovery of the ground state chelated enol is reported to occur via several pathways, including via the formation of transient-transient and transient-ground state dimers[17], and it is reported that this enhances the recovery.

In sunscreen formulations, the concentration of DBM is much higher than in the solutions studied here, as will be discussed in chapter 5. In a sunscreen formulation it is probable that interaction between transient molecules and chelated enol molecules or other transient molecules occurs extensively, and recovery of the chelated enol is fast.

4.2.2.4 Transient Decay Curve Fitting

For higher concentrations of both DBM and Parsol 1789, the transient decays, and recoveries of the enol did not seem to fit a first-order rate law, i.e. a single exponential curve, very well. This could imply that at higher concentrations, transient decay occurs via more than one pathway, e.g. via interaction of two transient molecules. This agrees with the effects of varying laser power reported earlier, where increased transient concentration caused an increase in the observed first order rate constant. As discussed earlier, reports in the literature have suggested that interaction of two transient molecules can enhance recovery of the chelated enol.

At these higher concentrations a double exponential fits more succesfully than a single exponential curve. This could also implicate the formation of more than one transient species, which decay with different rates.

4.2.2.5 Temperature Effects

The effect of varying the temperature on the transient recovery rate was studied. DBM in 2:1 isopentane : methylcyclohexane was studied over the temperature range 77-320 K, and the results obtained are shown in table 4.5 and figures 4.53 and 4.54. It must be noted that short decays, with lifetimes of approximately 0.02 s, were observed at 77 K using the technique of flash photolysis. As will be discussed later, the lifetime of this species at this temperature can be observed to be hours, using conventional absorption spectroscopy. It is probable that the action of the monitoring lamp in the flash photolysis experiments allowed localised heating, such that a faster transient decay was observed.

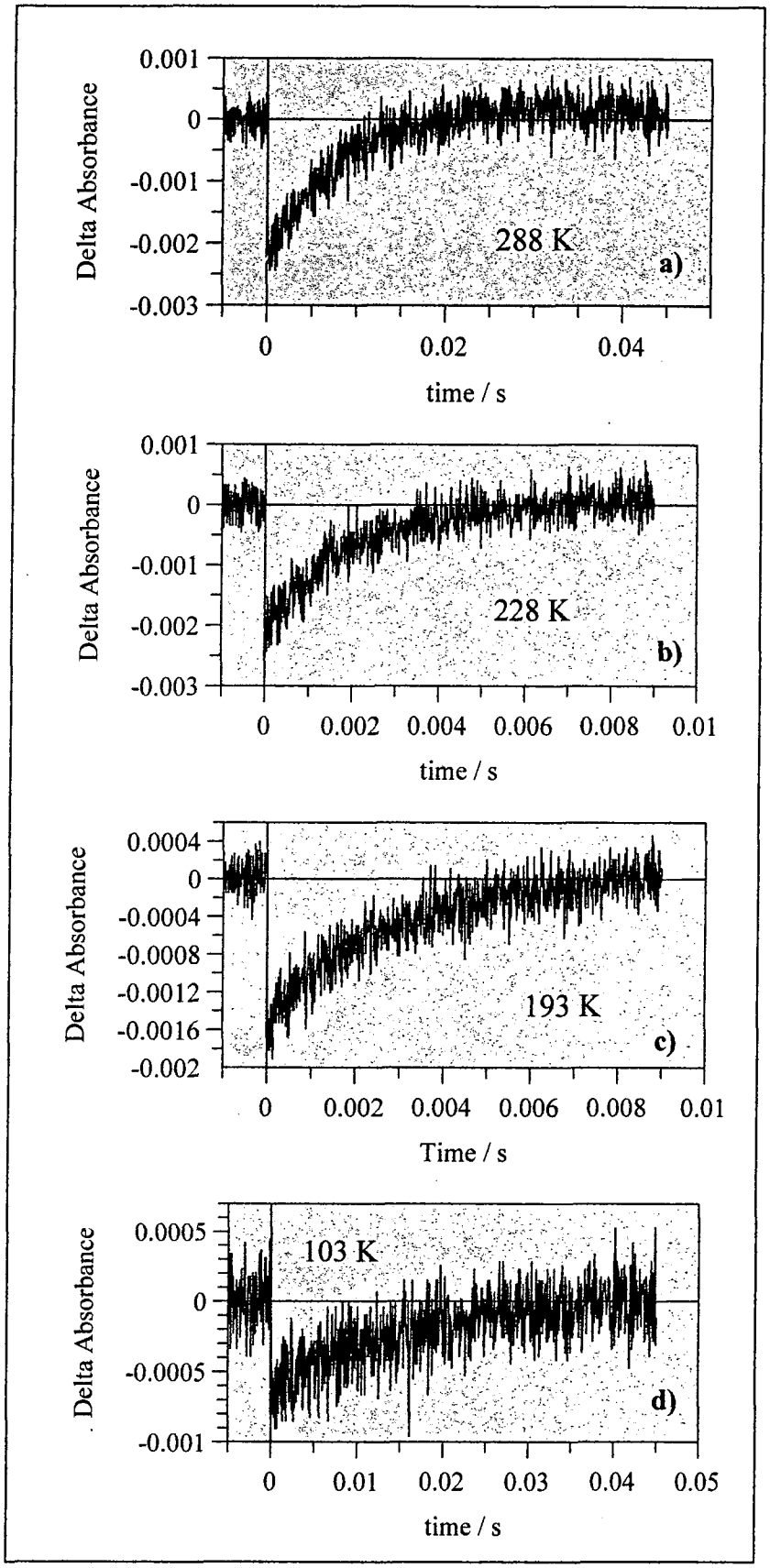

Figure 4.53 Typical transient decay curves for DBM in 2:1 isopentane : methylcyclohexane

Pumping at 340 nm, Transient decay curves observed at a) 288 K, b) 228K, c) 193 K, d) 103 K

Temperature / K	k / s^{-1} a)
77	56.8
103	58.5
123	86.6
173	85.2
193	332.3
203	436.4
213	426.2
223	417.7
228	482.7
233	493.6
238	443.4
243	380.1
248	354.4
253	341.7

Temperature / K	k / s^{-1} a)
258	279.6
263	267.0
268	214.4
273	166.0
278	160.8
283	147.7
288	125.0
288[b]	155.3
293[b]	138.5
298[b]	133.1
303[b]	122.1
308[b]	113.1
313[b]	107.1
318[b]	99.4

Table 4.5 Variation of the first order rate constant with temperature for the decay of the short-lived photo transient of DBM in 2:1 isopentane : methylcyclohexane

a) Average value, obtained from several k values calculated by probing at wavelengths 335-350 nm

b) Results obtained using waterbath, all other results obtained using cryostat

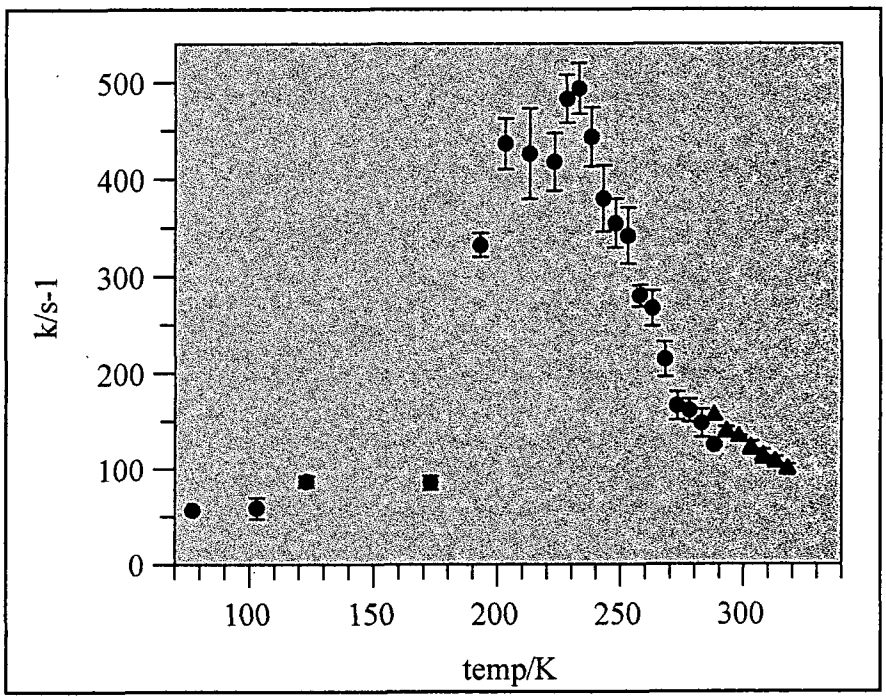

Figure 4.54 Variation of the first order rate constant with temperature for the decay of the short-lived photo transient of DBM in 2:1 isopentane : methylcyclohexane

(▲ Results obtained using water bath ● Results obtained using cryostat)

Average k values plotted, calculated by probing at wavelengths 335-350 nm. Errors shown are standard deviations.

The variation of rate constant with temperature has been reported by Tobita *et al*, where they report the expected results of an increase in first order rate constant with temperature for DBM in 3-methylpentane[19]. They have measured the activation energy to be 3.6 kcal mol^{-1}, however, they report their results only for the temperature range 155 - 260 K. The results obtained in this report agree over a similar range, approximately 150 - 230 K, where the expected behaviour is shown. It is odd that Tobita et al have chosen such an unusual range to study, and suggests that they may have also found a strange relationship between temperature and transient lifetime under normal conditions, but have not studied it in detail.

The reasons for this unusual temperature dependence are unclear. The melting points of isopentane and methylcyclohexane are 113 K and 146 K respectively[34], and therefore the melting point of the solvent system 2:1 methylcyclohexane : isopentane is likely to fall in the region where the graph displays the expected behaviour of increasing k with temperature. Thus change in solution properties at the melting point are unlikely to be a cause of the unusual effects observed at higher temperatures.

Changes in the solution properties on changing the temperature could, however, partly explain the results. The solution concentration increases as the temperature is lowered, due to solvent shrinkage. For the solvent system 2:1 methylcyclohexane : isopentane, the volume change is approximately $V_{77} / V_{293} = 0.78$ [37], and hence the solution concentration increases by a factor of 1.28 upon cooling. Concentration affects transient lifetimes, as reported previously, k increasing with increasing concentration, and so in this case with decreasing temperature. However concentration changes are unlikely to be greatly significant in the temperature range $\approx$ 230-300 K, which is well above the melting point. The absorption spectrum also changes on cooling, as was discussed in chapter 3. This effect, and the change in concentration, both result in higher DBM absorbances at 355 nm, and thus increased transient formation, with decreasing temperature. As discussed earlier, increased laser power, and therefore increased transient formation, resulted in increased values of k, and as such in this case k should increase with decreasing temperature, however the absorbance does not change dramatically, $\Delta Abs < 20\%$ at 355 nm, in the temperature range 230-300 K, where the unusual results are observed.

It was also observed was that the height of the transient signal increased approximately proportionally with increasing temperature, as shown in figure 4.55. This is in contrast to the effect of increasing DBM absorbance with decreasing temperature, as discussed above, suggesting that more transient was produced with increasing temperature, despite lower DBM absorbance.

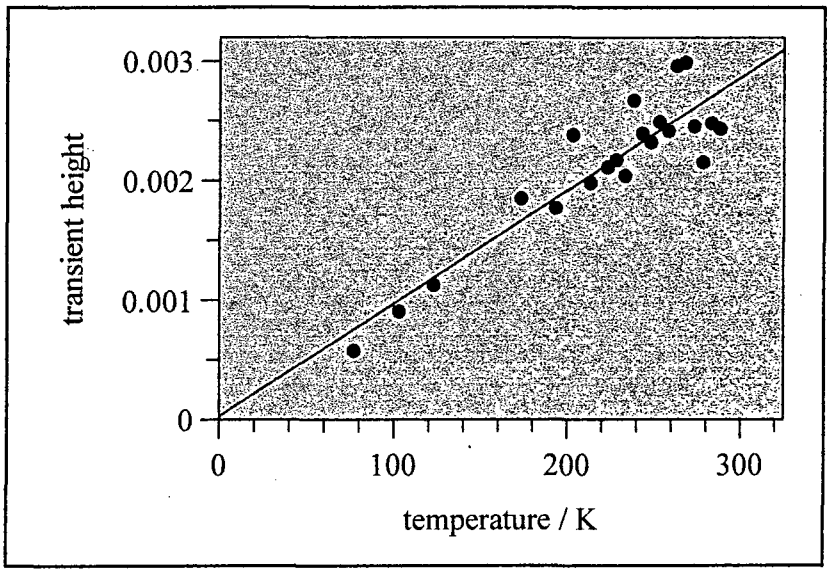

Figure 4.55 Variation in initial transient height with temperature, for decay of the short-lived photo transient of DBM in 2:1 isopentane : methylcyclohexane

(Best fit line shown, results obtained with cryostat shown)

Thus it is possible that the effects of increasing concentration and absorbance could partially explain the observed increase of k with decreasing temperature, however there must be other factors involved.

There are clearly conflicting effects causing the unusual shape of the temperature vs. rate constant of transient decay graph for DBM. It is probable that, although increased temperature causes an increase in the rate of transient decay as would be expected, there are other factors reducing the rate of decay with increasing temperature. This becomes of significance above 230 K, resulting in the inverted temperature-rate relationship. A possible explanation could be that with increasing temperature, due to decreased viscosity of the solvent and increased mobility of the molecules in solution, it is more likely that two or more non-chelated enol transients link up to form intermolecularly hydrogen bonded dimers or oligomers, which has the effect of stabilising the transients. Thus recovery to the intramolecular hydrogen bonded enol structure would be slowed with increasing temperature. However it would be expected that a similar decrease in transient decay rate with increasing concentration would occur, which is not the observed relationship, discussed earlier, where formation of dimers speeds up decay of the transient.

The observed variation of rate constant with temperature might be explained by considering the kinetics of systems where k falls with increasing temperature. First order reaction rate constants are determined by the activation energy, and always increase with temperature. In systems where such a rate constant is observed to decrease with increasing temperature, the reaction occurring can not be a simple one step reaction. For example consider the reaction shown in equation 4.4. If k_{obs} is observed to decrease with increasing temperature, one explanation is that a fast equilibrium is present between the reactant, A and an intermediate product in the reaction, B with equilibrium constant K, as shown in equation 4.5. This intermediate then reacts to form the product, with rate constant k, which is still the rate determining step,

as shown in equation 4.6. The rate of reaction is given by equation 4.7, provided the initial equilibrium is achieved much faster than the reaction rate. The equation shows that the observed rate constant is actually the product of the actual rate constant of the rate determining step and the equilibrium constant of the initial equilibrium.

$$A \xrightarrow{k_{obs}} \text{Product} \qquad \textbf{Equation 4.4}$$

$$A \underset{}{\overset{K}{\rightleftharpoons}} B \quad \text{fast equilibrium} \qquad \textbf{Equation 4.5}$$

$$B \xrightarrow{k} \text{Product} \qquad \textbf{Equation 4.6}$$

$$\text{Rate} = k[B] = kK[A] = k_{obs}[A] \qquad \textbf{Equation 4.7}$$

The rate constant k is related to the activation energy, E_a as described in equations 4.8 and 4.9. It is clear that this must increase with increasing temperature. K is related to the change in enthalpy, ΔH, of the equilibrium process, in a similar relationship, as described in equation 4.10 [38]. If the reaction is exothermic, and ΔH is negative, then it is clear that K will decrease with increasing temperature.

$$\frac{d\ln k}{d(1/T)} = \frac{-E_a}{R} \qquad \textbf{Equation 4.8}$$

$$k = A\exp\left(\frac{-E_a}{RT}\right) \qquad \textbf{Equation 4.9}$$

$$\frac{d\ln K}{d(1/T)} = \frac{-\Delta H}{R} \qquad \textbf{Equation 4.10}$$

Thus it is possible that on increasing the temperature, K decreases at a faster rate than k increases, resulting in a decrease in the observed rate constant on increasing temperature. Equation 4.9 makes the assumption that ΔH is constant with temperature. This is not actually the case, especially over large temperature ranges, and hence the rate of change of K with temperature will be also be affected by changes in ΔH (of the equilibrium process, equation 4.5). Activation energy (of the rate determining step, equation 4.7) will also vary with temperature. Thus if a balance exists between the rates of change of k and K with temperature, it is possible that over different temperature ranges the observed rate constant will show different trends with increasing temperature.

If the above reaction scheme and kinetics explains the observed recovery of the DBM non-chelated enol form, then the recovery is clearly not a one-step process. A fast equilibrium between the observed short-lived species, A, and another species, B, must occur, such that the reaction A→B is exothermic. The above kinetic discussion also requires that only species A must be observed in the decay kinetics, although with a low value for K it may be possible that observation of B is not noticed. It is not immediately clear what the other species could be. It is possible that species B is a complex with the solvent molecules, as suggested in the literature and discussed earlier. The introduction of a solvent molecule would not disrupt the kinetic scheme, as the solvent is present in excess. The recoveries in this section were, however, measured in non-polar aprotic solvent, (2:1 isopentane : methylcyclohexane), and thus the formation of solvent-non-chelated complexes is unlikely. E ↔ Z isomerisation of the non-chelated DBM is another possible explanation, and is discussed in a later section.

4.2.2.6 Quantum Yields of Transient Formation

The quantum yields of transient formation of dibenzoylmethane and Parsol 1789 in cyclohexane at room temperature were measured using the technique described earlier, over a range of concentrations. Formation of the non-chelated enol was measured by monitoring the loss of absorbance of DBM or Parsol 1789, by assuming that the non-chelated enol is the only product. Thus the loss of DBM or Parsol 1789 is directly equivalent to the formation of the non-chelated enol. Typical graphs of delta absorbance vs. laser power for Parsol 1789 and Aberchrome are shown in figure 4.56. The calculated quantum yields are given in tables 4.6 and 4.7.

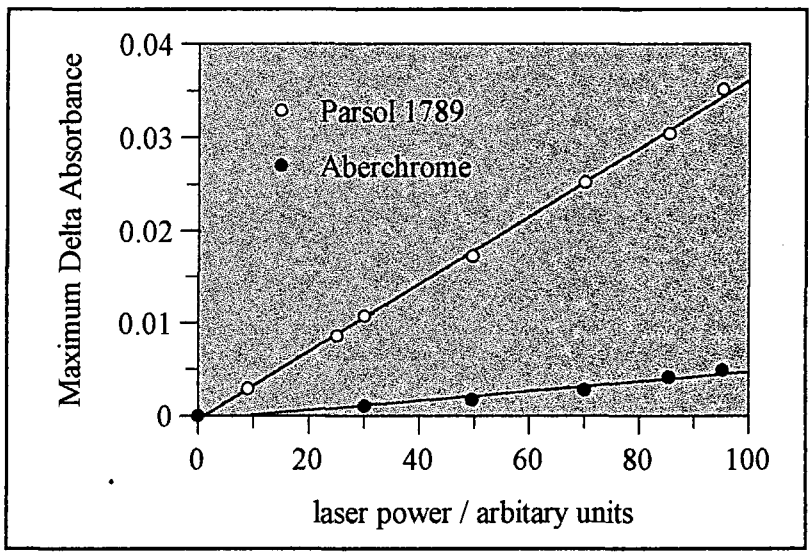

Figure 4.56 Change in absorbance vs. laser power for Parsol 1789 (probing at 358 nm) and Aberchrome 540 (probing at 494 nm), for irradiation at 340 nm

$10^5 \times$ Concentration / mol dm^{-3}	$\Phi_{Transient}$
1.8	0.45
2.6	0.46
3.0	0.58
3.9	0.41
5.4	0.55
average	**0.49 ± 0.07**

Table 4.6 Quantum yields of transient formation for DBM in cyclohexane

$10^5 \times$ Concentration / mol dm^{-3}	$\Phi_{Transient}$
1.2	0.39
1.9	0.39
2.1	0.44
2.6	0.34
4.0	0.48
average	**0.41 ± 0.05**

Table 4.7 Quantum yields of transient formation for Parsol 1789 in cyclohexane

These results compare to a literature value of Φ = 0.1-0.5 for DBM in isooctane[16]. As with the photoketonization quantum yields, the quantum yields of transient production do not show a variation with concentration, and hence $\Phi_{Transient}$ is independent of concentration. They show that $\Phi_{Transient}$ is significantly larger than the quantum yields observed for photoketonization, indicating a far more efficient process. The error associated with these values is also proportionally much smaller than that in the ketonization results.

4.2.3 Low Temperature Photo-conversion

4.2.3.1 Low Temperature Photochemistry

On irradiating a frozen solution of DBM at 77 K with UV light λ >300 nm, the absorption spectrum was seen to change, as shown in figure 4.57. The three peaks observed in the low temperature specturm

become smaller, as a new peak appears at $\lambda \approx 310$ nm. The new peak can be seen to be significantly different to both the room temperature and low temperature spectra. The original DBM spectrum is completely restored on warming the solution. The new species formed was observed to be stable for hours at 77 K, and it was not feasible to measure any possible decay over longer periods of time. This low temperature formation of a new species has been previously observed in a PhD thesis for 1,3-diketones including DBM[39], although it has not been reported elsewhere in the literature.

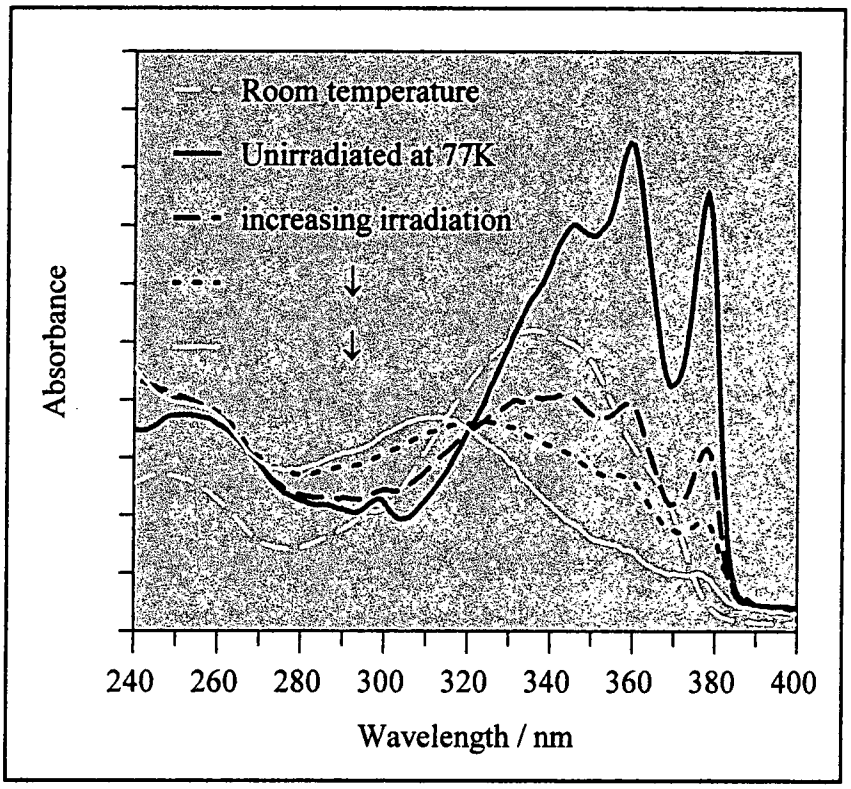

Figure 4.57 Changes in DBM absorption spectrum in 2:1 isopentane : methylcyclohexane with irradiation at 340 nm

This new peak is very similar to the that of the short-lived species observed by flash photolysis at room temperature. Thus it appears that on irradiation of DBM at low temperature the same species is formed as at room temperature, however because of the low temperature and solid nature of the solvent, the species is stable for hours. The extinction coefficient of the new species in EPA has been determined; $\varepsilon = 1.3 \times 10^4$ mol dm^{-3} cm^{-1} $\pm$ 0.2 $\times$ 10^4 mol dm^{-3} cm^{-1} at 311 nm. This is based on the assumption that the loss of DBM only corresponds to formation of the new species, and includes a correction for the change in solvent density on freezing.

The same effect is noticed with Parsol 1789, although the production of the new species appears to have a lower quantum yield, as longer irradiation periods are required. The formation of the short-lived species at room temperature was observed to occur more efficiently for DBM than for Parsol 1789, as described in section 4.2.2.6, and thus it is to be expected that the same effect would occur at low temperature. The efficiency of formation of the new species was studied qualitatively for DBM, Parsol 1789, 4,4'-dimethoxy dibenzoylmethane, (Parsol DAM), and 4,4'-di-tert-butyl dibenzoylmethane, (dtDBM). It was found that the rate of formation of the new species was DBM > dtDBM > Parsol 1789 > Parsol DAM, where DBM was the most efficient. Tertiary-butyl is a slightly electron donating group on the phenyl ring, whilst methoxy is a stronger electron donating group (in the para position, as in these compounds). It therefore appears that the addition of electron donating groups on the phenyl rings of DBM makes the formation of the non -chelated species on irradiation less favourable. This may be because in the chelaled enol of DBM, electron density is delocalised around the chelate ring, whereas in the excited state and non-chelalated enol, this is not possible to the same extent. Thus substituents that increase the electon density may be expected to destabilise the non-chelated enol form. It has been reported that for general 1,3-dicarbonyl compounds, electron donating substituents increase the intra-molecular hydrogen bond strength[40]. Thus formation of a non-chelated species is less favourable in these cases, as has been noted.

It was also discussed in chapter 3, that electron donating substituents on the phenyl ring of aromatic ketones result in a destabilisation of the n,π^* state relative to the ground and π,π^* states. Because transient formation is most likely to occur from the n,π^* state, where the oxygen is electron deficient, any structural changes that destabilises this state are likely to cause an increase in the π,π^* character of the lowest excited state. This would reduce the extent to which relaxation could occur by rotation to form a non-chelated enol. Thus the observed order of efficiency of forming the non-chelated enol, can be explained if transient formation occurs from the n,π^* state.

The absorption spectrum of the species produced on irradiation of DBM at 77K was observed to be slightly different for different irradiating wavelengths, as is shown in figure 4.58. The broadly irradiated sample, (approximately $340 < \lambda < 380$ nm) produced a species with a peak at $\lambda \approx 310$ nm, as descrided above. Irradiation at 378 nm produced a peak at $\lambda \approx 325$ nm, irradiation at 359 nm produced a peak at $\lambda \approx 315$ nm, and irradiation at 345 nm produced a peak at 310 nm, all for the same irradiation conditions, although the DBM absorbance, and irradiation power neccesarily varied for each experiment.

It was also found that broad band irraditaion of any of the above peaks resulted in the formation of a peak at $\lambda \approx 310$ nm, as was seen for initial broad irradiation. On formation of the peak on broad irradiation, the peak appears to shift to shorter wavelengths with increasing irradiation, simply as a result of the DBM spectrum converting to the spectrum of the new species. However, this is not the only effect occuring in this case; by comparing the size of the residual DBM vibrational bands in the spectra of the irradiated samples, it can be seen that irradiation at 359 nm has not converted as much DBM, yet the band due to the photoproduct is clearly at a shorter wavelength than that seen with irradition at 378 nm.

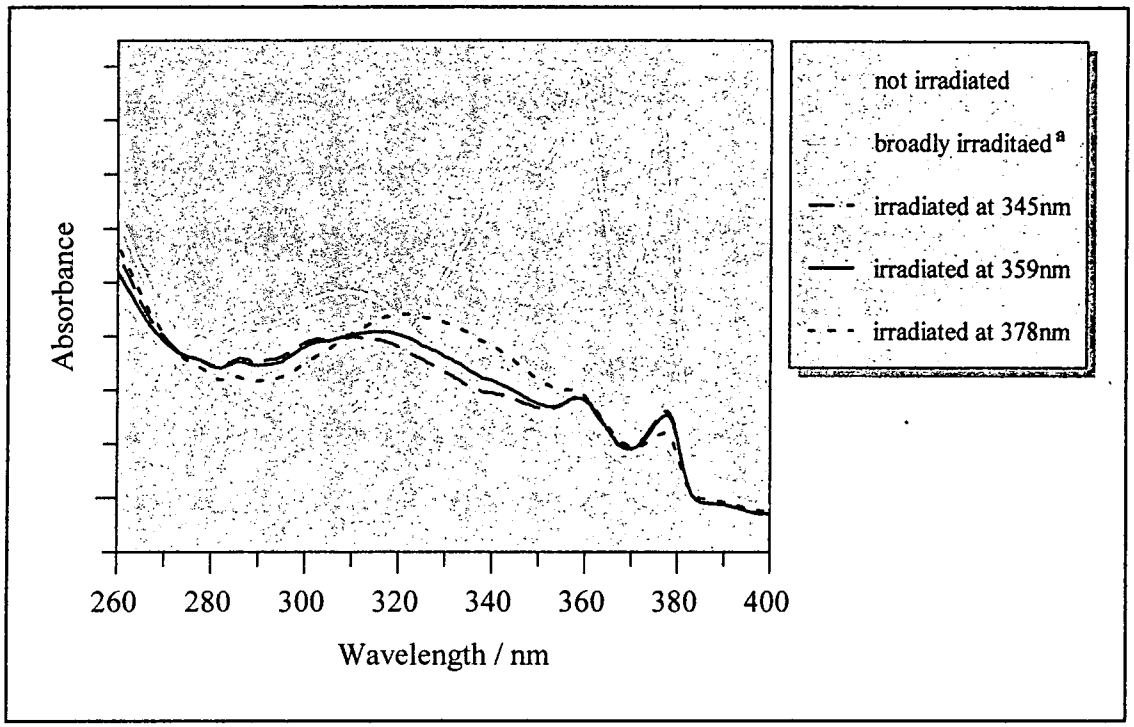

Figure 4.58 Changes in DBM absorption spectrum in EPA at 77 K with irradiation at varying wavelengths

(a: Spectrum not to same scale; see text for further irradiation details)

There is probably a link between the behaviour observed here and the E ↔ Z isomerisation of O-Methyl DBM, discussed earlier. The E and Z isomers of O-Methyl DBM were separated as described in chapter 2, and the low temperature spectra of the two isomers in EPA obtained, as described in chapter 3. Irradiation of the Z-isomer in EPA at 77K resulted in formation of the E isomer. The absorbance peak of the Z-isomer falls at $\lambda \approx 320$ nm, and that of the E-isomer at $\lambda \approx 310$ nm, as shown in figure 4.59.

It is possible that on irradiation of DBM, initially the Z-cis non chelated enol is formed on breaking of the hydrogen bond, followed by rotation about the C-O single bond. Further irradiation of this leads to the formation of the E-cis non chelated enol, via rotation about the C=C double bond, as shown in figure 4.60.

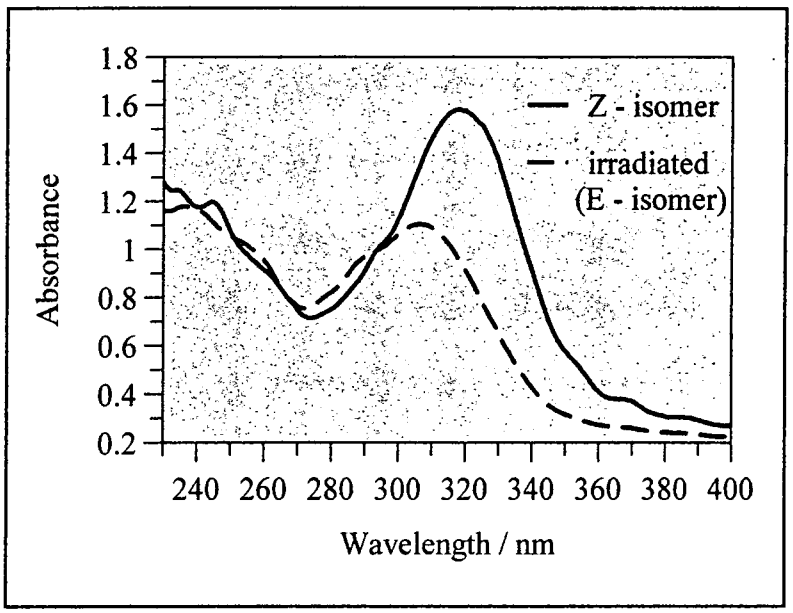

Figure 4.59 Absorption spectra of the Z-isomer of O-methyl DBM in EPA at 77 K, and that of the E-isomer formed by iradiation of the Z-isomer

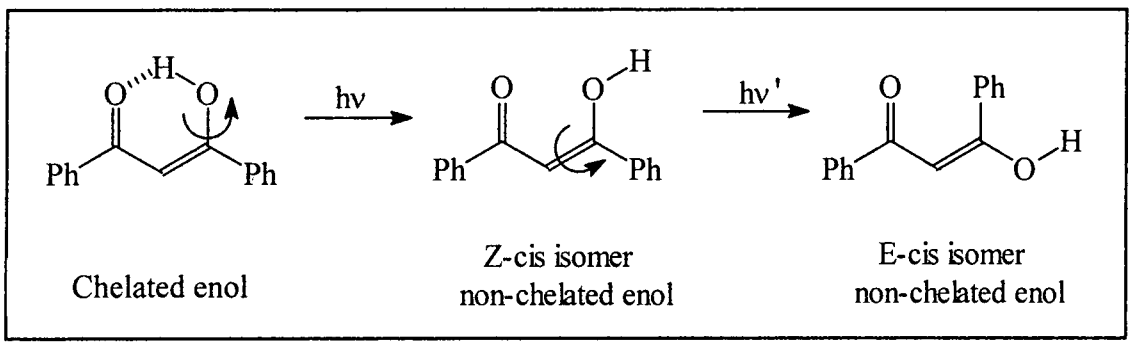

Figure 4.60 Possible rotations of DBM following irradiation

It is valid to assume that the non-chelated enols of DBM have similar UV absorption spectra to O-methyl DBM, as has been discussed. Therefore the E-cis isomer of DBM would have a peak shifted to shorter wavelengths with respect to the Z-cis isomer. On irradiation at 378 nm, only the DBM absorbs because the Z-cis non-chelated photoproduct does not have significant absorbance in this region. Thus little Z→E conversion takes place, and the spectrum of only the Z-cis isomer is seen. Irradiation at 345 nm causes Z→E conversion to take place, as the Z-cis isomer absorbs well in this region, and the overall result is formation of only the E-cis isomer. At wavelengths in-between, e.g. 359 nm, partial conversion occurs, and a mixed spectrum of Z-cis and E-cis isomers is seen.

Thus it is probable that irradiation of DBM at low temperature causes formation of a Z-cis non hydrogen bonded enol. Subsequent irradiation of this enol then causes Z→E isomerisation, and results in the formation of the E-cis non hydrogen bonded enol, or a mixture of the two isomers.

If this interpretation of the changes observed is correct, it does not necessarily follow that the same holds true for room temperature reactions. Although the transient is produced in one laser flash, the monitoring lamp is constant, and there may be sufficient UV light falling on the sample to convert the isomers. However, Z→E conversion may not take place in the time scale of the lifetime of the short-lived species, and thus the species produced at room temperature may be purely the Z-cis isomer. If some E-cis transient is formed, it follows that recovery to the ground state DBM must proceed via the Z-cis isomer, as the hydroxy and carbonyl groups must be brought physically close to reform the H-bond. It is thus possible that if a mixture of Z-cis and E-cis isomers were produced, a mixture of transient lifetimes would also be observed, because the E-cis isomer would take longer to recover. This may mean that the transient decay traces in fact would best be fitted to double exponential curves, for the two isomers, as was noted in section 4.2.2.4.

The possibility of E↔Z isomerisation was considered to see if it could explain the apparently anomalous temperature dependence of the observed rate constant of non-chelated enol decay, discussed in section 4.2.2.5. If on irradiation initially the Z- non-chelated enol is formed and then secondary photolysis converts this to the E isomer, e.g. by the action of the monitoring lamp, it is possible that with increasing temperature, the extent of Z→E conversion increases. If the E isomer has a longer lifetime, as discussed above, this could explain the decrease in k with increasing temperature.

Assuming that the above steps take place, such that photochemical production of the Z-cis isomer is followed by conversion to the E-cis isomer, then both these two isomers will be present in solution. Re-formation of the chelated enol from the main E-cis isomer product involves initial conversion back to the Z-cis isomer as discussed above. Thus if the kinetic scheme described in equations 4.4 - 4.7 in section 4.2.2.5 is valid, it may be possible that species A is the E isomer, whilst the intermediate species B, is the Z-isomer. However, it does not appear that this explanation is valid, because conversion from the Z to the E isomer is thermodynamically favourable (for O-methyl DBM), and thus reaction A→B, i.e. E→Z isomerisation in the DBM non-chelated enol, is not likely to be exothermic as is required in this theory.

4.2.3.2 Low Temperature Infra-red Spectroscopy

The infra-red spectrum of DBM in solution, e.g. in CCl_4, frozen at 77K, is very similar to that seen at room temperature in solution, or as a solid. The IR spectrum of DBM in CCl_4 at room temperature has been fully assigned by Tayyari and co-workers[40], as described in figure 4.61 and table 4.8. Because different workers report DBM to be symmetrical, and hence of C_{2v} symmetry, or not symetrical, C_s symmetry, as described in chapter 1, the vibrations of both of these symmetry groups are described.

IR band / cm^{-1}	Raman band / cm^{-1}	Approximate Description
1665 sh, vvw	-	ν (C=O) keto
1620	-	ν (C=O) keto
1602 vs	1620 (100), p	8a
(1560) vs		Q_1
(1560)	1560 w, br, p	Q_2
1487 m	1469 (7), p	19a
1370 m	-	Q_3
1438 sh	1446 (3), p	19b
1282 mw	1230 sh, dp	Q_4
1222 s	1230 sh, dp	ω
1182	-	δ (=CH)
975		γ (OH)
752 s		γ (=CH)
686 s	648 (8), p	ring-in-plane deformation
610 m	600 m	ring-out-of-plane deformation
363 m	-	ring-in-plane deformation
-	332 sh in CH_2Cl_2	γ (C-C_6H_5)
235 w	-	
204 sh	210 (2) in CH_2Cl_2	
105 w	-	torsion
	77	lattice mode

Table 4.8 Vibrational band frequencies of DBM[40]

(s = strong; m = medium; w = weak; v = very; sh = shoulder; br = broad;
The relative Raman intensities are denoted in brackets; p = polarised band; dp = depolarised band;
Q_1, etc., as indicated in Figure 4.61 ; ν=stretching; δ = in-plane bending; γ = out of plane bending;
8a, 8b, 19a and 19b refer to vibrations of the aromatic ring)

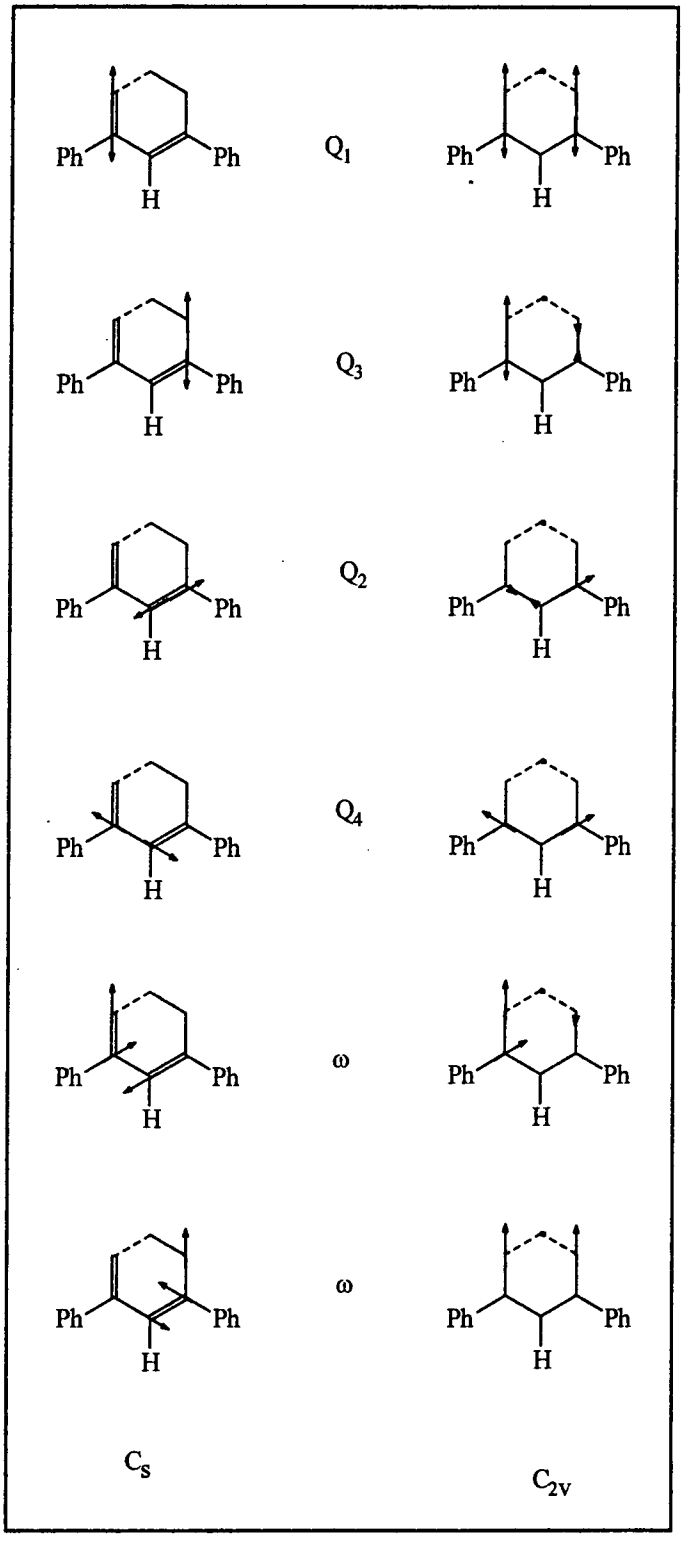

Figure 4.61 In plane vibrations of the chelate ring of DBM for the C_s and C_{2v} symmetry groups[40]

8a, 8b, 19a and 19b refer to vibrations of the aromatic ring. Q_1 and Q_3 are vibrations of the C=O group. As the hydrogen bonding in such chelate structures becomes stronger, the strength of the bond will decrease and these vibrations will shift to lower frequency. Q_2 represents vibration of the C=C double bond. In a strongly hydrogen bonded structure, the order of this bond is greatly reduced, and thus with increasing strength of H-bond, this vibration will shift to lower frequency. Q_4 is a vibration of the C-C bond, which increases in order, and thus strength with increasing strength of hydrogen bond. Thus the opposite behaviour is observed, and the vibration shifts to higher frequency with increasing H-bond strength. ω represents further vibrations of the C=O group. In 1,3-dicarbonyl compounds, there is also a very broad band spanning the region 3500-2200 cm^{-1}, centred at 2620 cm^{-1} for DBM. This is due to the O-H stretching vibration, however it is not always obvious due to the large range it covers. As the hydrogen bonding becomes stronger in such structures, the O-H vibration is found at lower frequencies[40].

The spectra obtained for DBM in CCl_4 and dichloromethane are shown in figures 4.62 and 4.63. Using the assignments in reference **40**, it has been possible to partially assign the low temperature spectrum, as shown on the spectra. Solvent bands in the regions of interest has meant that some peaks are distorted. There is also evidence of interference effects distorting the spectra, which can be seen as a regular pattern of oscillations on the baseline, increasing in intensity towards lower wavenumber.

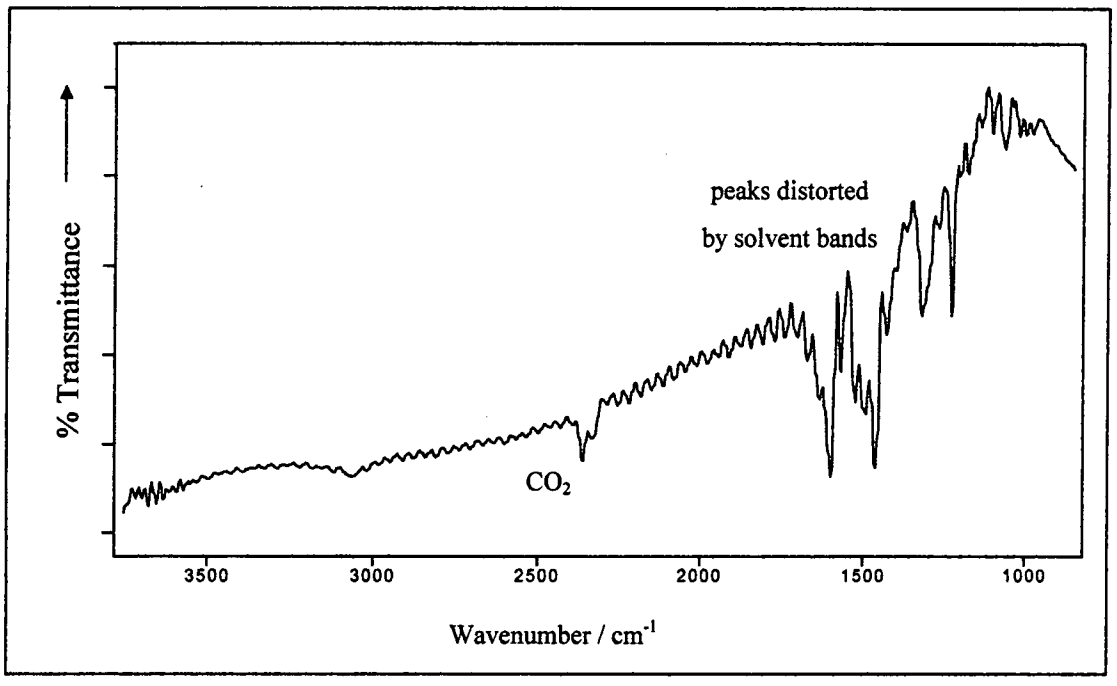

Figure 4.62 Infra-red spectrum of DBM in CCl_4 at 77 K, with solvent spectrum subtracted
(bands around 1500 cm^{-1} distorted due to solvent; also note interference effects)

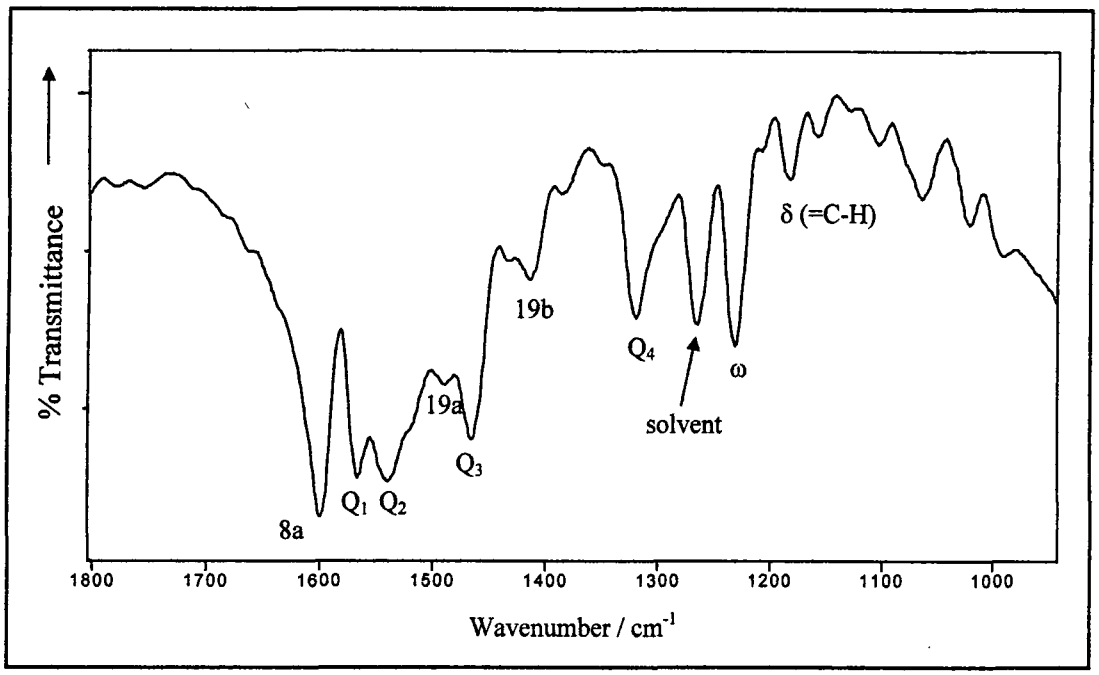

Figure 4.63 Infra-red spectrum of DBM in CH_2Cl_2 at 77 K, with solvent spectrum subtracted
(assignment of peaks based on table 4.8, from reference 40 ; some peaks may be distorted due to solvent)

The low temperature spectra of C-methyl DBM and O-methyl DBM in CCl_4 have also been obtained, and are shown below in figures 4.64 and 4.65. In the O-methyl DBM spectrum, where no hydrogen bonding is possible, the free enone C=O, peak can clearly be seen at 1644 cm^{-1}. The spectrum exhibits some similar features to DBM, due to the similarity in structures, and the aromatic ring vibrations are in similar positions, e.g. the 8a vibration occurs at 1602 cm^{-1}. For C-methyl DBM, the free C=O peaks falls at ≈ 1700 cm^{-1}, as would be expected for an aromatic ketone. The spectrum is quite different from that of DBM and O-methyl DBM, apart from the position of the aromatic vibrations, e.g. 8a occurs at 1597 cm^{-1}.

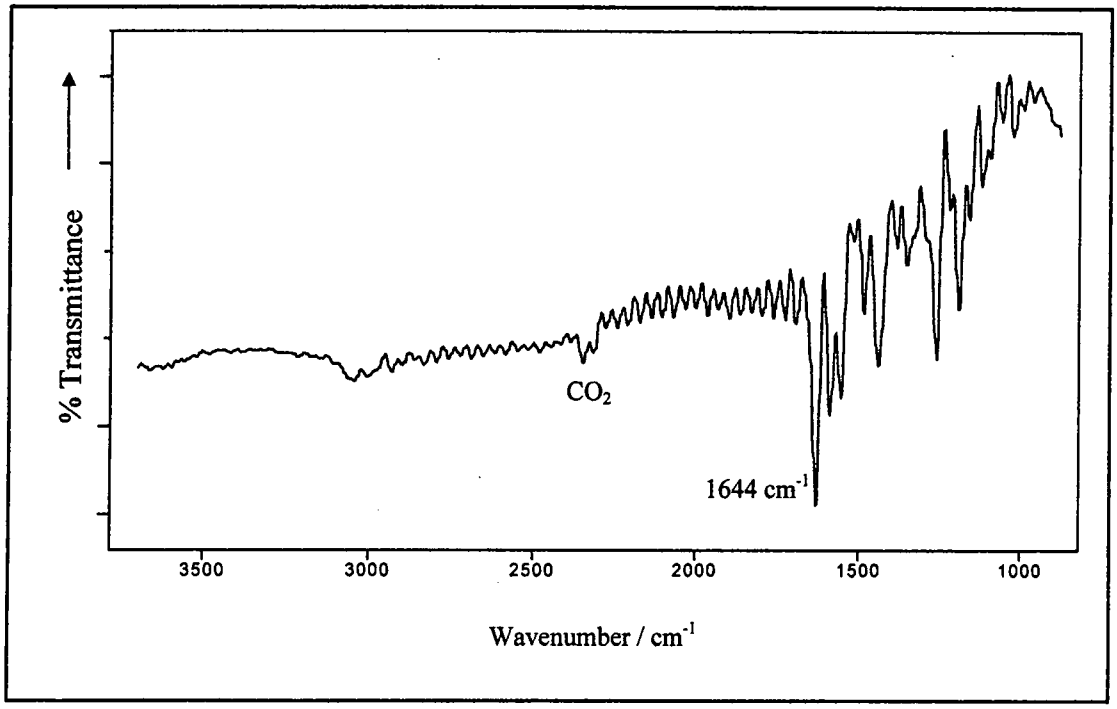

Figure 4.64 Infra-red spectrum of O-methyl DBM in CCl_4 at 77 K, with solvent spectrum subtracted

(bands around 1500 cm^{-1} distorted due to solvent; also note interference effects)

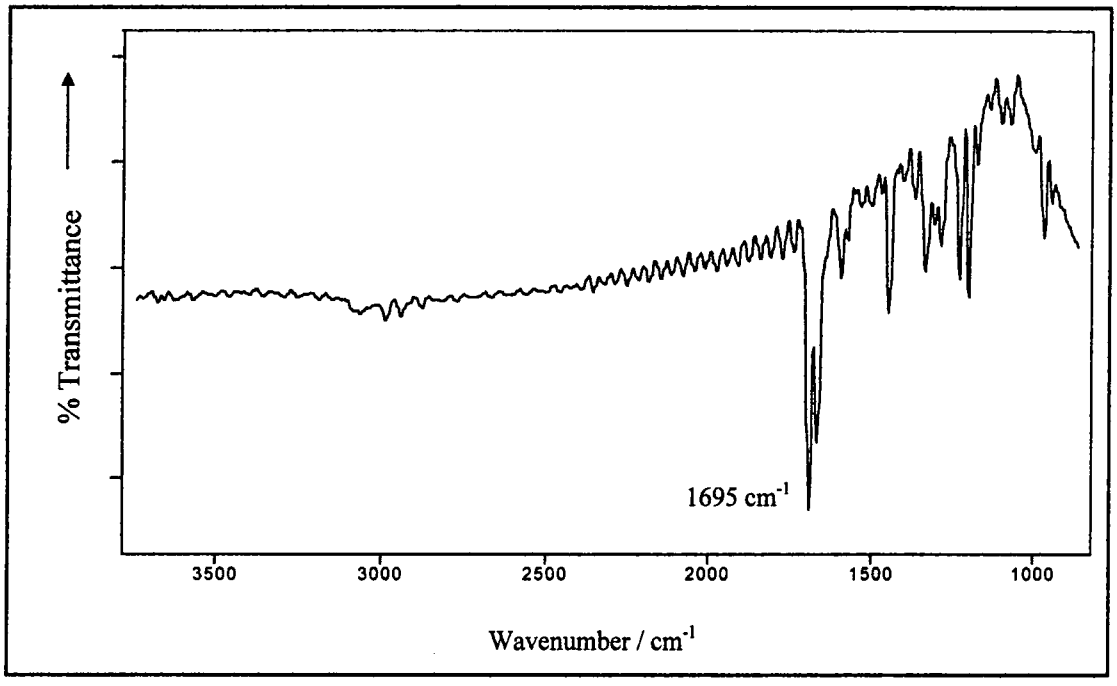

Figure 4.65 Infra-red spectrum of C-methyl DBM in CCl_4 at 77 K, with solvent spectrum subtracted

(bands around 1500 cm^{-1} distorted due to solvent; also note interference effects)

On irradiation of DBM, striking changes occur in the infra-red spectrum. Figure 4.66 shows the IR spectrum of the photoproduct, with the solvent and DBM spectra subtracted.

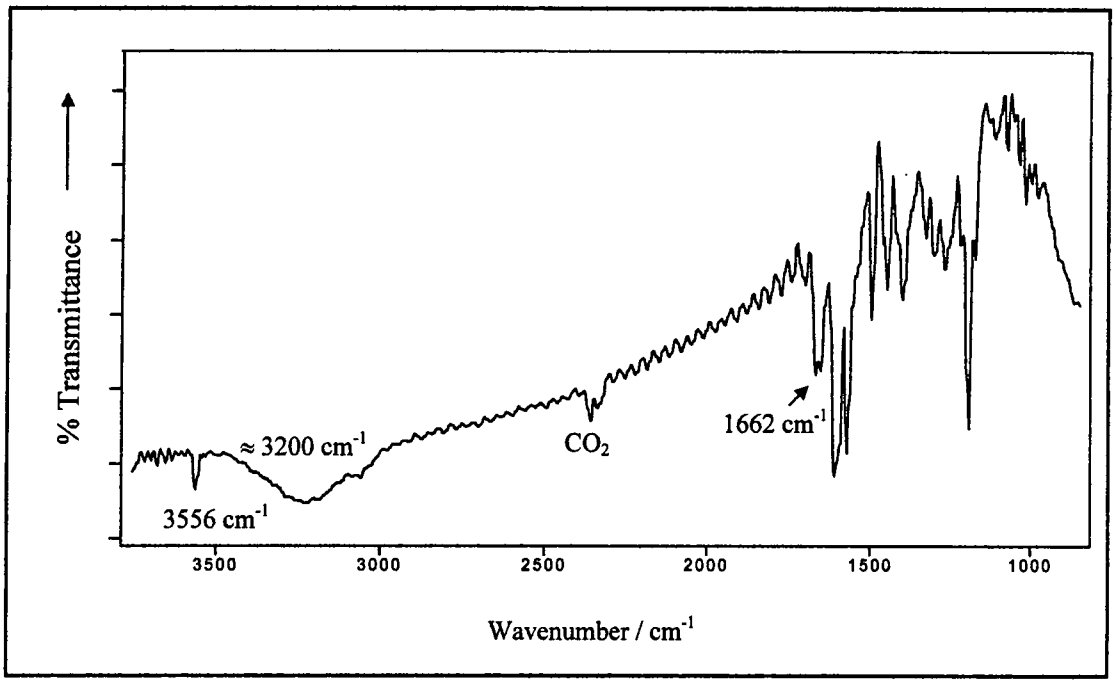

Figure 4.66 Infra-red spectrum of the photoproduct on irradiation of DBM in CCl_4 at 77 K, with solvent and DBM spectra subtracted

(bands around 1500 cm^{-1} distorted due to solvent; also note interference effects)

A sharp peak appears in the O-H region, at 3556 cm^{-1}, indicating a free O-H stretching vibration. A similar sharp peak in the range 3490-3575 cm^{-1} is observed in the IR spectra of 1,3-dicarbonyl compounds structurally fixed in a trans configuration[41], such as dimedone, figure 4.19. These compounds can not form an intra-molecular hydrogen bond, and as such the sharp peak in the infra-red spectrum is assigned to a free OH group. This provides clear evidence that the product on irradiation of DBM in solution at low temperature is a non-hydrogen bonded enol form. Also significant is the appearance of a peak at 1662 cm^{-1} which corresponds to a vibration of a free enone carbonyl, similar to that seen in the O-methyl DBM spectrum. Clearly the O-H bond has been broken on irradiation, and a non-hydrogen bonded species produced. There are other subtle changes from the original DBM spectrum, resulting in an IR spectrum quite similar to that of the O-methyl DBM. In Dichloromethane solution, similar changes are observed, however the sharp peak at 3556 cm^{-1} was not detected.

A broad peak is also obvious at approximately 3200 cm^{-1}. It was initially thought that this was due to water condensing on the IR cell over the extended irradiation and spectra acquisition times. However it is not formed to the same extent for non-DBM samples treated in the same way, and thus it is believed to be a new band, although possibly combined with an underlying water peak. Thus, it can be interpreted that on irradiation of DBM we see a hydrogen bonded O-H peak at higher frequency than for DBM. This is indicative of a weaker O-H bond, and suggests that some formation of intermolecular hydrogen bonds between neighbouring non-chelated enol molecules has occurred. The solutions were quite concentrated for this IR work (concentration $\approx$ 0.04 mol dm^{-3}), and although clearly some DBM molecules are isolated by solvent molecules, such that a free O-H peak is seen on irradiation, most are not, and can form intermolecular hydrogen bonds upon breaking of the intramolecular H-bonds upon irradiation.

A similar broad peak in the range 3200-3260 cm^{-1} is observed in the IR spectra of 1,3-dicarbonyl compounds structurally fixed in a trans configuration[41]. This is explained as being caused by inter-molecular hydrogen bonding between neighbouring molecules, and it is likely that the same interpretation for DBM is valid. Acetonitrile as a solvent is reported to form associates with the trans-enols, weakening the C-OH bonds, and disrupting inter-molecular hydrogen bonding[41]. In dichloromethane solvent no free O-H peak was observed. Dichloromethane, like acetonitrile, is a more polar solvent than CCl_4, and as such it is likely that a form of hydrogen bonding to the solvent occurs. Thus the broad O-H peak seen in the irradiated spectrum in this solvent may in fact be due to solvent-non-chelated enol interactions.

It is possible that inter-molecular hydrogen bonding could also be occurring at room temperature. Thus on irradiation, some transients produced could form intermolecular hydrogen bonds before eventually reverting to the intramolecular form. Solutions for study by flash photolysis, are necessarily less concentrated that for this IR work, so this may not be a significant effect. In polar and protic solvents such as ethanol, H-bonding to the solvent could easily take place as was observed in dichloromethane solution. The formation of solvent-non-chelated enol complexes has been suggested in the literature and discussed earlier. It is possible that intermolecular hydrogen bonding would stabilise the transient, resulting in a longer observed lifetime, although earlier results have suggested that the formation of transient dimers enhances the rate of transient decay.

The infra-red spectra of irradiated malonaldehyde, the simplest 1,3-dicarbonyl compound, in rare gas matrices have also been reported in the literature[27]. The appearance of a sharp, free OH stretching vibration in the range 3670-3535 cm^{-1} is reported on irradiation, and also the appearance of new carbonyl stretching vibrations, confirming the formation of a non-chelated isomer. Comparison of the theoretical calculations with the observed IR peaks suggests that the isomers shown in figure 4.67 are obtained on irradiation[27]. The comparison is not entirely valid, however, because the phenyl group substituents in DBM make a large difference to the structure, and to the stability of particular iosmers, compared with hydrogen atoms.

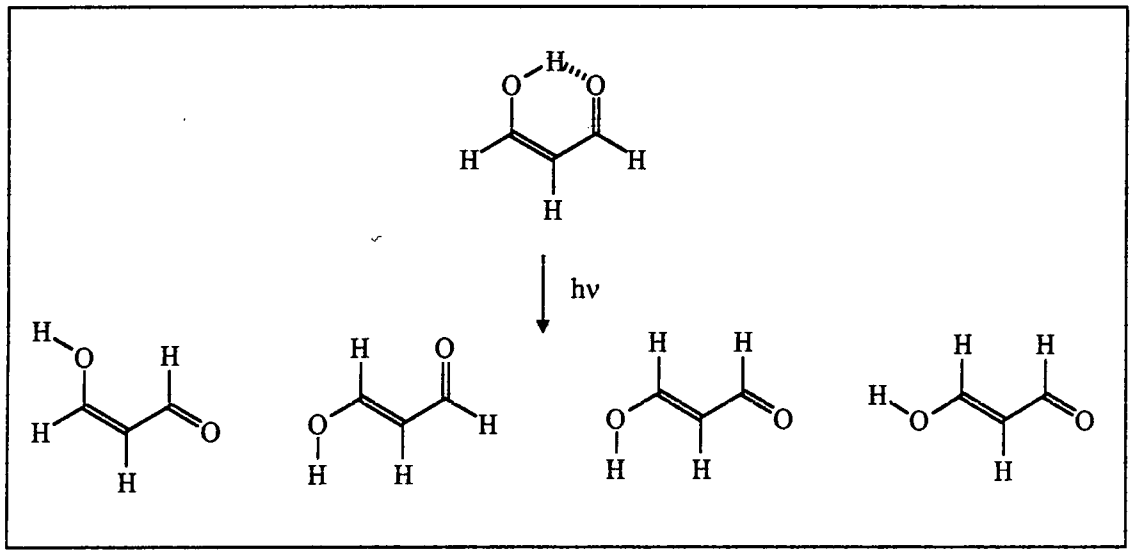

Figure 4.67 Non-chelated enol isomers of malonaldehyde formed on irradiation of the chelated enol form[27]

Having established conclusively that the photoproduct on irradiating DBM is the non-hydrogen bonded enol, the possibility of studying the E↔Z isomerisation discussed in the previous section was considered. The IR spectra of the two separate E and Z isomers of O-methyl DBM were obtained, by assuming a fresh solution is mainly the Z-isomer, and that on irradiation this converts to the E-isomer. The IR spectra obtained are shown in figure 4.68. A summary of some selected differences is given in table 4.9. The spectra are not particularly clear, and it appears that they do not represent the pure isomers, i.e. each spectrum contains a contribution from both isomers.

	Z-isomer		E-isomer	
	CCl_4	CH_2Cl_2	CCl_4	CH_2Cl_2
C=O	≈1640 cm^{-1}	≈1640 cm^{-1}	≈1667 cm^{-1}	≈1657 cm^{-1}
	≈1458 cm^{-1}	≈1457 cm^{-1}	≈1443 cm^{-1}	≈1447c m^{-1}

Table 4.9 Approximate selected infra-red absorption peak positions for E and Z isomers of O-methyl DBM in CCl_4 and CH_2Cl_2 at 77 K

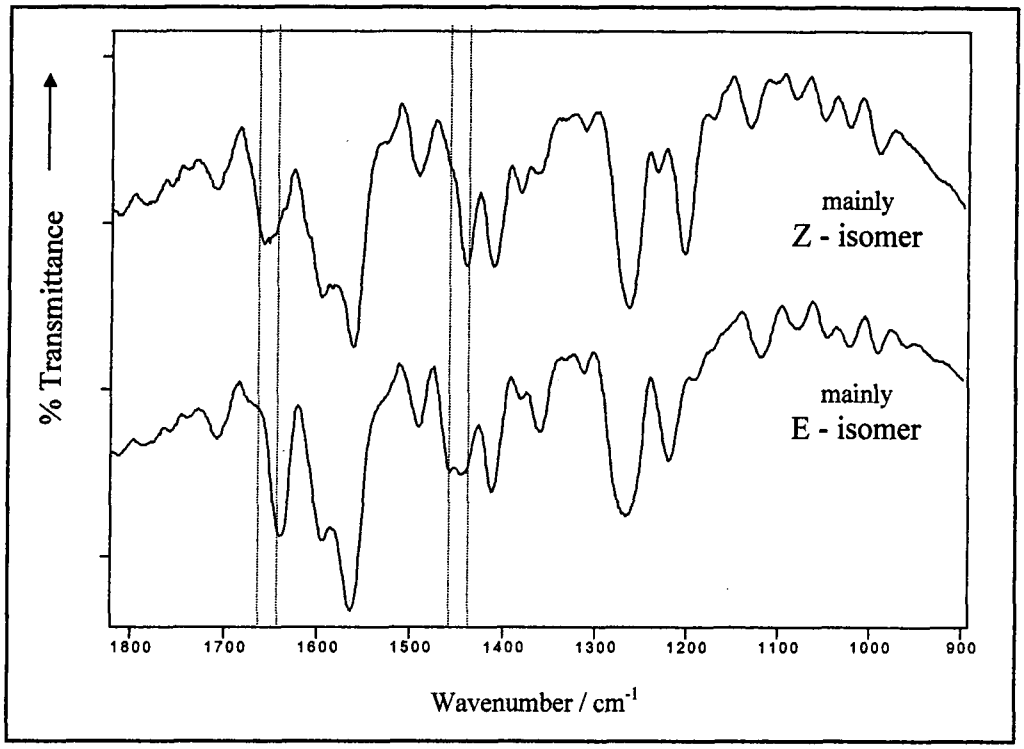

Figure 4.68 Infra-red spectrum of the E and Z-isomers of O-Me DBM in CH_2Cl_2 at 77 K, with solvent spectrum subtracted

(some peaks may be distorted due to solvent absorbance; also note interference effects)

As reported earlier, it is suggested that on irradiation of DBM at 77 K initially the Z-cis isomer of the non-chelated enol is formed, which then, on further irradiation, converts to the E-cis isomer. Irradiation at carefully selected wavelengths can prevent the secondary Z→E conversion, and allow study of the separate isomers. Thus by using a filter to block out UV light < 375 nm, it was hoped to produce mainly the Z-isomer, then by irradiating this product over a broad range, it should then be possible to convert it to the E-isomer, and hence the IR spectra of the two separate isomers can be observed. The results of such experiments are given in figure 4.69. There are subtle differences in the spectra, although again the spectra are not entirely clear, and it appears that each spectrum contains a contribution from the other. Selected comparison of the spectra is summarised in table 4.10.

	irradiation >375 nm	broad band irradiation
C=O	≈1653 cm^{-1}	≈1670 cm^{-1}
	≈1463 cm^{-1}	≈1448 cm^{-1}

Table 4.10 Approximate selected infra-red absorption peak positions for irradiation of DBM in CCl_4 at 77 K

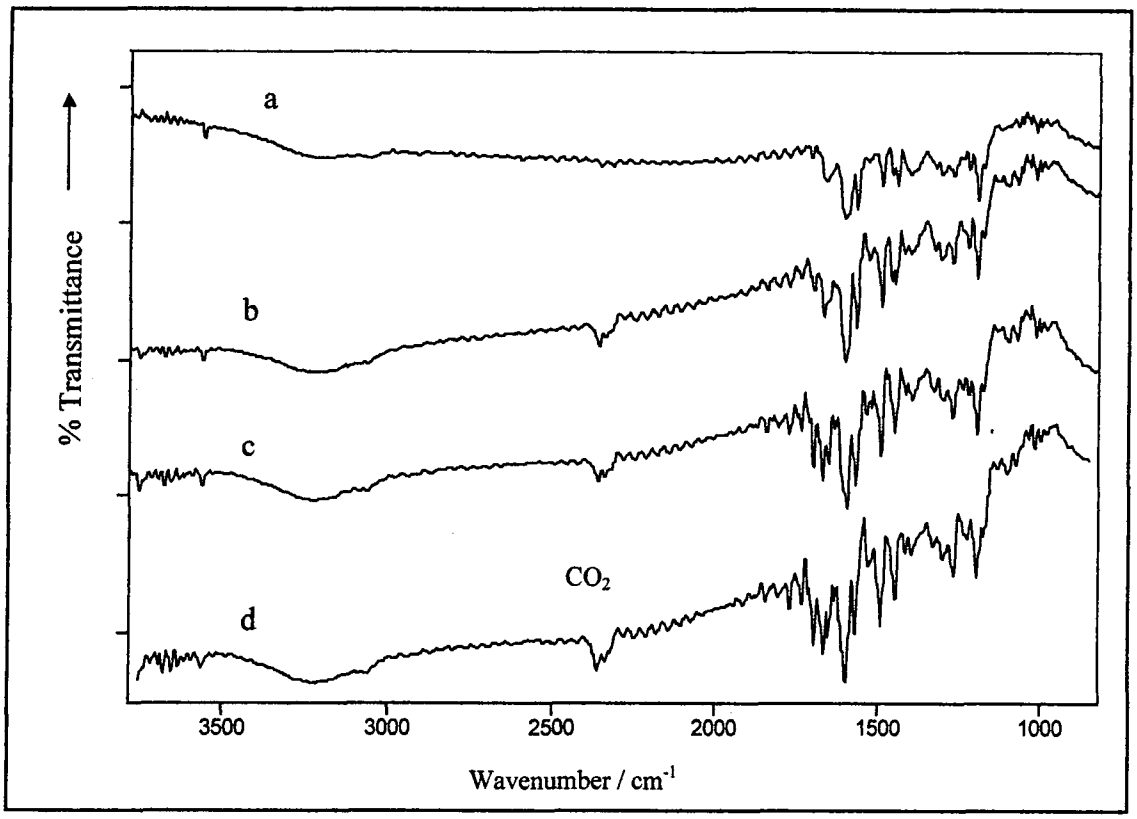

Figure 4.69 Infra-red spectra of irradiated DBM in CCl_4 at 77 K, with solvent spectra subtracted (a) → d) increasing irradiation; a) and b) irradiated < 375 nm ; c) and d) broad band irriadiation; bands around 1500 cm^{-1} distorted due to solvent; also note interference effects)

It can be seen that the spectrum of the sample irradiated > 375 nm does in fact show similarities to the Z-isomer of O-Methyl DBM, and after broad irradiation, it shows similarities to the E-isomer. This is further evidence that irradiation of DBM at low temperature does initially form the non-hydrogen bonded Z isomer, which converts with further irradiation to form the more stable E-isomer, as suggested by the UV results.

4.2.4 Time Resolved Resonance Raman Spectroscopy

The resonance Raman spectra of DBM, Parsol 1789, the O-methyl and C-methyl derivatives and acetophenone, in solutions of cyclohexane and trichlorotrifluoroethane were obtained using apparatus at the Rutherford Appleton Laboratories, as described in chapter 2, and in collaboration with Prof. G Truscott, Dr. D McGarvey and Miss. L Mulroy from the University of Keele. Trichlorotrifluoroethane was used as a solvent, because it does not posses any strong Raman bands in the region above 1250 cm^{-1}. Cyclohexane has strong bands in this region, which made it difficult to study the Raman bands of the compounds of interest, however similar spectra were obtained in this solvent.

Spectra were obtained in the range 1000 cm^{-1} to 2500 cm^{-1}. Attempts to study a higher range did not produce good quality spectra, because the O-H group is not part of the chromophore, and hence does not undergo resonance enhancement. There is also a lack of solvent Raman peaks in these regions, to assist in subtracting out ground state spectra. The Raman spectra presented in this work are noisy, which is partly due to the nature of the technique, but also due in some cases to significant sample fluorescence. The main problem encountered was with solvent and ground state subtraction. In many cases the strong solvent peaks have occurred with very slightly different peak widths in the probe only, than the pump and probe spectra. This has meant that the peaks do not subtract properly, and produce large positive and negative spikes. This effect might be due to heating of the solutions during experiments. Examples of the resonance Raman spectra obtained in 1,1,2 trichlorotrifluoroethane are given in Figures 4.70 to 4.73, and a summary of the peak positions is given in table 4.11. The spectrum of 1,1,2 trichlorotrifluoroethane is also given in figure 4.74.

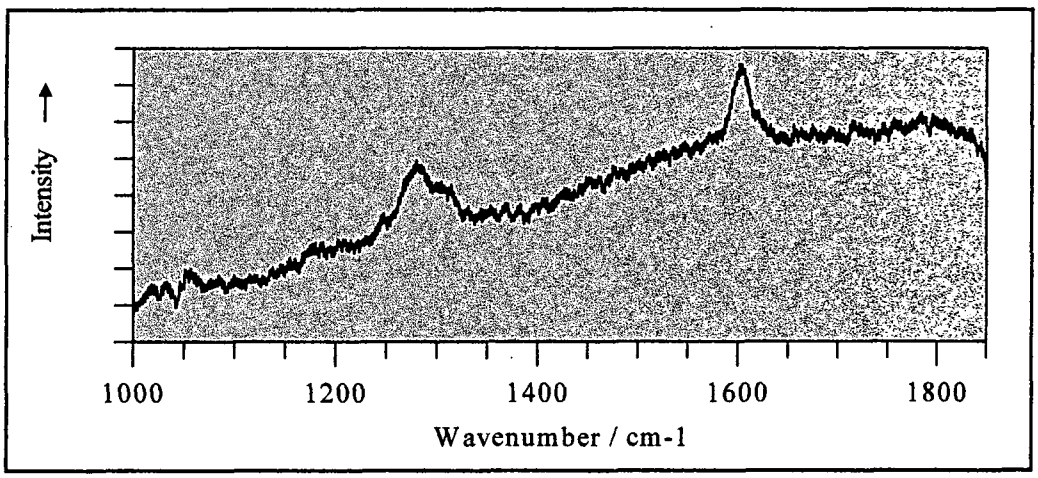

Figure 4.70 Resonance Raman spectrum of DBM in 1,1,2 trichlorotrifluoroethane; probing at 355 nm

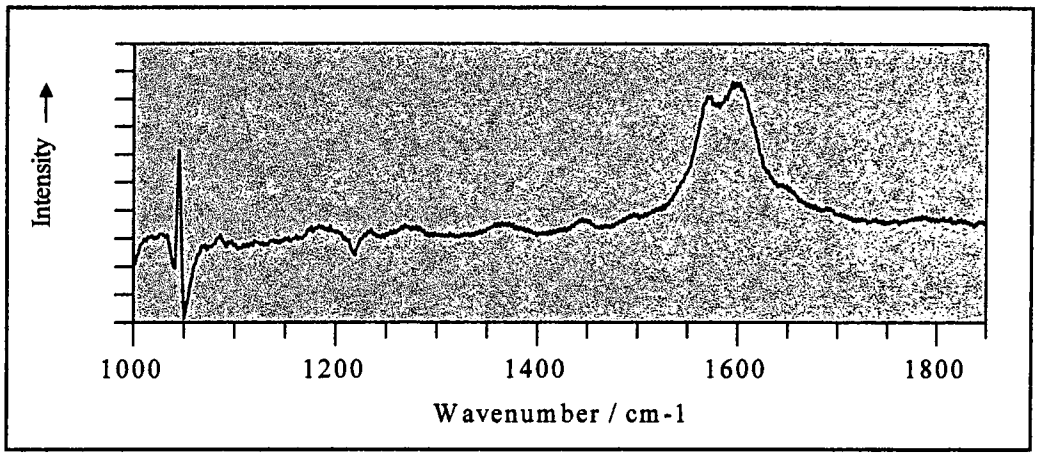

Figure 4.71 Resonance Raman spectrum of O-methyl DBM in 1,1,2 trichlorotrifluoroethane; probing at 295 nm

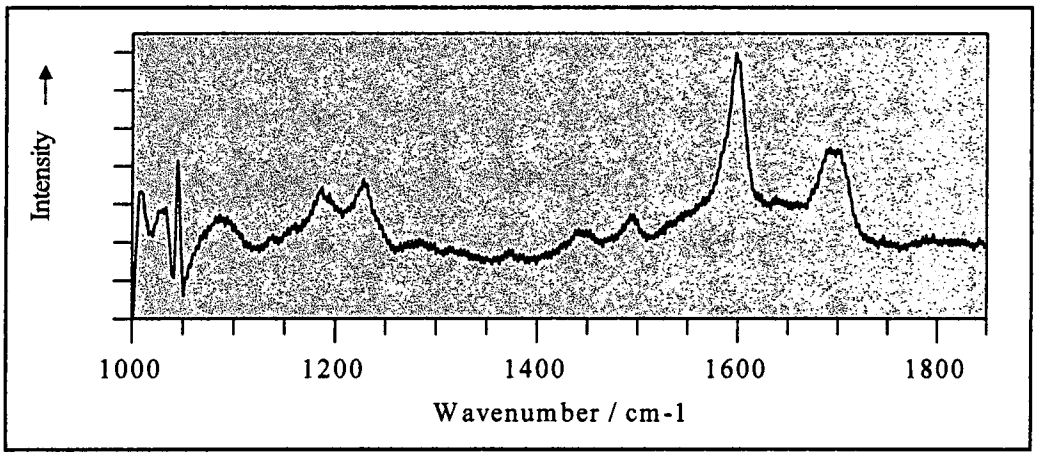

Figure 4.72 Resonance Raman spectrum of C-methyl DBM in 1,1,2 trichlorotrifluoroethane; probing at 295 nm

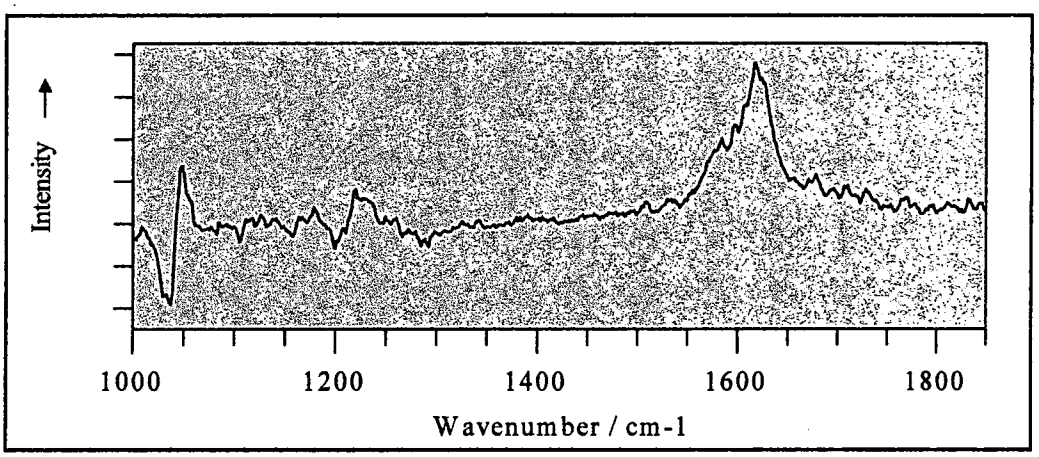

Figure 4.73 Time resolved resonance Raman spectrum of DBM in 1,1,2 trichlorotrifluoroethane; pumping at 355 nm, probing at 295 nm after 1 μs delay.

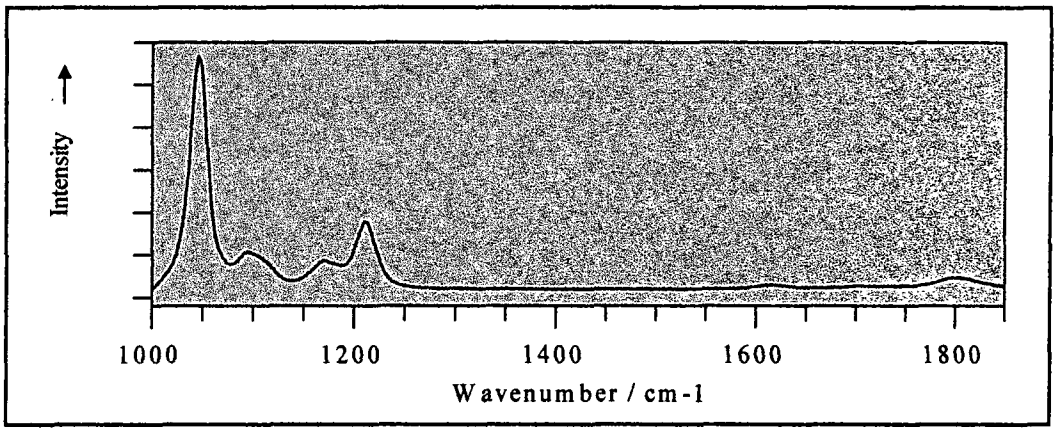

Figure 4.74 Resonance Raman spectrum of 1,1,2 trichlorotrifluoroethane

It can be seen in the ground state Raman spectra of DBM that there is a peak at 1600 cm^{-1} in CCl_2F-CF_2Cl or 1605 cm^{-1} in cyclohexane. This compares to a literature value of 1620 cm^{-1} in CCl_4 [40] (table 4.8). This peak corresponds to the 8a vibrational mode of the aromatic ring[40]. There are also peaks at 1280 cm^{-1} and 1305 cm^{-1}. The literature describes a quite broad peak at 1280 cm^{-1} with an apparent shoulder of higher wavenumber, in CCl_4 [40] (table 4.8), which appears to correspond to these peaks. It has been assigned to the Q_4, carbon-carbon single bond in-plane vibrations of the chelate ring [40] (table 4.8). Similar peaks are found for the ground state of Parsol 1789 at 1610 cm^{-1}, and ≈1290 cm^{-1}.

The O-methyl spectra show similar peaks at around 1600 cm^{-1}, which is consistent with this being a vibration of the aromatic ring. In the O-methyl DBM spectra this peak appears to be split into two. This could possibly be explained in terms of the loss of symmetry of the molecule, but why the same is not observed for the O-methyl Parsol spectra is unclear, although this peak does appear to be complex. In all O-methyl spectra, the peaks at ≈1300 cm^{-1} are no longer visible. This peak is less well defined, but possibly still visible in the IR spectra discussed in the previous section. It is possible that it has shifted to smaller wavenumber, and become overlaid by the solvent bands. A peak at 1180 cm^{-1} is observed for O-Methyl Parsol 1789 in 1,1,2 trichlorotrifluoroethane. On chelation the carbon-carbon single bond is strengthened, thus it would be expected that this vibration would be found at higher wavenumber in the chelated enol than in the O-methyl compounds where there is no chelation. There are possibly other small peaks in these spectra, of low intensity, which will not be discussed.

Spectrum	Solvent	Peak Positions / cm^{-1}
DBM	C	1280, 1305 sh, 1605
	T	1280, 1305 sh, 1600
O-Methyl DBM	C	doublet: 1570, 1600
	T	doublet: 1570, 1600
C-Methyl DBM	C	1600, 1700
	T	1600, 1695
Irradiated DBM (pumping at 355nm, probing at 295nm after 1 μ s delay)	C	1575 sh, 1600 sh, 1615
	T	1575 sh, 1620
Parsol 1789	C	1290, 1600
	T	1285, 1610
O-Methyl Parsol 1789	C	doublet: 1580, 1600
	T	1180, 1600
C-Methyl Parsol 1789	C	1178, 1605, 1690
	T	1175, 1605, 1680
Irradiated Parsol 1789 (pumping at 355nm, probing at 295nm after 1 μ s delay)	C	doublet: 1605, 1620
	T	1605, 1680 sh
Acetophenone	C	1600, 1695
	T	1600, 1695

Table 4.11 Position of peaks in resonance Raman spectra for DBM and related compounds
(C = cyclohexane; T = 1,1,2 Trichlorotrifluoroethane; sh = shoulder)

The C-methyl spectra once again show this strong peak at ≈ 1600 cm^{-1}. There is also an equally strong second peak at ≈ 1700 cm^{-1}, which can clearly be assigned to a stretching vibration of an aromatic carbonyl. The spectra observed for acetophenone show exactly the same structure (not shown). As with the spectra of the O-methyl compounds, the peaks at ≈ 1300 cm^{-1} are either not visible, or shifted to lower wavenumbers due to the absence of the intra-molecular hydrogen bond. There are also small peaks which will not be discussed.

In common with all the previous spectra, the transient spectra show the strong peak at ≈ 1600 cm^{-1}. The position of the peak has shifted slightly in both the DBM and Parsol 1789 transient spectra; (DBM transient: 1620 cm^{-1} in CCl_2F-CF_2Cl, 1615 cm^{-1} in cyclohexane; Parsol 1789 transient: 1605 cm^{-1} in CCl_2F-CF_2Cl, 1610 cm^{-1} in cyclohexane). These peaks were clearly observed to be in slightly different places to those of the corresponding ground state spectra, and thus are not merely magnifications of a poorly subtracted ground state. Such a small shift is not conclusive evidence in attempting to assign a structure to the transients, especially considering the apparent resolution of this experiment.

There are, however, obvious differences between the spectra of the transients and those of the ground state DBM and Parsol 1789, and the model compounds. Firstly the DBM transient peaks at ≈ 1600 cm^{-1}, appear to be split, which make them appear more like the O-methyl DBM spectra than like the ground state DBM spectra. This implies a similarity to the structure of the O-Methyl DBM and hence a loss of chelation in the transient. An important difference between the transient spectra, and those of the ground state is again the absence, or shift to shorter wavenumber, of the peaks at ≈ 1300 cm^{-1}. These peaks corresponded to C-C single bond in-plane vibrations of the chelate ring[40], as described earlier. This suggests a weakening of the C-C bond, i.e. loss of chelation. Therefore the intra-molecular hydrogen bond must have been broken on forming the transient species.

The results from the time resolved resonance Raman experiments are not as clear as the low temperature IR spectra, and attempts to obtain spectra in the OH stretching vibration region, to try and observe the free OH in the transient, were not successful as explained earlier. However these results do provide support for the theory that at room temperature the short-lived species produced on irradiation of dibenzoylmethanes is a non-chelated enol, as has been observed at low temperature.

4.3 Summary

The photochemical processes occurring on irradiation of dibenzoylmethane in solution have been studied over many years. The results, however, have been confusing, and explanations often contradictory. It has been generally suggested that the main process on irradiation is the formation of short-lived a non-chelated enol, however no direct evidence to confirm the structure of this species has been reported in the literature. Formation of the diketone form of DBM on prolonged irradiation in acetonitrile solution has also been studied.

In this work photoketonisation has been observed to occur in acetonitrile solution only, and the quantum yield of this process in has been measured to be $\Phi = 0.01 \pm 0.004$.

In this work, low temperature infra-red studies have produced direct spectroscopic evidence to prove that the short-lived species produced on irradiation is indeed a non-chelated enol. The infra-red studies also suggest that the non-chelated enol form of dibenzoylmethane does indeed form complexes with polar solvents, as has been proposed in the literature. This is the reason assumed in the literature for the great differences in the recovery rate of the non-chelated enol form at room temperature. The results in this work suggest that the recovery process is very sensitive to changes in solvent conditions, and throws doubt on many values quoted in the literature. Quantum yields of non-chelated enol formation in cyclohexane at room temperature have been measured to be $\Phi = 0.5 \pm 0.07$.

The results of varying the concentration and laser power at room temperature indicate that the rate of transient decay is enhanced by the interaction of the transient molecules with chelated enol molecules or other transient molecules. IR studies of low temperature transient formation confirm the interaction of transient molecules by the observation of inter-molecular hydrogen-bonding.

By comparison with O-Methyl DBM, which can exist as one of two isomers, it is suggested that at low temperature DBM initially forms a Z-cis non-hydrogen bonded enol, which then converts to an E-trans non-hydrogen bonded enol with further irradiation. A similar process may occur at room temperature, however the short lifetime of the non-chelated species may limit isomerisation. Kinetics for the enol recovery and an unusual temperature variation of k support the theory that there is more than one species formed.

Overall, this work has provided a clearer picture of the photochemistry of dibenzoylmethane and related molecules in solution.

4.4 References

[1] Gilbert A, Baggott J, "*Essentials of Molecular Photochemistry*", Blackwell Scientific Publications, Oxford, 1991

[2] Turro N J, "*Modern Molecular Photochemistry*", University Science Books, California, 1991

[3] Wagner P J, "*Topics in Current Chemistry 66 - Triplet States III; Chemistry of Excited Triplet Organic Carbonyl Compounds*", Springer-Verlag, New York, 1975, page 1

[4] Markov P, "Light-induced Tautomerism of β-Dicarbonyl Compounds", *Chem. Soc. Reviews,* **13** (1984), 69

[5] Sammes P G, "Photoenolization", *Tetrahedron*, **32** (1976), 405

[6] Dauben W G, Lodden G, Ipaktschi J, "*Topics in Current Chemistry 54 - Triplet States I; Photochemistry of β,γ-Unsaturated Ketones*", Springer-Verlag, New York, 1974, page 73

[7] Deflandre A, Lang G, "Photostability Assessment of Sunscreens", *Int. J. Cosmetic Science*, **10** (1988), 53

[8] Schwack W, Rudolph T, "Photochemistry of dibenzoyl methane UVA filters. Part I.", *J. Photochem. Photobiol. B: Biol.*, **28** (1995), 229

[9] Roscher N M, Lindemann M K O, Kong S B, Cho C G, Jiang P, "Photodecomposition of several compounds commonly used as sunscreen agents", *Photochem. Photobiol. A: Chem.*, **80** (1994), 417.

[10] Markov P, Radeva E, "Photoinduced Ketonization of some cyclic β-ketoesters in solution", *J. Photochem.*, **4** (1975), 179

[11] Veierov D, Bercovici T, Fischer E, Mazur Y, Yogev A, "Photoisomerization of β-Diketones and β-Keto Esters", *J. Am. Chem. Soc.*, **95** (1973), 8173

[12] Veierov D, Bercovivi T, Fischer E, Mazur Y, Yogev A, "Photoisomerization of the Enol Form of 1,3-Dicarbonyl Compounds", *J. Am. Chem. Soc.*, **99** (1977), 2723

[13] Markov P, Petkov I, "On the Photosensitivity of Dibenzoylmethane, Benzoylacetone and Ethyl Benzoylacetate in Solution", *Tetrahedron*, **33** (1977), 1013

[14] Markov P, Petkov I, Jeglova D, "Photochemistry of Enolizable β-Dicarbonyl Compounds: Study on the photoketonization of some Esters of Aroylacetic Acids", *J. Photochem.*, **8** (1978), 227

[15] Andrae I, Bringhen A, Böhm F, Gonzenbach H, Hill T, Mulroy L, Truscott T G, "A UVA filter (4-*tert*-butyl-4'-methoxydibenzoylmethane): photoprotection reflects photophysical properties", *J. Photochem. Photobiol. B:Biol.*, **37** (1997), 147

[16] Yankov P, Saltiel S, Petkov I, "Photoketonisation of Dibenzoylmethane in Polar Solvents", *Chem. Phys. Lett.*, **128** (1986), 517

[17] Yankov P, Saltiel S, Petkov I, "Photketonisation and Excited State Relaxation of Dibenzoylmethane in Non-polar solvents", *J. Photochem. Photobiol A:Chem.*, **41** (1988), 205

[18] Veierov D, Bercovici T, Mazur Y, Fischer E, "Effect of Additives and Solvents on the Fate of the Primary Photoproduct of 1,3 Dicarbonyl Compounds", *J. Org. Chem.*, **43** (1978), 2006

[19] Tobita S, Ohba J, Nakagawa K, Shizuka H, "Recovery mechanism of the reaction intermediate produced by photoinduced cleavage of the intramolecular hydrogen bond of dibenzoylmethane", *J. Photochem. Photobiol. A:Chem.*, **92** (1995), 61

[20] Yankov P, Saltiel S, Petkov I, Markov P, "Study of the Relaxation Rate of the Transient Form of the Photoexcited Enol form of Dibenzoylmethane", *Bulg. J. Phys.*, **12** (1985), 629

[21] Yankov P D, Saltiel S M, Tomov I V, Markov P J, Petkov I K, "Measurements of the Relaxation Kinetics of Photo-Excited Enol Form of Dibenzoylmethane", *Laser Chem.*, **5** (1985), 107

[22] Kittel G, Köhler G, Getoff N, "Sensitised Ketonisation of Ethyl Acetoacetate. A Method for the Determination of Triplet Quantum Yields", *J. Phys. Chem.*, **83** (1979), 2174

[23] Nikolov P, Fratev F, Petkov I, Markov P, "Dimer Fluorescence of some β-Dicarbonyl compounds", *Chem. Phys. Lett.*, **83** (1981), 170

[24] a) Beeby A, "A Flash Photolysis study of Dibenzoylmethane", *Annual Report to Central Laser Facility,* (1993), 160, RAL-93-031
b) Beeby A, Parker A W, "The Photochemistry of Dibenzoylmethane; An Enolised 1,3-Diketone", *Annual Report to Central Laser Facility,* (1994), 186, RAL-94-042

[25] Markov P, Fratev F, "A CNDO/S Study of the Photoinduced Tautomerization", *Comptes rendus de l'Académie bulgare des Sciences*, **28** (1975), 771

[26] Rhoads S J, Pryde C, "Enolic Concentrations in β-Keto Esters. Correlation of Bromometric and Ultraviolet Absorption Data", *J. Org. Chem.*, **30** (1965), 3212

[27] Chiavassa T, Verlaque P, Pizzala L, Allouche A, Roubin P, "Experimental and Theoretical Studies of the Photoisomerization of Malonaldehyde Isolated in Rare Gas Matrices", *J. Phys. Chem.*, **97** (1993), 5917

[28] Baker A W, Shulgin A T, "Intramolecular Hydrogen Bonds to π-Electrons and other weakly basic Groups", *J. Am. Chem. Soc.*, **80** (1958), 5358

[29] Baitinger Jr. W F, Schleyer P von R, Mislow K, "Hydrogen Bonding in *ortho*-Substituted Biphenyls", *J. Am. Chem. Soc.*, **87** (1965), 3168

[30] Devaquet A, "Potential Energy Sheets for the n,π* and π,π* Triplet States of α-β-unsaturated ketones", *J. Am. Chem. Soc.*, **94** (1972), 5160

[31] St Nikolov G, Markov P, "Photochemical Hydrogen Abstraction as a Radiationless Transition in the Photoketonization of β-dicarbonyl compounds", *J.Photochem.*, **16** (1981), 93

[32] Courtot P, Le Saint J, "Un Nouveau Système Photochrome: Les Énols Chélatés cis et trans de Diaroylacétates D'Éthyle. Etude en Photolyse à Éclairs", *Tetrahedron Lett.*, **33** (1973)

[33] Gould E S, "*Mechanism and Structure in Organic Chemistry*", Henry Holt and Company, New York, 1959

[34] Weast R C, "*Handbook of Chemistry and Physics*", 61st Edition, CRC Press, Florida, 1980

[35] Dai G, Qin X, Zhang J, Wu S, "Phototautomerization of β-diketones", *Youji Huaxue (Organic Chemistry)*, **2** (1987), 155, *(English Translation)*

[36] Kiuchi F, Chen X, Tsuda Y, "Z-E Isomerization of β-Methoxychalcones: Preferred Existence of E-Isomers in Naturally Occurring β-Methoxychalcones", *Chem. Pharm. Bull.*, **38** (1990), 1862

[37] Muro S L, Carmichael I, Hug G L, "*Handbook of Photochemistry*", Marcel dekker Inc., New York, 1993

[38] Atkins P W, "*Physical Chemistry*", 4th Edition, Oxford University Press, Oxford, 1990, page 777

[39] Kuo J, "UV Spectroscopic and Nuclear Magnetic Resonance Studies of the Enol-Keto Tautomerism in β-Diketones", PhD thesis, Louisiana State University, 1966

[40] Tayyari S F, Zeegers-Huyskens T, Wood J L, "Spectroscopic study of hydrogen bonding in the enol form of β-diketones - I. Vibrational assignment and strength of the bond", *Spectrochimica Acta.*, **35** (1979), 1265

[41] Grens E, Grinvalde A, Stradins J "Intra- and Intermolecular Association and I.R. Spectra of Dicarbonyl Compound Enol Forms", *Spectrochimica Acta,* **31** (1975), 555

Chapter 5

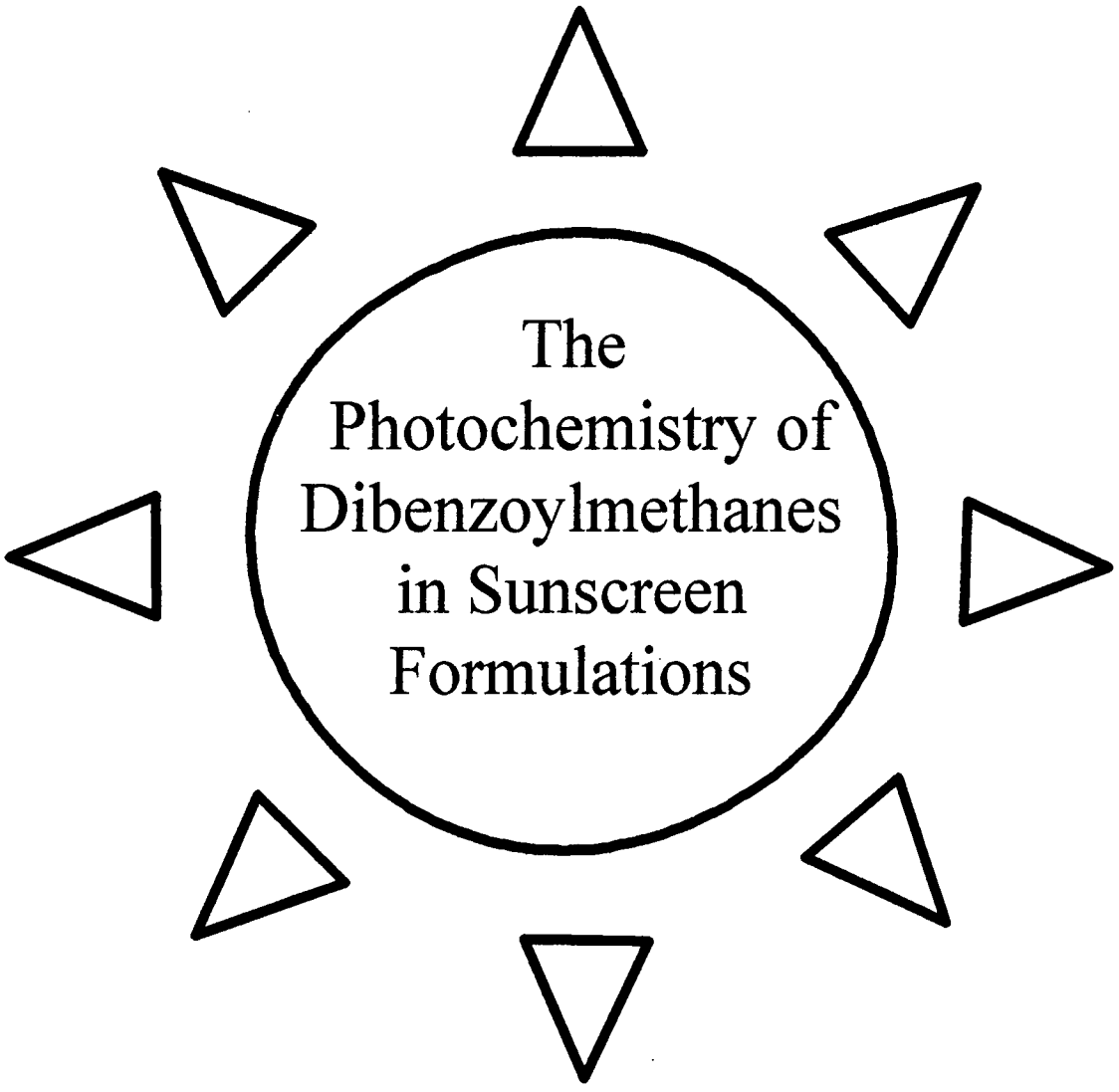
The
Photochemistry of
Dibenzoylmethanes
in Sunscreen
Formulations

5.1 Introduction

It has already been seen in chapters 3 and 4 that different solvent environments can have a significant effect on the photophysical and photochemical properties of UV absorbers such as dibenzoylmethanes. Solvent polarity, pH, hydrogen-bonding effects and possible molecular associations are all important factors. It is not surprising, therefore, that the exact formulation in which a sunscreen chemical is present can profoundly influence the properties of the sunscreen, and hence its effectiveness as a UV filter.

5.1.1 Sunscreen Formulations[1,2]

The formulation of sunscreen products is a complex mixture of art and science. Early products were very basic and were developed mainly by trial and error. Modern products are the result of careful study of scientific principles and exhaustive testing procedures.

There are many general factors involved in choosing the best formulation for a sunscreen product. At the most basic level these include the desired usage, the target SPF required, the market area considered, the cost of materials, the other required properties such as perspiration and water resistance, the legal and environmental requirements, the packaging, and the general aesthetics. More specifically, in order to function as a good sunscreen, there are many factors that must be taken into account. The product must be able to be spread on the skin such that it forms an even, continuous film on the surface of the skin. A patchy coverage results in unprotected areas and a drop in the achievable SPF. To attain high SPFs the layer must generally be thick, although in most cases transparency is desirable for cosmetic reasons. The ingredients used must be non-toxic and non-irritating, and there must be a compatibility of the ingredients such that the sunscreen chemical does not lose effectiveness and no harmful by-products result. The formulation must be stable over the expected shelf-life for the relevant storage conditions and in the high temperatures associated with use in the sun. Ideally the formulation should also be non-greasy and non-drying to the skin, easy to apply, and with no unpleasant odour.

The main types of sunscreen formulations in use today are emulsions, (lotions or creams), oils, gels, sticks, mousses, aerosol sprays and ointments. Sunscreens are also increasingly being incorporated in other every-day products such as hair preparations and make-up. The different types of formulations cover the range of consumer demands in terms of sun-protection requirements, ease to use and aesthetic factors. Brief descriptions of the main types of formulations are given below

5.5.1.1 Types of sunscreen formulations

Emulsions[1]

Emulsions are the most popular and most common type of formulation on the market. These consist of the sunscreen in the oil phase of an oil-in-water or water-in-oil emulsion, and depending on the viscosity these can be lotions or creams, which can form thick uniform films. Emulsions can accommodate a wide range of materials and allow easy incorporation of sunscreens which are commonly oils or can be easily emulsified. They are prepared with a large amount of water and are therefore cheap, however this can make it difficult to impart waterproof properties.

Oils[1]

Sunscreens simply dissolved in oils are one of the oldest types of formulation, although they are not in common usage today. They consist of a single phase, and as such are easy to manufacture, and easy to apply. However, only thin films are possible on application which reduces the effectiveness and limits the SPF possible.

Gels[1]

Gels are clear gelatinous products, and typically belong to one of three main types, aqueous gels, hydroalcoholic gels and microemulsions. Aqueous gels use either water-soluble sunscreens or solubilisers, which limits the choice of sunscreen chemical, and hence SPF range, and prevents any water resistant properties. Hydroalcoholic gels contain ethanol which results in a refreshing and cooling effect as the ethanol evaporates on use. However, as for aqueous gels, waterproofing is a problem. There is also a high level of irritation to the eyes and face. The evaporation can also mean that a uniform film is not left on the surface of the skin, which reduces the effectiveness and limits the SPF. Microemulsion gels are the essentially same as emulsions, with the exception of a very small particle size, so that the product appears clear. These products are very good because a thick uniform film can be achieved, however, high levels of emulsifiers make the product expensive, limit the water resistant properties and can increase irritation to the skin.

Sticks and Ointments[1]

Sticks are generally for specialist usage such as for applying protection to the lips and nose. These consist mainly of oils and oil-soluble sunscreens thickened by wax and petrolatum. They have an oily and greasy feel, but are very waterproof. Ointments are similar to sticks, but with less rigidity. They are not particularly aesthetic, but are very waterproof. They tend to have specialist uses, such as on prescription from dermatologists for light-sensitive diseases.

Aerosol Sprays and Mousses[1]

Aerosol sprays are oil-based or emulsuion formulations designed to be sprayed directly on the skin, eliminating the need for rubbing. It is difficult with such products to ensure an even sunscreen coverage,

and there is a risk of spraying onto sensitive areas such as the eyes. Mousses typically consist of an oil or emulsion lotion with a pressurised propellant, in a specialist dispenser, such that the product is applied as a creamy foam.

5.5.1.2 Formulating Emulsions[1]

Emulsions are by far the most common sunscreen formulation in. They consist of a dispersion of one immiscible liquid in another, and are thermodynamically unstable, with unfavourable inter-molecular interactions driving the formulation to separate into the constituent oil and water phases over time. The goal in formulation is to make the emulsion as stable as possible; a stability of 3 years at room temperature is the typical basic requirement. Emulsifiers or surfactants are used to stabilise the emulsion and are always key ingredients, but the preparation method can have as much influence to the overall product stability as exact ingredient choice and quantity.

The stability of an emulsion can be predicted by Stoke's law, equation 5.1, which describes the velocity of sedimentation, V, where d = diameter of the particles in the dispersed phase, p_1 = specific gravity of the dispersed phase, p_2 = specific gravity of the external phase, g = gravitational constant, and n = viscosity of the external phase.

$$V = \frac{d^2(p_1 - p_2)g}{18n} \qquad \textbf{Equation 5.1}$$

To stabilise emulsions, formulators act to minimise V, by using a variety of methods designed to maximise n, and minimise d and $(p_1 - p_2)$. These include adding thickeners to the external phase to increase the viscosity, and utilising homogenising techniques to ensure small, even particle sizes. The theories behind formulations and the methods used are the subject of many books. Readers are referred to references **1** and **2** for further details and discussion.

5.5.1.3 Emulsion Ingredients[3]

The basic ingredient list for a typical sunscreen emulsion consists of a sunscreen, water, oils and other fatty substances and emulsifiers. In practice other compounds such as preservatives, fragrances and moisturising agents are also included, and often many types of each ingredient group are used. The choice of ingredients can vary with the country of manufacture and change regularly as new products become available. Table 5.1 lists the main ingredient types, their uses and typical proportions used, as determined by a survey of products available in Finland[3].

Ingredient	Use	Typical proportion % by weight
Sunscreens	To absorb UV radiation	10 8
Solvents		50
Fatty Substances	To solubilise non-water soluble ingredients also to soften and moisturise the skin can act as emulsifiers or auxiliary emulsifying agents	29
Emulsifiers	To stabilise emulsion by reducing surface tension	Varying
Cosmetic Active Substances	To soothe and moisturise skin To revitalise skin by increasing blood circulation and metabolism	7 8
Preservatives	To protect against microbial attack	1
Silicones	To increase hydrophobic properties	
Excipients	e.g. substances for pH adjustment	0 7
Chelates	Bind small amounts of metallic impurities - also preservatives	0 1
Antioxidants	To prevent fats becoming rancid	0 2
Fragrances	To mask unpleasant odour and improve marketability	0 4
Thickeners	to increase Viscosity	Varying

Table 5.1 Ingredients in typical sunscreen emulsions[1, 3]

The exact choice of ingredients and quantities is very specific to particular companies, and is often protected by commercial patents. The maximum amount of each sunscreen which can be included in a formulation is set down by legislation, which differs from country to country. Manufacturers tend to include a variety of different sunscreens in any one product to increase the overall proportion to achieve higher SPFs, and also to allow broad spectrum protection. Approved proportions vary from approximately 1% to 10% by weight, depending on the sunscreen[1,4]. In the EC Parsol 1789 can be used in proportions up to 5% of the formulation weight[1, 3]. These figures compare to the typical concentrations used to study the behaviour of DBM in previous chapters, 1×10^{-5}mol $dm^{-3} \approx 0.0002\%$ by weight.

It is clear that the actual solvent conditions experienced by sunscreen chemicals vary widely and differ greatly from the simple single solvent solutions studied in previous chapters. There are many other species present in the emulsions, all of which may interact and influence the photochemistry of the sunscreens. The concentration of sunscreen is also much higher than can be readilly studied in solution phase photochemical studies. Thus the need to be able to study the photochemistry of sunscreens such as the

dibenzoylmethanes under conditions more representitive of actual formulations is important, however there is very little evidence in the literature that this has been attempted.

5.1.2 Usage Conditions

The formulation is the main factor governing the properties of sunscreens, however the way in which a product is used can have marked effects on its efficacy in preventing UV-induced damage to the skin. The thickness and eveness of the sunscreen film on the skin is an important factor. The way the product is applied varies greatly in practice, and depends on individual preferences, the physical properties of the formulation, and also the cost of the product. Studies show a large variation in applied film thickness for different users, from 0.6 - 20 mg cm^{-2} [3,4].

The treatment received by the sunscreen product on the skin is also important in determining the protection offered against UV radiation. Perspiration and swimming may wash off the sunscreen, reducing protection. Perspiration, whilst consisting of 99% water, also contains traces of other compounds including lactate, urea, ammonia and sodium chloride[4]. Swimming in pools allows chlorine bleaches and other chemicals to come into contact with the skin and sunscreen, whilst sea water contains a variety of salts. Any of these compounds could potentially influence the properties of the sunscreen. Interaction with the chemicals in other skin products such as cosmetics could also be important.

Products may also be absorbed into the stratum corneum outer layers of the skin[2,5]. This is generally considered as desirable, because such sunscreens can then not be easily washed off or removed by abrasion. This obviously places the sunscreen in a different environment, where the UV filtering properties may be different. Sunscreens may, however, also pass into the deeper layers of the skin, and even diffuse into the bloodstream, which is highly undesirable[2]. As well as having serious implications for safety, this clearly also reduces the protective ability of the sunscreen.

The temperatures at which the product is used, for example on a hot, sunny beach, or in cold, bright, snowy conditions, may affect film thickness and stability, and hence product performance. The source of the UV light is also clearly important, whether this be natural sunshine on a beach, or at high altitude, or from an artificial source such as a sunbed, all of which can be expected to have a differing spectral distribution.

All these potential problems and variations must be considered when formulating sunscreen products, such that they can efficiently fulfil their function. These factors must also be taken into consideration when testing and evaluating sunscreens.

5.1.3 Measuring UV Protection Factors

5.1.3.1 Measuring UVB Sun Protection Factors

As discussed in chapter 1, sunscreens were originally designed and developed to protect against inflammatory erythema (sunburn) which is most effectively caused by UVB radiation. It is not surprising, therefore, that sunscreen products are usually studied and tested, throughout the world, in terms of the protection given against this response. This is measured in terms of the sun protection factor, SPF, which was first suggested in 1974 [1].

The SPF of a product is defined as shown in equation 5.2, where MED = Minimum Erythemal Dose. An MED is defined as the minimal dosage of UV light that produces a uniform skin erythema with clearly defined margins, determined using the eye, and is measured in units of J cm^{-2} [1].

$$SPF = \frac{\text{MED for protected skin}}{\text{MED for unprotected skin}} \qquad \textbf{Equation 5.2}$$

SPFs are measured *in-vivo* using a test group of human volunteers and a solar simulator. Because of the many variables in the way in which sunscreen products are used, as discussed in the previous section, the techniques for measuring SPF are highly regulated and standardised, although they vary slightly from country to country. The general technique involves applying an even layer of thickness 2 mg cm^{-2}, (1.5 mg cm^{-2} in German tests), onto skin on the back or abdomen that has not been previously exposed to sunlight. A template then divides this area and a control, unprotected area, into smaller areas which receive varying doses of UV radiation. The MED of the protected and unprotected skins are then determined, and the SPF calculated[1,3].

The United States guidelines surrounding the choice of a solar simulator state that the spectral output should model that of sunlight at sea level, from the sun at a zenith angle of 10°. In practice this means the source must have a continuous emission spectrum in the UVA and UVB ranges (290-400 nm), with less than 1% of the energy <290 nm and no more than 5% of the energy >400 nm. Xe arc lamps with appropriate filters are commonly used[4].

The determination of SPFs by this method carries a high degree of error. This is because of many factors including the variation of application method, irradiation source, and the subjective nature of determining an MED. Because of slight procedural differences, an SPF may vary from one country to the next for the same product. SPFs are time consuming and expensive to determine in this manner, mainly because of the

involvement of human test subjects. However SPFs are required by law and widely understood by consumers, and *in-vivo* methods are currently the only legally approved testing procedures.

5.1.3.2 Measuring UVA protection

The incorporation of UVA sunscreens into sun-protection products in recent years has been accompanied by a range of claims of UVA protection. These were often largely unsubstantiated and products with only minimal quantities of UVA sunscreens were marketed as protecting the skin from UVA damage. There has therefore been much work and discussion on devising testing procedures for UVA protection, to authenticate and standardise claims[6].

The major problem with such testing is that SPF determination, as used for UVB protection is not a suitable method for measuring UVA protection. The amount of UVA radiation required to produce the erythema response is over 1000 times greater than the amount of UVB required, and long irradiation times would therefore be necessary. This coupled with further problems of heating effects contributing to the observed erythema, and a non-linear power dependence of the response, means that this method is generally impractical for estimating UVA protection factors. Perhaps more significantly, it is not even clear if the erythema response is a representative measurement of the sum total of UVA damage to the skin. It is not possible to conclusively determine action spectra for harmful effects e.g. photoageing and skin cancer. Even reported action spectra for erythema and pigmentation responses differ greatly. This is also a problem with UVB SPF testing, although the effects of UVB radiation are better understood[1,7].

UVA testing is a subject of great study, and many *in-vivo* and *in-vitro* testing procedures have been, and are being developed. Such methods may also be proposed as possible alternatives to lengthy and costly SPF testing for UVB protection.

5.1.3.3 *In-vivo* Testing Methods for UVA protection[1,7]

Actual *in-vivo* responses to UVA on human volunteers are generally considered to give the only reliable results predicting UVA protection, thus *in-vivo* UVA tests are generally designed to mimic the SPF tests but using only UVA radiation. The choice of endpoint is different because of the unreliable and impractical nature of using the inflammatory erythema response. Other skin changes proposed are the immediate and delayed pigment darkening reactions, or tanning. These are not generally satisfactory, because the immediate pigment darkening reaction produces unclear and short-lived endpoints, and the delayed pigment darkening, like the erythema response, requires long irradiation times.

An alternative procedure is to photosensitise the skin by the application or ingestion of photosensitising chemicals, e.g. 8-methoxypsoralen or anthracene. This ensures that only short periods of irradiation produce inflammatory erythema. The validity of such tests are disputed, as it can be expected that the photosensitised action spectrum will differ to that of normal skin. There are also serious safety considerations in using such drugs.

SPF-like tests on animals instead of humans are often proposed as an alternative to using humans. The hairless mouse is the most common animal used, because of the ease of caring for and testing such animals. The vascilature and pigmentation of mouse skin differs to that of human skin, and in mice the usual response to UV is edema, as opposed to erythema. For these reasons, the validity of using mouse skin as a model for human skin is not always accepted. Pig skin is reported to closely resemble human skin, but pigs are more difficult and expensive to care for and test.

Other biological responses to UVA radiation have been proposed as endpoints for SPF-like tests. These include changes in the mechanical properties of the skin, the suppression of DNA synthesis, and the microscopic study of the production of sunburn cells. Some of these responses are proposed as being more reflective of the photoageing or skin cancer-forming properties of UVA radiation, but the validity is still under investigation. These are also invasive techniques, requiring the removal of biological samples. These are generally only performed on animals, usually requiring the sacrifice of the animal.

5.1.3.4 *In-vitro* UVA Testing Methods

The lack of an accepted and reliable *in-vitro* testing method for UVA sunscreen protection, as well as the time and costs involved in such procedures has led to the development of *in-vitro* methods.

The simplest *in-vitro* method is a simple measurement of the UV transmittance spectrum of a dilute solution of the sunscreen product. SPFs are then calculated by taking into account the contribution that each wavelength makes to the solar spectrum, and the relative ability of each wavelength to cause erythema, or the response under consideration. Thus an equation such as that in equation 5.3 is used, where $E(\lambda)$ = Contribution to the solar spectrum of wavelength λ, $\varepsilon(\lambda)$ = Relative ability of wavelength λ to cause erythema (or response under consideration), and T= Spectral transmittance at wavelength λ. SPFs for UVA protection only are calculated by limiting the range of wavelengths over which the protection factor is measured[8].

$$SPF = \frac{\sum_{\lambda} E(\lambda)\varepsilon(\lambda)}{\sum_{\lambda} E(\lambda)\varepsilon(\lambda)T(\lambda)} \qquad \textbf{Equation 5.3}$$

The main problem with such *in vitro* methods is that they consistently overestimate the SPF values of sunscreens. This is because these methods do not take into account the usage conditions, such as the way the film is applied. The behaviour of sunscreens in formulations may be vastly different to the behaviour in solution, and these methods can not be used for sunscreens containing physical sunscreens such as TiO_2, because these are insoluble. Improved *in-vitro* methods involve using essentially the same method, but using thin films, of 2 mg cm^{-2} of the sunscreen products on quartz plates, in place of solutions. However such methods still ignore the effect of the texture of skin, and sunscreen-skin interactions including the effects of temperature and pH[1,8]. Water resistance tests can also not usually be carried out successfully using *in-vitro* systems.

Improved *in-vitro* methods use actual layers of excised skin from mice or unwanted human skin, instead of a quartz slide. Plastic casts of skin, to mimic the texture, have also been used. Such methods provide better estimates of SPF, however the results are not always reliable. The preparation of excised skin or skin casts is also time-consuming, and natural skin-sunscreen interactions are still not adequately modelled[1,6,8,9].

Other *in vivo* methods have been used to estimate the actual transmittance of sunscreens on living skin. These include measuring the autofluorescence of protected and unprotected skin[10], and by the use of photoacoustic spectroscopy[11]. Such techniques are experimentally difficult, and are still being tested and developed. All these spectral techniques still rely on calculating the predicted erythema response. As discussed, this may not be a valid indicator for UVA damage, and action spectra are still debated.

In-vivo testing methods also do not take into account photostability of sunscreens. *In vivo* SPF tests allow for changes in sunscreen protection over the irradiation times, however *in-vitro* tests usually make one measurement at the beginning of irradiation. Attempts have been made to consider this factor, by pre-irradiating samples, but this is still the subject of controversy[1,5].

5.1.3.5 The Star Rating System for UVA protection[6]

In 1992 the UK company Boots introduced compulsory UVA protection testing and labelling on all sun-products for sale in their shops in an attempt to standardise UVA claims[12]. The *in-vitro* test procedure is based on a method developed by Diffey and Robson[13], and uses a thin-layer spectroscopic technique similar to those described in the previous section. The method involves using 2 mg cm^{-2} layers of a sunscreen product on a polymer-based surgical tape with a textured surface, to simulate skin (Transpore tape).

Boots argue that it is not fully understood as to which wavelengths of UV are important in causing biological damage, and it is therefore desirable to have a broad, even protection from all solar UV wavelengths. The ratio of UVA absorbance per unit wavelength, to UVB absorbance per unit wavelength

is then used to determine how balanced the protection is across the spectrum. This eliminates the need to consider an action spectrum for erythema, or any other response. The ratio can thus range from 0 - 1, from no UVA protection to balanced UVA and UVB protection. Stars are awarded based on this ratio, and this label considered in addition to the SPF of the product.

This system is not without criticism, particularly because it can not be used for oil-based products which can dissolve the tape. Many of the problems associated with *in-vitro* testing methods are still not overcome with this technique. However, because Boots is the largest retail seller of sunscreen products in the UK, accounting for 48% of sales in 1993 [14], this system has been adopted by most manufacturers in the UK.

5.1.4 Photochemistry of Sunscreens in Formulations

The various formulations, usage conditions and testing procedures for sunscreens have been discussed to highlight the problems that are involved in measuring the properties of these systems. In attempting to study the photochemistry of sunscreens under usage conditions, all of the above must be taken into account. A formulation or model system must be chosen, a test method developed, and deviation from actual usage conditions must also be considered.

Very little has been reported in the literature on the study of the photochemistry of sunscreens in formulations, or on skin, despite the wealth of studies attempting to measure protection factors. There are many technical problems to overcome, and in most cases compromises have to be made, such that the study of real formulations under exact usage conditions is an unrealistic goal.

5.1.5.1 Photochemistry of Dibenzoylmethanes in Sunscreen Formulations

Dibenzoylmethane based UVA sunscreens are relatively new, and as chapter 4 has illustrated the solution-state photchemistry is not yet completely understood. It is perhaps not surprising that there are less than a handful of reports in the literature studying aspects of the photochemistry in conditions other than simple solutions.

Photostability studies of dibenzoylmethanes in thin layers of model or actual sunscreen emulsions, under solar simulated conditions have been reported[15,16]. Such studies are concerned with the loss of absorbance of the sunscreen, and hence protective ability, studied by changes in the absorption spectrum. Any products, or the photochemical processes occurring have not been considered in such reports.

Studies of the behaviour of dibenzoylmethanes in cell cultures have also been reported. One report discusses the possible mutagenic effect of dibenzoylmethanes, with no reference to the photochemistry or

mechanisms occurring[17]. The effects of including Parsol 1789 in solutions of human lymphoid cells on the cell death by irradiation has been reported[18]. It was observed that at high Parsol 1789 concentrations, protection against UVA was displayed by a reduction in the fraction of cell deaths on UVA exposure. At low Parsol 1789 concentrations no UVA protection was provided, but significant UVB protection was observed. This was interpreted as being due to conversion of the chelated enol of DBM to the non-chelated transient species. It is suggested that the sunscreen adsorbs onto the cells in solution, possibly stabilising the non-chelated intermediate, and such that this effect is only noticed at low concentrations. However, no actual study of the photochemistry in this system was made, and the interpretation is speculative. The possibility of photoketonisation or decomposition was not considered. Both these processes would result in a loss of absorbance in the UVA region, and hence a reduction in UVA protection, and an increase in UVB absorbance and protection. These effects could explain the reported results.

Thus while the photochemistry of dibenzoylmethanes has been studied in various types of solvents, there have been no photochemical studies in sunscreen formulations or biological systems, other than simple absorption spectra measurements. It has been the aim of this chapter to study the photochemistry of DBM in systems other than simple solutions, and specifically to study the photochemistry in sunscreen formulation systems.

5.2 Results and Discussion

As discussed in section 5.1.1, there are a great variety of possible formulations and ingredients for sunscreen products, and these can be expected to change frequently. Information on exact ingredients, proportions and formulation methods is commercially sensitive information. It would therefore be impossible to study the photochemistry of dibenzoylmethanes in all possible environments found in commercial products, and only a very selective study has been undertaken in this work.

5.2.1 Photochemistry of Dibenzoylmethanes in Micellar Systems

As a basic model for oil-in-water emulsion systems, micellar solutions in water can be studied. Absorption spectra and flash photolysis studies of DBM in such systems have already been reported in chapters 3 and 4.

Details of the absorbance maxima for solutions of DBM and Parsol 1789 in aqueous Triton-X-100 reduced, from chapter 3, are reproduced in table 5.2 for ease of reference. It was observed that the main π,π^* absorption peak was shifted to longer wavelengths, compared to non-polar solvents. This is consistent with the increase in the polar nature of the aqueous micellar solution, as discussed in chapter 3.

However, the peak is shifted to similar, or longer wavelengths, than in solutions of pure water. In chapter 3 it was observed that the peak positions did not always follow the trend expected for changes in polarity, and this may be a further example of this. If more than one DBM molecule was contained within one micelle, it is possible that interactions between the molecules could result in the shift of the absorption peak - solid samples have longer wavelength absorptions, as will be shown later. The estimated ratio of DBM molecules : Triton-X-100 micelles ≈ 1:10, in a 1 x 10^{-5} mol dm^{-3} solution of DBM in 1% Triton-X-100 reduced in water, and thus it is possible that the occupancy of some micelles will be >1. Varying the concentration of Triton-X-100 reduced resulted in small peak shifts, but with no general directional trend, as can be seen in table 5.2.

	Solvent	λ_{max} / nm
Dibenzoylmethane	Cyclohexane	337
	Ethanol	344
	Water	346
	1% Triton-X-100 Reduced in water	347
	2% Triton-X-100 Reduced in water	345.5
	5% Triton-X-100 Reduced in water	346
Parsol 1789	Cyclohexane	355.5
	Ethanol	358
	1% Triton-X-100 Reduced in water	359.5

Table 5.2 Absorption maxima for DBM and Parsol 1789 in various solvents at room temperature
(reproduced from tables 3.1 and 3.2, chapter 3)

Flash photolysis studies of DBM in Triton-X-100, as reported in chapter 4, revealed that the transient absorption spectrum was similar to that observed in other solvents such as ethanol, as shown in figure 5.1. The lifetimes of the non-chelated enol species were, however, much shorter than those observed for other solvents, as was reported in chapter 4, and repeated in table 5.3 for ease of reference.

Solvent	k / s^{-1}	τ / ms
Cyclohexane	300	3.4
Ethanol	3900	0.25
1% Triton-X-100 reduced in water	60000	0.017
2% Triton-X-100 reduced in water	52000	0.019
5% Triton-X-100 reduced in water	52000	0.019

Table 5.3 Transient lifetimes for DBM in various solvents
(reproduced from table 4.4, chapter 4)

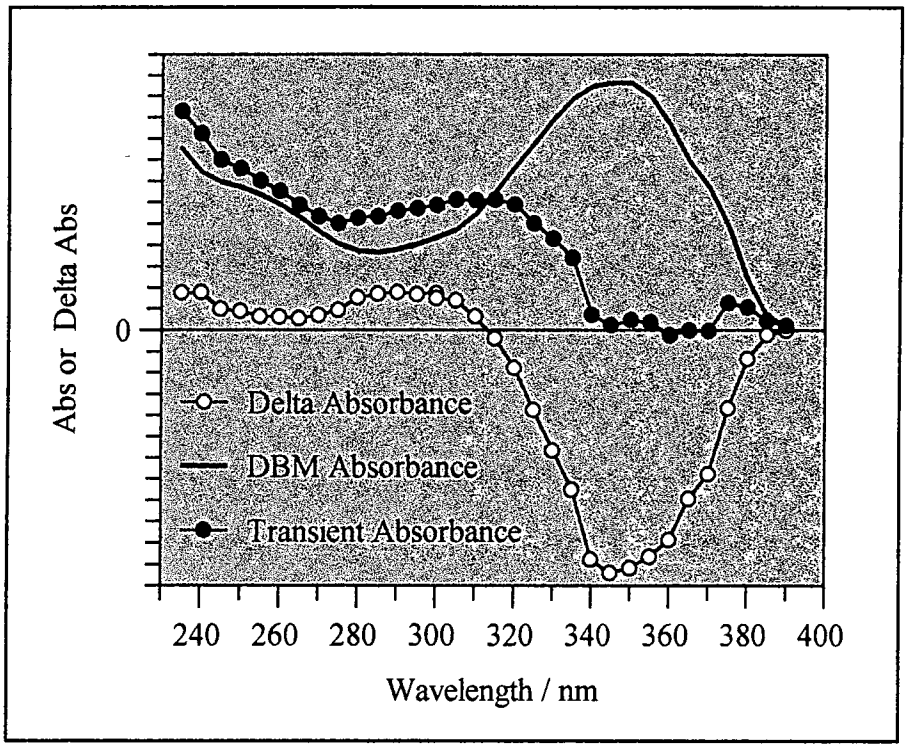

Figure 5.1 Transient absorption spectrum for DBM in 1% Triton-X-100 reduced in water, pumping at 355 nm

Concentration studies, discussed in section 4.2.2.4, showed that the rate constant of transient decay increased with increasing concentration. In a micellar solution, the effective concentration of DBM could be greater than in a single solvent of equivalent total concentration. This could occur if more than one DBM molecule were contained within each micelle. If this were the case it would be expected that DBM micellar solutions would exhibit the properties of solutions of higher concentrations in other solvents, and have much shorter lifetimes, as was observed. Little difference to the lifetime was noted on increasing the concentration of Triton-X-100 reduced in the solution, however the results could show that the lifetime increases with increasing surfactant concentration. This could be consistent with the reduction of the local DBM concentration by increasing the number of the micelles, and decreasing the number of DBM molecules in each micelle. Such concentration effects are probably the main factor affecting the observed transient lifetime, however as was discussed in chapter 4, the lifetime is sensitive to many influences, and other factors may well be involved.

The results of studying micellar systems show that the same photochemical processes, governed by the same factors occur in these systems as in simple solutions. The excited state energies and rates of the processes vary, reflecting the different solvent environment, and effective concentrations.

5.2.2 Photochemistry of Dibenzoylmethane in Emulsion Systems

5.2.2.1 The Emulsion System

The photochemistry of dibenzoylmethane in a sunscreen formulation emulsion system was studied. The chosen formulation was based on an official United States FDA recipe for preparing a standard sunscreen for SPF testing[4]. This is an oil-in-water emulsion system, typical of sunscreen formulations, and uncomplicated by purely cosmetic ingredients such as fragrances and moisturising agents. The sunscreen ingredient, homosalate, (homomenthyl salicylate), was replaced by varying concentrations of dibenzoylmethane. The small quantities of preservatives, only included to increase the shelf-life of the product, were not included, to allow easier study of DBM. No other changes were made, to retain the exact emulsion conditions as far as possible. Details of the preparation are given in chapter 2, and the composition is repeated in table 5.4 for ease of reference.

Ingredient	Percentage by Weight
Lanolin (Wool Fat)	5.0
Dibenzoylmethane	Y
Mineral Oil	2.5
Stearic Acid (Octadecanoic Acid)	4.0
Ethylene diamine tetraacetic acid, disodium salt (EDTA)	0.05
Proplyene Glycol (1,2 Propanediol)	5
Triethanolamine	1
Purified Water	82.45- Y
TOTAL	100%

Table 5.4 Composition of the model sunscreen formulation

(See section 2.8, chapter 2 for more information)

5.2.2.2 Absorption Spectra of DBM in the Emulsion System

An unquantified thin layer of the model formulation containing 1% DBM by weight was spread onto Transpore tape, itself stuck on a quartz plate. Transpore tape is a substrate which has been used to model the textured surface of human skin, as described in section 5.1.3.5. The absorbance spectrum of the thin layer on the tape was measured by transmission spectroscopy, against an identical reference without the DBM, and is shown in figure 5.2. The spectrum below 250 nm is very noisy and partially distorted, due

to a high level of background absorbance from other ingredients in the cream and the Transpore tape. There is also a degree of scattering caused by the cream and Transpore tape, the effect of which is enhanced at short wavelength. However it can be seen that the spectrum has the same profile as the solution state spectra observed in chapter 3, in simple solutions. The peak falls at λ_{max} = 345 nm, which compares to the positions in polar solvents and the micellar solutions, as can be seen from table 5.2.

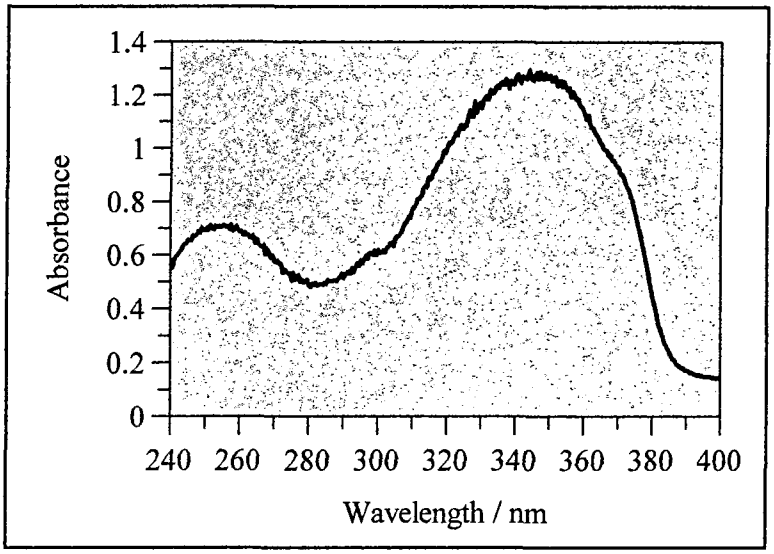

Figure 5.2 Absorbance spectrum of 1% DBM in model emulsion system
(Unquantified thin layer of cream spread on Transpore tape on quartz slide,
vs reference of cream with no DBM spread on Transpore tape on quartz slide.)

The absorption properties of DBM in this formulation were also studied using the technique of diffuse reflectance absorbance spectroscopy as described in chapter 2. This technique allows the study of DBM in the opaque, highly scattering emulsion system, and eliminates the need for spreading a thin layer onto an appropriate surface.

The absorption spectrum of 0.005% w/w DBM in the model formulation obtained by this method is shown in figure 5.3. The amount of DBM incorporated in the formulation must be quite small, in the same way that transmission spectroscopy requires dilute solutions of highly absorbing materials in order to ensure accuracy. Unfortunately this means that the background absorbance of the other ingredients becomes significant. The spectrum below 300 nm is extremely noisy and unreliable. This is because of the low sensitivity of the spectrometer used for these measurements, a lower power output of the source and the high absorbance of other ingredients in the formulation in this region. The main peak also appears slightly distorted, due to background absorbance. With these limitations in mind, it can be seen that the spectrum above 300 nm resembles the transmission spectrum of the thin layer on Transpore tape, although the peak appears more shifted to longer wavelengths.

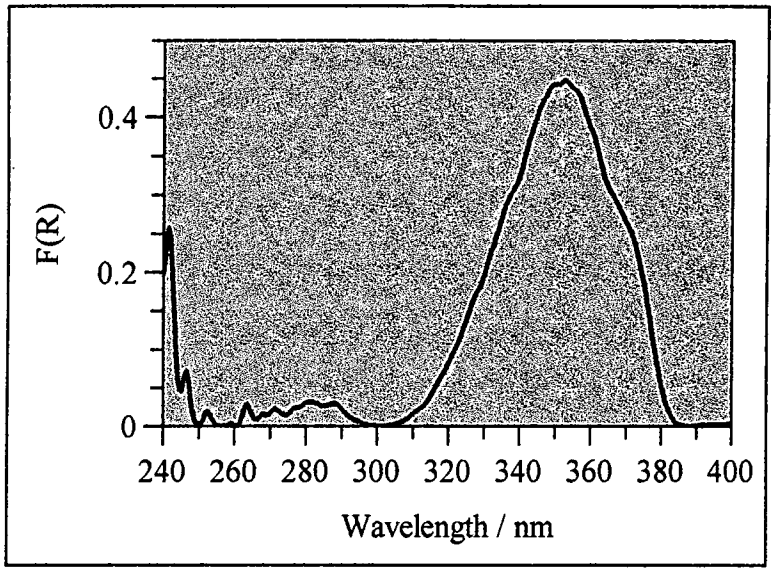

Figure 5.3 Diffuse reflectance absorption spectrum of 0.005% DBM in the model formulation

It was not possible to measure the extinction coefficient of DBM in this system, partly because of the inability to control the concentration carefully enough in the preparation method. Carefully defined layer thicknesses were not possible for the transmission spectroscopy, and this would also prevent accurate extinction coefficient measurement. The level of accuracy of the diffuse reflectance spectra would also prevent measurement of an extinction coefficient. It would also be difficult to relate such an extinction coefficient to a transmission extinction coefficient.

5.2.2.3 Diffuse Reflectance Flash Photolysis of DBM in the Emulsion System

Diffuse reflectance flash photolysis study of DBM in the model formulations revealed the formation of a short-lived species, analogous to that found in the solution work in chapter 4. The new species decayed following first order kinetics, and a typical change in reflectance vs. time curve for the transient decay is shown in figure 5.4. The resulting difference spectra are shown in figure 5.5. As was observed for the diffuse reflectance absorption spectra, this technique is less sensitive below 300 nm because of significant absorbance from other ingredients in the formulation.

The spectrum obtained is similar to those observed for simple solvents, described in chapter 4, and for micellar solutions, described in the previous section. The absorbance peak of the short-lived species appears to be slightly shifted towards longer wavelengths, but an exact peak position cannot be determined because of the difficulties in obtaining a ground state absorption spectrum. No formation of an enolate species was observed.

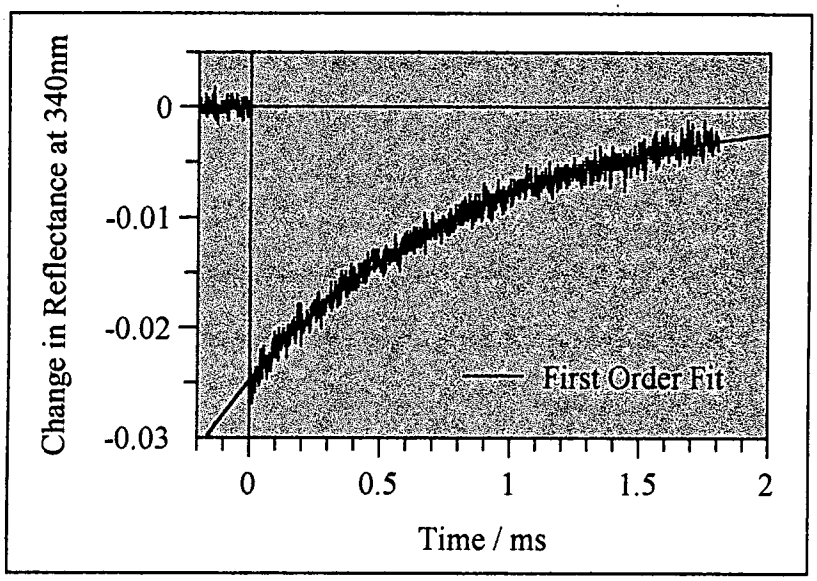

Figure 5.4 Typical transient decay curve for 0.005% DBM in model formulation; pumping at 355 nm, probing at 340 nm

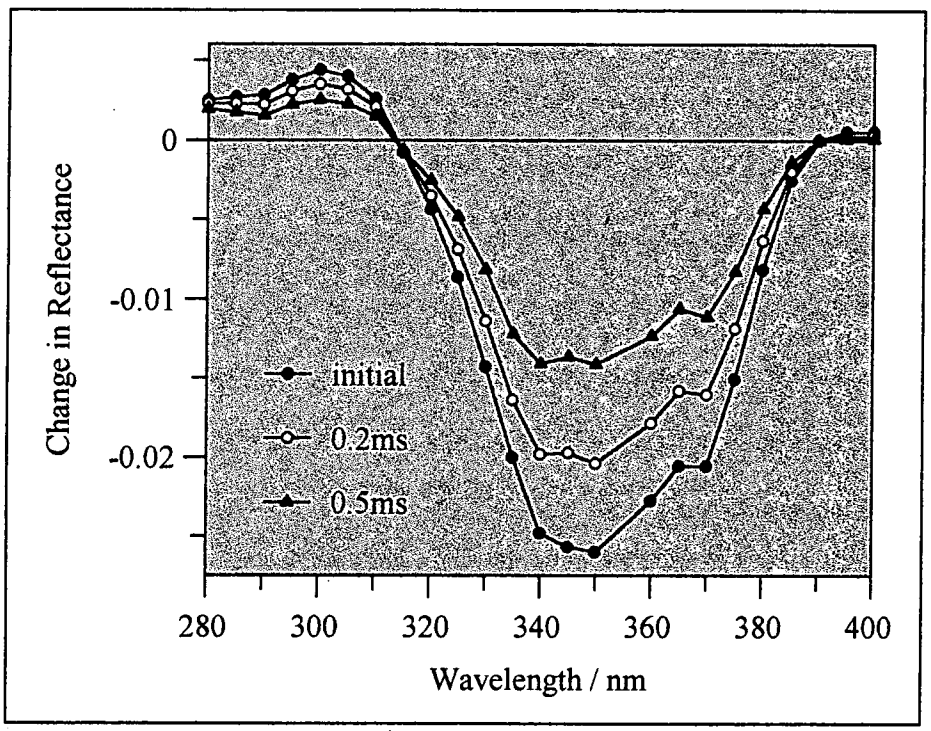

Figure 5.5 Diffuse reflectance flash photolysis difference spectrum after various time intervals for 0.005% DBM in the model formulation, pumping at 355 nm

The first order rate constant for decay of the short-lived species was measured to be $k \approx 1200\ s^{-1}$, and the lifetime to be $\tau \approx 0.9$ ms, for 0.005% DBM in the model formulation. Thus the non-chelated species

decays faster than in non-polar solvents such as cyclohexane, but much slower than in polar solutions such as ethanol and micellar solutions in water. The micellar solutions may be expected to be the best model for the formulation, and it might have been expected that the lifetimes would be similar to those systems. However there are other ingredients in the system which may influence the decay of the non-chelated enol. The addition of triethanolamine has been observed in the literature to increase the non-chelated species lifetime, as was discussed in chapter 4. This is an ingredient of the model formulation, and may play a similar role. The polarity of the environment surrounding the DBM molecules in the formulation is also unknown, and it was observed in chapter 4 that the solvent polarity can play a significant role in the decay kinetics.

5.2.2.4 Photodegradation of DBM in the Emulsion System

The stability of the emulsion model formulation, and the quality of diffuse reflectance absorption spectra, prevented study of the degradation or possible photoketonisation of DBM in the emulsion. The effect of UV light on the absorption spectrum of DBM could not be accurately determined using the techniques here, although it appears that some loss of absorbance does occur, possibly photoketonisation, which slowly recovers.

5.2.2.5 Summary

This study has shown that with dibenzoylmethanes, similar photochemistry occurs in emulsion systems as in simple solvents, and micellar solutions. The excited state energies and rates of the photoprocesses occurring vary, as would be expected of different solvent environments.

5.2.3 The effect of Amides

Recently published patents, filed by L'Oreal, suggest that incorporating amides into sunscreen formulations containing DBMs results in increased photostability[19]. Incorporation into formulations as a solvent, of up to 10% amide by weight is reported to result in significant improvement in the photostability of Parsol 1789, present as 2% by weight. The patent covers a wide range of amides, of the general structure shown in figure 5.6, with N,N diethyl-m-toluamide and N-butyl-N-acetylaminopropionate specifically mentioned.

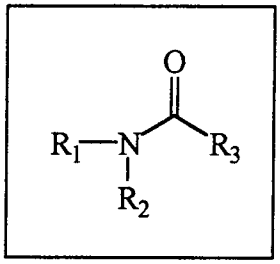

Figure 5.6 General structure of amides covered by patent[19]

(R_1 and R_2 = C_1-C_{12} linear or branched alkyl or phenyl, R_3 = as R_2 or monovalent radical with ester)

No reasons for the increased photostability are given in the patent information. The mechanism is not likely to be caused by the quenching of DBM excited states, as the triplet energy of amides is too large[6]. In this work, the photochemical properties DBM in solutions containing the amide have been investigated, to attempt to understand the mechanisms of photoprotection.

The photochemistry of DBM in N,N-dimethylformamide has already been discussed in chapters 3 and 4. Flash photolysis of this system resulted in the formation of an enolate species from the non-chelated photoproduct, which reverted back to the chelated enol. This would, however, tend to suggest a reduced photostability, as it was observed in chapter 3 that the formation of the enolate in basic solution results in a slow decomposition of DBM.

The photochemistry of DBM in cyclohexane solutions containing N,N-diethyltoluamide in cyclohexane was studied, as this compound was specifically referred to in the patents. Increasing the solvent mixture from 100% cyclohexane to 100% N,N-diethyltoluamide resulted in a progressive shift of the DBM π,π^* absorbance maximum from 337 nm to 350 nm, as would be expected from the increasing polarity of the solvent mixture. No significant change in the extinction coefficient was observed.

Flash photolysis studies of DBM in varying concentrations of N,N-diethyltoluamide in cyclohexane from 100% cyclohexane to 100% N,N-diethyltoluamide were carried out. The strong absorption bands of the N,N-diethyltoluamide prevented the accurate measurement of the transient absorption spectrum below 300nm. In the region above 300 nm the spectrum observed was the same as found for other solvents, described in chapter 4. The first order rate constant increased with increasing proportion of N,N-diethyltoluamide, as would be expected from an increase in the polarity of the solvent, and as shown in figure 5.7. No formation of an enolate species was observed in concentrations of up to 5% w/w N,N-diethyltoluamide in cyclohexane.

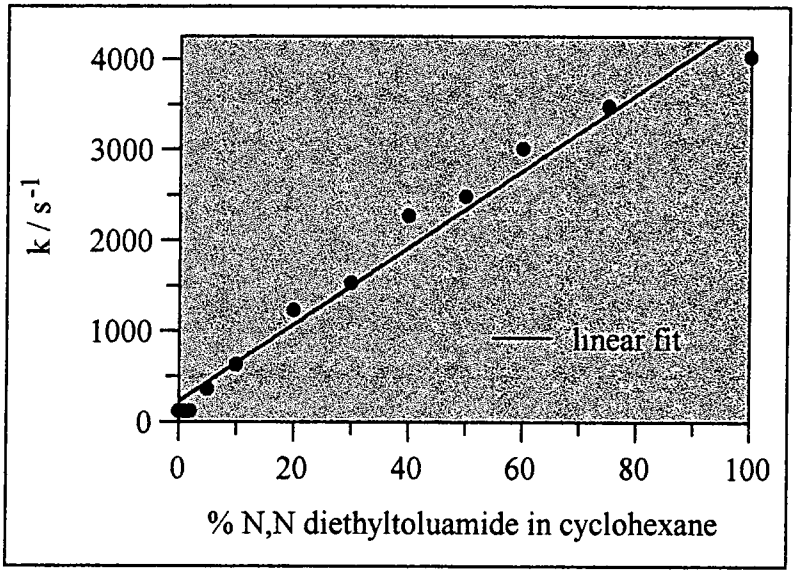

Figure 5.7 Variation of first order rate constant of transient decay for DBM with % N,N-diethyltoluamide in cyclohexane

This study of DBM in amide solutions has not revealed any factors different to other solvent systems, to suggest a mechanism for the reported improved photostability. It could be that the amides interact with another component of the sunscreen formulation, limiting the ability of this other component to influence the decomposition of the DBM.

5.2.4 Photochemistry of Dibenzoylmethanes in Oil-based Systems

Oil-based sunscreen formulations, as discussed in section 5.5.1.2 are not in common usage today, but products based on this type of formulation, such as sticks, aerosols and ointments are sold commercially. In this work, the photochemistry of DBM in mineral oil solutions has been studied, as a model for this type of formulation. Mineral oil is a viscous, long-chained hydrocarbon, and it might be expected that the photochemistry would mirror that observed in solvents such as cyclohexane.

The absorption spectrum of DBM in mineral oil was measured as a thin layer between quartz plates. The absorption spectrum observed was the same as those found in chapter 4 for other solvents, with the main π,π^* absorbance peak in mineral oil positioned at 340 nm.

Photodegradation and possible photoketonisation was difficult to study because of changes in layer thickness over time, especially with heat from the irradiation source. UV spectra appear to show a reversible loss in absorbance of DBM with irradiation, as is shown in figure 5.8. The absolute intensities can not be accurately compared due to differences in layer thickness and density caused by changes in

temperature. By comparing the ratio of the peak intensities of the chelated enol peak and the diketone peak, it appears that on irradiation this ratio decreases, and on being left to recover for several days in the dark, the ratio increases again.

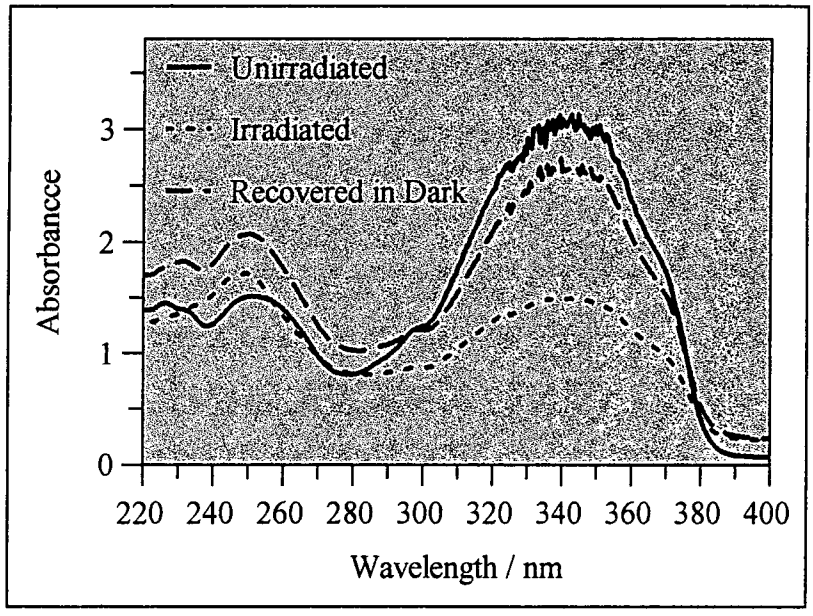

Figure 5.8 Changes in the absorbance spectra of a thin layer of DBM in mineral oil on a quartz plate, with UV irradiation, and on being left to recover for several days in the dark

In order to try and clarify the changes, IR spectra of similar thin layer samples, between KBr plates were measured. The samples were more concentrated that in the absorbance spectra above, and changes in layer thickness prevented subtraction of the background mineral oil and KBr spectra. The spectra obtained are shown in figure 5.9. Full recovery to the original spectrum was observed over weeks in the dark.

The IR spectra show the appearance of a sharp peak at approximately 1660 cm^{-1}, and a broad peak at approximately 3450 cm^{-1}, with irradiation. This compares to the changes observed in the low temperature IR spectra in chapter 4, where irradiation of DBM produced a sharp peak at 3556 cm^{-1}, a broad peak at approximately 3200 cm^{-1}, and a peak at 1662 cm^{-1}. These correspond to a free O-H stretch, a hydrogen bonded O-H stretch and an enone carbonyl stretching vibration respectively. Thus it appears that formation of a non-chelated enol may be formed in solutions of DBM in mineral oil. This, however, does not correspond with the UV absorption spectra described earlier, where no evidence of a non-chelated absorbance was seen. Similarly no IR peak was observed in the region of 1700 cm^{-1} – 1750 cm^{-1}, as seen for C-Methyl DBM, corresponding to a carbonyl stretching frequency, indicating that no photoketonisation had occurred.

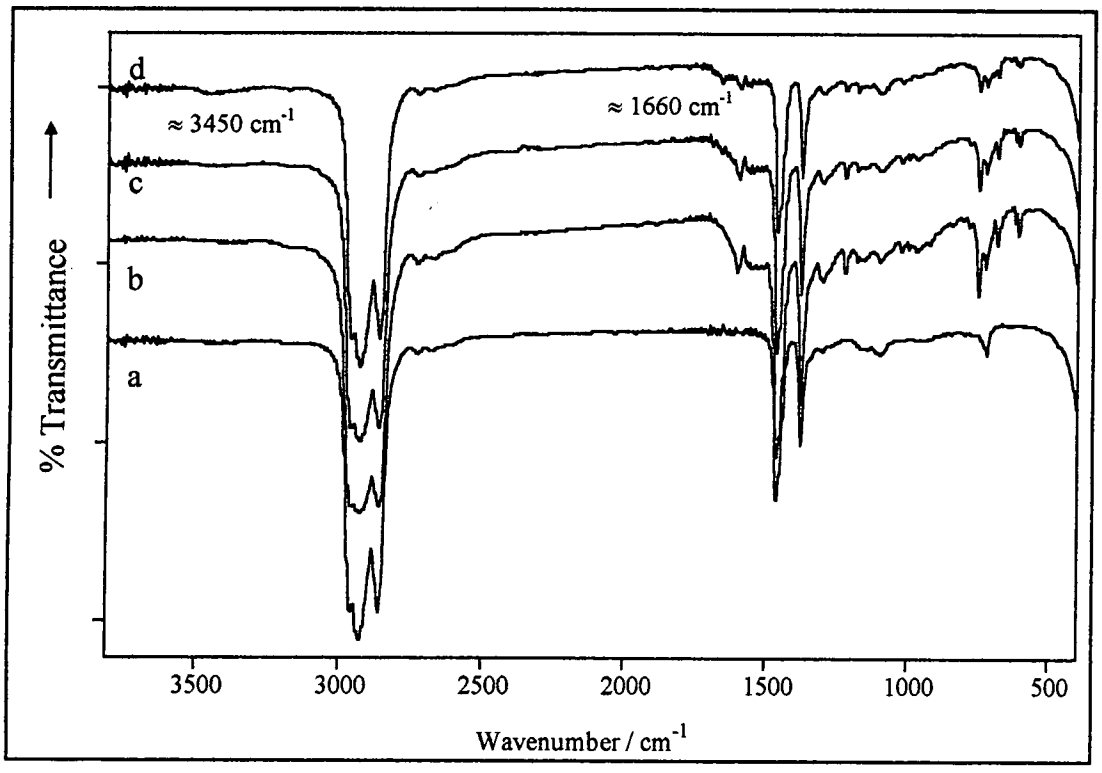

Figure 5.9 Changes in the IR spectrum of a thin layer of DBM in mineral oil between KBr plates with irradiation

a) Mineral oil only between KBr plates (background spectrum)

b) DBM in mineral oil between KBr plates

c), d) as for b with increasing irradiation

It is not clear what photoprocesses are occurring in DBM in mineral oil, as the UV and IR data seem to contradict. The IR data is perhaps more reliable, and does appear to show the formation of a long-lived non-chelated species on irradiation of DBM. These results are discussed further in the next section.

5.2.5 Photochemistry of Dibenzoylmethane as a Solid

If dibenzoylmethane sunscreens are incorporated into hydroalcoholic gels, as described in section 5.5.1.3, then DBM may be deposited as a thin solid layer onto the skin, as the alcohol evaporates. Thus it is of interest to understand the photochemistry of dibenzoylmethanes as solids, and this has been studied.

It is extremely difficult to obtain transmission absorbance spectra of solid samples of DBM, due to the highly scattering nature of solids. Pure DBM is too highly absorbing to allow study by diffuse reflectance, unless a white scattering material is used to dilute it, which will be discussed in the following section.

To eliminate these problems, a concentrated solution of DBM in ether was spotted onto a quartz plate and the ether allowed to evaporate, such that a thin solid layer of DBM was deposited onto the plate. The changes to the absorption spectrum of this solid layer with irradiation were studied; the spectra are shown in figure 5.10. The absolute intensities cannot be compared, because the non-uniform nature of the thin solid layer, and the inability to ensure that exactly the same portion was studied for each spectrum. However, the ratio of chelated enol absorbance to diketone absorbance can be compared, and is seen to decrease with irradiation, and increase again on being left to recover for several days in the dark.

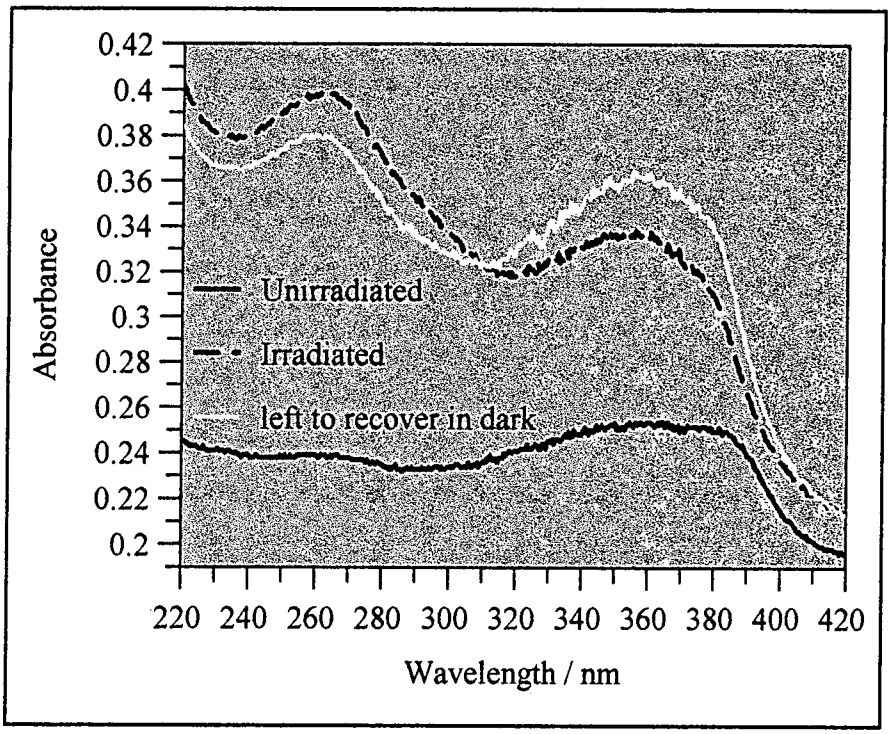

Figure 5.10 Changes in the absorption spectrum of a thin solid layer of DBM on quartz plate with irradiation and on being left to recover for several days in the dark

This could correspond to a degradation of DBM. The apparent recovery could be due to the analysis of a thicker portion of the layer, where less degradation would have taken place. It is also possible that a photoketonisation process has occurred, although a contribution from degradation is probable.

The IR spectrum of a thin solid layer of DBM deposited directly onto the Golden Gate attenuated total reflection accessory, by evaporation from ether solution, was obtained. The changes to this on UV irradiation were studied, and the results are shown in figure 5.11. No recovery was observed after several days, and it was not possible to study the possible recovery over a longer period of time due to equipment availability.

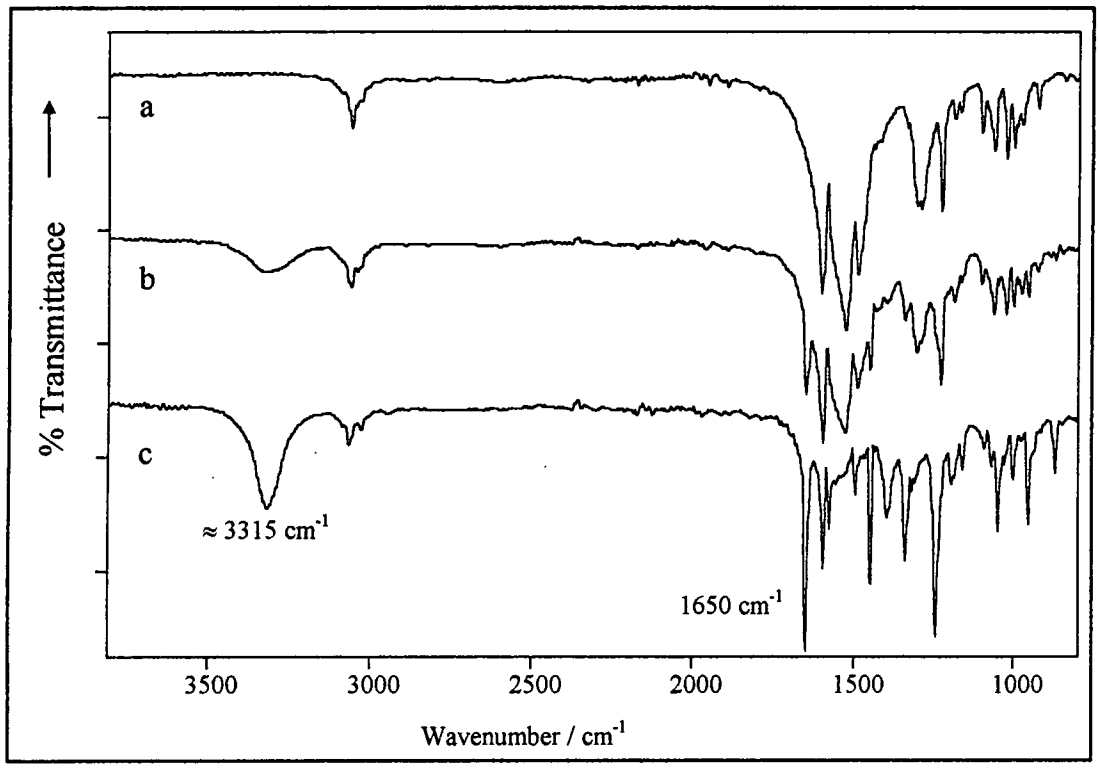

Figure 5.11 Changes to the IR spectrum of a thin solid layer of DBM with irradiation

a) DBM; b),c) with increasing irradiation

On irradiation of solid DBM, similar changes to those observed after the irradiation of DBM in mineral oil can be seen. Included in the many changes observed, there is a grow in of a broad peak at approximately 3315 cm^{-1}, and a sharp peak at approximately 1650 cm^{-1}. The broad peak suggests some form of inter-molecular hydrogen bonding being formed, which clearly can not involve a solvent. The peak at 1650 cm^{-1} can be assigned to a enone carbonyl stretching frequency. The irradiated spectrum can be compared to those of the model compounds C-methyl and O-methyl DBM, as shown in figure 5.12.

It can clearly be seen that the irradiated DBM spectrum bears many similarities to the spectrum of O-methyl DBM, and does not resemble that of C-methyl DBM. Thus it appears that irradiation of the solid DBM results in a long-lived non-chelated species, as was observed for the low temperature solutions. However, as for the study of DBM in mineral oil, these results are not confirmed by UV absorption spectroscopy. Because it is not possible to study any recovery, it is possible that the change observed is not reversible, and is in fact decomposition. Decomposition of Parsol 1789 in solution on irradiation has been studied in the literature, and is discussed in chapter 4. Some of the species formed do possess an O-H bond, and this could be the source of the observed inter-molecular hydrogen bond formation.

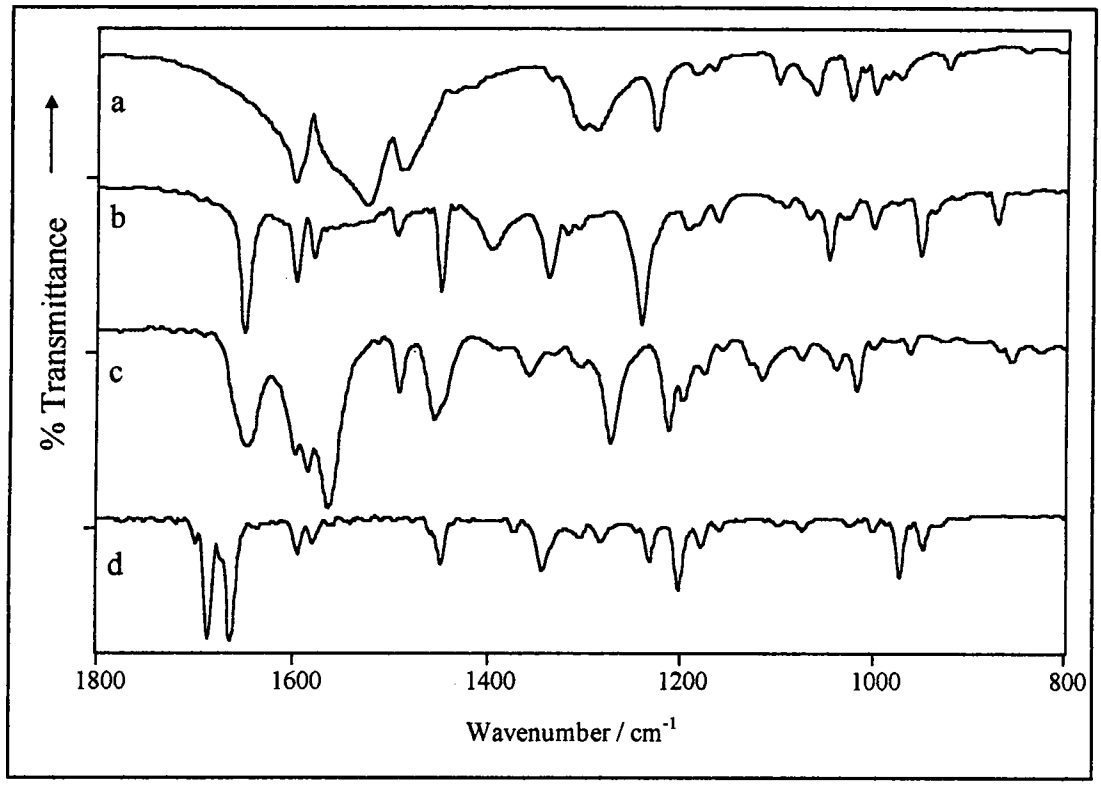

Figure 5.12 Comparison of IR spectra of DBM, irradiated DBM,O-methyl DBM and C-methyl DBMs

a) DBM; b) irradiated DBM; c) O-methyl DBM; d) C-methyl DBM

(Spectra of thin solid layers)

Further work would have to be undertaken to study both the mineral oil and solid systems, in order to clarify the results obtained here. The most likely explanation is the decomposition of DBM, and not the formation of a diketone or non-chelated enol species. Whatever the products, any long-term change in UVA absorbance of a dibenzoylmethane in a sunscreen formulation has serious consequences for the effectiveness in terms of UVA protection.

5.2.6 Photochemistry of Dibenzoylmethane Adsorbed on Cellulose

The photochemistry of DBM adsorbed on cellulose has been studied, although this is clearly not a sunscreen formulation. Cellulose can be used as a convenient white standard in which to dilute solid DBM in order to study its properties by diffuse reflectance spectroscopy, however it must be realised that DBM will interact with the cellulose, via hydrogen-bonding, which is likely to have an effect on the observed photochemistry. Cellulose is also commonly used to build structure in gel formulations, as discussed in section 5.5.1.3. In a hydroalcoholic gel, it is possible that the layer of sunscreen on the skin after evaporation of the alcohol could be more accurately modelled as DBM adsorbed on cellulose.

Cellulose is a polymer of β-D-glucopyranose units, found in plant cell walls. The structure is shown in figure 5.13, which shows that cellulose has many possible sites available for hydrogen bonding to molecules such as DBM[20].

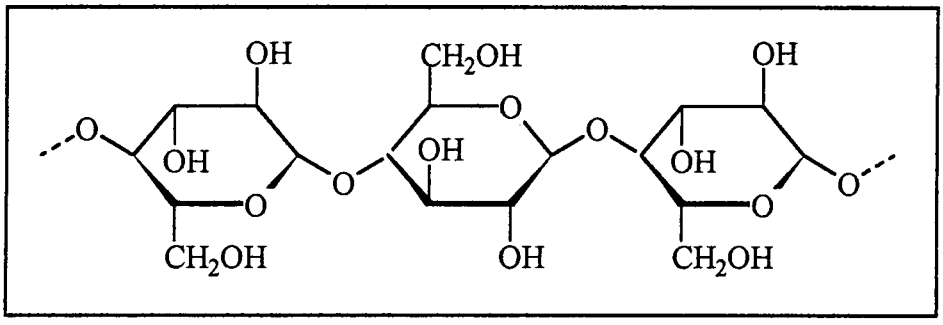

Figure 5.13 Structure of cellulose[20]

The diffuse reflectance absorption spectrum of DBM adsorbed on cellulose has been measured, and is shown in figure 5.14. The spectrum can be seen to be similar to those obtained in solution, with the main π,π^* absorption band falling at approximately 355 nm. The technique is less sensitive below 280 nm, and thus the spectrum in this region is less reliable. It was not possible to study the photodegradation, or possible photoketonisation of DBM using this technique due to the quality of the spectra, however loss of DBM absorbance with irradiation was noted in flash photolysis experiments, which is likely to correspond to photodegradation.

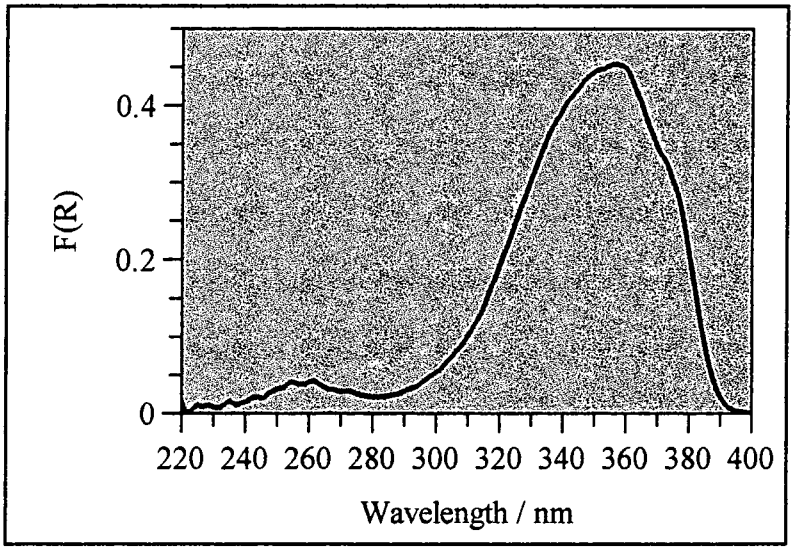

Figure 5.14 Diffuse reflectance absorption spectrum of 0.5 mg/g DBM adsorbed on cellulose

The formation of the non-chelated enol species has been observed by diffuse reflectance flash photolysis, and the spectra obtained are shown in figures 5.15 and 5.16. The transient spectrum has a similar profile to that observed for DBM in solution, described in chapter 4.

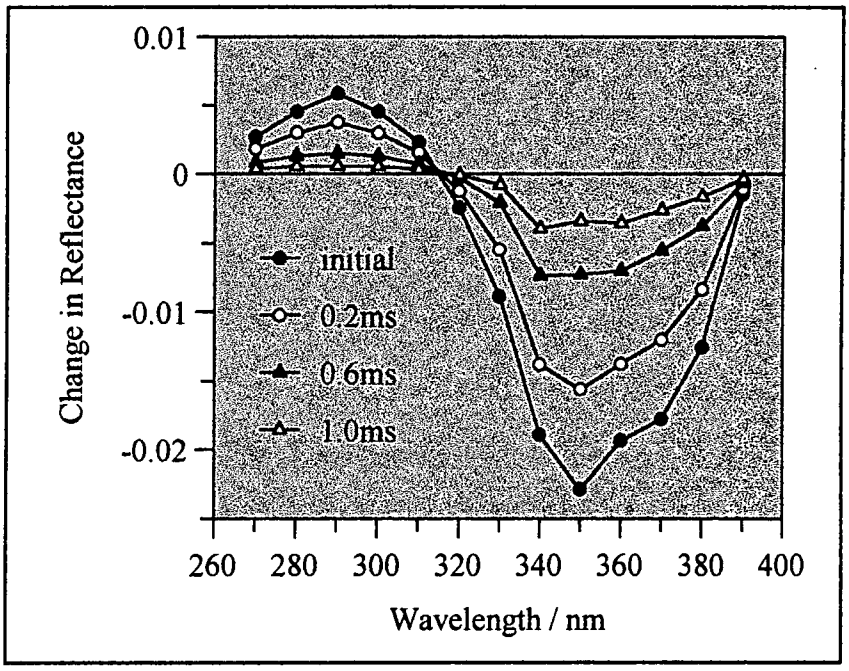

Figure 5.15 Difference spectrum after various time intervals for 0.6 mg/g DBM adsorbed on cellulose, pumping at 355 nm

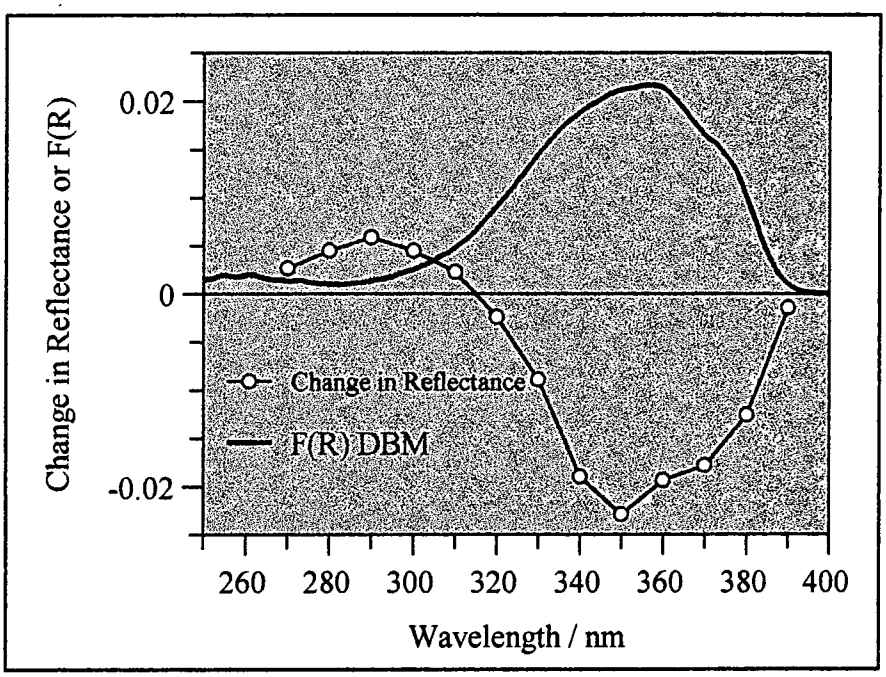

Figure 5.16 Transient difference spectrum for 0.6 mg/g DBM adsorbed on cellulose, pumping at 355 nm

(initial change in reflectance values plotted)

The transient decay curves were fitted to first order, single exponential decays; a typical decay is shown in figure 5.17. However, it is probable that there are different sites in the cellulose structure onto which the DBM can be adsorbed, resulting in a number of different environments. Thus the non-chelated enol of DBM would exhibit slightly different decay rates depending on the adsorbed site, and the nature of the DBM-cellulose interactions, and a range of rate constants should describe the kinetics of recovery.

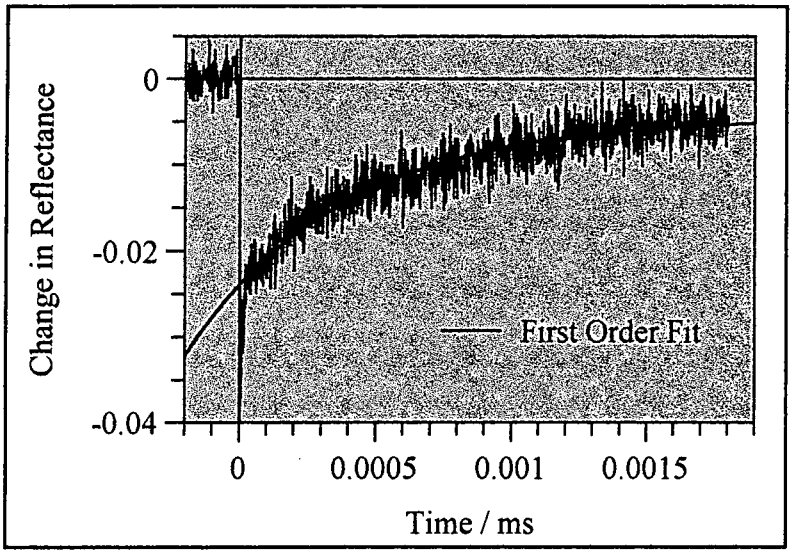

Figure 5.17 Typical transient decay curve for 0.6 mg/g DBM adsorbed on cellulose; pumping at 355 nm, probing at 340 nm

The average first order rate constants measured for a range of concentrations are given in table 5.5. The estimated error on the concentration values is high, because the sample preparation method does not guarentee good sample homogeneity. With the exception of the first value, the first order rate constant can be seen to increase with increasing concentration, as was observed in chapter 4 for DBM in solution. The values are similar to those observed for DBM in polar solutions, but because the first order rate constants vary with concentration it is difficult to compare the values directly.

Concentration of DBM adsorbed on Cellulose / mg/g ± 20%	k / s^{-1}	τ / ms
0.2	2560	0.39
0.4	1490	0.67
0.6	2000	0.50
0.8	2060	0.49
1.0	3030	0.33

Table 5.5 Variation of first order rate constant with concentration for the decay of the non-chelated enol species of DBM when adsorbed on cellulose

Thus again it can be seen that the photochemistry of DBM adsorbed on cellulose mirrors that seen in solution.

5.3 Summary

The photochemistry of DBM in a variety of different environments has been studied. It is possible that irradiation of DBM as a solid, or dissolved in mineral oil, results in the formation of a long-lived non-chelated enol. The observed results could however merely be as a result of photodegradation, and further work would be necessary to clarify the results obtained here.

In emulsions, the most common sunscreen formulation, it has been shown that the photochemistry occurring on irradiation is the same as that observed in solutions. This is an important result, as it indicates that simple solutions are a good model for actual sunscreen formulations, and leads the way for the study of sunscreen photochemistry *in vivo*.

Only a very selective study of DBM in sunscreen formulations has been carried out in this work. With more knowledge of commercial formulations, it should be possible to further study the photochemistry of sunscreens in the formulation environments. The results reported here generally have involved smaller concentrations of DBM than would be found in actual formulations, and the usage conditions have not been considered. These are clearly limitations of the validity of these results, and need to be considered in future work. However, considering the lack of information in the literature concerning of the photochemistry of DBM in systems other than solutions, these results are of significance.

5.4 References

[1] Lowe N J, Shaath N A, "*Sunscreens - Development, Evaluation, and Regulatory Aspects*", Marcel Dekker Inc., New York, 1990

[2] Balsam M S, Sagarin E, "*Cosmetics - Science and Technology*", 2nd Edition, Volume 1, 1972

[3] Sainio E-L, "The ingredients, safety, efficacy and stability of sunscreens", *National Consumer Administration Publications Series 16 / 1995*, National Consumer Administration, 1995, Helsinki

[4] "Sunscreen drug products for over-the-counter human use", Federal Register, **158(90)** (1993)

[5] Blank I H, Cohen III J H, Anderson R R, Jaenicke K F, Parrish J A, "Observation on the Mechanism of the Protective Action of Sunscreens", *J. Investigative Dermatology*, **78** (1982), 381

[6] a) "UVA: Skin Response, Protection and the Consumer", International Conference, 21-22 March 1995, The Commonwealth Institute, London

b) "Broadspectrum Sun Protection: The Issues and Status", International Conference, 11-12 March 1997, The Commonwealth Institute, London

[7] 6th Congress of the European Society for Photobiology, 3-8th September 1995, Churchill College, University of Cambridge

[8] Sayre R M, Poh Agin P, LeVee G J, Marlowe E, "A Comparison of In Vivo and In Vitro Testing of Sunscreening Formulations", *Photochem. Photobiol.*, **29** (1979), 559

[9]Brown S, Diffey B L, "The Effect of Applied Thickness on Sunscreen Protection: In Vivo and In Vitro Studies", *Photochem. Photobiol.*, **44** (1986), 509

[10] Utz S R, Knuschke P, Sinichkin Y P, "In Vivo Evaluation of Sunscreens by Spectroscopic Methods", *Skin Research and Technology*, **2** (1996), 114

[11] Giese K, Nicolaus A, Sennihenn B, "Photoacoustic In Vivo Study of the Penetration of Sunscreen into Human Skin", *Can. J. Phys.* **64** (1986), 1139

[12] "Boots Star System for UVA Adopted by Manufacturers", *The Pharmaceutical Journal*, Nov. 16 1991, 660

[13] Diffey B L, Robson J, "A New Substrate to Measure Sunscreen Protection Factors Throughout the Ultraviolet Spectrum", *J. Soc. Cosmet. Chem.*, **40** (1989), 127

[14] "*Sunscreens and the Consumer - Consumer Understanding of Sunscreens, their Use and Labelling*", London, Health Authority, 1996

[15] Kammeyer A, Westerhof W, Bolhuis P A, Ris A J, Hische E A, "The Spectral Stability of Several Sunscreening Agents on Stratum Corneum Sheets", *Int. J, Cosmetic Science*, **9** (1987), 125

[16] Deflandre A, Lang G, "Photostability Assessment of Sunscreens. Benzylidene camphor and dibenzoylmethane derivatives", *Int. J. Cosmetic Science*, **10** (1988), 53

[17] Kowland J, McKenzie E A, McHugh P J, Cridland N A, "Sunlight-induced Mutagenicity of a Common Sunscreen Ingredient", *FEBS.*, **324** (1993), 309

[18] Andrae I, A Bringhem, Gonzenbach H, Hill T, Mulroy L, Truscott T G, "A UVA Filter (4-tert-butyl-4'-methoxydibenzoylmethane): Photoprotection Reflects Photophysical Properties", *J. Photochem. Photobiol. B: Biol.*, **37** (1997), 147

[19] "Process for the Light Stabilization of Sunscreen Agents Derived from Dibenzoylmethane, Light - Stabilised Cosmetic Sunscreen Compositions thus obtained, and Uses Thereof", Patent no 94-14930, France, 12/12/94, L'Oreal, Paris. (EP 0 717 982 A1)

[20] Mark, Bikales, Overberger, Menges, "*Encyclopaedia of Polymer Science and Engineering*", 2nd Edition, Wiley-Interscience, 1985, pg 90

Chapter 6

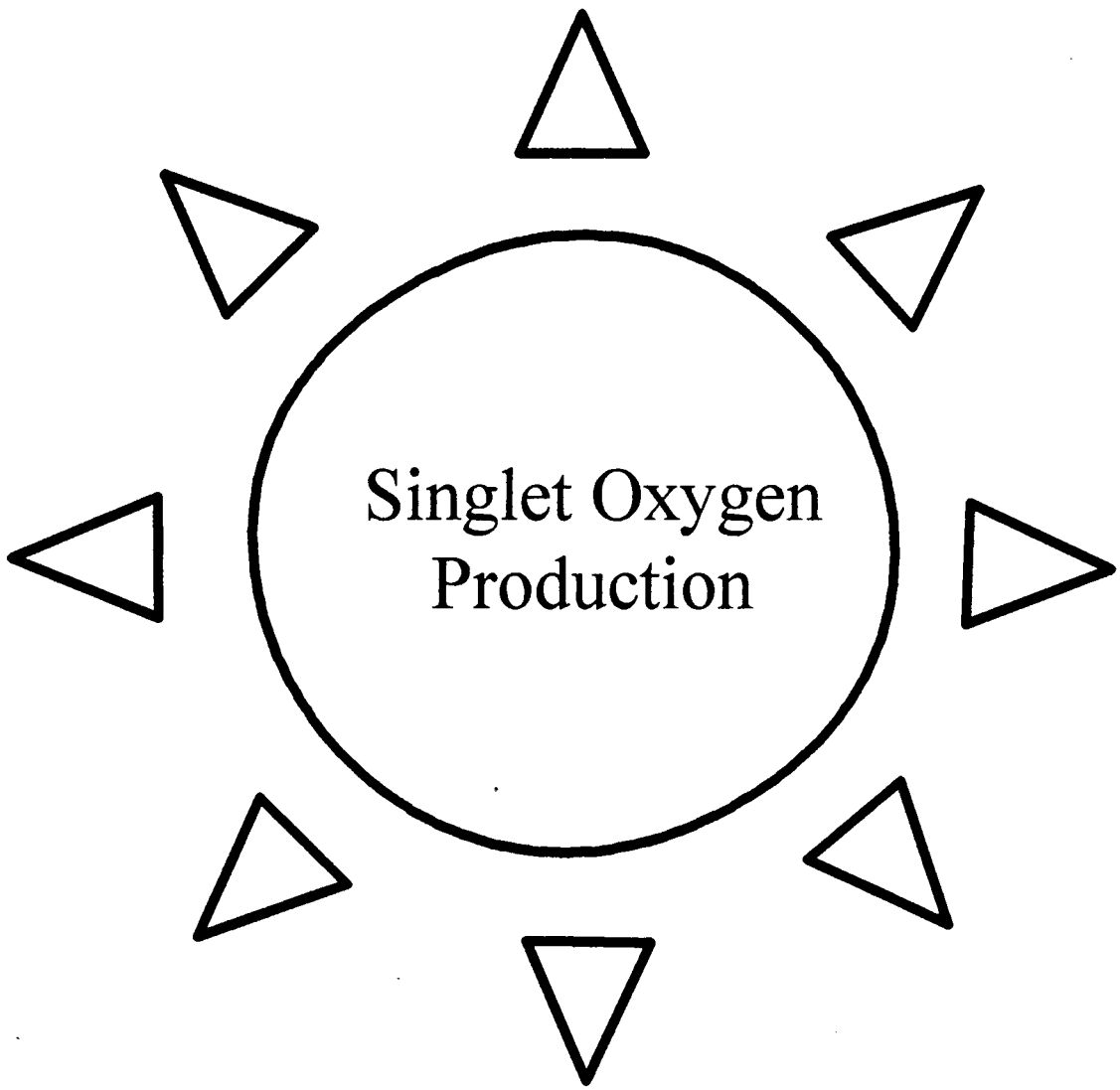

6.1 Introduction

Molecular oxygen, O_2, is highly abundant on our planet, and is an essential part of all life. Singlet molecular oxygen can be formed by energy transfer from an electronically excited states of a sensitiser molecule. It is a very important species biologically because it is highly reactive and capable of causing damage to biological materials such as proteins and lipids[1]. This can have effects detrimental to health, as will be discussed later. If sunscreens are capable of acting as sensitisers for singlet oxygen, this would have serious consequences, and thus it is important to study the singlet oxygen generating properties of sunscreens.

6.1.1 Electronic states of molecular Oxygen

The molecular orbitals of O_2, derived from linear combination of atomic orbitals, are shown in figure 6.1.

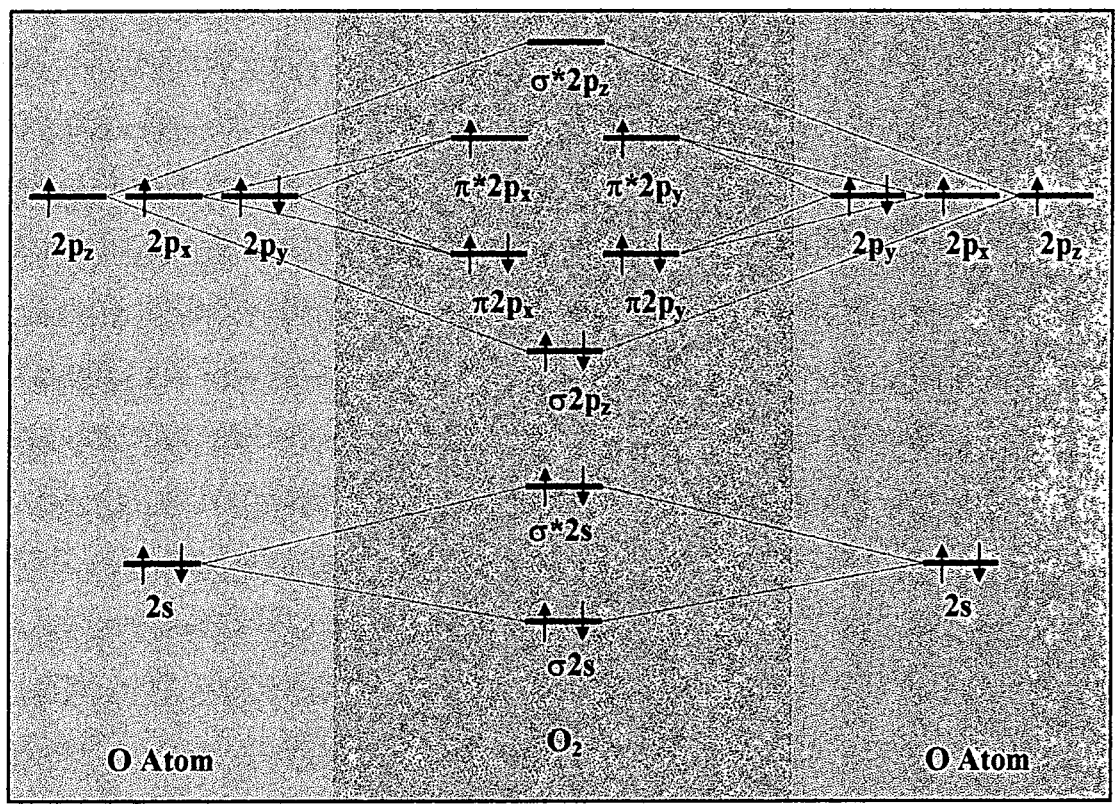

Figure 6.1 Schematic molecular orbital diagram for molecular oxygen[2]

(Molecular axis in z-axis; * denotes anti-bonding orbital)

Because the π_x^* and π_y^* orbitals are degenerate, Hund's rule predicts that the lowest energy state will be that of highest multiplicity[3]. The ground state of molecular oxygen is therefore a triplet state, and is described by the term symbol $^3\Sigma_g$.

Some possible electronic excited states of oxygen are described in figure 6.2. The first two excited states of oxygen are singlet in nature, i.e. having only spin paired electrons. Molecules in either of these excited states are referred to as "singlet oxygen" or "singlet molecular oxygen".

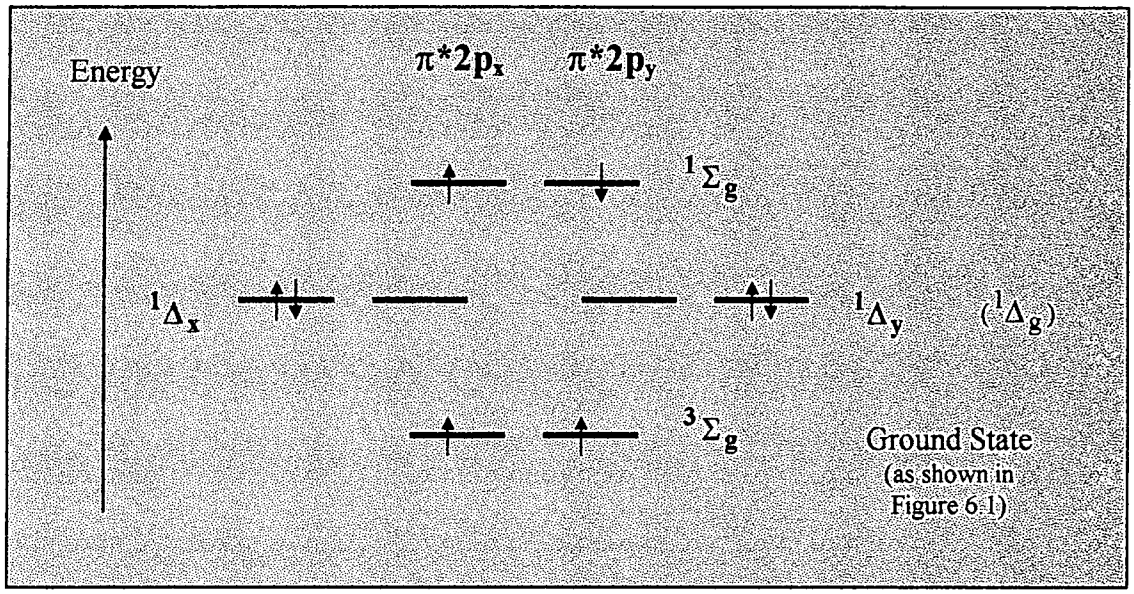

Figure 6.2 Some electronic excited states of molecular oxygen

(occupancy of π^*2p_x and π^*2p_y orbitals shown only; all lower levels are occupied as shown in figure 6.1)

Electronic transitions between the ground and higher states of oxygen, shown in figure 6.3, involve transition from a triplet state to a singlet state, and as such are strongly forbidden.

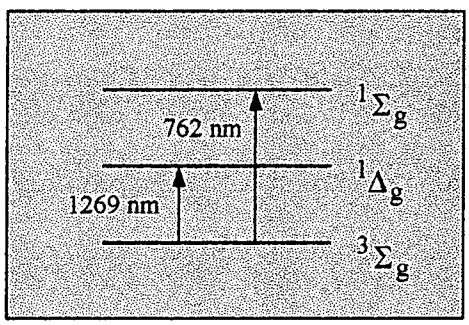

Figure 6.3 Electronic transitions of molecular oxygen

Such transitions do occur directly in the upper atmosphere, where absorption and emission at 1269 nm and 762 nm (for $v'_0 \leftrightarrow v''_0$ transitions) can be observed[4]. In the gas phase the radiative lifetimes of the $^1\Delta_g$ and $^1\Sigma_g$ excited singlet states are 64 minutes and 16 s respectively, however, in solution, the lifetimes are

very short[4], as will be discussed in section 6.1.4.1. In fact, the lifetime of the $^1\Sigma_g$ state is so short that very little is known about it, and most excited state chemistry is believed to arise from the $^1\Delta_g$ singlet state. Thus it is the properties of the $^1\Delta_g$ state that are of interest, and the terms "singlet oxygen" and "singlet molecular oxygen", and the symbol $^1O_2$, usually refer exclusively to this state, and will do so in this report.

6.1.2 Singlet oxygen generation by photosensitisation

Because the electronic transition $^1\Delta_g \leftarrow {}^1\Sigma_g$ is highly forbidden, the generation of singlet oxygen, is usually only achieved by indirect methods. It can be a product of certain chemical reactions, but singlet oxygen is usually generated by photosensitisation. This is as a result of energy transfer from an electronically excited state of a sensitiser molecule to a ground state oxygen molecule. In theory, this could occur from either the singlet or triplet states of the sensitiser molecule, as indicated in schemes 6.1 and 6.2, where "Sens" represents a sensitiser molecule, and "Sens*" represents an excited state of the sensitiser.

$$^1\text{Sens}^* + O_2(^3\Sigma_g) \longrightarrow {}^3\text{Sens}^* + O_2(^1\Delta_g) \qquad \textbf{Scheme 6.1}$$

$$^3\text{Sens}^* + O_2(^3\Sigma_g) \longrightarrow {}^1\text{Sens} + O_2(^1\Delta_g) \qquad \textbf{Scheme 6.2}$$

Clearly for scheme 6.1 to be possible, the difference between the energy of the singlet state, E_S, and the energy of the triplet state, E_T, of the sensitiser must be greater than or equal to the energy of the singlet state of oxygen, E_Δ, i.e. $E_S - E_T \geq E_\Delta$. For scheme 6.2, $E_T \geq E_\Delta$.

There are many other possible quenching interactions between molecular oxygen and a sensitiser excited state, including chemical reactions[4]. These do not, however, result in $O_2(^1\Delta_g)$ generation, and will not be discussed in detail in this report.

The lifetime of a triplet state is generally much larger than the lifetime of the corresponding singlet state, and therefore triplet photosensitised $O_2(^1\Delta_g)$ production, as shown in scheme 6.2, is the most common

route by which singlet oxygen is generated. Triplet photosensitised singlet oxygen generation is considered to proceed via electron exchange energy transfer[3,5], as shown in figure 6.4.

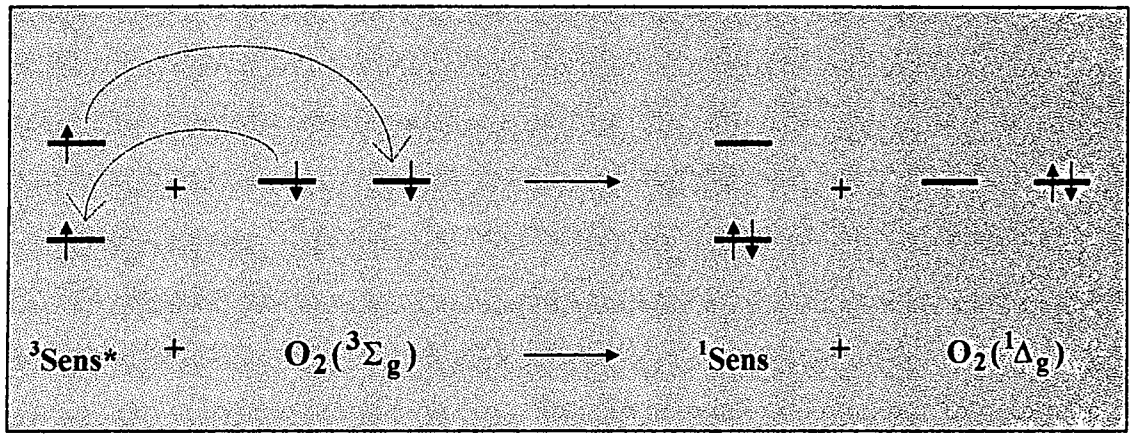

Figure 6.4 Electron transfer between a sensitiser, Sens, and molecular oxygen[3,5]

The energy difference between the ground state, ($^3\Sigma_g$), and first excited state, ($^1\Delta_g$), of oxygen is small, (1269 nm = 92 kJ mol^{-1}), and a wide range of compounds can act as photosensitisers for singlet oxygen, including many aromatic hydrocarbons and carbonyl compounds. Examples of photosensitisers include Rose Bengal, E_T = 164 kJ mol^{-1}, and C_{60}, E_T = 151 kJ mol^{-1} [6].

The rate of formation of singlet oxygen by photosensitisation is extremely fast in solution, (In aerated solutions, $k_{O_2} \approx 10^{8\text{-}9}$ mol^{-1} dm^3 s^{-1} [6]), and the kinetics can be complicated because of the many possible types of interaction between O_2 and sensitiser excited states. These kinetics will be briefly discussed in section 6.1.4.2.

6.1.3 Quantum Yields of Singlet Oxygen Production

The quantum yield of singlet oxygen production, Φ_Δ, by photosensitisation is defined in equation 6.1.

$$\Phi_\Delta = \frac{\text{number of molecules of } {}^1O_2 \text{ produced}}{\text{number of photons absorbed by sensitizer}} \qquad \textbf{Equation 6.1}$$

The theoretical maximum quantum yield is therefore 2, if schemes 6.1 and 6.2 occurred sequentially, with 100% efficiency, to give scheme 6.3. Such an occurrence is very uncommon, although there are compounds with Φ_Δ values of greater than unity, e.g. rubrene in oxygen saturated toluene, $\Phi_\Delta = 1.8$ [4].

$$^1\text{Sens} + h\nu \longrightarrow {}^1\text{Sens}^*$$

$$^1\text{Sens}^* + O_2(^3\Sigma_g) \longrightarrow {}^3\text{Sens}^* + O_2(^1\Delta_g) \qquad \textbf{Scheme 6.3}$$

$$^3\text{Sens}^* + O_2(^3\Sigma_g) \longrightarrow {}^1\text{Sens} + O_2(^1\Delta_g)$$

For most sensitisers, the process of singlet oxygen generation has to compete with other rapid excited-state deactivation pathways. These include internal conversion, vibrational relaxation and fluorescence from the singlet state to the ground state, inter-system crossing to form the triplet state, and internal conversion, inter-system crossing, vibrational relaxation and phosphorescence from the triplet state to the ground state. Direct chemical reactions between excited states and molecular oxygen can also compete. Thus the quantum yield of singlet oxygen production will be very much less than 2. Generally compounds with longer lived excited states have higher yields of singlet oxygen. Quantum yields can also be dependant on oxygen concentration, with maximum yields being found in oxygen saturated solutions. Clearly excited states with energies (or energy differences) lower than the energy of the singlet state of oxygen, 92 kJ mol^{-1}, will not act as sensitisers.

6.1.4 Photophysical Properties of singlet oxygen

6.1.4.1 Non-Radiative Lifetime

Singlet oxygen has a very long intrinsic lifetime due to the highly forbidden nature of the transition $^1\Delta_g \rightarrow {}^3\Sigma_g$. The intrinsic lifetime is reported to be 45 minutes[7], however in solution, rapid, nonradiative, quenching back to the ground state occurs, such that singlet oxygen has a very short lifetime. The lifetime in solution is highly solvent dependant, as the quenching efficiency of solvents varies[8]. Lifetimes in alcohols and water are very short, e.g. in ethanol $\tau \approx 10$ μs and in water $\tau \approx 4$ μs [8]. Singlet oxygen in hydrocarbon and aromatic solvents generally have longer lifetimes, e.g. in cyclohexane $\tau \approx 23$ μs and in benzene $\tau \approx 30$ μs [8], and halogenated solvents have exceptionally long lifetimes, e.g. in tetrachloromethane

$\tau \approx$ 1000-30000 μs (sources vary) and in chlorobenzene $\tau \approx$ 1200 μs [8]. Solvent deuteration also greatly increases the lifetime of the singlet oxygen in solution[8,9].

Singlet oxygen - solvent interactions result in energy transfer from the excited singlet oxygen to vibrational energy levels of the solvent, but the exact mechanisms are not well understood. The electronic to vibrational energy transfer process occurs most rapidly when the accepting oscillators are of high frequency, e.g. X-H, and the observed quenching efficiencies of various solvents can be related to the vibrational frequencies of the X-H bonds present[9]. Relaxation of singlet oxygen can theoretically occur to leave the molecule in any of the excited vibrational states of the ground state triplet, as shown in figure 6.5.

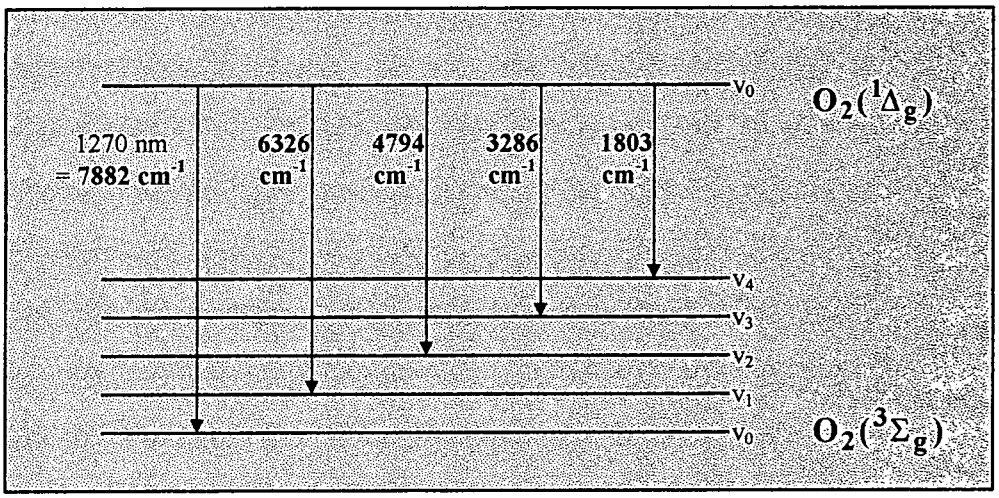

Figure 6.5 Electronic transitions from the singlet state to different vibrational energy levels of the triplet ground state of oxygen[9]

The Franck-Condon principle indicates that transitions from the v = 0 state of the singlet state to higher vibrational states of the triplet state are less favoured than transitions to lower vibrational states, because of a smaller integral overlap[9].

The vibrational stretching frequencies of different hydrogen and deuterium bonds are listed in table 6.1. By comparing these energies with those shown in figure 6.5 for excited state relaxation, it can be seen that vibrational excitation of the different bond types can relax singlet oxygen to different vibrational energy levels. For example vibrational excitation of an O-H bond can relax singlet oxygen to (a higher rotational energy level of) the v_2 vibrational level of the ground state, whereas a C-H bond can only relax the singlet oxygen to the v_3 vibrational energy level, which is a less favourable process[9]. Consequently solvents containing O-H bonds more efficiently relax singlet oxygen than solvent with only C-H bonds, and in these solvents singlet oxygen has a shorter lifetime. A similar explanation can explain the effect on the singlet oxygen lifetime of solvent deuteration[9].

Bond	Vibrational Stretching Frequency / cm^{-1}
O-H	3500
C-H	3050
O-D	2550
C-D	2240

Table 6.1 Vibrational stretching frequencies for various hydrogen and deuterium bonds[9]
(listed in order of descending ability of each bond to quench singlet oxygen)

There are other non-radiative deactivation pathways for singlet oxygen, including singlet-singlet annihilation[10], which can result in the observation of a dependence of the singlet oxygen lifetimes upon excitation source intensity[9].

Since the "concentration" of the solvent involved in singlet oxygen relaxation is very large compared to the singlet oxygen concentration, the decay of singlet oxygen follows pseudo first order kinetics as indicated in equation 6.2.

$$\frac{d\left[{}^1O_2\right]}{dt} = -k_D\left[{}^1O_2\right] \qquad \textbf{Equation 6.2}$$

6.1.4.2 Kinetics of Formation and Decay

The observed rates of formation and decay of singlet oxygen depend on the mechanisms and excited states involved. As described in the previous section, the decay of singlet oxygen follows first order kinetics, however a simple first order decay curve will only be observed if the rate of formation of singlet oxygen is fast compared to the decay.

The rate of formation of singlet oxygen is described in equation 6.3, and the rate of decay is given above in equation 6.2. The overall observed rate of singlet oxygen decay is therefore given by equation 6.4, which can be integrated to give the singlet oxygen concentration at time = t, shown in equation 6.5.

$$\frac{d\left[{}^1O_2\right]}{dt} = k_{O_2}\left[Sens^*\right]\left[O_2\right] \qquad \textbf{Equation 6.3}$$

$$\frac{d[^1O_2]}{dt} = k_{O_2}[Sens^*][O_2] - k_D[^1O_2] \qquad \textbf{Equation 6.4}$$

$$[^1O_2] = \frac{k_{O_2}[O_2]}{k_D - k_{O_2}[O_2]} \times \left(\exp(-k_M[O_2]t) - \exp(-k_D t)\right)[Sens^*]$$

Equation 6.5

For generation of singlet oxygen by a typical triplet state sensitiser, the rate of formation, equation 6.3, is very fast compared to the rate of decay of singlet oxygen, equation 6.4, and only the decay of singlet oxygen is observed. At low concentrations of oxygen, however, the rate of singlet oxygen formation becomes smaller, and comparable to the rate of decay, and a "grow-in" of the singlet oxygen can be observed in the decay trace, as shown in figure 6.6.

Singlet oxygen formation is not the only route by which the sensitiser excited state can decay, but competes with other deactivation pathways such as vibrational relaxation and luminescence. The rate of the rise of the $^1O_2$ signal is dependant on the lifetime of the sensitiser excited state, which is clearly also directly linked to the concentration of dissolved oxygen, especially in the case of compounds with high quantum yields of singlet oxygen generation. An excited state that is long-lived in the absence of oxygen results in a slow rise time for the singlet oxygen signal. Instrumental response limits the ability to measure the grow-in of the signal for excited states that are very short lived in the absence of oxygen, where an instantaneous rise is observed, even at low oxygen concentrations.

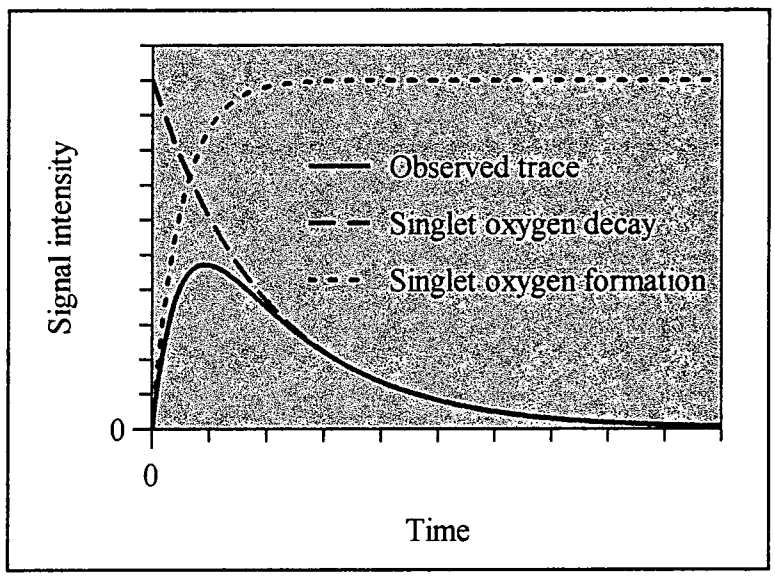

Figure 6.6 Schematic diagram showing the decay kinetics of singlet oxygen, split into the contributions due to formation and decay

6.1.4.3 Luminescence

Despite the highly forbidden nature of the singlet oxygen $^1\Delta_g \rightarrow {}^3\Sigma_g$ transition, luminescence at 1269 nm resulting from this transition can be observed to occur weakly, using sensitive IR detectors[4]. The amount of luminescence produced from singlet oxygen, i.e. the quantum yield of luminescence, Φ_p^{Δ}, depends greatly on the solvent nature[10]. This is partly due to the variation of the rates of non-radiative decay pathways, described above, where less luminescence will be observed from singlet oxygen in a solvent in which rapid quenching occurs, e.g. water. The phosphorescence rate constant, k_p, is also solvent dependant, and can be correlated to the solvent polarisablity[11]. Values of k_p are observed to be large in benzene solution, and small in aqueous solution[11]. Again, detailed mechanisms to explain these variations are not generally agreed upon.

Direct observation of $^1O_2$ by the study of luminescence at 1269 nm is increasingly becoming the most effective method for detecting and monitoring singlet oxygen formation and decay in solution[4]. This is generally easier in solvents where singlet oxygen has a high probability of luminescence and a long non-radiative lifetime. In practice it is most difficult to study singlet oxygen in aqueous media, which is often of the greatest interest, although D_2O is often used a substitute.

6.1.4.4 Singlet Oxygen Quenching

Singlet oxygen can also be physically or chemically quenched by interaction with other molecules in solution, including the sensitiser, reducing the observed lifetime. Chemical quenchers undergo chemical reactions with singlet oxygen, to produce oxidised products, whilst physical quenchers undergo energy transfer with singlet oxygen, e.g. causing excitation of the quencher to higher vibrational energy levels, but are not chemically altered.

The rate of decay of singlet oxygen in the presence of a quencher is given by equation 6.6, where k_D is the rate constant for decay in the absence of the quencher, k_Q is the quenching rate constant, and [Q] is the concentration of quencher.

$$\frac{d[^1O_2]}{dt} = -\left(k_D[^1O_2] + k_Q[Q][^1O_2]\right) \qquad \textbf{Equation 6.6}$$

If it is assumed that the concentration of quencher is much greater than the singlet oxygen concentration, or does not change during the decay, then the rate equation becomes that shown in equation 6.7, where k_Δ is the observed rate constant of singlet oxygen decay, defined in equation 6.8.

$$\frac{d[^1O_2]}{dt} = -k_\Delta[^1O_2] \qquad \textbf{Equation 6.7}$$

$$k_\Delta = k_D + k_Q[Q] \qquad \textbf{Equation 6.8}$$

Efficient quenchers have large values of k_Q, e.g. α-tocopherol (Vitamin E), $k_Q = 2 \times 10^8$ dm^3 mol^{-1} s^{-1} [8], but these are generally still considerably less than the rate constants for diffusion controlled reactions, $k \approx 10^{10}$ dm^3 mol^{-1} s^{-1}.

6.1.5 Chemical Properties and Biological effects of singlet oxygen

Singlet oxygen is a highly reactive species, and will undergo a great variety of chemical reactions with organic molecules. These include addition, [2+2] and [4+4] cycloaddition reactions, and oxygenation [3,5]. Further information on the reactions of singlet oxygen can be found in reference 5.

Biologically, singlet oxygen is highly toxic, due to its high reactivity. Species such as proteins, amino acids, nucleic acid bases, and lipids are all susceptible to oxidation by singlet oxygen[1]. At the cellular level, singlet oxygen has been shown to produce physical rupture of cell membranes, impair membrane transport functions, inactivate internal organelles such as mitochondria, and even cause oxidative damage of DNA and RNA including DNA scission[12]. Singlet oxygen is implicated as a cause of physiological damage such as inflammation, cardiovascular diseases and cancer. Indeed, ageing and maximum life expectancy are related to oxidative damage, including that caused by singlet oxygen[13].

These damaging effects can be made use of, for example in photodynamic therapy, where cancers are destroyed by photosensitised generation of singlet oxygen in tumour cells[14]. Clearly, however, formation of singlet oxygen in the body is generally undesirable. The body does have some natural defences against attack by singlet oxygen, including antioxidants such as Vitamin E (α-tocopherol) and carotenoids, which act as efficient quenchers and can limit or prevent damage[13].

Singlet oxygen is not the only harmful reactive oxygen species which can be formed in the body under the action of light. Peroxyl radicals (ROO$^\bullet$), hydroperoxyl radicals ($HO_2^\bullet$), hydroxyl radicals (HO$^\bullet$), and

superoxide anion radicals ($O_2^{\bullet -}$), can also be formed under certain circumstances[13]. The formation and effects of species such as these are difficult to separate from that of singlet oxygen, especially considering that they can form, and be formed from, singlet oxygen[7,15]. Singlet oxygen is, however, considered to be the most important photogenerated oxygen species, and these others will not be considered in this report.

6.1.6 Singlet Oxygen Generation by Sunscreens

As described in Chapter 1, chemical sunscreens are designed to protect the skin from damage caused by UV radiation, by absorbing the UV light and dissipating the energy via safe pathways. If a sunscreen were to act as a photosensitiser for singlet oxygen, this would potentially be a serious problem, as the sunscreen could cause photochemically induced damage to skin, instead of protecting against it.

The lifetime of singlet oxygen in cellular media is a few microseconds in the surrounding and internal watery phases of the cells, and 10s of microseconds in the fatty lipid environments such as cell membranes, hence the singlet oxygen species can only diffuse about 10^{-7} m during its lifetime. This compares to typical cell diameters of 10^{-5} m and membrane thicknesses of 10^{-8} m [12]. Therefore, it is important to note that biological damage will only occur close to a site where singlet oxygen is generated.

Porphyrins are very good singlet oxygen photosensitisers used in photodynamic therapy, but it has been reported that they do not cause damage when applied topically to the skin[1]. This is because the stratum corneum of the skin acts as a barrier, and prevents the porphyrin entering living cells.

Because sunscreens are applied topically, assumptions are usually made that they remain on the outer surface of the skin, and the singlet oxygen photosensitising properties are therefore rarely investigated. However, virtually all chemicals placed on the surface of the skin can diffuse to some extent through the stratum corneum to lower layers, and then into the bloodstream where they can be spread to all parts of the body[16]. This is known as percutaneous absorption.

Some studies have been undertaken to determine the extent of percutaneous absorption of sunscreens[17,18], and these indicate that topically applied sunscreens do enter the stratum corneum and lower skin layers. Studies have also shown that some sunscreens can be detected in the blood stream or in urine after application to the skin[16]. As mentioned in chapter 5, it is often desirable for a sunscreen to partially locate in the stratum corneum, as it is then resistant to removal by washing and abrasion[16,19]. However the stratum corneum is the main external barrier of the skin, and if the sunscreen can penetrate this, it is likely to pass through to lower layers of the skin.

There have been many reports of allergies and dermatitis from sunscreens[20,21]. An allergic response must be generated by interaction with living cells; further evidence that sunscreens do get absorbed into living

parts of the skin. Other factors to be considered include the fact that people with injured or damaged skin will also use sunscreens, and clearly the risk of sunscreens being absorbed is much higher in these cases.

Sunscreen users often spend extended periods of time in the sunshine, exposing themselves to large quantities of UV radiation, and even a layer of SPF 15 sunscreen still transmits approximately 7% of the incident UV light. Therefore any singlet oxygen photosensitising ability of a sunscreen which has been absorbed and is present in living cells could have serious consequences, in terms of biological damage. In fact, it has been suggested that photoallergic responses to illuminated sunscreens are indeed caused, at least in part, by singlet oxygen production[22]. If the sunscreen has been transported to other parts of the body, it could then be located in areas that are not protected from UV light. It is thus important to study the singlet oxygen generating properties of sunscreens.

Some sunscreens are known to generate singlet oxygen. Sunscreens including p-aminobenzoic acid (PABA), 2-ethyl-hexyl p-(dimethylamino) benzate (ODPABA), 2-ethylhexyl salicylate (OMC), and 2-ethylhexyl p-methoxy cinnamate (OCR) have all recently been studied in solution and shown to generate singlet oxygen [22,23].

6.1.7 Singlet Oxygen Generation by Dibenzoylmethane Sunscreens

As discussed in Chapter 1, dibenzoylmethanes are currently the most common UVA sunscreens in Europe, being present in most sunscreens claiming to have UVA protection. Since their introduction there have been many reports of allergic and photoallergic reactions[21,20,24,25]. It has also been reported that DBM becomes toxic, and mutagenic towards cultivated yeast cells when illuminated[26]. Despite these reports, very little work has been done on investigating the singlet oxygen photosensitising properties of DBMs, which could be responsible, or partly so, for the above effects.

As discussed in chapter 4, reports differ as to whether oxygen affects the lifetimes and quantum yields of photoprocesses of DBM in solution. Some workers suggest it does not, whilst others suggest oxygen has a slight effect. It has been reported that DBM can generate singlet oxygen, via its diketo form[27], which is present in very small concentrations in solution but can be formed on irradiation as discussed in chapter 4. Few details are given in this reference, and no quantum yields are reported. Beeby and Parker have measured the quantum yield for singlet oxygen generation by DBM in cyclohexane solution to be $\Phi_{\Delta} = 0.03$ [28]. They also reported that no singlet oxygen was observed in solutions of acetic acid, acetonitrile, ethanol, pyridine and toluene. There have otherwise been no reports to date, studying the singlet oxygen properties of DBM, and none reporting studies of Parsol 1789. There also appears to have been no investigations made of the ability of DBMs to quench singlet oxygen.

The potential for DBMs to act as singlet oxygen sensitisers, has been further investigated in this work.

6.2 Results and Discussion

6.2.1 Quantum Yields of Singlet Oxygen Generation

Photosensitised singlet oxygen generation by dibenzoylmethanes and model compounds has been studied in various solvents. The quantum yields of singlet oxygen generation have been measured directly using the method of observing luminescence at 1269 nm as described in chapter 2.

A typical trace showing the decay of the singlet oxygen signal, (observed for sensitisation by DBM in benzene), and the fitted single exponential decay curve are shown in figure 6.7. Traces obtained for standards, where quantum yields of singlet oxygen generation were larger, had a much greater signal to noise ratio.

A typical plot of singlet oxygen signal intensity vs. relative laser power (for sensitisation by DBM in benzene), is shown in figure 6.8.

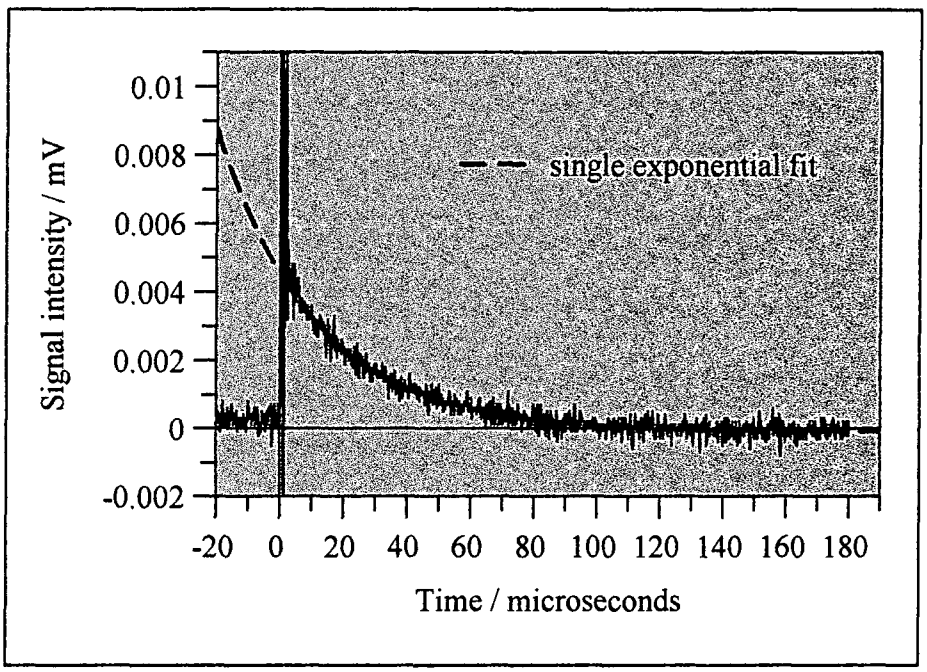

Figure 6.7 Singlet oxygen decay for photosensitisation by DBM in benzene, as studied by observing 1269 nm luminescence

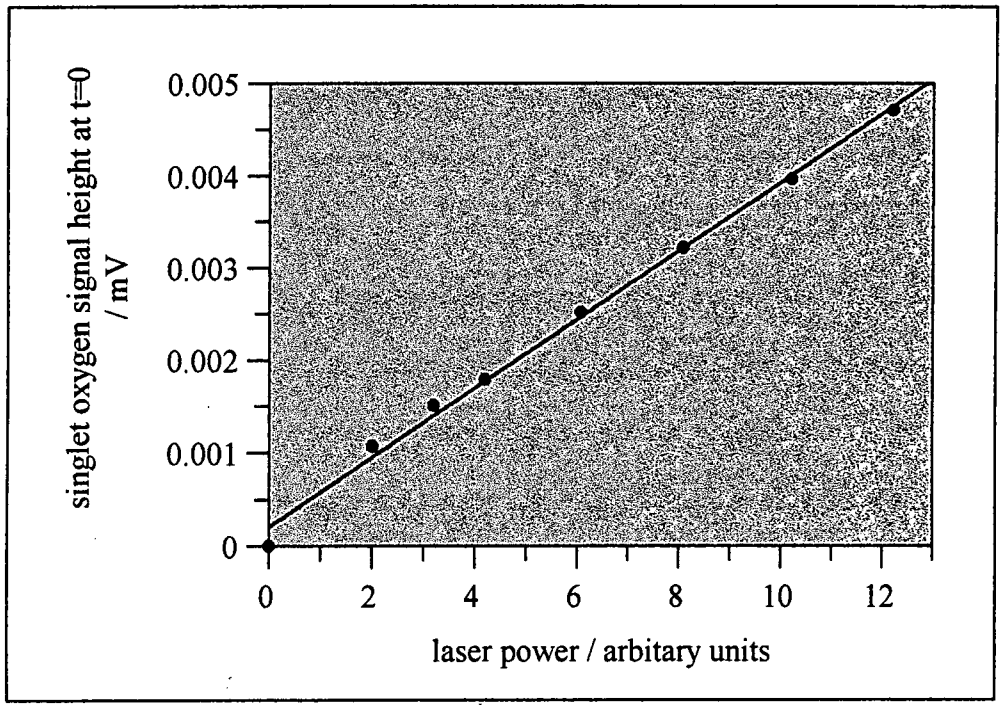

Figure 6.8 Singlet oxygen luminescence signal intensity vs. laser power for photosensitised generation by DBM in benzene

Measured singlet oxygen lifetimes and quantum yields obtained in methanol, acetonitrile and benzene are given in tables 6.2-6.4. Two standards were considered for each solvent, to ensure accuracy. The reference compound used to calculate the quantum yields is indicated with an asterisk. Literature values are given in brackets.

Compound	τ / μs ±0.5 μs	Φ_Δ ±10%
Rose Bengal*	10.0	(0.80[a])
Anthracene	10.0	0.67, (0.7[a])
Dibenzoylmethane	n	n
C-Methyl DBM	9.8	0.11
O-methyl DBM	n	n
Parsol 1789	n	n
	(10.4[b])	

Table 6.2 Singlet oxygen quantum yields and lifetimes for photosensitisation in air saturated methanol solution

a) Reference 4, b) Reference 7, * Standard used in calculations, n) no signal detected

Compound	τ / µs ± 0.5 µs	Φ_Δ ± 10%
Rose Bengal	79	0.56, (0.54[a])
Acridine*	81	(0.82[a,b])
Dibenzoylmethane	n	n
C-Methyl DBM	76	0.13
O-methyl DBM	n	n
Parsol 1789	n	n
	(58.3 - 69[c])	

Table 6.3 Singlet oxygen quantum yields and lifetimes for photosensitisation in air saturated acetonitrile solution

a) Reference 4, b) in O_2 saturated solution, c) Reference 7, *) Standard used in calculations, n) no signal detected

Compound	τ / µs ± 0.05-0.1 µs	Φ_Δ ± 10%
C_{60}*	31	(0.97[a])
Anthracene	31	0.88, (0.66[a])
Dibenzoylmethane	33	0.009
C-Methyl DBM	31	0.16
O-methyl DBM	32	0.006
Parsol 1789	35	0.005
Parsol DAM	31	0.005
	(26.7- 31.2[b])	

Table 6.4 Singlet oxygen quantum yields and lifetimes for photosensitisation in air saturated benzene solution

a) Reference 4, b) Reference 7, *) Standard used in calculations

It can be seen that the singlet oxygen lifetimes obtained in these experiments for standards in methanol and benzene solutions agree well with literature values, and less so for the acetonitrile solutions. In methanol and acetonitrile solutions, singlet oxygen has a low rate of radiative decay and a low luminescence quantum yield. This resulted in very small signals, and none could be detected for most of the compounds studied. This does not necessarily mean that these compounds do not generate singlet oxygen in these

solvents, but that if they do the quantum yields are lower than the detection limit of the equipment, i.e. approximately $\Phi_\Delta < 0.01$. In benzene solution, signals were nearly 10 times as large, due to a larger luminescence quantum efficiency for singlet oxygen in this solvent, and signals were detected for all compounds. These signals were not detected on degassing the solutions.

C-Methyl DBM has a significant singlet oxygen quantum yield, which is consistent with its aromatic ketone structure; c.f. benzopheneone in benzene, $\Phi_\Delta=0.36$ [4]. Excited states of dibenzoylmethanes are rapidly deactivated by formation of the non-chelated enol, as described in chapter 4, hence oxygen quenching, i.e. formation of singlet oxygen would not be expected to occur particularly readily. DBM, O-Methyl DBM (the model for the non-chelated enol) and the Parsols studied do in fact have small yields, showing them to be singlet oxygen sensitisers, although very poor ones. The diketone form of DBM and Parsol 1789 has a negligible absorbance at 355 nm, as was reported in chapter 3, and therefore the photosensitisation ability of DBMs it is not due entirely to the small contribution from the diketone form acting as sensitiser, as suggested by previous workers[27].

O-methyl DBM has a singlet oxygen yield comparable to those of DBM and Parsol 1789, which could indicate that it is the non-chelated enol form of dibenzoylmethanes which acts as a singlet oxygen sensitiser. However this could only be the case if the non-chelated enol was formed in an excited state, as the singlet oxygen is produced in one flash in these experiments. It is also significant that the quantum yields of non-chelated enol formation are approximately 0.5, as measured in chapter 4, and hence if it were the non-chelated enol of DBM generating singlet oxygen it would not be expected that the quantum yields would be comparable for O-methyl DBM and DBM.

6.2.2 Variable Oxygen Concentration

The effect of varying the concentration of oxygen on the kinetics of the decay of singlet oxygen generated by DBM was investigated to give an insight into the nature of the excited state of DBM generating singlet oxygen.

The oxygen concentration in solutions of DBM and C_{60} were varied using the method described in chapter 2. For C_{60} in benzene solution, changes in the singlet oxygen decay trace were observed on lowering the oxygen concentration. At low oxygen concentrations a grow-in of the singlet oxygen signal is observed, as shown in figure 6.9.

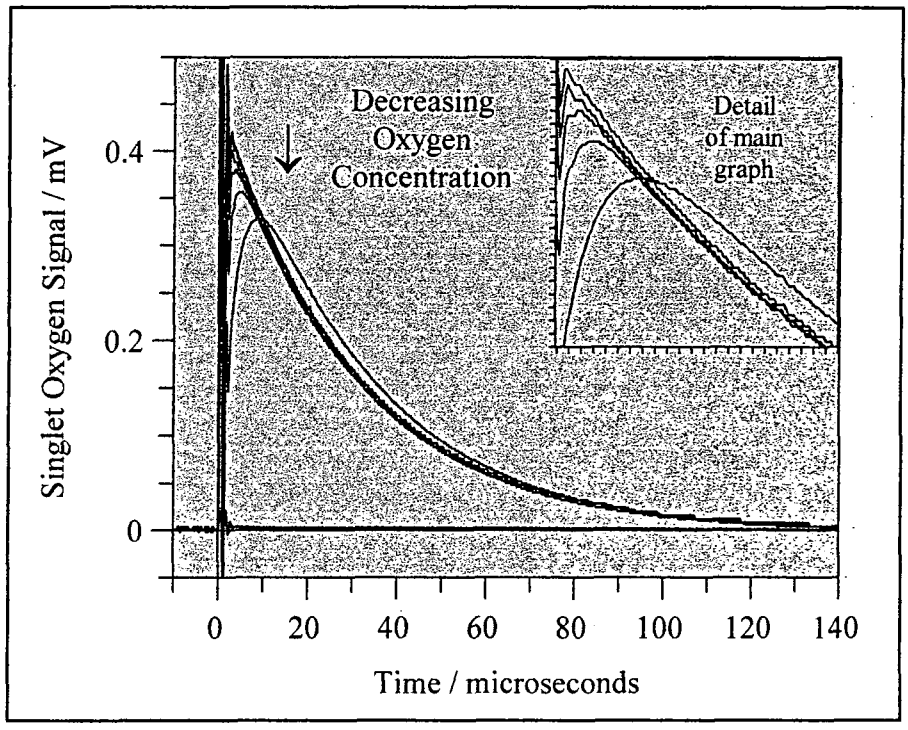

Figure 6.9 Singlet oxygen decay traces for varying oxygen concentrations, for photosensitised generation of $^1O_2$ by C_{60}

The traces can be fitted to bi-exponential function, where the kinetics of the rise of the singlet oxygen signal reflect the kinetics of the decay of the C_{60} triplet, and changes with oxygen concentration (equation 6.5). The rate of the decay of the signal are identical for all traces, $k_\Delta \approx 30$ μs, reflecting the lifetime of singlet oxygen in benzene solution, as discussed earlier. These results are as would be expected for C_{60}, following the reasoning in section 6.1.4.2, because it is well known that it is the long-lived triplet state that generates singlet oxygen[4].

The results for DBM in benzene solution show a different pattern; no grow-in of the singlet oxygen signal is observed, even at low oxygen concentrations. All traces instead follow similar kinetics, being fitted to single exponential curves, as shown in figure 6.10. Because of the low quantum yield of DBM, the decay traces had a large noise to signal ratio, and thus only the fitted curves are shown in figure 6.10.

The grow-in of the singlet oxygen decay is faster than the detection limit of this system, and is effectively instantaneous, i.e. the lifetime is approximately $\tau < 1$ μs. This indicates that a very short lived singlet state, or a triplet state state of DBM in responsible for generating singlet oxygen.

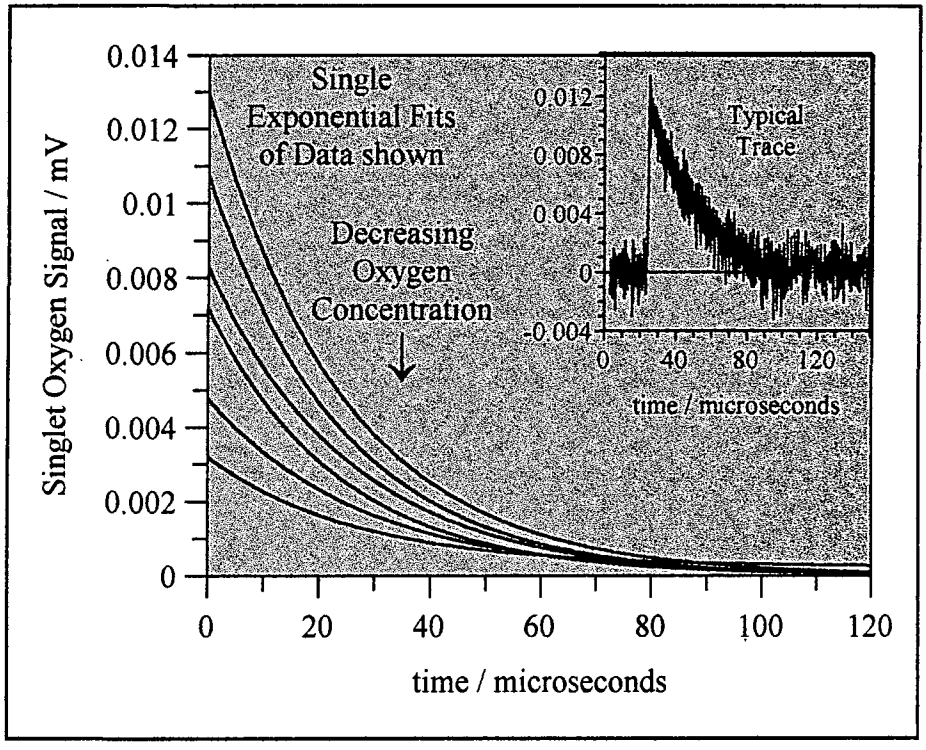

Figure 6.10 Singlet oxygen decay traces for varying oxygen concentrations, for photosensitised generation of $^1O_2$ by DBM

(Single exponential fits of data shown for clarity; typical trace shown in inset)

The signal height, and thus the quantum yield of singlet oxygen production, increases with increasing oxygen concentration. The quantum yield of singlet oxygen production, as defined in equation 6.1, can also be expressed as shown in equation 6.9, where k_{other} is the sum of rate constants for other excited state deactivation processes for DBM.

$$\Phi_\Delta \propto \frac{k_{O_2}[O_2]}{k_{other} + k_{O_2}[O_2]} \qquad \textbf{Equation 6.9}$$

Equation 6.9 can be rearranged to give equation 6.10, where C is a constant of proportionality. A graph of 1 / (initial signal height) vs. 1 / (singlet oxygen concentration) is shown in figure 6.11, where it can be seen the points fall on a straight line as expected.

$$\frac{1}{\Phi_\Delta} = C\left(\frac{k_{other}}{k_{O_2}[O_2]} + 1\right) \qquad \textbf{Equation 6.10}$$

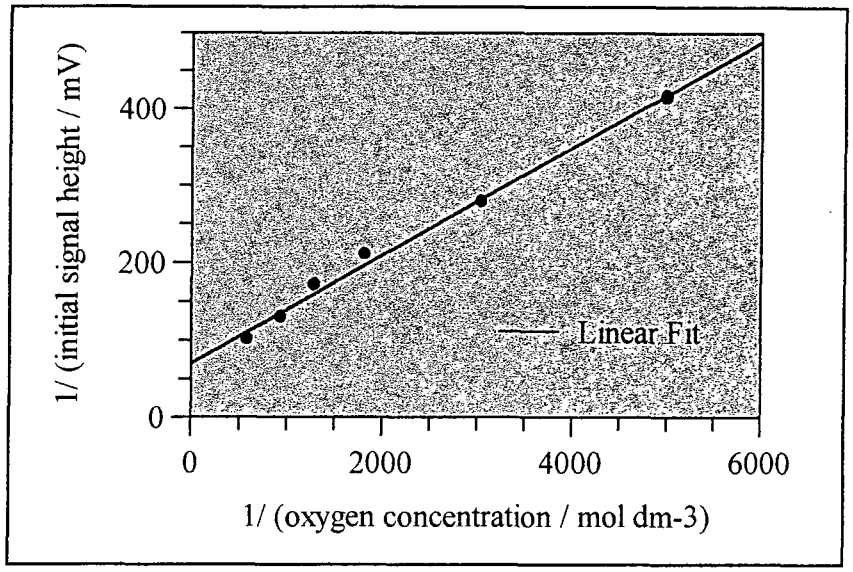

Figure 6.11 Variation of (1 / initial signal height) vs. (1 / oxygen concentration) for the photosensitised generation of singlet oxygen by DBM in benzene

In chapter 4, the nature of the excited state leading to non-chelated enol formation was discussed. Literature studies suggest that the triplet state is involved, because of rapid inter-system crossing from the singlet state. This would suggest that the triplet state of DBM is also likely to be responsible for singlet oxygen generation. Assuming that $k_{O_2} \geq 2 \times 10^9$ dm^3 mol^{-1} s^{-1}, the results in this section indicate that the lifetime of the triplet state of DBM must be very short, i.e. $\leq$ 100 ns, which would be consistent with a rapid formation of the non-chelated enol. Alternatively, these results could provide support for the theory that the formation of the non-chelated enol of DBM results from the singlet excited state, and as such inter-system crossing to form the triplet state does not occur efficiently.

6.2.3 Quenching of Singlet Oxygen

The ability of DBM and Parsol 1789 to quench singlet oxygen was studied using the method described in chapter 2, using zinc 2,9,16,23-tetra-tert-butyl-[29H,31H]-phthalocyanine to generate singlet oxygen by excitation at 680 nm.

A typical graph of Parsol 1789 concentration vs. observed rate constant for singlet oxygen decay is shown in figure 6.12, and the values obtained for the rate constants of quenching, k_Q, defined in equation 6.8, are given in table 6.5

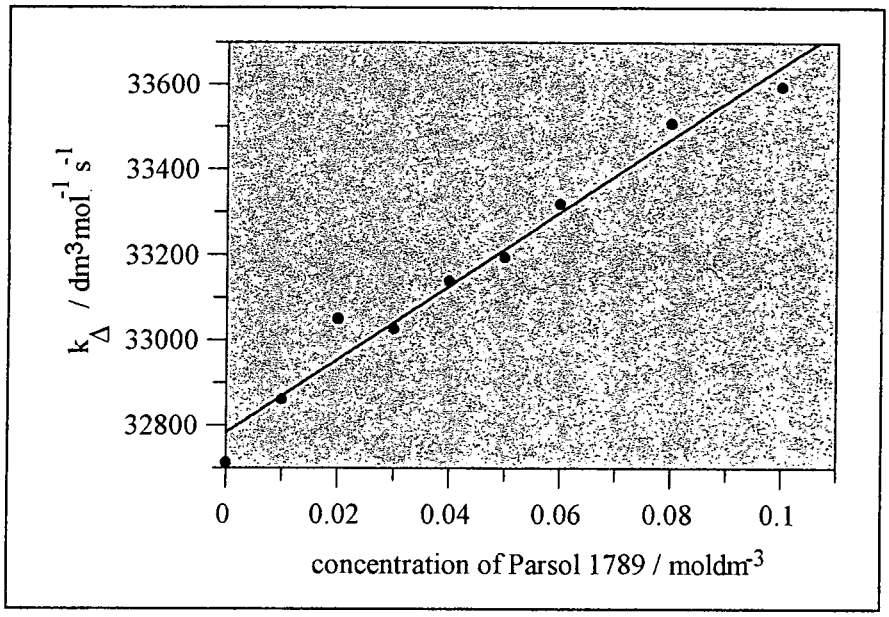

Figure 6.12 Concentration of Parsol 1789 vs. observed rate constant for singlet oxygen decay for quenching of singlet oxygen by Parsol 1789 in benzene

	k_Q / 10^7 dm^3 mol^{-1} s^{-1}	
	in Benzene	in Ethanol
Dibenzoylmethane	5.1± 0.6	2.5 ± 0.8
Parsol 1789	8.6 ± 0.6	6.7 ± 0.2

Table 6.5 Singlet oxygen quenching rate constants for DBMs

The values for k_Q are very small with very little quenching observed even at 0.1 M concentrations. The concentrations used were very large, (0.1 mol dm^{-3} Parsol 1789 in ethanol ≈ 4% by weight), and certainly comparable to any amount present in a sunscreen, e.g. the legal limit for Parsol 1789 is <5% by weight[20]. DBMs are therefore unlikely to offer any significant protection from the singlet oxygen generated by another source, or indeed from the singlet oxygen they generate.

6.2.4 Sunscreen Formulations and Cellular Environments

No attempt was made to measure the singlet oxygen quantum yields by photosensitisation or quenching abilities of DBMs in sunscreen formulations, to model conditions actually found when sunscreens are used. As mentioned earlier, singlet oxygen must be located in living material to cause damage, i.e. the DBMs must have been absorbed into the skin, and so conditions under actual use should refer to DBMs in

a cellular environment, and not in a sunscreen formulation or solution. When this is realised, it becomes clear that, because little is known about absorption of DBMs into the skin, developing a valid model system would be largely guesswork. Another problem would then be that cells, or cellular model systems, e.g. micellar solutions, tend to be aqueous in character. As described earlier, water is one of the most difficult solvents to study singlet oxygen production by the methods used in this work, due to the short lifetime, and low luminescence quantum yield. No singlet oxygen signals due to photosensitisation by DBM were detected in ethanol, and hence attempting to measure singlet oxygen generation in an aqueous environment is unlikely to be successful for these compounds. Other problems include the difficulty of measurement in an opaque or scattering environment, and for accurate quantum yield measurements, the finding a suitable standard; a compound in which the singlet oxygen quantum yield in the model environment was known.

Despite these limitations, it can be seen from chapter 3 that the photochemistry of dibenzoylmethanes occurring in solution is similar to that in micellar solutions or the model sunscreen emulsion system used. Hence it is sensible to suggest that if DBMs are found to produce singlet oxygen in solution, they will be capable of doing so in more complicated environments.

6.3 Summary

It can be seen from these results, that dibenzoylmethane sunscreens do generate singlet oxygen by photosensitisation, with quantum yields $\Phi_\Delta \approx 0.005\text{-}0.01$. Whilst it is true that this is a very low efficiency, singlet oxygen is a highly reactive species capable of causing serious biological damage, and hence any ability of a sunscreen to produce singlet oxygen is undesirable.

The lifetime of the excited state of DBM involved has been shown to be very short, approximately $\tau < 1$ μs, even at low oxygen concentration. From previous discussions, it is likely that the excited state generating singlet oxygen is the triplet state, and hence these results indicate a very short-lived triplet state of the chelated enol form of DBM.

The ability of dibenzoylmethanes to quench singlet oxygen was also found to be very small, with the rate constants for quenching, $k_Q \approx 3000\text{-}9000$ $dm^3\ mol^{-1}\ s^{-1}$. This is not likely to offer significant protection against the singlet oxygen generated by other molecules, or indeed by the DBMs themselves.

6.4 References

[1] Coyle J D, Hill R R, Roberts D R, "*Light, Chemical Change and Life - a Source Book in Photochemistry*", Open University Press, Milton Keynes, 1982

[2] Greenwood N N, Earnshaw A, Chapter 14, "Oxygen" in "*Chemistry of the elements*", Permagon Press, Oxford, 1989, page 706

[3] Turro N J, Chapter 14 "Singlet Oxygen and Chemiluminescent Organic Reactions" in "*Modern Molecular Photochemistry*", University Science Books, California, 1991, page 578

[4] Wilkinson F, Helman W P, Ross A B, "Quantum Yields for the photosensitised formation of the lowest electronically excited singlet state of Molecular Oxygen in Solution", *J. Phys. Chem. Ref. Data.*, **22**, No 1, 1993

[5] Gilbert A, Baggott J, "*Essentials of Molecular Photochemistry*", Blackwell Scientific Publications, Oxford, 1991

[6] Murov S L, Carmichael I, Hug G L, "*Handbook of Photochemistry*", 2nd edition, Marcel Dekker Inc., New York, 1993

[7] Khan A U, "Activated Oxygen: Singlet Molecular Oxygen and Superoxide Anion", *Photochem. Photobiol.*, **28** (1978), 615

[8] Gorman A A, Rodgers M A J, Chapter 10 "Singlet Oxygen" in "*Handbook of Organic Photochemistry*", ed. Scaiano J C, Volume 2, CRC Press, Florida, 1989

[9] Hurst J R, Schuster G B, "Nonradiative Relaxation of Singlet Oxygen in Solution", *J. Am. Chem. Soc.*, **105** (1983), 5756

[10] Losev A P, Byteva I M, Gurinovich G P, "Singlet Oxygen Luminescence Quantum Yields in Organic Solvents and Water", *Chem. Phys. Lett.*, **143** (1988), 127

[11] Schmidt R, Afshari E, "Effect of Solvent on the Phosphorescence Rate Constant of Singlet Molecular Oxygen ($^1\Delta_g$)", *J. Phys. Chem.*, **94** (1990), 4377

[12] Parker J G, "The Importance of Singlet Delta Oxygen in Cancer Photoradiation Therapy", *John Hopkins APL Technical Digest*, **5(1)** (1984), 48

[13] Bensasson R V, Land E J, Truscott T G, Chapter 4 "*Activated forms of Oxygen*" in "*Excited States and Free radicals in Biology and Medicine*", Oxford University Press, Oxford, 1993, page 101

[14] MacRobert A J, Phillips D, "Photodynamic Therapy", *Chemistry & Industry*, (1992), 17

[15] Nill Q J, Mendenhall G D, "Yields of Singlet Molecular Oxygen from peroxyl Radical Termination", *J. Am. Chem. Soc.*, **114** (1992), 165

[16] Balsam M S, Sagarin E, Chapter 7 "Suntan Preparations" in "*Cosmetics Science and Technology*", 2nd Edition, Volume 1, 1972 , page 241

[17] Blank I H, Cohen J H, Anderson R R, Jaenicke K F, Parrish J A, "Observations on the Mechanism of the protective Action of Sunscreens", *J. Invest. Dermatol.*, **78** (1982), 381

[18] Giese K, Nicolaus A, Sennhenn B, Kölmel K, "Photoacoustic in vivo study of the penetration of sunscreen into human skin", *Can. J. Phys.*, **64** (1986), 1139

[19] N J Lowe, N A Shaath, "*Sunscreens: Development, Evaluation, and Regulatory Aspects*", Marcel Dekker Inc, New York, 1990

[20] Saninio E-L, "The Ingredients, safety, efficacy and stability of sunscreens", *National Consumer Administration Publications Series 16 / 1995*, National Consumer Administration, 1995, Helsinki

[21] Schauder S, Ippen H, "Photoallergic and allergic contact dermatitis from dibenzoylmethanes", *Photodermatology*, **3** (1986), 140

[22] Allen J M, Gossett C J, Allen S K, "Photochemical Formation of Singlet Molecular Oxygen in Illuminated Aqueous Solutions of Several Commercially Available Sunscreen Active Ingredients", *Chem. Res. Toxicol.*, **9** (1996), 605

[23] Allen J M, Gossett C J, Allen S K, "Photochemical formation of singlet molecular oxygen ($^1O_2$) in illuminated aqueous solutions of p-aminobenzoic acid (PABA)", *J. Photochem. Photobiol. B:Biology*, **32** (1996), 33

[24] DeLeo V A, Suarez S M, Maso M J, "Photoallergic Contact Dermatitis", *Arch. Dermatol.*, **28** (1992), 1513

[25] Dromogoole S H, Maibach H I, "Sunscreening Agent Intolerance: Contact and Photocontact Sensitization and Contact Urticana", *J. Am. Acad. Dermatol.*, **22** (1990), 1068

[26] Knowland J, McKenzie E A, McHugh P J, Cridland N A, "Sunlight-induced mutagenicity of a common sunscreen ingredient", *FEBS Letters*, **324** (1993), No. 3, 309

[27] Dai G, Qin X, Zhang J, Wu S, "Phototautomerization of β-Diketones", *Youji Huaxue*, **2** (1987), 155

[28] Beeby A, Parker A W, "The Photochemistry of Dibenzoylmethane; An Enolised 1,3-Diketone", *CLF Rutherford Appleton Laboratory Report*, RAL-94-042, (1994), 186

Appendices

1. Publications and Presentations

"A Time-Resolved Resonance Raman Study of Enolised 1,3-Diketones used as UV-A Sunscreens", A Beeby, C Coultous, D J McGarvey, L Mulroy, S Tavender, *Central Laser Facility, Rutherford Appleton Laboratory, Annual Report 1994-95, RAL Report TR-95-025,* pg 132

"Time-Resolved Spectroscopy of Enolised 1,3-Diketones used as UV-A Sunscreens", oral presentation at 6th Congress of the European Society for Photobiology, 3rd-8th September 1995, *University of Cambridge*

2. Courses attended

2.1 External Courses

EPSRC Summer School in Laser Spectroscopy, 4th-10th September 1994, *University of East Anglia, Norwich*

2.2 Internal Courses

Physical chemistry of polymers, Prof. R W Richards, *Dept. of Chemistry, University of Durham*

Practical nuclear-magnetic resonance, Dr. A M Kenwright, *Dept. of Chemistry, University of Durham*

Optics, Dr. R Bower, *Dept. of Physics, University of Durham*

3. Seminars and Lectures attended

"Determining Molecular Structure - the INADEQUATE NMR Way", Prof. N L Owen, *Brigham Young University, Utah*

"Some Aspects of Ag(II) and Ag(III) Chemistry", Prof. N Bartlett, *University of California*

"Real or Imaginary 3rd Order Non-Linear Optical Materials" Dr. G Rumbles, *Imperial College, University of London*

"The Manipulation of Electronic and Structural Diversity in Metal Complexes - New Ligands for New Properties", Dr. P G Edwards, *University of Wales, Cardiff*

"Polymers do it at interfaces", Dr. T Cosgrove, *Bristol University*

"Chemical Aspects of Photo-Dynamic Therapy", Prof. R. Bonnett, *Queen Mary's College, University of London*

"C60 - a Celestial Sphere which fell to Earth", Prof. H W Kroto, *University of Sussex*

"Low Temperature Crystallography - Experiences with a 20K X-Ray Diffractometer", Prof. P Lugar, *Frei University, Berlin*

"Chemical Reactions in Organised Systems: Peracid reactivity in Surfactant Micelles and Cyclodextrin Hosts", Dr. M. Davies, *University of Northumbria, Newcastle*

"Explosions", Dr. C J Ludman, *University of Durham*

"Chemistry of Smart Fluids", Prof.B H Robinson, *University of East Anglia, Norwich*

"A Water of Glass? Luminescence Studies of Water Soluble Polymers", Prof. I. Soutar, *Lancaster University*

"Drug Abuse in Sport", Dr. P D Levy, *Drug Control Centre, King's College London*

"Sonochemistry", Prof T J Mason, *Coventry University*

"Terahertz Laser Spectroscopy of Water Clusters; Towards a Genuine Molecular Model of the Liquid", Prof. J Saykally, *University of California, Berkeley*

"Liquid Crystals - More Than Meets the Eye", Prof. J W Emsley, *Southampton University*

"Soft Soaps and Surfaces", J Penfold, *ISIS Facility, Rutherford Appleton Laboratories, CCLRC*

"New Perspectives in NMR Imaging", Prof. E W Randall, *Queen Mary and Westfield College, University of London*

"Laser Cooling in the Condensed Phase: the Tale of a Novel Observation", Dr. G Rumbles, *Imperial College, University of London*

"Supramolecular Photochemistry", Prof. V Balzani, *University of Bologna, Italy*

"Triplet State Interactions in DNA Model Systems", P D Wood

"Synthetic Polymers for Biomedical Application - can we meet Nature's Challenge?", Prof. B J Tighe, *Dept. of Molecular Sciences and Chemistry, University of Aston*

"The Purpose of Experiment - A Look at Davy and Faraday", Prof. D M Knight, *Dept. of Philosophy, University of Durham*

"New Materials - Fact or Fantasy?", Prof. R J Young, *Manchester Materials Centre, UMIST*

"Assembly of Complex Molecules by Palladium-Catalysed Queueing Processes", Prof. R E Grigg, *University of Leeds*

"Surface Light Scattering: Ripples and Relaxation", Prof. J Earnshaw, Queens University, Belfast

"Molecular Tubes and Sponges", R Templar, *Imperial College, University of London*

"A Little Light Relief", Prof D Phillips, *Imperial College, University of London*

"Chemical Applications of Very High Resolution ZEKE Photoelectron Spectroscopy", Prof. K Muller-Dethlefs, *York University*

"Polyketones", Neil Cooley, *BP Chemicals, Sunbury*

"High-Speed Automation of Chemical Reactions", Mr. D Rudge, *Zeneca Pharmaceuticals*

"The Dynamics of Dissociation at Surface and Fuel Cell Catalysts", Prof. B Hayden, *University of Southampton*

"From Runways to Non-Metallic Metals - New Chemistry Based on Sulphur", Dr. A J Banister, *University of Durham*

"Tinkering with Biosynthesis: Towards a new Generation of Antibiotics", Dr. J Staunton, *University of Cambridge*

"My Dialogues with Medicinal Chemists", Prof. Sir James Black, *Imperial College, University of London / Sir James Black Foundation*

"The Enantioselective quenching of Lanthanide Complexes", Prof J H Riehl, *Michigan Technology University*

"The Structure, Properties and Design of Blue Copper Proteins", Prof. A G Sykes, *University of Newcastle*

"Some Very Heterocyclic Chemistry", Prof. C W Rees, *Imperial College, University of London*

"Probing Dynamical Processes with Photoelectrons", Dr. Katherine Reed, *University of Nottingham*

"Ozone Depletion and Skin Cancer - Alarming or Alarmist?", Prof. B Diffey, *Dept. of Medical Physics, Dryburn Hospital, Durham*

"Polymers both enable and limit the discovery of protein alterations in studies ranging from gene regulation to mad cow disease", Prof. M Harrington, *Caltech, Pasedena*

North East Graduate Colloquia 1995-1997, *University of Durham* (1995), *University of Sunderland* (1996), *Universtiy of Newcastle* (1997)

Acknowledgements

There are many people who have helped me over the past few years, all contributing to some extent to the production of this thesis. This note cannot do justice to my gratitude, and to attempt to name everyone here would probably result in accidentally leaving out some key people. So, I would simply like to say a general thank-you to everyone who played their part - although it's a bit of a cliché, I couldn't have done it without you all.

There are, however a few bodies and people who I would like to specifically mention.

I must acknowledge my PhD supervisor, Dr. Andrew Beeby. Thanks too to Steve Faulkner for proof-reading this thesis.

For funding I am indebted to the EPSRC (for initial project funding) and the Department of Chemistry at the University of Durham (for main funding).

For assistance with the Time Resolved Resonance Raman spectroscopy, I would like to thank the Rutherford Appleton Laboratories for use of their facilities, and particularly Sue Tavender.

I would also like to thank David Worrall and Prof. Frank Wilkinson's group at the dept of Chemistry at Loughborough University for showing me their diffuse reflectance spectroscopy equipment, and the basic principles of this technique. I would also like to thank Prof. Wilkinson for additional suggestions regarding the analysis of some of the data presented here.

On a personal level let me thank Allison, Claire, Mum and Dad, and especially Graham for all their support.

And finally, special thanks to Daphne, Olivia, Todd and Di for keeping me sane.